Curtin University Medical School

Pharmacy

Bile acids for probucol formulations applications in drug induced ototoxicity

Corina Mihaela Ionescu

0000-0002-8966-0448

This thesis is presented for the Degree of

Doctor of Philosophy

Curtin University

August 2024

Declaration

To the best of my knowledge and belief this thesis contains no material previously published by any other person except where due acknowledgment has been made.
This thesis contains no material which has been accepted for the award of any other degree or diploma in any university.

Signature:  .....

Date: 25.08.2024

Table of Contents

Table of Figures

Table of Tables

Abbreviations

BSC	Biopharmaceutical Classification System
FDA	Food and Drug Administration
ROS	Reactive Oxygen Species
PB	probucol
CDDP	cisplatin, cis-diamminedichloroplatinum II
CDCA	chenodeoxycholic acid
CA	cholic acid
UDCA	ursodeoxycholic acid
TCA	taurocholic acid, T-conjugated bile acid
DCA	deoxycholic acid
LCA	lithocholic acid
T-	taurine-conjugated bile acids
G-	glycine-conjugated bile acids
hyo-DCA	hyo-deoxycholic acid
HEI-OC1	House Ear Institute-Organ of Corti 1 cell line
RAW 264.7	Macrophage cell line (ATCC®, TIB-71™)
F1,2,3…10	Formulation 1,2,3…10
F1,2,3…10+	Formulation 1,2,3…10 with stressors
*α/β*CD-PB	*α/β*-CD-probucol
*α/β*CA-PB	*α/β*-CD-bile acid type-probucol
DMSO	dimethyl sulfoxide
ER	endoplasmic reticulum
HO1	heme oxygenase 1
SOD2	superoxide dismutase 2
Bcl-2	B cell lymphoma-2
BK	large Ca^{2+}-activated K^{+}
VDR	vitamin D receptor
SIRT1	Silent information regulator transcript-1
Nrf2	nuclear factor erythroid 2-related factor
TNF-α	tumour necrosis factor alpha
MCP-1	monocyte chemoattractant protein-1

IL-6	interleukin-6
ABR	auditory brainstem response
P2X	Purinergic Ion-ligand receptors
P2Y	Purinergic G-protein-coupled receptors
ATP	adenosine triphosphate
UPR	unfolded protein response
CHOP	high CCAAT-enhancer-binding protein homologous protein
GRP78	chaperone glucose-regulating protein 78
mAchR or M	muscarinic acetylcholine receptors
ERK	extracellular signal-regulated kinase
ATM	ataxia telangiectasia mutated
S1PR2	Sphingosine-1-phosphate receptor 2
miR	non-coding micro ribonucleic acid
SOX2	SRY-Box Transcription Factor 2
FOXO3	forkhead box O3
BBB	blood-brain-barrier
BLB	blood-labyrinth-barrier
P-gp	P-glycoprotein
Oatp1a4	Organic anion-transporting polypeptide 1a4
FRX	farnesoid X receptor
TGR5	Takeda G-coupled protein receptor 5
SREBP	Sterol responsive element-binding protein
ATP8B1	ATPase phospholipid transporting 8B1
OSPL2	Oxysterol-binding protein like 2
AMPK	AMP-activated protein kinase
Apo	apolipoprotein
IC50	inhibitory concentration
DCF	2', 7' –dichlorofluorescein
API	active pharmaceutical ingredient
PVP	polyvinylpyrrolidone
PVA	polyvinyl acetate
PEG	polyethylene glycol
CD	cyclodextrin
beta- or β-CD	β-cyclodextrin

alpha- or α-CD	α-cyclodextrin
gamma- or γ-CD	γ-cyclodextrin
PFA	paraformaldehyde
MTT	3-(4,5-dimethylthiazol-2-yl)-2,5-diphenyltetrazolium bromide
WST-1	water-soluble tetrazolium salt assay
DMEM	Dulbecco's Modified Eagle Medium
PBS	Phosphate buffer saline
FBS	Foetal bovine serum
SEM	Scanning electron microscope
EDS	Energy Dispersive X-Ray Spectroscopy
UATR	attenuated total reflection accessory
FT-IR	Fourier-transform infrared
OMY	oligomycin
ROT	rotenone antimycin A
FCCP	carbonyl cyanide-4 (trifluoromethoxy) phenylhydrazone
ECAR	extracellular acidification rates
SNHL	sensorineural hearing loss
Trypsin-EDTA	trypsin-ethylenediaminetetraacetic acid
PG	polypropylene glycol
TGel	transonic gel
BCA	pierce bicinchoninic acid protein assay kit
HPLC	high-performance liquid chromatography analysis
PDI	polydispersity index
BOILED-Egg	Brain Or IntestinaL EstimateD permeation method

Acknowledgements

I would like to acknowledge the funding body Australian Postgraduate Award and Curtin Research Scholarship that allowed me to pursue this PhD scholarship.

Many thanks go to my main supervisor Dr Hani Al-Salami, co-supervisor Dr Armin Mooranian and co-supervisor Dr Daniel Brown for your constant support, supervision, advice and independence offered in the laboratory, writing and presenting. I appreciate the knowledge of drug delivery and pharmacy-related expertise that the project was focused on, and for the introduction to hearing research, training in vivo techniques, critical thinking, ideas on how to use bile acid, and lessons on collaborations and scientific integrity.

Thank you to the seniors and junior students – Bozica Kovacevic, Melissa Jones, Louise Carey, Susbin Wagle, Patrick Lim, Thomas Foster – from the Biotechnology and Drug Development Research Laboratory for the support, exchange of ideas and protocols, and for your presence in the laboratory, office and during meetings.

I am grateful to have used the House Ear Institute-Organ of Corti 1 cells provided from Prof. Federico Kalinec and Dr. Young Joon Seo. I appreciate and thank Dr. Young Joon Seo for his knowledge on in vitro techniques and teachings on how to perform organ of Corti microdissections.

Thank you, Dr Giuseppe Luna for your advice, endless laboratory etiquette examples, inductions and introduction to organic chemistry synthesis. Sei sempre "Beato Tra" gli studenti.

Thank you, Jorge Martinez, for your encouragement and wise words, and more importantly for access and introductions to pharmaceutical equipment.

Many thanks to Ms Elaine Miller for the Tescan Clara Scanning Electron Microscopy induction at the John de Laeter Centre Electron Microscope Facility at Curtin University.

I would like to acknowledge Curtin Health Innovation Research Institute (CHIRI) as the core facility for this project. I would like to acknowledge the use of CHIRI laboratory equipment and the scientific and technical assistance throughout the years.

Thank you, Dr Joanna Kelly, Pat Metharom, Dr Rob Steuart, Dr Rob Trengove, Dr Ben Dwyer, Mr Sam Siem, Mr Michael Nesbit, and to the DGR support from Dr Kylie Munyard and Dr Cyril Mamotte.

I am glad to have met wonderful individuals, and I thank you Dr Aria Van Alin, Natali Vasilevski, Melissa Jones, Bozica Kovacevic, Susbin Wagle, Daniel Walker, Patrick Lim, Amy O'Keefee, Dr Thellie Ponto, Dr Gae Elisson, Victor Olet, Thomas Foster, Usha Vyshu Chidella, Arazu Sharif, Amelia Radesich, Katherine Sussato and Michel Nesbit for the tearoom chats.

Thank you to all the people and trainees from Swordfish Fencing Club, UWA Fencing Club and WA Fencing to regain confidence through sport and maintain "Mens Sana in Corpore Sano".

Special thank you to the lasting friendship, mentoring, and for the pursuit for scientific outreach – Dr Maria Suciu, Dr Alexandra Ciorîță, Dr Diana Felicia Panait, Dr Lucian Barbu-Tudoran and Tech. Septimiu Tripon from the Electron Microscopy Centre "Constantin Crăciun" team from Cluj-Napoca.

Lastly, yet more importantly, thank you to my extended family and for your many examples in pursuing dreams far away from home.

Copyright Statement

I have obtained permission from the copyright owners to use any third-party copyright material reproduced in the thesis (e.g. artwork), or to use any of my own published work (e.g. journal articles, reviews) in which the copyright is held by another party (e.g. publisher, co-author).

Attachments and further information can be found in Appendix I.

Country Acknowledgement

We acknowledge that Curtin University works across hundreds of traditional lands and custodial groups in Australia, and with First Nations people around the globe. We wish to pay our deepest respects to their ancestors and members of their communities, past, present, and to their emerging leaders.

Abstract

The majority of commercial drugs and molecules with therapeutic potential have poor water solubility and decreased tissue absorption. With limited commercial application, the lipophilic antioxidant probucol requires pre-formulation and encapsulation technologies to improve bioavailability.

Within this thesis, probucol's otoprotective application is assessed *in vitro* on House Ear Institute-Organ of Corti 1 (HEI-OC1) using three different formulation methods; 1) spray dried, 2) chitosan films or 3) supramolecular aggregates. To improve pre-formulation stability and drug loading, probucol is tested in combination with unconjugated and conjugated bile acids (cholic acid, deoxycholic acid, chenodeoxycholic acid, ursodeoxycholic acid, taurocholic acid, lithocholic acid).

Pre-formulation rheology, particle characterisation including functional groups identification, surface morphology, zeta potential, drug loading, drug dissolution, matrix swelling recordings and calorimetry measurements were performed. The biological impact on model cells for oxidative stress (cytotoxicity) were assessed using reactive oxygen species accumulation, viability and bioenergetics assays.

Bile acids as excipients improve spray dried and chitosan film formulation stability, surface appearance as well as drug loading, dissolution and release. Supramolecular particle aggregation is greatly influenced by low concentrations of bile acids. Fewer yet stable nanoparticle formations were recorded with the addition of lithocholic acid. Bile-probucol (ursodeoxycholic acid, cholic acid) formulations are compatible with HEI-OC1 and maintain cell survival against stressor pre-conditioning.

Bile acids used in formulations influence and enhance differently drug release we show that slower drug release favours HEI-OC1 cell survival against oxidative stress *in vitro*. A combination (*e.g.* method 1 & 3, method 2 & 3) or additional methods other than the ones specified (*e.g.* metallic nanoparticles, quantum dots, nanoprecipitation) could be used to enhance probucol's therapeutic efficacy and drug delivery in the future.

List of Primary Publications

This PhD hybrid thesis comprises of five publications that are submitted, in press or under revision. The publications are presented as chapters. Copyrights are attached in Appendix I.

1. **Corina M. Ionescu,** Melissa A. Jones, Susbin R. Wagle, Bozica Kovacevic, Thomas Foster, Momir Mikov, *Armin Mooranian and *Hani Al-Salami - Bile Acid Application in Cell-Targeting for Molecular Receptors in Relation to Hearing: A Comprehensive Review. *Current Drug Targets*, Volume 25, Issue 3, 2024, Page 158 – 170. DOI: 10.2174/0113894501278292231223035733

2. **Corina M. Ionescu,** Melissa A. Jones, Susbin R. Wagle, Bozica Kovacevic, Thomas Foster, Momir Mikov, *Armin Mooranian and *Hani Al-Salami – Could Bile Acids Modulate Hearing Loss? – To be published

3. **Corina M Ionescu**, Bozica Kovacevic, Melissa A Jones, Susbin R Wagle, Thomas Foster, Momir Mikov, *Armin Mooranian and *Hani Al-Salami - Probucol-Ursodeoxycholic Acid Otic Formulations: Stability and In Vitro Assessments for Hearing Loss Treatment. *Journal of Pharmaceutical Sciences*, 2024, 10:S0022-3549(24)00159-X. DOI: 10.1016/j.xphs.2024.04.032

4. **Corina M Ionescu**, Bozica Kovacevic, Susbin R Wagle, Thomas P Foster, *Armin Mooranian and *Hani Al-Salami - Secondary Bile Acid-Polymer Based Micro-Films for Ear-Targeted Delivery of The Drug Probucol: Applications for Treating Hearing Loss. – To be published

5. **Corina M Ionescu**, Thomas P Foster, Bozica Kovacevic, Susbin R Wagle, *Armin Mooranian and *Hani Al-Salami - Cyclodextrin Probucol Bile Acid Particles and Their Effects on HEI-OC1 Cells. – To be published

List of Secondary Publications

The following list of 42 co-authored papers do not encompass the theme of this thesis.

1. Sangeetha Mathavan, **Corina M Ionescu**, Bozica Kovacevic, Momir Mikov, Svetlana Golocorbin-Kon, Armin Mooranian, Crispin R Dass, *Hani Al-Salami – Formulation buoyancy of nanoencapsulated gliclazide using primary, conjugated and deconjugated bile acids. *Therapeutic Delivery*, Volume 10, No. 9, 2019. DOI: 10.4155/tde-2019-0058

2. Sangeetha Mathavan, **Corina M Ionescu**, Bozica Kovacevic, Momir Mikov, Svetlana Golocorbin-Kon, Armin Mooranian, Crispin R Dass, *Hani Al-Salami – Histological effects of pharmacologically active human bile acid nano/micro-particles in Type-1 diabetes. *Therapeutic Delivery*, Volume 11, No. 3, 2020. DOI: 10.4155/tde- 2019-0079

3. Armin Mooranian, Nassim Zamani, **Corina M Ionescu**, Ryu Takechi, Giuseppe Luna, Momir Mikov, Svetlana Goločorbin-Kon, Božica Kovačević, *Hani Al-Salami – Oral gavage of nano-encapsulated conjugated acrylic acid-bile acid formulation in type 1 diabetes altered pharmacological profile of bile acids, and improved glycaemia and suppressed inflammation. *Pharmacological Reports*, 72(2), 368 – 378, 2022. DOI: 10.1007/s43440-019-00030-z

4. *Armin Mooranian, Nassim Zamani, Bozica Kovacevic, **Corina Mihaela Ionescu**, Giuseppe Luna, Momir Mikov, Svetlana Goločorbin-Kon, Goran Stojanovic, Sanja Kojic and *Hani Al-Salami – Pharmacological effects of secondary bile acid microparticles in diabetic murine model. *Current Diabetes Reviews*, Volume 18, Issue 1, 2022. DOI: 10.2174/1573399816666200626213735

5. *Maria Suciu, **Corina M. Ionescu**, Alexandra Ciorita, Septimiu C. Tripon, Dragos Nica, Hani Al-Salami, and Lucian Barbu-Tudoran – Applications of superparamagnetic iron oxide nanoparticles in drug and therapeutic delivery, and

biotechnological advancements. *Beilstein Journal of Nanotechnology*, Volume 11, 1092 – 1109, 2020. DOI: 10.3762/bjnano.11.94

6. Susbin Raj Wagle, Bozica Kovacevic, Daniel Walker, **Corina Mihaela Ionescu**, Melissa Jones, Goran Stokanovic, Sanja Kojic, Armin Mooranian, *Hani Al-Salami – Pharmacological and Advanced Cell Respiration Effects, Enhanced by Toxic Human-Bile Nano-Pharmaceuticals of Probucol Cell-Targeting Formulations. *Pharmaceutics*, 12(8), 708, 2020. DOI: 10.3390/pharmaceutics12080708

7. Susbin Raj Wagle, Bozica Kovacevic, Daniel Walker, **Corina Mihaela Ionescu**, Umar Shah, Goran Stojanovic, Sanja Kojic, Armin Mooranian, *Hani Al-Salami – Alginate-based drug oral targeting using bio-micro/nano encapsulation technologies. *Expert Opinion on Drug Delivery*, Volume 17, Issue 10, Page 1361 – 1376, 2020. DOI: 10.1080/17425247.2020.178958

8. Melissa Jones, Daniel Walker, **Corina Mihaela Ionescu**, Bozica Kovacevic, Susbin Raj Wagle, Armin Mooranian, Daniel Brown & *Hani Al-Salami – Microencapsulation of Coenzyme Q10 and bile acids using ionic gelation vibrational jet flow technology for oral delivery. *Therapeutic Delivery*, Volume 11, No. 12, 2020. DOI: 10.4155/tde-2020-0082

9. Armin Mooranian, Melissa Jones, **Corina Mihaela Ionescu**, Daniel Walker, Susbin Raj Wagle, Bozica Kovacevic, Jacqueline Chester, Thomas Foster, Edan Johnston, Momir Mikov, *Hani Al-Salami – Advancements in Assessments of Bio-Tissue Engineering and Viable Cell Delivery Matrices Using Bile Acid-Based Pharmacological Biotechnologies. *Nanomaterials*, 11(7), 1861, 2021. DOI: 10.3390/nano11071861

10. Chester, J; Johnston, E; Walker, D; Jones, M; **Ionescu, CM**; Wagle, SR; Kovacevic, B; Brown, D; Mikov, M; Mooranian, A, *Al-Salami, H – A Review on Recent Advancement on Age-Related Hearing Loss: The Applications of Nanotechnology, Drug Pharmacology, and Biotechnology. *Pharmaceutics*, 13(7), 1041, 2021. DOI: 10.3390/pharmaceutics13071041

11. Armin Mooranian, Thomas Foster, **Corina M. Ionescu**, Daniel Walker, Melissa Jones, Susbin Raj Wagle, Bozica Kovacevic, Jacqueline Chester, Edan Johnston, Elaine Wong, Marcus D. Atlas, Momir Mikov, *Hani Al-Salami – Enhanced Bilosomal Properties Resulted in Optimum Pharmacological Effects by Increased Acidification Pathways. *Pharmaceutics*, 13(8),1184, 2021. DOI: 10.3390/pharmaceutics13081184

12. Susbin Raj Wagle, Bozica Kovacevic, **Corina Mihaela Ionescu**, Daniel Walker, Melissa Jones, Louise Carey, Ryusuke Takechi, Momir Mikov, *Armin Mooranian, *Hani Al-Salami – Pharmacological and Biological Study of Microencapsulated Probucol-Secondary Bile Acid in a Diseased Mouse Model. *Pharmaceutics*, 13(8), 1223, 2021. 10.3390/pharmaceutics13081223

13. Armin Mooranian, **Corina Mihaela Ionescu**, Susbin Raj Wagle, Bozica Kovacevic, Daniel Walker, Melissa Jones, Jacqueline Chester, Thomas Foster, Edan Johnston, Momir Mikov, Marcus D. Atlas, *Hani Al-Salami – Probucol Pharmacological and Bio-Nanotechnological Effects on Surgically Transplanted Graft Due to Powerful Anti-Inflammatory, Anti-Fibrotic and Potential Bile Acid Modulatory Actions. *Pharmaceutics*, 13(8), 2021, 1304. DOI: 10.3390/pharmaceutics13081304

14. Armin Mooranian, **Corina Mihaela Ionescu**, Susbin Raj Wagle, Bozica Kovacevic, Daniel Walker, Melissa Jones, Jacqueline Chester, Edan Johnston, Maja Danic, Momir Mikov, Crispin Dass, *Hani Al-Salami – Chenodeoxycholic Acid Pharmacology in Biotechnology and Transplantable Pharmaceutical Applications for Tissue Delivery: An Acute Preclinical Study. *Cells*, 10(9), 2021, 2437. DOI: 10.3390/cells10092437

15. Mooranian A, Foster T, **Ionescu CM**, Carey L, Walker D, Jones M, Wagle SR, Kovacevic B, Chester J, Johnstone E, Kuthubutheen J, Brown D, Atlas MD, Mikov M, *Al-Salami H – The Effects of Primary Unconjugated Bile Acids on Nanoencapsulated Pharmaceutical Formulation of Hydrophilic Drugs:

Pharmacological Implications. *Drug Design, Development and Therapy*, Volume 2021:15, Page 4423 – 4434. DOI: 10.2147/DDDT.S328526

16. Armin Mooranian, **Corina Mihaela Ionescu**, Susbin Raj Wagle, Bozica Kovacevic, Daniel Walker, Melissa Jones, Jacqueline Chester, Thomas Foster, Edan Johnston, Sanja Kojic, Goran Stojanovic, Momir Mikov, *Hani Al-Salami – Polyelectrolytes Formulated with Primary Unconjugated Bile Acid Optimised Pharmacology of Bio-Engineered Implant. *Pharmaceutics*, 13(10), 2021, 1713. DOI: 10.3390/pharmaceutics13101713

17. Thomas Foster, **Corina Ionescu**, Daniel Walker, Melissa Jones, Susbin Wagle, Božica Kovacevic, Daniel Brown, Momir Mikov, *Armin Mooranian, *Hani Al-Salami – Chemotherapy-induced hearing loss: the applications of bio-nanotechnologies and bile acid-based delivery matrices. *Therapeutic Delivery*, Volume 12, No. 10, 2021. DOI: 10.4155/tde-2021-0050

18. Carey, L, Walker, D, Jones, M, **Ionescu, C**, Wagle, S, Kovacevic, B, Brown, B, Mikov, M, Mooranian, A, *Al-Salami, H – Bile acid-permeation enhancement for inner ear cochlear drug-pharmacological uptake: bio-nanotechnologies in chemotherapy-induced hearing loss. *Therapeutic Delivery*, 12(12), 2021. DOI:10.4155/tde-2021-0048

19. Mooranian, A, Jones, M, **Ionescu, CM**, Walker, D, Wagle, SR, Kovacevic, B, Chester, J, Foster T, Johnston, E, Mikov, M, *Al-Salami, H - Pharmaceutical formulation and polymer chemistry for cell encapsulation applied to the creation of a lab-on-a-chip bio-microsystem. *Therapeutic Delivery*, 13(1), 2021. DOI:10.4155/tde-2021-0067

20. Armin Mooranian, Louise Carey, **Corina Mihaela Ionescu**, Daniel Walker, Melissa Jones, Susbin Raj Wagle, Bozica Kovacevic, Thomas Foster, Jacqueline Chester, Edan Johnston, Momir Mikov, *Hani Al-Salami – The Effects of Accelerated Temperature-Controlled Stability Systems on the Release Profile of Primary Bile Acid-Based Delivery Microcapsules. *Pharmaceutics*, 13(10), 2021, 1667. DOI: 10.3390/pharmaceutics13101667

21. Armin Mooranian, Melissa Jones, **Corina Mihaela Ionescu**, Daniel Walker, Susbin Raj Wagle, Bozica Kovacevic, Jacqueline Chester, Thomas Foster, Edan Johnston, Jafri Kuthubutheen, Daniel Brown, Momir Mikov, *Hani Al-Salami – Artificial Cell Encapsulation for Biomaterials and Tissue Bio-Nanoengineering: History, Achievements, Limitations, and Future Work for Potential Clinical Applications and Transplantation. *Journal of Functional Biomaterials*, 12(4), 2021, 68. DOI: 10.3390/jfb12040068.

22. Armin Mooranian, **Corina Mihaela Ionescu**, Daniel Walker, Melissa Jones, Susbin Raj Wagle, Bozica Kovacevic, Jacqueline Chester, Thomas Foster, Edan Johnston, Jafri Kuthubutheen, Daniel Brown, Marcus D. Atlas, Momir Mikov, *Hani Al-Salami – Single-Cellular Biological Effects of Cholesterol-Catabolic Bile Acid-Based Nano/Micro Capsules as Anti-Inflammatory Cell Protective Systems. *Biomolecules*, 12(1), 2022, 73. DOI: 10.3390/biom12010073

23. Armin Mooranian, **Corina Mihaela Ionescu**, Susbin Raj Wagle, Bozica Kovacevic, Daniel Walker, Melissa Jones, Jacqueline Chester, Thomas Foster, Edan Johnston, Sanja Kojic, Goran Stojanovic, Momir Mikov, *Hani Al-Salmi – Taurine Grafted Micro-Implants Improved Functions without Direct Dependency between Interleukin-6 and the Bile Acid Lithocholic Acid in Plasma. *Biomedicines*, 10(1), 2022, 111. DOI: 10.3390/biomedicines10010111

24. Melissa Jones, **Corina Mihalea Ionescu**, Daniel Walker, Susbin Raj Wagle, Bozica Kovacevic, Jacqueline Chester, Thomas Foster, Edan Johnston, Jafri Kuthubutheen, Daniel Walker, Marcus D. Atlas, Momir Mikov, *Armin Mooranian, *Hani Al-Salami – Biguanide Pharmaceutical Formulations and the Applications of Bile Acid-Based Nano Delivery in Chronic Medical Conditions. *International Journal of Molecular Sciences*, 23(2), 2022, 836. DOI: 10.3390/ijms23020836

25. Armin Mooranian, Melissa Jones, Daniel Walker, **Corina Mihaela Ionescu**, Susbin Raj Wagle, Bozica Kovacevic, Jacqueline Chester, Thomas Foster, Edan

Johnston, Jafri Kuthubutheen, Daniel Brown, Marcus D. Atlas, Momir Mikov, *Hani Al-Salami – Pharmacological Dose-Effect Profiles of Various Concentrations of Humanised Primary Bile Acid in Encapsulated Cells. *Nanomaterials*, 12(4), 2022, 647. DOI: 10.3390/nano12040647

26. Bozica Kovacevic, Melissa Jones, **Corina Ionescu**, Daniel Walker, Susbin Wagle, Jacqueline Chester, Thomas Foster, Daniel Brown, Momir Mikov, *Armin Mooranian, *Hani Al-Salami – The emerging role of bile acids as critical components in nanotechnology and bioengineering: Pharmacology, formulation optimizers and hydrogel-biomaterial applications. *Biomaterials*, Volume 283, 2022, 121459 DOI: 10.1016/j.biomaterials.2022.121459

27. Bozica Kovacevic, **Corina Mihaela Ionescu**, Melissa Jones, Susbin Raj Wagle, Michael Lewkowicz, Maja Danic, Momir Mikov, *Armin Mooranian, *Hani Al-Salami – The Effect of Deoxycholic Acid on Chitosan-Enabled Matrices for Tissue Scaffolding and Injectable Nanogels. *Gels*, 8(6), 2022, 358. DOI: 10.3390/gels8060358

28. Armin Mooranian, Jacqueline Chester, Edan Johnston, **Corina Mihaela Ionescu**, Daniel Walker, Melissa Jones, Susbin Raj Wagle, Bozica Kovacevic, Thomas Foster, Momir Mikov, *Hani Al-Salami – Reduced Cytokine Tumour Necrosis Factor by Pharmacological Intervention in a Preclinical Study. *Biomolecules*, 12(7), 2022, 877. DOI: 10.3390/biom12070877

29. Kovacevic, B, Wagle, SR, **Ionescu, CM**, Jones, M, Lewkowicz, M, Wong, EY, Kojic, S, Stojanovic, G, Danic, M, Mikov, M, Mooranian, *A, Al-Salami, H – Novel hydrogel comprising non-ionic copolymer with various concentrations of pharmacologically active bile acids for cellular injectable gel. *Colloids and Surfaces B-Biointerfaces*, 222, 113014, 2023. DOI: 10.1016/j.colsurfb.2022.113014

30. Armin Mooranian, **Corina Mihaela Ionescu**, Susbin Raj Wagle, Bozica Kovacevic, Daniel Walker, Melissa Jones, Jacqueline Chester, Edan Johnston, Momir Mikov, Karmen Stankov, Magdy Elnashar, *Hani Al-Salami – Low-dose

nano-gel incorporated with bile acids enhanced pharmacology of surgical implants. *Therapeutic Delivery*, Volume 14, No. 1, 2023. DOI: 10.4155/tde-2022-0037

31. Jones, M, Kovacevic, B, **Ionescu, CM**, Wagle, SR, Quintas, C, Wong, EYM, Mikov, M, Mooranian, A, *Al-Salami, H – The applications of targeted delivery for gene therapies in hearing loss. *Journal of Drug Targeting*, 31(06), 2023. DOI: 10.1080/1061186X.2023.2216900

32. Wagle, SR, **Ionescu, CM**, Kovacevic, B, Jones, M, Foster, T, Lim, P, Lewkowicz, M, Danic, M, Mikov, M, Mooranian, A, *Al-Salami, H – Pharmaceutical characterization of probucol bile acid-lithocholic acid nanoparticles to prevent chronic hearing related and similar cellular oxidative stress pathologies. *Nanomedicine*, 18(12), 923-940, 2023. DOI: 10.2217/nnm-2023-0092

33. Kovacevic, B, Wagle, SR, **Ionescu, CM**, Foster, T, Danic, M, Mikov, M, Mooranian, A, *Al-Salami, H – The biocompatibility and the metabolic impact of thermoresponsive, bile acid-based nanogels on auditory and macrophage cell lines. *European Journal of Pharmaceutics and Biopharmaceutics*, 190, 248-257, 2023. DOI: 10.1016/j.ejpb.2023.08.003

34. Thomas Foster, Michael Lewkowicz, Christina Quintas, **Corina Mihaela Ionescu**, Melissa Jones, Susbin Raj Wagle, Bozica Kovacevic, Elaine Y. M. Wong, *Armin Mooranian, *Hani Al-Salami – Novel Nanoencapsulation Technology and its Potential Role in Bile Acid-Based Targeted Gene Delivery to the Inner Ear. *Small*, Volume 19, Issue 8, 2022, 2204986. DOI: 10.1002/smll.202204986

35. Bozica Kovacevic, **Corina Mihaela Ionescu**, Susbin Raj Wagle, Melissa Jones, Michael Lewkowicz, Elaine Y.M. Wong, Maja Đanić, Momir Mikov, *Armin Mooranian, *Hani Al-Salami – Impact of Novel Teflon-DCA Nanogel Matrix on Cellular Bioactivity. *Journal of Pharmaceutical Sciences*, Volume 112, Issue 3, 2023, Page 700-707. DOI: 10.1016/j.xphs.2022.09.008

36. Lewkowicz, M, Jones, M, Kovacevic B, **Ionescu, CM**, Wagle, S, Foster, T, Mikov, M, Mooranian, A, *Al-Salami, H - Potentials and limitations of pharmaceutical

and pharmacological applications of bile acids in hearing loss treatment. *Therapeutic Delivery*, 13(10) 2023. DOI: 10.4155/tde-2022-0033

37. Thomas Foster, **Corina Mihaela Ionescu**, Melissa Jones, Susbin Raj Wagle, Bozica Kovacevic, Patrick Lim, *Armin Mooranian & *Hani Al-Salami – Poly-L-lysine as a crosslinker in bile acid and alginate nanoaggregates for gene delivery in auditory cells. *Nanomedicine*, Volume 18, No. 19, 2023. DOI: 10.2217/nnm-2023-0152

38. Bozica Kovacevic, Melissa Jones, Susbin Raj Wagle, **Corina Mihaela Ionescu**, Thomas Foster, Maja Đanić, Momir Mikov, *Armin Mooranian & *Hani Al-Salami – Influence of poly-L-ornithine-bile acid nano hydrogels on cellular bioactivity and potential pharmacological applications. *Therapeutic Delivery*, Volume 14, No. 8, 2023. DOI: 10.4155/tde-2023-0034

39. Kovacevic, B, **Ionescu, CM**, Jones, M, Wagle, SR, Foster, T, Lewkowicz, M, Wong, EYM, Danic, M, Mikov, M, Mooranian, A, *Al-Salami, H – Novel polysaccharides-bile acid-cyclodextrin gel systems and effects on cellular viability and bioenergetic parameters. *Therapeutic Delivery*, 15(2), 2024. DOI: 10.4155/tde-2023-0063

40. Kovacevic, B, Jones, M, Wagle, SR, **Ionescu, CM**, Foster, T, Danic, M, Mikov, M, Mooranian, A, *Al-Salami, H – The effect of deoxycholic acid-based hydrogels on hepatic, muscle and pancreatic beta cells. *Therapeutic Delivery*, 15(1), 41-45, 2024. DOI10.4155/tde-2023-0054

41. Foster, T, Lim, P, Kovacevic, B, Wagle, SR, Ionescu, CM, Mooranian, A, *Al-Salami, H - Effect of ursodiol on alginate/PLL nanoparticles with non-ionic surfactant for gene delivery. *Journal of Nanoparticle Research*, 26(3), 39, 2024. DOI: 10.1007/s11051-024-05939-y

42. Wagle, SR, Kovacevic, B, Ionescu, CM, Foster, T, Jones, M, Mikov, M, Wise, A, Mooranian, A, *Al-Salami, H – Probucol-bile acid based nanoparticles protect

auditory cells from oxidative stress: an in vitro study. *Therapeutic Delivery*, 15(4), 2024. DOI: 10.4155/tde-2023-0099

*Equal Corresponding Author(s)

List of Conference Presentations

The Chapter information, including candidacy, has formed the basis of the following three conference poster presentations.

Poster and Rapid Fire Presentation

Ionescu C.M., Mooranian A., and Al-Salami H. Self-Assembled β-Cyclodextrin – Bile Acid Based Microparticles for Targeted Drug Delivery. *Drug Delivery Australia*, December 2023.

Online Poster Presentation

Ionescu C.M., Kovacevic B., Walker D., Wagle S.R., Jones M., Oluyede F., Mooranaian A., Brown D., *Al-Salami H. Spray Dried Probucol/Bile Acid Particle for Trans-Tympanic Delivery. *International Conference on Medical and Biological Engineering, CMBEBIH*, Bosnia and Herzegovina, April 2021.

Ionescu C.M., Kovacevic B., Walker D., Wagle S.R., Jones M., Oluyede F., Mooranaian A., Brown D., *Al-Salami H. Inner Ear Drug-Delivery of Probucol and Bile Acid for Inflammation Relief: Study Design and Limitations. *Drug Delivery Australia*, Australia, November 2020.

Chapter 1

General Introduction

Drug delivery is limited by the solubility and absorption of the active pharmaceutical ingredient (API) impairing around 40% of drugs and more than 90% newly discovered molecules application (1). Such drugs and molecules benefit from inclusion into polymer and polysaccharide-based formulations to increase drug-water miscibility, optimise delivery release and drug targeting to tissues.

1.1. Probucol

Probucol (4,4'-(isopropylidenedithio)bis(2,6-di-tert-butylphenol), biphenabid or Lorelco) is a known antioxidant with historic use as a hypolipidemic drug with limited commercial availability to some countries (*e.g.* China, Japan). *In vivo*, probucol has a half-life of 12-500 hours (2) and is mainly eliminated from the body through faeces, although high concentrations of probucol show affinity to white adipose tissue as well as the brain (3). From a molecular characteristic, probucol is highly lipophilic (octanol-water partition coefficient log P = 8.92) and has a molecular weight of 516.8, basic pKa (10.29) and polar surface area of 40.46 Å^2 (2). With poor water solubility of 5 ng/mL (4), probucol is a class II type drug based on the Biopharmaceutical Classification System (BSC) (5) and in violation of two of *Lipinski's* rules (high molecular with and log P) that limits the molecule's diffusion through lipid membranes (6). Probucol as an API has diverse applications pre-clinically in improving cellular oxidative survival in neurodegeneration (7), diabetes (8) and ischemic (9) models. More recently, our research group reviewed the possible benefits of using probucol delivery in relation to inner ear pathologies (10). For drug delivery, probucol shows better absorption properties by incorporating the drug into formulations obtained from grinding or solid-dry dispersions containing for example polyvinylpyrrolidone (PVP). Since probucol's large crystalline size can affect drug dissolution, reducing its size by either mechanical milling or incorporating the drug in water-soluble polymeric formulations can improve surface-area contact with water (11-14). This process improves the drug's controlled release, dissolution ability, and absorption parameters (5) in solutions in a time-dependent manner (15). There are other methods for obtaining probucol delivery systems based on emulsions (16, 17) or mesoporous

particles, for example increase probucol dissolution, and offer a better antioxidant response in cell culture (18). However, no research has undergone in optimising probucol formulation or explored the antioxidant effects in terms of ototoxicity or hearing loss.

1.2. Ototoxicity and Drug Delivery

Hearing loss caused by ototoxicity refers to a set of environmental, genetic, medication, age-associated or a combinatory effect of factors linked to an increased oxidative stress response in the inner ear, notably within the mechanosensory epithelium and neurons. Combating ototoxicity requires strategies to limit exposure, monitor hearing loss and improve delivery by developing and selecting better therapeutic candidates (19-21). Common ototoxic medications include antibiotics (aminoglycosides such as gentamicin and kanamycin), and chemotherapeutic agents (*e.g.,* cisplatin) (22). Research has focused on discovery and delivery of therapeutic treatments to combat ototoxicity using an array of molecules, predominantly antioxidants (23, 24). There are few clinical trials testing Food and Drug Administration (FDA) approved drugs (antioxidants, statins, antihistamine-like blockers) and new synthetic molecules (25). Dexamethasone for example, is a lipophilic statin (log P = 1.93) (2) researched against an array of hearing loss causes, limited by systemic administration including reduced blood-labyrinth-barrier (BLB) permeability and increased occurrence of side effects (26). The preferred administration route of the drug involves a more invasive approach through trans-tympanic delivery, this allows for a higher drug concentration bolus applied and in direct contact with the inner ear. Dexamethasone incorporation into formulations improves delivery outcomes (27). Dexamethasone's crystalline size is also a limiting determinator in permeability (< 500 nm) (28), however it allows for prolonged drug attachment to the round window membrane and to slowly permeate for hours (29). The additional use of a lipophilic compound together with dexamethasone improves drug retention on the round window membrane (30). Toxicity experiments done on model inner ear-derived cells positively respond to dexamethasone by showing a reduction of cisplatin-induced apoptosis (31) and reactive oxygen species (ROS) production (30). Although dexamethasone's lipophilicity is lower than probucol, it will be referred to as a model for permeation prediction within this study.

1.3. Bile Acids as Excipients

As part of our previous research group findings, bile acids used as excipients stabilise probucol formulations using the Ionic Gelation Vibrational Jet Flow technique (3, 32, 33). Bile acids are hydrolysed steroid structures produced from cholesterol in the liver to aid digestion by promoting fat emulsification and absorption. Bile acids have several transporters in various tissues including the blood-brain-barrier (BBB) that facilitate bile acid transport (34, 35). There are few FDA-approved uses for bile acids limited to chenodeoxycholic acid (CDCA) (36) cholic acid (CA) (37) and ursodeoxycholic acid (UDCA) (38). The amphipathic properties depend on the hydroxyl groups of each bile acid structure and determines micelle self-assembly or supramolecular aggregates assembly (39). As formulation excipients, bile acid can stabilise mixed micelles, lipid particles (40, 41), polymer nanoparticles (42, 43), metal nanoparticles (44) emulsions (45) and improve drug uptake and sustain drug release pattern (46). The bile acid's low anionic surfactant effects (log $P > 3.5$) can stabilise colloidal suspensions by increasing the zeta potential of the polymer-molecule interaction within solutions (47). As for permeability, bile micelles or salts can improve drug targeted delivery by enhancing permeability though cellular membranes. Reversible and concentration-dependent tissue permeation can have negative effects on cellular viability (48), however both UDCA and taurocholic acid (TCA) show protective effects against intestinal permeation (49) and protect the blood-retinal-barrier from damage (50). Results from various permeation models including the BBB, intestine, and colorectal cells indicate that some bile acids such as deoxycholic acid (DCA) (51-54), CDCA (54-56), CA and TCA (48) selectively increase paracellular influx attributed by modulating tight junction proteins.

1.4. Ototoxicity Models

Both *in vitro* and *in vivo* models offer information for drug applications and tolerable dosing levels. *In vivo* ototoxicity affects firstly the outer hair cells of the cochlear basal turn progressively damaging the apical region as well. The application of antioxidants helps by reducing induced cellular stress. *In vivo* models offer important information on the permeation of molecules, and the drug accumulation pattern in perilymph (base to apical gradient) as well as hearing threshold data. Rats and guinea pigs are more susceptible than mice to ototoxic drugs, therefore the use of mice explants might be better suited for screening purposes (57). However, *ex vivo* pig

round window membrane explants are more relevant to simulate permeation patters as they resembles the human round window membrane histology (58). An initial formulation screening can be conducted *in vitro* on mouse auditory cell line House Ear Institute-Organ of Corti 1 (HEI-OC1) that are sensitive for ototoxic applications as well (59). As many drugs require solvents such as dimethyl sulfoxide (DMSO) for direct applications, the HEI-OC1 and in general inner ear cells can be affected by DMSO (60), and < 0.5% DMSO is shown to affect explants hair cell survival (61) further emphasising the need to incorporate drugs such as probucol into formulations rather than direct solvent dilutions.

1.4.1. Systemic *versus* Local Delivery

Systemic delivery requires drug trafficking across the BLB that can be modulated by changes in blood flow or, for example, by application of histamine (62), inflammation (63), mannitol (64), sound conditioning (65), noise-exposure (66), diuretics (67). However, the more invasive local delivery through trans-tympanic injections to the middle ear minimises systemic side effects and improves steroid drug entry to the inner ear perilymph and endolymph (68) represent the salvage therapy for sensorineural hearing loss (26, 69). The round window membrane remains the entry point to the inner ear; it comprises of three layers and is 40-70 μm in thickness (70). With selective permeability to molecules and more importantly to nanoparticles depending on their size, charge and functional moieties (71), the round window membrane represents the preferred entry point for many drug delivery therapies (72). Magnetic or biodegradable nanoparticle formulations, hydrogels and polymer formulations can be used to improve round window permeability (73). Prolonged repetitive exposure can induce local inflammation, thickening of the round window and highlight the need for prolonged drug release strategies rather than multiple dose applications. Drug entry to the inner ear following trans-tympanic applications depends on the rate of drug passage though the round window membrane and rate of clearance into the nasopharynx through the Eustachian tube (74). Therefore, ensuring drug contact with the round window membrane during animal studies and clinical settings is essential. This can be achieved by simply resting the head on one side for at least 30 minutes (71). Drug entry is not uniform and complete; there is a stronger gradient at the base of the round window and is dictated in part by a molecule's characteristics. Therefore, increased drug contact with the round window membrane

or sustained release is more favourable for trans-tympanic delivery and to decrease ototoxicity.

1.4.2. Round Window Membrane Permeability

Lipophilic (log *P* >5) molecules can pass through cellular membranes by diffusion, with less lipophilic compounds such as fluoresceine, gentamicin, dexamethasone phosphate pass faster through an artificial round window membrane (70). The more hydrophobic compounds such as dexamethasone increase inner ear drug entry by hours (28) or days (75) when applied to the round window in a simple formulation. Round window modulation by reducing tight junction (76) with chitosan (77), sonoporation (78, 79) or microneedles (80, 81) could increase lipophilic drug entry to the inner ear. Besides lipophilicity the formulation type, particle surface charge measured through zeta potential can greatly influence permeation as well. For example, cationic-polymer and neutral particles (~200 nm) pass through mucus layers resembling the round window membrane, however the neutral and cationic particles accumulate more in hearing representative cells (82). Highly cationic particles are not entirely safe as these particles interact with cell membranes and are readily internalised showing higher toxicity compared to anionic particles (26). Generally, the particle size is crucial for cellular entry and uptake can be facilitated by micropinocytosis (0.2-10 μm) and caveolin mediated endocytosis uptake (83). In order for particles to diffuse or actively pass through the round window membrane, researchers have characterised that particles ranging from 10-300 nm (84) or ~ 500 nm (28) are ideal to minimise toxicity.

1.4.3. Drug Lipophilicity and Diffusion

Irrespective of formulation preparation time, the drug lipophilicity in combination with hydrophilic polymers show a slower release pattern compared to more hydrophilic compounds (85). Lipophilicity comes with advantage in sustained release from polymeric matrix, and the degradation of matrix is dependent on the drug p*K*a. For example, slower degradation is observed for basic p*K*a hydrophobic drug combinations (86). Although advantageous, lipophilicity influences a drug's ability to permeate and diffuse through membranes and could limit therapeutic dosing. Lipinski's rule of 5 in an important element to screen drug membrane permeability especially for oral administrated drugs. Better permeability refers to molecules that

have less than 500 molecular weight, no more than 5 hydrogen bond donors, no more than 10 hydrogen bond acceptors and less than 5 log *P* octanol-water partition coefficient (6). However, probucol violates two of these rules that restrict oral absorption into the blood stream. Consequently, if systemic delivery relies on BLB entry, probucol's applicability and efficiency may be limited. It is important to note that there is a discrepancy in the literature regarding log *P* values and blood-barrier permeability, which is better discussed in the context of BBB permeability (87). With this rationale, targeted delivery to the middle ear through trans-tympanic injections may improve drug absorption by localising drug entry. This also applies for dexamethasone by improving absorption to the inner ear as well as minimising systemic side effects. Additionally, dexamethasone ionisation to dexamethasone phosphate further improves absorption and permeation by decreasing the drug's lipophilicity (by 0.3-7.87 log *P* units (88)) albeit with an increase in the molecular weight. This approach is turn may be better suited for smaller molecular weight molecules rather than probucol or dexamethasone. Generally, among lipophilicity, polar surface area is predictive of passive absorption (89, 90) and should be considered for tissue permeation as well (29). Compared with the less lipophilic dexamethasone (94.83 $Å^2$) or dexamethasone phosphate (147.02 $Å^2$) (2), probucol's polar surface area (40.46 $Å^2$) is lower than the predicted value for oral (<120 $Å^2$) and BBB (<80 $Å^2$) permeation (91, 92). Given its molecular characteristics and well-documented antioxidant effects, probucol emerges as a strong candidate for testing its efficacy within the inner ear.

1.5. Thesis Overview

This thesis collection is comprised of published, under review and accepted with revisions results collected through the PhD program.

The overarching structure is based on the rationale for optimising probucol formulations for preventing cytotoxicity *in vitro.* The drug release patterns from formulations are studied and presented using two different methods (spray dried and gel formulations). Optimising probucol particle size (supramolecular aggregates) represents a crucial aspect for reaching permeability thresholds for future *in vivo* studies. The use of bile acids as excipients into formulations is assessed as well and differences in probucol dissolution are evaluated.

1.6. Hypothesis

Probucol formulations are suitable for drug delivery for an *in vitro* ototoxicity model, and formulation stability can be modulated with the addition of bile acids as excipients.

Aims

- Develop and characterise probucol formulations that are compatible with *in vitro* HEI-OC1 cells.
- Develop probucol formulations that promote *in vitro* HEI-OC1 cell survival against cytotoxic stressors (cisplatin, H_2O_2).
- Determine bile acids as excipients and their modulatory effects on formulation stability.
- Develop nanoparticles based on probucol that can be used as formulations.
- Assess bile acids and their limitations in the inner ear (review).

Significance

- Provide evidence for a new antioxidant as probucol in relation to otic therapy.
- Formulate probucol stable water-based formulations.
- Expand the use of bile acids for probucol formulations (CA, DCA, CDCA, UDCA, TCA and lithocholic acid (LCA)).
- Proof of concept for cyclodextrin-probucol inclusion formation and how bile acids impact particle self-assembly.
- Understand the use and drawbacks of bile acids in the inner ear (review).

Limitations

This thesis acknowledges certain limitations. Firstly, investigations on probucol's *in vitro* and *in vivo* permeability are lacking posing areas for future research. Secondly, the absence of testing probucol powder *in vitro*. This arises from probucol's tendency to remain trapped on the surface tension barrier in culture media, limiting exposure to the adhered cells layer.

1.7. Chapter Overview

Chapter 2 discusses bile acids therapeutic potential to the organ of Corti and is comprising of two publications. The first part of the Chapter covers bile acids targets that are common to the inner ear tissues and how the different bile acid might interfere

with hearing function through active interaction with proteins, improving cell viability or modulating microRNAs. In the second half of the chapter, bile acid pool imbalance is discussed in terms of the possible negative effects it may hold on hearing loss through cholesterol levels and lipoproteins, or BBB disturbance.

Chapter 3 investigates the use of the bile acid UDCA on probucol particle formation and drug availability and activity on HEI-OC1 treated with cisplatin cells. To facilitate probucol *in vitro* applications, a mixture of polymers and polysaccharides together with UDCA are presented as spray dried solid dispersions and characterised. The use of UDCA improved probucol solubilisation and solid dispersion probucol content as well as increased probucol dissolution. *In vitro*, the solid dispersions probucol-UDCA increased cellular viability under cisplatin-induced stress and significantly reduced associated cellular ROS accumulation over a 24 hour period.

Chapter 4 assesses the probucol's stability in formulation with DCA and chitosan for film formation, swelling, drug content, degradation and dissolution as well as *in vitro* assessment on HEI-OC1 and macrophage RAW 246.7 cells viability and cytokine production. DCA improved chitosan film water absorption (swelling), degradation properties and improved probucol incorporation within the film matrix. Probucol and DCA film formulations are compatible with both cell lines in terms of viability after three days. HEI-OC1 cells treated with probucol films showed minimal improvement in viability compared to cisplatin-treated cells without probucol. However, DCA films slightly improved macrophage viability challenged by cisplatin and enhanced cytokine production.

Chapter 5 presents a method for probucol loaded particles consisting of bile acids and cyclodextrin inclusion complexes. Bile acid concentration and cyclodextrin type (alpha-, beta-cyclodextrin; α- β-CD) are important for determining particle formation. The chapter further explores α-CD and β-CD bile-probucol particle effect on HEI-OC1 cells, showing that CA-, DCA-, LCA- and to some extent DCA-probucol particles are better tolerated. The use of β-CD bile-probucol outperforms α-CD in terms of particle formation and particle drug content, however, show minimal impact under induced cellular oxidative stress conditions (H_2O_2) for HEI-OC1.

Chapter 2

Literature Review

Bile acids and the organ of Corti Targets

2.1. Publications

1. **Corina M. Ionescu,** Melissa A. Jones, Susbin R. Wagle, Bozica Kovacevic, Thomas Foster, Momir Mikov, Armin Mooranian and Hani Al-Salami - Bile Acid Application in Cell-Targeting for Molecular Receptors in Relation to Hearing: A Comprehensive Review. *Current Drug Targets*, Volume 25, Issue 3, 2024, Page 158 – 170. DOI:10.2174/0113894501278292231223035733

**Graphical Abstract Retrieved from Publication 1.*

2. The work in this chapter is developed for publication as:

Corina M. Ionescu, Melissa A. Jones, Susbin R. Wagle, Bozica Kovacevic, Thomas Foster, Momir Mikov, Armin Mooranian and Hani Al-Salami – Could Bile Acids Modulate Hearing Loss?

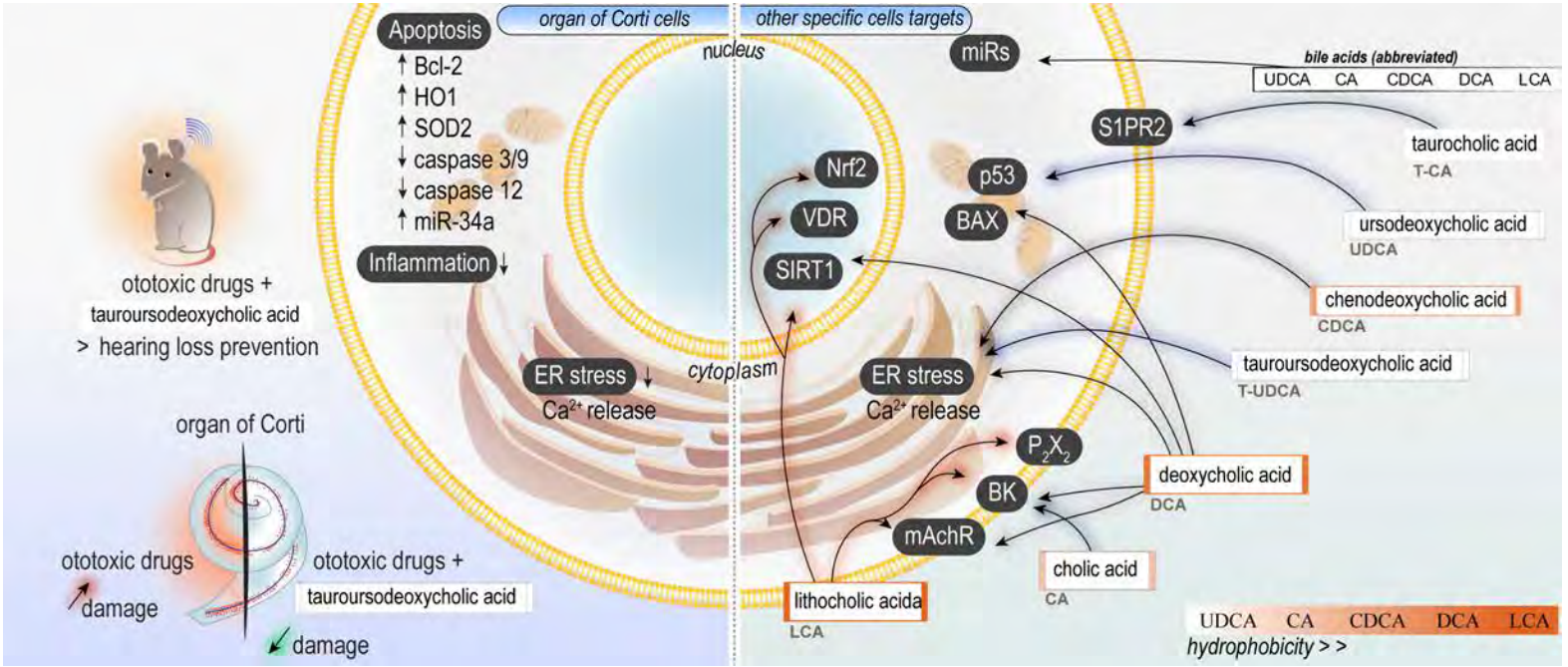

*Graphical abstract 1. Bile acids and the inner ear targets.

Left panel: Tauroursodeoxycholic acid is a hydrophilic bile acid applied *in vitro* and *in vivo* for hearing loss research by preventing organ of Corti cellular apoptosis, reducing inflammation markers and relives endoplasmic reticulum (ER) stress. In ototoxic-challenged mice, it improves hearing thresholds and prevents organ of Corti damage (red shading). Right panel: Bile acids present in the human body and their molecular targets as documented in the literature. The represented molecular targets are also expressed in the auditory system, although the extended effects of bile acids are unknown regarding the organ of Corti. Abbreviations: endoplasmic reticulum, ER; lithocholic acid, LCA; cholic acid, CA; deoxycholic acid, DCA; tauroursodeoxycholic acid, T-UDCA; chenodeoxycholic acid, CDCA; ursodeoxycholic acid, UDCA. Bottom left corner, bile acid classification from most hydrophilic (UDCA) to most hydrophobic (LCA).

2.2. Introduction

Based on PubMed searches (93) there are less than ten research papers on the importance of tauroursodeoxycholic acid (T-UDCA) for preventing drug-induced hearing loss. T-UDCA is mostly preferred for its low toxicity, and that it protects the endoplasmic reticulum (ER) under ototoxic stress. The chapter presents a literature collection of both primary (CA, CDCA) and secondary (LCA, DCA, UDCA) bile acids. The effects captured in more than 27 *in vitro* and *in vivo* models of various tissues are presented in relation to few common targets found within the inner ear structure. If fully explored, LCA and TCA, respectively, could be strong candidates for targeted drug delivery against hearing damage. To note that out of all the bile acids and the effects retrieved for these publications, DCA appears to negatively modulate cells and tissues the most, while UDCA can reverse the tumour-induced effects caused by DCA. Key contributors to these effects include the variation in concentrations applied to the cells (LCA ~3-45 μM, DCA ~100-1000 μM) within the context of the specific models exposed and the necessary dosing requirements, which will be later discussed. The topic of bile acid pool dysfunction in relation to liver pathologies, cognition decline, and cholesterol metabolism are debatable, with no resources on the effects on hearing function. This could be better explored in terms of how bile acids and bile pool changes affect blood-barriers. There is limited information on the BLB, although similar in structure and function with the BBB and blood-retinal-barrier. An increase in hydrophobic bile acids (DCA, LCA, CDCA) have potential modularity effects on blood-barrier permeability by disruption of tight junction proteins and increasing permeability.

2.3. Summary

T-UDCA and UDCA applied *in vitro* or *in vitro* have previously been used as treatments to prevent ER stress, reduce apoptosis, restore antioxidant protein expression or lower auditory brain stem response thresholds that are disturbed by gentamicin and cisplatin. Some bile acid targets expressed within the hearing epithelium or associated tissue are important for structural integrity and modulate hearing function, however they are not studied in relation to bile acid treatment or targeting. Although the unconjugated UDCA may protect cells and tissues, including blood-retinal barrier integrity, DCA and CDCA can increase blood-barrier

permeability and interact with cholesterol microdomains. The dual nature of bile acids, and bile acid imbalance requires further attention in relation to hearing and in the inner ear. Therefore, understanding the literature on bile acids and their effects of these targets serves as guide for the selection of bile acid formulations prepared and discussed in the later chapters. To fully consider bile acids and their effects to the inner ear, data on permeability through the round window membrane and BLB is crucial. Appendix VI contain simulated predictions of bile acids permeation through the round window membrane.

Publication 1

Abstract

Bile acids play important roles in lipid and glucose metabolism, signalling and aid in digestion. Changes associated with production and ratios can be used as markers for various liver pathologies. In addition to their functional effects in modulating inflammatory responses and cellular survivability, the unconjugated or conjugated, secondary or primary nature of bile acids accounts for their various ligand effects.

The common hydrophilic bile acids have been used successfully as local treatment to resolve drug-induced cell damage or to ameliorate hearing loss. From various literature references, bile acids show concentration and tissue-dependent effects. Some hydrophobic bile acids act as ligands modulating vitamin D receptor, muscarinic receptors and calcium-activated potassium channels, proteins that are important and present in the inner ear system.

Currently there are limited resources investigating the therapeutic effects of bile acid on hearing loss, little to no information on detecting bile acids in the peripheral ear system. This review focuses both on hydrophilic and hydrophobic human bile acids along with their tissue-specific effects in modulating cellular integrity thus bringing in consideration the possible effects and extended therapeutic applicability of bile acids to the inner ear tissue.

Key words: cochlea, bile acids, bile acid receptors, hearing loss, micro RNAs, cellular stress

2.4.1. Introduction

The recent concept of bile acids and their implication in hearing impairment is gaining practical interest. Bile acids are well characterized in the metabolic field, with surprising benefits shown in the field of neuroscience. There are few descriptive reports of the effects bile acid hold in reducing apoptosis during ototoxic insults, however these studies lack in understanding the mechanisms that confer protective effects and refer only to a limited set of bile acids (94, 95). There are even fewer mentions that identify bile acids in the ear system. One paper found that bile acids form up to 32% of children's middle ear otitis media secretions (96). The finding correlates the possible presence of bile acids in the middle ear by oesophageal refluxes. Trans-tympanic application of CDCA reveals a small degree of middle ear inflammation, with noticeable metaplasia of epithelial cells towards gland-like structural cells in both CDCA and pepsin tested groups (97). To our knowledge, there are no direct correlations of bile acid levels in the inner ear. One main disadvantage in investigating bile acid levels would be limited by cochlear tissue and fluid (perilymph) analytical optimisation.

T-UDCA is one of the most hydrophilic bile acids researched for its protective effects *in vivo* and *in vitro* on neurodegenerative and ocular disorders (98), as well as ischemia (99). T-UDCA has been reported in improving neuron survival, acting as a Ca^{2+} agonist, reducing endoplasmic reticulum (ER) stress and maintaining ER homeostasis, decreasing apoptosis markers (tumour protein p53, caspase 3, caspase 12, cytochrome C), blocking ROS, and modulating cellular pathways (100). There are few mentions showing the potential of bile acid as treatment in preventing organ of Corti trauma, oxidative stress, and noise-induced hearing loss in various models (**table 2.1**). For example, a *Cdh23*$^{erl/erl}$ deficient murine model for progressive hearing loss shows that T-UDCA reduced apoptosis and hearing thresholds in the first weeks of hearing loss onset compared with control deficient mice (101). Cisplatin-treated rats present high hearing loss thresholds, low heme oxygenase 1 (HO1) and superoxide dismutase 2 (SOD2) protein expression, and increased hair cell apoptosis, effects that are reversed by T-UDCA administration concomitantly with cisplatin (94). Cisplatin and aminoglycosides interfere with cochlear ER function leading to ER stress-dependent apoptosis, however T-UDCA reverses cisplatin's effect (95, 102). Against gentamicin, T-UDCA-treated murine auditory cell line (HEI-OC1) and organ of Corti explants show increased anti-apoptotic B cell lymphoma-2 (Bcl-2) expression and suppressed

ER stress (103). Therefore, the remainder of the review reports literature mentions of bile acid cellular implications with the goal of demonstrating the importance on researching bile acid in the context of hearing function and disease (**figure 2.1**). Bile acids are natural modulators of some important membrane and nuclear receptors. Not all bile acid receptors have been previously described in the inner ear system. We bring forth possible cochlear tissue receptor targets and gene expression modulators that might be suitable candidates for bile acid drug targeting and would require further research to establish a broader therapeutic potential against progressive hearing loss.

2.4.2. Hydrophobic Bile Acids and the Activity on BK channels

The large Ca^{2+}-activated K^+ (BK) channel is a membrane protein expressed in multiple tissues, with important cochlear signalling roles in excitable and non-excitable cells (104). It consists of subunits forming pores or with roles in voltage- and calcium-sensing. The β_1 subunit is shown to increase blood flow in neuronal tissue and its activity can be modulated by LCA and glycine-conjugated DCA (G-DCA) at low concentrations (105, 106). The BK channel is expressed in the auditory hair cell membrane, spiral ganglions and stria vascularis (107). Deletion of the BKα subunit is linked to mild progressive hearing loss and presbycusis (108). BK channel activation might be promoting pericyte disassociation from endothelial cells as seen in an age-related hearing loss mouse model (109). Furthermore, channel expression levels vary with age in the auditory midbrain region responsible for sound processing (110). Experiments done on chick spiral ganglion and sensory auditory cells show that apoA-I binds to, and inhibits BK channels hyperpolarization and tuning activity (111). Evidence on cisplatin-induced apoptosis shows that the ototoxic effects follow BK channel activation in spiral ligament fibrocytes (112). Furthermore, β-CD can disrupt cholesterol microdomains that are important in regulating BK voltage-gated channels (113). More importantly bile acids could potentially act in the same manner when used at detergent concentrations or lower (later discussed in Chapter 2.5.4). Dopico et al. (2002) found that bile acids can increase BK channel activity dependent on the plane polarity and critical micellar concentration (LCA > DCA > cholic acid (CA); **table 2.2**) (114).

2.4.3. Vitamin D Receptor and the SIRT1/Nrf2 Pathway in Relation to Bile Acids

LCA is a bile acid with antagonistic action on the nuclear vitamin D receptor (VDR), an important receptor affecting cellular antioxidant responses, modulating apoptosis, maintaining and regulating of calcium uptake and reabsorption in the intestinal epithelium (115). Silent information regulator transcript-1 (SIRT1) is a transcription factor that can modulate VDR and is implicated in activating oxidative stress and inflammation and is responsible for the release of nuclear factor erythroid 2-related factor (Nrf2). Nrf2 acts as an oxidant sensor and can translocate from the cytoplasm to the nucleus to target upregulation antioxidant defence genes (*e.g.* SOD, HO-1). Small intestinal enterocytes exposed to tumour necrosis factor alpha (TNF-α) leads to mucosal barrier dysfunction, in part protected through VDR activation by LCA *via* upregulation of SIRT1, Nrf2 and HO-1 (116). LCA promotes *Cyp24a1* expression in the ileum similar to the active vitamin D (calcifediol) yet does not lead to Ca^{2+} accumulation in VDR knocked-out mice (117). In the inner ear, vitamin D deficiency may be associated with tinnitus (118), and hearing loss in older adults (119). Hypervitaminosis D as well is shown to aggravate age-related hearing loss in a Klotho mouse model (120). Compared to adult wild type mice, VDR adult mutant mice present elevated auditory brainstem responses (ABR), decreased capsase-3 expression, and loss of basal spiral ganglions. The authors also reported that VDR is expressed in osteocytes nuclei in the bulla, spiral ganglion, Reissner's membrane cells, auditory hair cells, inner sulcus, and the cytoplasm of some spiral ligament fibrocytes and stria vascularis in the cochlea tissue (121).

2.4.4. Lithocholic Acid as Purinergic Receptors Modulator

Ion-ligand receptors (P2X) and G-protein-coupled receptors (P2Y) are purinergic membrane receptors regulated by compounds including fatty acids, cholesterol and neurosteroids expressed in various tissues including the cochlea (122). Both P2X and P2Y receptors are sensitive to nucleotides, such as adenosine triphosphate (ATP) and are implicated in cochlear micromechanics (123), influencing BBB blood flow (124), regulating sound transduction and modulating inner ear gap junctions, perilymph and intracellular Ca^{2+}, Na^{+} and K^{+} levels (125). P2X is present in excitable cells, as well as brain endothelial cells and pericytes, with protein ultrastructural localization showing deposits at the cytoplasmic levels and mitochondrial outer membrane (126). In the organ of Corti, $P2X_2$ is found on the endolymphatic membranes of cells, and stereocilia

(124), while $P2X_4$ is detected on endothelial cells and pericytes, providing necessary blood flow following ATP stimulation (127). Overstimulation and mutation of $P2X_2$ leads to noise-related and progressive hearing loss (128). Interestingly enough, LCA and analogues strongly modulate P2X receptors, for example $P2X_2$ is inhibited while $P2X_4$ activity is potentiated (129). Authors reported that 3 μM LCA is sufficient to potentiate $P2X_4$ and inhibit $P2X_2$, while CDCA, DCA and UDCA require a higher dose to act in the same manner as LCA on these receptors. LCA at 10-30 μM can potentiate $P2X_7$; a receptor present predominantly on immune cells known for its pro-inflammatory activity in other tissues (130), and detected at the glial level surrounding spiral ganglion cells in adult mice (131). In a different study $P2X_2$ showed species-specific inhibitory responses for other bile acids; T-LCA, T-hyo-DCA, T-CDCAT-DCA and T-UDCA (132).

2.4.5. Hydrophilic Bile Acids and the Endoplasmic Reticulum Stress Response

UDCA and the conjugated T-UDCA were reported as a highly effective "chemical chaperon" against ER stress. As a response to endoplasmic unfolded or misfolded proteins, chaperon proteins recruitment can activate the unfolded protein response (UPR) and pro-apoptosis protein activation. Aminoglycosides are a class of antibiotics that can cause an increase ER chaperone expression with subsequent loss of hearing function, especially in the outer hair cells of the basal cochlear turn. Mutant mice lacking a gene responsible for UPR activation show gentamicin-induced ER stress protein increases and promotes apoptosis in spiral ganglion cells. These haploinsufficient XBP1 mice lacking the essential transcription function for UPR had an improvement in hearing function after systemic administration of T-UDCA (102). A similar effect has been observed in auditory hair cell cultures and explants treated with T-UDCA which decreased ER stress (103). In a similar manner to aminoglycosides, cisplatin can cause ER stress and hearing loss. Besides hearing loss in mice, authors report a noticeable increase in ER cisplatin-dependent apoptosis marked by high CCAAT-enhancer-binding protein homologous protein (CHOP), chaperone glucose-regulating protein 78 (GRP78), calreticulin and calnexin expression in the stria vascularis and the outer hair cells to which T-UDCA aids in preserving hearing thresholds (95). T-UDCA's ability to attenuate protein aggregation in the presence or absence of cisplatin might be the key factor in restoring cellular ER function during an insult (133). In a different example, T-UDCA effects are due to its

ability to mediate caspase-12 dependent apoptosis (134). Thus providing a possible explanation to T-UDCA's effects against cisplatin-induced intracellular calcium accumulation that hinders Ca^{2+} currents and synaptic vesicle release from hair cells (135). On the other spectrum of bile acid activity, DCA has shown concentration-dependent apoptosis effects (100-200 μM DCA) with intracellular Ca^{2+} increase (<600 μM DCA) in human gastric cancer cells (136). Although in a different cell line 750 μM DCA > CDCA > T-DCA increase intracellular Ca^{2+} (137, 138), with DCA showing effects on membrane hyperpolarisation. DCA as well as CDCA and LCA present negative implication by sustaining ER stress, UPR markers and can induce Golgi fragmentation (139).

2.4.6. Bile Acids Interaction with Muscarinic Acetylcholine Receptor

Research undertaken in resolving cochlear physiology questions in part the intracellular location and function of the five muscarinic acetylcholine receptors (mAchR; M). Literature present $M_{1\text{-}5}$ expression in the organ of Corti, spiral ganglions or in the spiral ligament in young and adult mice. Loss of M_2/M_4 activity may be implicated in high frequency noise resistance (140), possibly by mAchRs inhibition that influences the fusiform cells responsible for integrating cochlear auditory information (141). With unknown effects to the cochlea, DCA and conjugates show strong receptor antagonistic effects, for example, at physiological concentrations, the bile acids are more potent than atropine in inhibiting M_3-mAchR and do not undergo degradation by acetylcholinesterase. In terms of the strongest interaction with muscarinic receptors, T-DCA conjugates are followed in affinity by G-DCA > T-LCA > LCA > DCA > G-LCA. Other than M_3, the human metabolite *S*-lithocholyltaurine shows binding affinity to M_1 while the synthetic lithocholylcholine binds more strongly to M_3 and $M_{1\text{-}2}$ compared to T-LCA alone (142-144). Adding to the effects on mAchR, the interaction between DCA and macrophages hints to a possible cause of colonic inflammation triggered by macrophage polarization as a result of M_2-mAchR upregulation thus leading to TNF-α, interleukin 6 and nitric oxide release (145). This could represent a sensitive path as inflammation and macrophage recruitment can cause detrimental effects on hearing loss (146).

2.4.7. Bile acid and Apoptotic Activity

P53 is a protein modulating cell survival and death-induced by genotoxic insults. In part, increased p53 expression promotes tumour suppression, while reduced p53 activity could strategically represent a way to counteract cochlear cell apoptosis. From an early age-induced hearing loss model, mice exhibit high levels of p53 and SIRT-1 compared to control mice (147, 148). In cell cancer models, UDCA modulated apoptosis by increasing p53 and BAX activity, negatively influencing cellular migration. UDCA is viewed as a chemo-protectant agent in this manner, reversing cancer cell phenotype triggered by another bile acid (DCA) on bile duct and colon cancer cells (149, 150). DCA effects vary by tissue. In cancer cells DCA activates extracellular signal-regulated kinase (ERK) promoting p53 proteasome-degradation reducing p53 protein levels without affecting p53 mRNA expression (151). Alternatively, DCA can affect rat primary hepatocytes and liver tissue alike by increasing p53 levels (152). Considering hearing research, pathways that block p53 appear to protect inner and outer hair cells affected by cisplatin treatment which increased apoptosis by activating p53 *via* ataxia telangiectasia mutated (ATM). Hair cell survival and better hearing thresholds were observed in tumour bearing-cisplatin-treated mice with noted enhanced anti-neoplastic effects from systemically inhibiting p53 (153). Interactions with other proteins for example SIRT1 deacetylates p53 and downregulates protein activity (154). Lastly resveratrol fed mice had SIRT1 upregulation which led to reduced p53 levels in outer hair cells and inner hair cells, with notable decrease of age-related hearing loss (155).

2.4.8. G protein-coupled Receptors and Taurocholic Acid

Part of the transmembrane G protein-coupled receptor family, the sphingosine-1-phosphate receptors promote lipid metabolism, proliferation, cytoskeletal organisation, modulates inflammation, influences angiogenesis and myelinisation. Sphingosine-1-phosphate receptor 2 (S1PR2) represents a subtype highly expressed in various tissues including the liver, cochlea, and vestibule. In terms of the receptor's cochlear localisation, S1PR2 is expressed within inner and outer hair cells, the stria vascularis, spiral ganglion nuclei and spiral ligament fibrocytes. S1PR2 can be activated by sphingosine-1-phosphate and to a certain degree by taurine-conjugated bile acids including T- conjugated CA (TCA), T-UDCA, T-DCA as well as G-CA and G-DCA (156). Human genetic variants affecting the S1PR2 gene are associated with

hearing loss (157). Studies on S1PR2 knocked-out mice reveals ear and vestibule structure alterations, changes in stria vascularis vasculature, and hearing loss. Since a reduced endocochlear potential has been associated with the development of progressive hearing loss in the S1PR2 knock-out model this opens the possibility of targeted delivery with agonists (158). For example, sphingosine-1-phosphate applied against gentamicin can protect hair cell loss. However, in the same study, the positive effects of the agonist are aggravated by the addition of S1PR2 antagonist that further increase cell damage and apoptosis (159). The search and use of new agonists could lead to better outcomes against ototoxicity. In a model for cisplatin-induced ROS accumulation, a synthetic agonist protects and reduces cellular damage both *in vitro* and *in vivo* (160). Neither the use of T-UDCA nor other bile acids have been used in the same context to observe the effects on S1PR2. To note that previous applications of T-UDCA show great potential in protecting against ototoxic hearing loss and neurosensory damage (95, 98), the question remains valid as to what extent bile acid S1PR2 activation can account for otoprotection. Another aspect that requires investigation would be the use of local *versus* systemic application of such agonists. Local delivery implies the use of more invasive strategies to administer drugs to the middle ear. On the other hand, systemic administration is massively restrictive and can require the use of higher drug doses to reach the cochlea and pass through the blood-labyrinth-barrier. Current information about the S1P2 regulatory effects on blood-brain-barrier would require further investigation to understand the receptor importance on the blood-labyrinth-barrier. Considering the S1P2 expression in blood barrier epithelium, research shows that antagonistic targeting of the receptor can reduce oxidative damage associated tight junction disorganisation (161).

2.4.9. MicroRNAs and Hearing Loss

The last portion of the review will focus on bile acids and their influence on non-coding micro ribonucleic acid (miRNA or miR) molecules. Concentration, exposure time and bile acid type are presented from different tissues. These findings are observed in relation of miRs and their effects on hearing loss (**figure 2.2**). In the rat cochlear nucleus brain region a noticeable decrease in miR-199a-5p and SIRT1 increase is associated with exposure to noise (162). As previously discussed, hepatocyte expression of miR-199a-5p acts to preserves ER function after bile acids (DCA) treatment (163). Two very robust research papers on the effect of acidic (a

mixture of bile salts) or neutral (DCA or CDCA) bile on laryngeal mucosa and on hypopharyngeal cells show varied miR responses dependent on pH. They point to an increase in miR-21, miR-155, miR-192 and decrease of tumour suppressor miR-34a, miR-375 and miR-451a levels following acidic bile acid treatment. Opposite patterns were observed in neutral bile acid treatment and highlight the importance of pH in promoting pro-neoplastic effects in this model. However, it is important to mention there have been exceptions in which miR-21 and miR-192 show lower levels than the control, in two different cell lines (164). Although the study does not present untreated controls, unconjugated DCA and CDCA lowered miR-21, miR-155, miR-192 while miR-34a, miR-375 and miR-451a increased compared to acidic bile acids (165). Rudnicki *et al.*, (2014) demonstrated that lipopolysaccharide stimulation of the mouse inner ear triggers inflammation pathways by increasing miR-155 and miR-224 levels, suggesting to new therapeutic targets against inflammation (166). In case of primary biliary cholangitis tissue, the negative effects of highly expressed miR-155 and low miR-21 levels in hepatic cell culture are representative of inflammation and onset of disease, effects all reversed upon UDCA treatment (167).

UDCA applied as treatment *in vitro* and *in vivo* decrease miR-34a levels and ameliorates autophagic flux associated with age-related hearing loss (168). Furthermore, diabetic mice express high levels of miR-34a and a downregulation of SIRT1, revealing a possible mechanism of hyperglycaemia-associated hearing impairment (169). In an opposite model, primary human hepatocarcinoma and rat hepatocytes miR-34a levels decrease when treated with CDCA, T-UDCA or UDCA, while the opposite effects are seen from CA and G-CA treatments (170-172). Higher miR-34a in association with p53 upregulation and SIRT1 downregulation reported following DCA treatment *in vitro* and *in vivo* (152). Surprisingly, miR-34a shows important implication in murine age-related hearing loss revealed by higher miR-34a with decreased Bcl-2 in the auditory cortex (173). Other tissues are also affected in aged mice showing higher miR-29a, miR-34a and miR-124 levels in the organ of Corti, heart, liver, and plasma. Moreover, older mice have low circulating plasma levels of SIRT1, miR-29a and miR-124 that corroborate with human results (174). MiR-34 levels fluctuate thought the development of external auditory squamous cell carcinoma reaching low levels as the tumour progresses (175).

Humans exposed to occupational noise reveal low miR-21-5p plasma levels along with low miR-92a-3p (176). The opposite can be said about vestibular Schwannomas and

cholesteatomas revealing increased miR-21 levels (177). In regards to ischemic injury, miR-21 overexpression protects against neuron cell damage (178), with similar effects noticed after traumatic brain injury (179). When mice undergo cochlear ischemic reperfusion the application of miR-21 rich exosomes derived from neural progenitor cells reduce ABRs and apoptosis markers, furthermore, showing little impact on macrophages in terms on toxicity (180). Results from a different study using primary spiral ganglion cell derived exosomes were found to downregulate inflammatory markers and to upregulate miR-21-5p, miR-26a-5p and miR-181a-5p after 7-days of treatment (181). With miR-21 expression higher in the tumour microenvironment, authors tested LCA, DCA, CA and CDCA on various colorectal cancer cell lines and reported that (<100 μM) LCA and to a lesser degree DCA, upregulated miR-21 via ERK1/2 signalling promoting cancer cell proliferation (182). In a concentration-dependent manner, DCA increases miR-21 in gastric intestinal metaplasia cells with subsequent SRY-Box Transcription Factor 2 (SOX2) downregulation (183). Although it requires high concentrations, DCA applied to primary liver cells decreases miR-21 and negatively affects cell viability (184). Interestingly, SOX2 overexpression appears to protect against noise-induced insults (185), and perhaps the concentration-dependent modulatory effect of DCA or UDCA may be taken in consideration for further research. In context of partial hepatectomy, UDCA's protective effects are greater than DCA in terms of increasing miR-21 following a bile acid diet in rats (186). Adding to the varied set of examples of how important tissue-specificity is in obtaining beneficial effects in a different model, rats recovering from artery hyperplasia are better protected by UDCA administration displaying lower miR-21 (187).

A recently published research paper on hearing levels of paint workers exposed to volatile solvents revealed a significant correlation between hearing loss to a decrease in plasma levels of miR-122-5p and miR-195-5p. Further associated with the workers was a decrease in distortion product otoacoustic emission with lower miR-206, miR-495p and miR-92b-5p (188). Lower miR-122-5p levels are present after ROS induction through tert-butyl hydroperoxide (189). Furthermore, stimulation of *in vitro* auditory cells with H_2O_2 overexpress miR-122-5p holds protective effects by forkhead box O3 (FOXO3) downregulation (190). From a different perspective, higher miR-122 circulating levels are negatively associated with liver heath; however, UDCA administration in healthy and non-alcoholic fatty liver disease patients lowers plasma and liver miR-122 (191). In regard to miR-92b-5p, higher levels are correlated with

low gallbladder cancer patient survival, although hope lies in the effects seen in a xerograph mouse model and rely on DCA administration to improve the outcome of disease (192). Circulating miR plasma levels differ in noise-exposed and noise induce hearing loss male textile workers. The study reveals statistically lower levels of miR-24-3p, miR-185-5p and miR-451a (193). On a positive note, miR-185-5p overexpression may promote *in vitro* hepatocyte proliferation by stimulating CA production in stellate cells (194).

The miR-96/182/183 cluster is important to stereocilia and hair bundle formation. The cluster is essential for both peripheral and central auditory system maturation and mutations within these genes are associated with non-syndromic progressive hearing loss (195). Besides the negative effects on auditory hair cell survival, cisplatin reduces miR-96/182/183 levels. The addition of miR-182 mimetics restores in part cisplatin-induced cell survival via mitochondrial-dependent pathways (196). From zebra fish lateral line neuromasts we learn that short-term pre-conditioning to neomycin increases miR-96/182/183 and in fact protects against acute neomycin-damage to the sensory epithelium (197). As for bile acids, intestinal chemical sequestration proves important in increasing miR-96/182/183 hepatic levels (198).

2.4.10. Conclusions

Bile acids compose a specific set of molecules important in maintaining human lipid and glucose metabolism signalling. The hydrophobic nature of bile acids shows a detrimental role to cells exposed to high concentrations. In part, the hydrophobic-hydrophilic balance is essential; the more hydrophilic in nature, the higher the molar concentration required to reach micelles the more damaging in effects they can be, and vice-versa. The bile pool is mostly recycled at the intestine with only a small fraction of bile reaching the plasma and could act as markers for bile acid dysfunctions. So far there are few references on the therapeutic effects of hydrophilic T-UDCA and UDCA respectively against drug-induced apoptosis, progressive hearing loss and to preserve organ of Corti cellular integrity *in vitro* or *in vivo*. Some bile acids such as UDCA, LCA, CDCA and DCA may supress endoplasmic reticulum activity or prove to negatively influence apoptosis. In fact, the results vary from target to target, concentration, and intensity damage. MiRs could represent important plasma markers for hearing loss onset. Bile acids (CA, DCA, CDCA, UDCA, LCA) modulate miR levels associated with hepatic, hypopharyngeal and tumour cell insults, yet could be

used to develop systemic targeting strategies that reduce occupational, and noise-induced hearing loss. In terms of bile acid receptors expressed in the inner ear, there are few cross-references that may prove important for auditory hair cell, spiral ganglion neurons and stria vascularis function. As covered in this review, muscarinic receptor function is affected by increased noise-exposure and some synthetic bile acids may act as strong muscarinic activity inhibitors. In regard to muscarinic activity, DCA requires attention as the bile acid has been recorded in activating intestinal macrophages. Should this effect overlap with cochlear macrophage activation during targeted delivery, it could have negative effects since increased and prolonged inflammation exacerbates hearing loss. LCA is an antagonist of P2X receptors, although the effects in preventing the receptor's overstimulation during noise and progressive hearing loss remain unknown. Similarly, LCA's strong agonistic effect on VDR and BK channels are documented on monocytes, artery, and intestinal cells, with potential interest in restoring VDR and BK reduced activity that can cause tinnitus and age-related hearing loss. Lastly, S1PR2 activation during cisplatin-induced ototoxicity could represent a valuable strategy in reducing auditory hair cell apoptosis. More research is required to establish S1PR2 agonists therapeutics candidates and taurine-conjugated bile acids may be advantageous. Although amphipathic in nature, bile acid could influence cellular interaction and may benefit drug delivery. It is important to note that bile acid's critical micellar concentrations are much lower than the treatment concentrations described in this review and could be essential in establishing bile acid treatments. With lower treatment concentration, both systemic and local drug delivery strategies may develop to manage progressive hearing loss. Although systemic drug delivery to reach the inner ear is limited, long term side effects may be controlled by low-dose treatments or even subsequent bile acid sequestrant administration. Local middle ear drug delivery requires small drug volumes however implies the use of stable formulations that may permit fast drug diffusion to the inner ear and delay middle ear clearance through the Eustachian tube. In sum more research is requires as previous bile acid trans-tympanic therapies have not attributed the beneficial effects to bile acid receptors expressed in the inner ear. Two aspects should be considered for establishing bile acid effects in regard to the cochlear architecture – 1) pharmacokinetics and pharmacodynamics of circulating bile acids plasma and locally applied treatments, as well as 2) bile acid receptors activity and effect in healthy and hearing loss models.

Publication 2

Abstract

Bile acids are commonly known in digestion and liver research and hold important therapeutic potential. Besides the application of T-UDCA acid to the inner ear *in vitro* and *in vivo,* there is little information of the other bile acids and their effects, let alone the baseline levels in relation to the cochlea. In this review, some important bile acid effects are presented in correlation with the auditory system. We provide information of hyperlipidaemia, the blood-barrier integrity and some types of liver dysfunctions that lead to abnormal bile pool. Future experimental research on the subject is required to test the suitability of both hydrophobic and hydrophilic bile acids against hearing loss.

Key words: apolipoprotein, cochlea, cholesterol, bile acids, blood labyrinth barrier, hearing loss

2.5.1. Introduction

Bile acids are amphipathic molecules that are synthetised from cholesterol in the liver and stored in the gallbladder (199). The two primary bile acids CA and CDCA, which can be conjugated with either taurine (T-) or glycine (G-) form the more hydrophobic bile salts that aid lipid solubilisation in the intestine. Once in the intestine, secondary bile acids are formed from primary bile acids through a process of partial dihydroxylation by gut bacteria to form LCA, from CDCA, and DCA, from CA (200). Bile acids form micelles based on their critical micellar concentration and can be reabsorbed through enterohepatic circulation. The bile acid synthesis and reabsorption in part controls cholesterol metabolism, in addition to acting as cell signalling molecules resembling hormones (201). Due to their amphipathic nature (**figure 2.3**), the cellular properties could be referred as “double-edged” in part protecting and promoting cellular homeostasis yet potentially toxic depending on concentration. Various studies (*e.g.* gastric cancer cells (137, 138), laryngeal mucosa (165), oesophageal (139)) reveal strong tissue-specific, concentration-dependent and bile acid-specific effects (149, 150) that vary due to the pH (164) and the hydrophobic nature of bile acids. The BBB is often referred to be similar to the BLB; it is the main blood exchange path for lipophilic and ligand-based molecules, restricting exogenous

entry (202). Due to the similarities of the two barriers, we will discuss the effects bile acids hold on the permeability of the blood barrier and bring it into context in regards to the BLB (203). Early development of bile duct obstruction and a fatty diet changes lipid and bile secretion from a conjugated bile acid profile (204) to a more hydrophobic profile with less T-UDCA or UDCA present in the brain tissue (205), changes that can lead to inflammation and damage. An array of liver diseases associated with bile acid metabolic (52, 206-213) and cholesterol (213-216) changes present some degree of idiopathic hearing loss (217-229). The authors aim to bring in perspective bile acid dysfunction with known effects in relation to hearing loss. The role of cholesterol, apolipoproteins and blood-barrier integrity and function influenced by bile acids is presented.

2.5.2. Bile Acid Influence on the Blood Brain and Labyrinth Barriers

The cochlear blood supply flows through the terminating spiral modiolar artery, which branches into two systems surrounding the spiral ligament and stria vascularis forming four microvessel networks. The BLB is comprised of the basilar membrane supporting a population of endothelial cells, pericytes and perivascular resident macrophages that conform and maintain barrier integrity (230, 231). BLB cells are connected through tight junction proteins, and imbalances brought through chemical or mechanical disturbance can potentially be detrimental to the hearing organ (232-236). P-glycoprotein (P-gp) is a transmembrane efflux transporter (coded by *mdr1a*, *mdr1b* and *mdr2* genes) constituent of the BBB. Cerebral ischemia elevates P-gp levels in BBB endothelia, however the transporter can be pharmaceutically silenced to restore BBB integrity (237). To note, P-gp is found on BLB endothelial cells and other cochlear cells populations and holds an important role in preventing ototoxic drug accumulation (238-240). Cyclosporine A exposure changes bile acid gallbladder transport in the absence of mdr2, the effect is reversed with the addition of TCA (241). UDCA and CDCA can reduce P-gp overexpression induced by doxorubicin in hepatocarcinoma cells (242).

Bile acids Modulate Blood Barriers Permeability

The BLB functions as a protective network by having selective permeability solutes, various molecules including drugs and nutrients. The BLB stimulates blood flow entry to the inner ear in a similar manner and function to the blood-retina-barrier or the BBB (203). Rats perfused with DCA and T-CDCA salts at concentrations above 1.5 mM present brain and BBB cell ultrastructural changes (243). It is worthy to mention that 1.5 mM represents a much higher concentration than the total bile acid levels in serum (210, 244), yet it is lower than the critical micellar concentration that DCA and CDCA can form micelles and act as detergents. Endothelial cells are found in conjunction with pericytes at a ratio of 1:1 in the retina, 1:2 in the brain and 1:5 in the BLB (230). In a diabetic retinopathy model, UDCA prevented retinal vessel enlargement (245) and reduced leakage through the blood-retina-barrier (50) preventing pericyte population loss by interfering and reversing endoplasmic reticulum stress (246). Interestingly, bile duct ligation cholestasis in a rat model increases BBB permeability. Similarly, treatment with CDCA or DCA disturbed endothelial tight junctions and increased BBB permeability, with G-CDCA, T-CDCA and UDCA reported to pass the BBB (55). Conjugated G-UDCA is also mentioned to pass the BBB *in vitro,* yet UDCA was shown to reduce, to some degree, apoptosis markers caused by elevated bilirubin levels and prevented BBB permeability (247). This demonstrates that different bile acids present systemically can modulate blood-barriers and may represent a therapeutic approach for targeted BLB entry.

Blood Barrier Targets

Organic anion-transporting polypeptide 1a4 (Oatp1a4) is an important transporter of endogenous and xenobiotic compounds including bile acids such as TCA (248). The Oatp1a4 is expressed sex-specifically at the BBB level in mice (249) and interestingly, mutations to the transporter gene can alter bile pool predominantly in male mice (250). When affected by liver disease, the bile acid pool changes followed by farnesoid X receptor (FXR) downregulation and Takeda G-coupled protein receptor 5 (TGR5) upregulation (52). Bile acids are ligands for FXR and activate the receptor (CDCA > LCA > DCA > CA) (251). FXR is expressed in both animal and human neuronal tissue (252) and can regulate amyloid B deposit on hippocampal neurons (253). Bile acids

are endogenous agonists for TGR5, with LCA having the strongest receptor affinity followed by other unconjugated, taurine and glycine conjugated bile acids (254). Interestingly, TGR5 activation is reported to reduce BBB permeability in a cerebral vascular occlusion model (255). In regard to hepatic encephalopathy, TGR5 upregulation in the frontal cortex is associated with neuroinflammation effects that can overcome by TGR5 agonist preconditioning (256). Furthermore, TGR5 activation negatively affects microglia in a lipopolysaccharide inflammation model, however the effects are reduced upon hyo-DCA application (257).

2.5.3. Bile acids, Cognition and Hearing loss

The bile acid pool is dysregulated in some diseases thus presenting a possible disruption to the BBB (258, 259), with some pathology cases enlisting hearing loss as a side effect. Bile acids have been reported in brain tissue, with the ability to pass the BBB in both disease and normal conditions (**table 2.1**). Neurological complications are associated with chronic liver disease. Alcoholic cirrhosis patients, regardless of neomycin treatment, present increased hearing loss (260). A total of 14 bile acids were reported to increase in alcoholic cirrhosis patients serum compared to control, non-alcoholic fatty liver disease, and virus liver disease patients alike (261). Liver fibrosis risk has been associated with age-related hearing loss in an older population (220), with another cohort study on the same disease model find associative changes in G-conjugated bile acid with a marked increase in serum LCA (209). Data on the pathophysiology of Alzheimer's disease report cognitive decline in patients may be correlated with lower CA plasma levels and a subsequent increase in DCA (262). A different study presented increased LCA serum levels in patients considered at risk before and after the onset of Alzheimer's disease. Mild cognitive impairment participants revealed higher G-DCA and G-LCA compared to the control (263). Circulating CA level imbalance may point to a reduction in brain glucose metabolism, furthermore, the G-DCA to CA ratio appears to be associated with amyloid deposition in patients (264). Multiple sclerosis development is another subject for blood-barrier integrity (265, 266) that can also relate to altered DCA and CA circulating levels; with one report presenting T-UDCA (20-70 μM / 500 mg/Kg) supplementation as a means for preventing spinal cord demyelination (267).

2.5.4. Bile Acid Micelles and Cholesterol

Cholesterol and protein rich lipid-rafts modulate auditory hair cell mechanics and maintain hearing acuity (268, 269). Depending on concentration, cholesterol associated with the outer hair cell motor protein prestin is shown to reduce electromotility (270) and represents the means by which 2-hydroxypropyl-β-CD is responsible for ototoxicity (271). As a rule of thumb, the detergent action of bile acids appears to be dependent on both lipid membrane composition, bile acid type and concentration. Hydrophobic bile acids are known for their strong detergent effects at the millimolar range that can lead to membrane disturbance and cellular lysis. At higher concentrations, bile acids assemble into micelles dependant on their critical micellar concentration that can include lipids as well (272, 273). Similar to methyl-β-CD, CDCA can decrease caveolae formation in aorta epithelial cells, effect restored by the addition of cholesterol to experimental groups (274). CA and UDCA diet supplementation stimulate gallbladder biliary release as well as increase biliary phospholipids and cholesterol production (248) and interestingly in *in vitro* conditions, T-UDCA (at high 10 mM concentration) may selectively remove sphingomyelin from membranes containing phosphatidylcholine regardless of cholesterol levels (275) .

Cholesterol Cellular Homeostasis and Hearing Loss Markers

ATPase phospholipid transporting 8B1 (ATP8B1) represents a major flippase protein described in the liver and other tissues (276, 277). It is recognized as the cause of progressive familial intrahepatic cholestasis type 1 (213, 228, 278). ATP8B1 deficient mice present an increase in cholesterol to phospholipid levels as a result of bile acid transport changes (216). ATP8B1 is also present in the hair cell stereocilia and spiral ganglion neurons and has been associated with early hearing loss onset. Sterol responsive element-binding protein (SREBP) is a transcription factor responsible for sterol biosynthesis and homeostasis, overexpression of this protein contributes to intracellular cholesterol accumulation (214, 279, 280). SREBP-2 activation is modulating the miR cluster 96/182/183 that provide a feedback loop for SREBP-1/2 activity dependent on cholesterol and bile acid levels (198, 281, 282). Oxysterol-binding protein like 2 (OSPL2) is a transporter protein important in cholesterol-homeostasis and it is expressed in auditory hair cell and supporting cell cilia (283). Mutations to this protein are associated with autosomal dominant non-syndromic

hearing loss by inhibiting AMP-activated protein kinase (AMPK) activity that triggers SREBP-2 leading to cholesterol-induced oxidative stress accumulation (223, 284).

Bile Acid and Cholesterol Levels in Relation to Hearing Loss

The risk of idiopathic hearing loss and hypercholesterolemia is still a contested subject in humans (285). An array of risk factors investigated in cisplatin-treated cancer survivors reports higher changes of progressive hearing loss and tinnitus in patients with hypercholesterolemia (286). Cholesterol synthesis in the liver, and secretion from the gallbladder are modulated by the bile acid hydrophobicity (287) so much that changes from CA to CDCA increase bile acid biosynthesis enzymes, promotes cholesterol elimination and lower plasma cholesterol in mice (288). Humans who underwent supplementation with CDCA showed a change in the bile acid pool, while DCA supplementation minimally decreased lipid levels (289). In rats cholesterol levels and the bile acid pool change with age (290), similar results have been reproduced in a small human study where they show age-associated cholesterol increase predominantly in men. Interestingly enough, in female participants that have undergone gallbladder removal follow a similar trend (291). On a larger dataset study focused on collecting information from long term use of lipid lowering medications found that older male participants are slightly protected against hearing loss (292). Bile acid sequestrants represent a type of medication used for lowering cholesterol levels, although statins are a more efficient treatment class in this regard. A very good systematic review covers more animal and human studies of statin use and their effects in regards to ototoxicity, tinnitus, vertigo and histology (293).

2.5.5. Bile Acid and Apolipoprotein Level Changes in Hearing Loss

Apolipoprotein E (apo; apoE) APOE-ε4 allele genotype may be associated with the populational decline in hearing acuity (294, 295) and is better known as a variant allele marker associated with cognitive impairment (296). Finding a clear association between cognitive decline and hearing loss is a recent topic, with various cohort studies offering multifaceted results based on patient selection and differences in analysis and input criteria (297-301). A larger population study found a possible implication of bile acid sequestrates to a relative increase of vascular dementia brain markers, with tissue-

specific increases of CA and CDCA (302). As briefly mentioned in the previous subsection, cholesterol lowering statin use shows better hearing thresholds, an effect also observed in apoE deficient atherosclerotic mice which present accentuated age-related hearing loss (303) with higher spiral ganglion ROS (304, 305) and noticeable increase in stria vascularis apoptosis markers (306). Moreover, apoE$^{-/-}$ transgenic mice present variations in their bile pool levels with seemingly increased CA levels compared to non-transgenic mice (307). Interestingly, lipid profile dysregulation with low apoA and high apoB levels may be predictive of sensorineural hearing loss (229). A seven day noise-exposure experiment in pigs prompts cochlear apoE and apoA-I levels, pointing to the implication of cholesterol metabolism for early hearing recovery (229, 308). ApoA-I transgenic mice fed CA are the representative atherosclerotic mouse model and it shown that CA feeding compensated with high fat diet significantly reduced apoA (309). Regardless of diet type, CA can lead to increases in apoE and apoB levels in these mice (310). ApoA-I is responsible in transporting cholesterol and phospholipids from tissues to the liver where cholesterol is used to synthesise new bile acids. Cholestasis increases bile acid to higher than normal physiological levels to the point that human apoA-I transgenic mice show higher FXR activity which further influences bile acid synthesis and circulation (311, 312). From an older study, it is presented that the effects of bile acid sequestration are slightly increasing apoA levels and decreasing apoE (313). Although, small scale human-based studies, demonstrate that, to a degree, bile acid oral intake can affect and change bile acid homeostasis along with circulating lipid levels. Both DCA and UDCA uptake show modulatory effects either by decreasing (314) or increasing apoA levels (315). ApoA-I/II can form micelles depending on their concentrations in serum levels and bile salts can dissociate or aggregate with apoA-I/II micelles dependent on the bile acid hydrophobicity (244).

2.5.6. Conclusions

Bile acids control an important part of liver metabolism, and their circulating levels represent a means to detect pathogenesis. References on blood-barrier permeability, brain concentration and associated bile acid tissue-specific concentrations are made to better understand the effects that might be observed in the cochlea. We see that p-glycoprotein upregulation can affect blood-barrier integrity and both UDCA and

CDCA can help modulate the transmembrane efflux pump activity. Furthermore, UDCA reduces pericyte associated diabetic retinopathy stress and blood-retinal leakage. There is no direct implication of the bile acids effects to the BLB. We could only discuss the relation between bile acids and the BBB. It is thus important to consider that G-CDCA, and UDCA are both reported to pass through the BBB. TGR5 activation reduces BBB permeability, and CDCA as well as LCA act as receptor agonists. Hyo-DCA can also reduce microglial inflammation associated to TGR5 activation. The protective effect of some bile acids might be obscured by the cell-damaging hydrophobic bile acids. With bile pool change, blood-barrier permeability leads to accumulation of hydrophobic bile acids in the brain, effect associated with cellular accumulation, damage, and cognitive decline including idiopathic hearing loss to a degree. Another important role of bile acids is in modulating cholesterol levels. Cholesterol is an integral element in auditory cell function, and some important proteins in cholesterol homeostasis are linked to hearing loss. Moreover, hypercholesterolemia itself is documented in affecting both cognition and to some degree may lead to progressive hearing loss. Cholesterol chelation can reduce prestin electromotility and bile acids should be taken in consideration and tested for similar results. Hydrophobic bile acids can act as detergents at lower than micellar concentrations. CDCA for example prevents cholesterol dependent membrane caveolae formation. It is regarded that cholesterol overexpression and accumulation increases hearing loss in disease models, however it is important to consider that CA and UDCA supplementation in mice increases cholesterol production as well. Some reports correlate age-related hearing loss with high cholesterol, notoriously Apo E/A in murine studies. Although in some studies statin use improved hearing loss thresholds and reduced spiral ganglion damage, the use of bile acid sequestrants that lower cholesterol as well should be further examined. A long-term study on bile acid sequestrants use shows association between CA and CDCA accumulation in brain tissue and vascular dementia onset in men. Literature references are sought to bring correlations of bile acids pool changes and effects in relation to known diseases that enlist hearing loss side effects. Thus, bile acid implication on blood barriers, cholesterol and associated proteins requires future research and can potentially be useful for developing drug delivery strategies to prevent hearing loss onset.

Competing Interests

All other authors have no completing interest to declare.

Acknowledgments

The authors want to acknowledge the Australian Postgraduate Award (APA) and Curtin Research Scholarship (CRS).

Funding

Curtin Faculty ORS-WAHAI Consortium, the Australian National Health and Medical Research (APP9000597).

Data Availability

Data sharing not applicable to this article as no datasets were generated or analysed during the current study.

Author contribution

CMI, MM, AM and HAS conceptualised and designed the project. The main draft of the manuscript was prepared and assisted by all authors, who contributed effectively to the final draft.

Target / Insult	*In vitro, In vivo model*	*Bile acid dose and delivery route*	*Bile acids used*	*Effect*	*Reference*
Spiral ganglions and hair cells of the organ of Corti – gentamicin toxicity	Cochlea explants and XBP1+/- CBA/J mice	500 mg/Kg S.C. after 3 hours - 3 and 6 days	T-UDCA	Prevents ER stress after gentamicin in a compromised UPR model. Improved hearing	(102)
Cellular apoptosis and ER stress – gentamicin toxicity	HEI-OC1 cells and BALB/c cochlear explants	<200 μM - 4 and 24 hours	T-UDCA	Increased Bcl-2, Bip, CHOP expression, promoted survival and auditory hair cell count after gentamicin exposure	(103)
Cochlea – cisplatin toxicity	Sprague-Dawley rats	100 mg/Kg I.P. - 5 days	T-UDCA	Reduced hearing thresholds after cisplatin toxicity	(95)
***Cdh23*$^{erl/erl}$ mutant mice**	C57BL/6J homozygous *Cdh23*$^{erl/erl}$ *r*epresentative of non-syndromic recessive deafness *DFNB12* in humans.	100 mg/Kg I.P. every other day for 8 weeks, starting post-natal day 7. Follow-up I.P. once per week.	T-UDCA	Low caspase-3/9 expression by week 10. Hearing loss onset and low thresholds shift from 4 weeks to 12 weeks following T-UDCA treatment.	(101)
Rat hearing – cisplatin toxicity	Sprague-Dawley rats	100 mg/kg I.P. for 3 days with or without cisplatin, 5 mg/kg. ABR taken 10 days from treatment	T-UDCA	T-UDCA cisplatin-treated group had protective effects; lower ABR thresholds, higher HO1 and SOD2 expression, and low caspase 3 detection.	(94)
Organ of Corti – electrode insertion trauma	Organ of Corti explants from three-day post-natal	50 μM, 100 μM or 200 μM	T-UDCA	T-UDCA groups with reduced morphological damage and reduced apoptosis markers after electrode implant	(316)

	Sprague-Dawley rats				
Sensory hair cells and organ of Corti explants – cisplatin insult	HEI-OC1 cells, Sprague-Dawley rats, and explants	500 mg/kg/day I.P. for 3 days or 0.5 mg/mL T.T. in rats. 1 mM for explants and 1.6 mM for cells	T-UDCA	Reduced ABR thresholds of T-UDCA treated rats after I.P. and T.T. compared with cisplatin. Increased hair cell survival, decreased CHOP, caspase-12, calreticulin, UGGT1 and OS9.	(133)
Autophagy and miR-34a levels – age-related hearing loss	HEI-OC1	10 μM	UDCA	UDCA reduced overexpression of miR-34a-induced apoptosis	(168)

Table 2.1.

Collection of references that have applied bile acids as treatment for cochlear morphology and functional hearing studies. A description of the target and type of insult used to model the experiments. The bile acid type, dose and delivery route are presented at which effects were observed. Abbreviations; subcutaneous, S.C.; intraperitoneal, I.P.; trans-tympanic, T.T.; B-cell lymphoma 2, Bcl-2; binding immunoglobulin protein, Bip; UDP-glucose ceramide glucosyltransferase-like 1, UGGT1; OS9 ER lectin, OS9; auditory brainstem response, ABR.

Target / Insult	***In vitro, In vivo model***	***Bile acid dose and delivery route***	***Bile acids used***	***Effect***	***Reference***
ER dependent apoptosis	Huh7 human liver cell line	400 μM/L - 18-24 hours	T-UDCA	Inhibited elevated cytosolic calcium, and caspase-12 activation caused by thapsigargin.	(134)

Duodenum, ileum and jejunum	(Vdr(−/−)) mice and wild-type mice (Vdr(+/+)) C57BL/6J mice	Gavage 0.3-0.8 mM/Kg	LCA	Weak VDR ligand. Increased *Cyp24a1* gene expression, but not the Ca^{2+} Trpv6 transporter.	(117)
Caco-2 cells	Epithelial barrier dysfunction	20 μM - 12 hours	LCA	Upregulates SIRT1, Nrf2 and HO-1, and activates the VDR against 100 ng/mL TNF-a for 24 hours.	(317)
Muscarinic receptors	Chinese hamster ovary cells, macrophages	100 μM	DCA, LCA and derivatives	Agonist/antagonist action on M_1, M_2, M_3. Less potent than atropine as anti-muscarinic action. Can determine macrophage pro-inflammatory polarization	(142, 144, 145)
p53 activity	SNU-245 squamous carcinoma, HCT116 (ATCC) human colorecta carcinoma cells	100-500 μM/L	DCA, UDCA	UDCA reversed DCA insult by increasing p53 and BAX activity, reduced ERK activity; as a tumour suppressor effect.	(149, 150)
p53 activity	HCT116 (ATCC) human colorecta carcinoma cells	200 μM	DCA	Reduced p53 protein levels, p53 proteasome-degradation, partial ERK stimulation promoting tumorigenesis.	(151)
Non-alcoholic steatohepatitis	Wistar rats' tissue and primary rat hepatocytes	Gavage 250 mg/kg or 10-400 μM on cells.	DCA	Concentration-dependent increase in p53 with decrease in SIRT1	(152)
BK_{Ca2+} channel	Sprague-Dawley rat *β*-KO and C57BL/6 mice myocyte and arteries	45 μM	LCA	Causes reversible vasodilatation by activation of BK channels *β*1 subunit.	(318)

BK_{Ca2+} channel	Smooth muscle artery, pulmonary artery, and gallbladder cells	100 μM and as low as 3 μM	DCA, CA, LCA and T-LCA	Increase BK channel activity in cell-attached or inside-out patch clamp models.	(114)
Purinergic receptors	HEK293T cells expressing rat P2X2, P2X4 and P2X7 receptors, and Wistar rat primary pituitary gonadotrophs expressing P2X2 and P2X4	3, 10-30 μM LCA and analogues, 10-30 μM CDCA, DCA and UDCA	LCA and analogues	LCA and structural analogue 4-dafachronic inhibit ATP-stimulated $P2X_2$ and potentiate $P2X_4$, including $P2X_7$ at higher doses.	(129)
Purinergic receptors	Rat receptor cloned in Xenopus laevis oocytes	20 μM	taurine-conjugated -LCA, -hyo-DCA, -CDCA	Taurine-conjugated bile acids inhibited $P2X_2$. T-LCA potentiated $P2X_4$ and had more effect on human $P2X_2$ than the rat homologue. Effects not restricted to the taurine moiety, but to the hydroxyl groups.	(132)
Intracellular Calcium release	SCM1 human gastric cancer cells	600 and 1000 μM	DCA	Induced intracellular calcium concertation release from ER in a concentration-dependent manner. Concentrations of 100-500 μM that induced apoptosis.	(136)
Vascular nitric oxide production associated with cirrhosis	Human umbilical and calf aortic endothelial cells	100-750 μM	DCA, CDCA, CA, and taurine-conjugates	All show increased intracellular calcium release, except CA. DCA and CDCA increase nitric oxide production that may involve pathogenesis.	(137)

Intestinal chlorine secretion	T84 colonic cell line	750 μM, 100 μM minimum	T-DCA and TCA	Induced intracellular calcium currents followed by reversible potassium and chlorine currents. Effects not observed by TCA.	(138)
Cholestasis ER stress model	BNL-CL2 and HL-7702/L02 hepatocytes, bile duct-ligated mouse liver, HEK293 cells	200 μM	DCA	miR-199-5p protects against ER stress caused by DCA. DCA might promote cell death by IRE1α activity.	(163)
Sphingosine-1-phosphate receptor 2	Primary rat hepatocytes and S1P(2) (-/-) KO mice	5-100 μM for cell culture and 36 μM/100 g rat/hour for 3 hours infusions	TCA, T-UDCA, T-DCA, G-CA, G-DCA	Agonistic action on receptor. TCA activity on S1PR2 is mediated by ERK1/2 and AKT activation. The addition of an antagonist on the receptor represses bile acid activity.	(156)

Table 2.2.

Collection of bile acid references and their impact on tissues and cells other than the cochlea. A description of the target and type of insult used to model the experiments. The bile acid type, dose and delivery route are presented at which effects were observed. Abbreviations; knock-out, KO; tumour necrosis factor alpha, TNF-α; Bcl-2-associated X protein, BAX; zonula occludens-1/2, ZO-1/2; transient receptor potential cation channel subfamily V member 6, TRPV6; extracellular signal-regulated kinase, ERK; inositol-requiring transmembrane kinase endoribonuclease-1α, IRE1α; protein kinase B, AKT; Sphingosine-1-phosphate receptor 2, S1PR2.

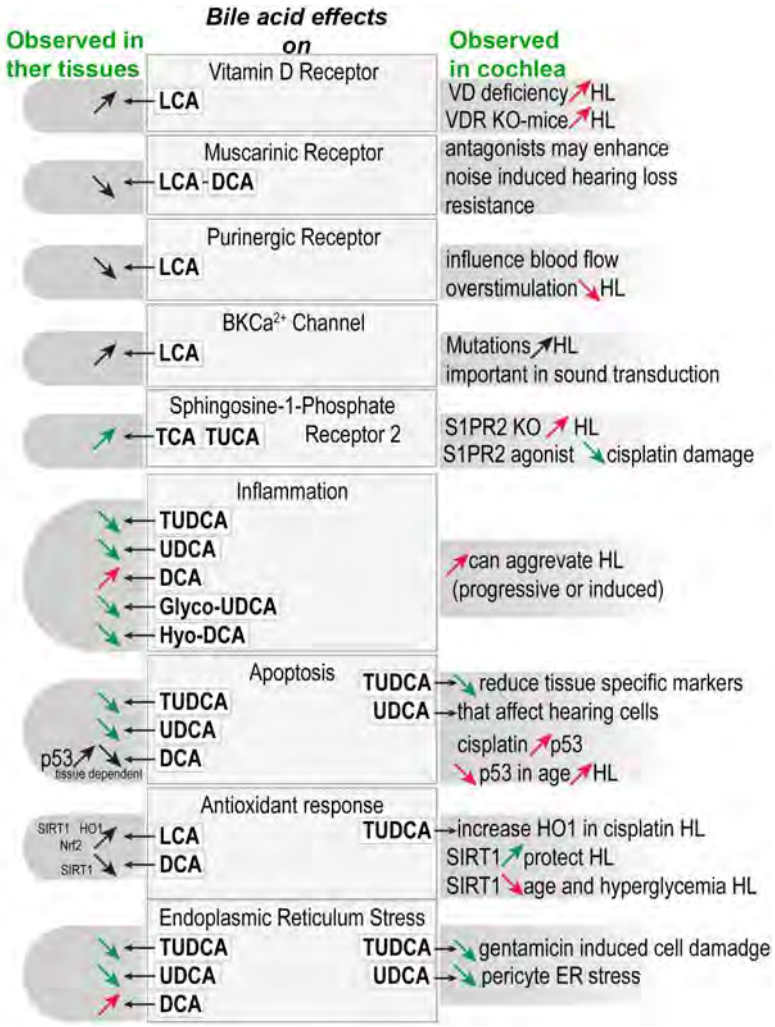

Figure 2.1.

Summary figure of bile acids and their discussed effects on modulating receptors, inflammation, apoptosis, antioxidant response and endoplasmic reticulum stress observe in other tissues as well in the cochlea. More information on the cochlear effects is described in Table 2.1. The observed effects of bile acids in other tissues are described in table 2.2 and correspond to an array of models (murine intestinal cells, ovary cell and macrophages, oocytes and pituitary cells, myocytes and arteries, human hepatocytes, endothelial cells, gastric cells and colorectal carcinoma, squamous carcinoma). Abbreviations: vitamin D, VD; vitamin D receptor, VDR; knock-out KO; hearing loss, HL; endoplasmic reticulum, ER; bile

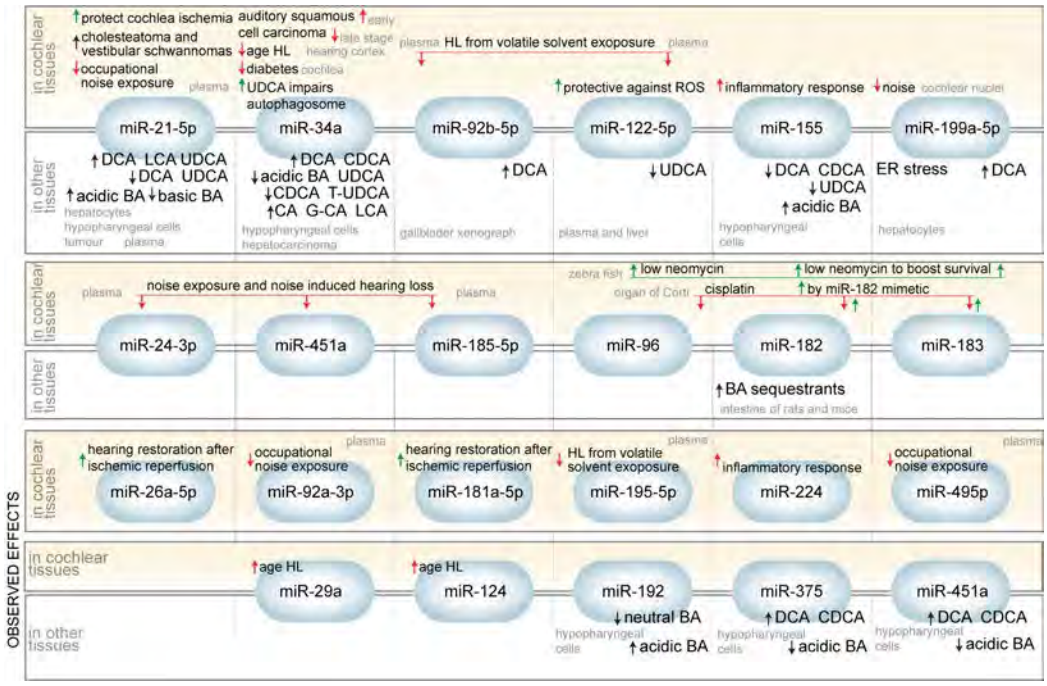

Figure 2.2.

Literature descriptions of bile acids and their effects on miR levels. Some miRs expressed in the cochlea tissues show a positive or negative association with hearing loss development (yellow box). The effects of bile acids from other models (hypopharyngeal cells, plasma, intestine, hepatocytes, gallbladder xerographs) are presented to highlight the possible implications of miRs on the hearing organ. Bile acid therapeutic application could potentially modulate hearing insult associated miRs. So far, UDCA has been used on auditory cell cultures to reduce apoptosis associated miR-34a activity. Abbreviations: hearing loss, HL; endoplasmic reticulum, ER; bile acid, BA.

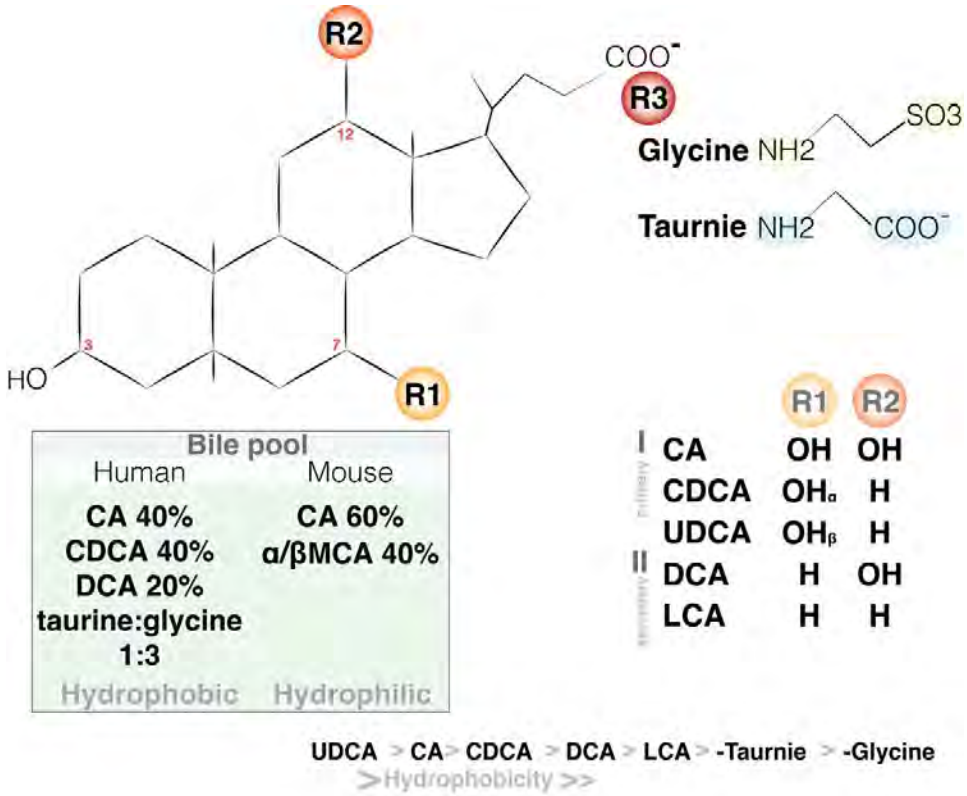

Figure 2.3.

Steroid structure of a bile acid listing the structural changes that form the main human bile acid components: cholic acid (CA), chenodeoxycholic acid (CDCA), deoxycholic acid (DCA), with lithocholic acid (LCA) and ursodeoxycholic acid (UDCA) found in trace amounts. Mouse bile pool mostly contains CA and α/β muricholic acid (MCA). Bile acids are conjugated to glycine (G-) and taurine (T-) to form bile salts that promote bile acid synthesis, and gallbladder excretion into the intestines to facilitate lipid absorption. In terms of hydrophobicity, unconjugated bile acids with multiple hydroxyl groups (-OH) are more hydrophilic than taurine and glycine-conjugated bile acids.

Target / Insult	*In vitro, In vivo model*	*Bile acid dose and delivery route*	*Bile acids used*	*Effect*	*Reference*
Spinal cord injury	Sprague-Dawley rats	10 µL	T-UDCA	Reduced neuroinflammation markers; TNF-α, IL-1β, IFN-ϒ, and IL-6	(100)
Cholestasis model	Swiss albino mice	0.5% or 1% - 7 days	CA, UDCA	Both diets downregulated Oatp1/4 and increased glutathione. CA upregulate mrp2, mdr1a/b and increased cholesterol and phospholipid levels. mdr1a and Mrp2 was also upregulated by higher UDCA supplementation.	(248)
Diabetic retinopathy	C57BL/6 J mice	100 mg/kg S.C.	UDCA	Protected the capillary wall and retinal integrity	(245)
Diabetic retinopathy	C57BL/6 mice	Gavage 15, 30 mg/kg for one month	UDCA	Protected the retinal integrity and reduced inflammation of the blood-retina barrier	(50)
Diabetic retinopathy	C57BL/6NCrSlc mice. Pericyte culture	*In vivo* 100 mg/kg I.P. *in vitro* 100 µM	UDCA	Protected the blood retinal barrier integrity, restored UPR and ER stress. Protected pericyte viability	(246)
Cholestasis model or bile acid treatment	Sprague Dawley rats.	3 µg/day - 1- or 5-days I.V. *In vitro* rat brain microvascular endothelial cells (RBMECs) 10 µM or 100 µM/ 24 hours	DCA CDCA *in vivo*. CDCA, DCA, G-CDCA, T-CDCA, or UDCA *in vitro*	Higher circulating bile acid increased blood-barrier permeability. BBB markers occluding, ZO-1, ZO-2 downregulated by DCA CDCA chow	(55)
Severe jaundice model	HBMEC cell line	50 µM - 4 or 24 hours	UDCA, G-UDCA	G-UDCA reduced capsase-3, IL-6. UDCA, reduced cytokine release. Both pass cell monolayers	(247)
Middle cerebral artery occlusion	BV2 cell lines, C57BL/6 mice	Gavage 25, 50, 100 mg/kg/ 7 days *in vivo*. 100 µM *in vitro*	Hyo-DCA	Decreased inflammation markers in microglial cells via TGR5 activation	(257)

Hepatic encephalopathy model	C57Bl/6 or cytochrome p450 7A1 KO (Cyp7A1(-/-)) mice	Fed before liver failure with 0.2% CA, 0.3% DCA, 3% UDCA	CA, DCA, UDCA	Induced liver failure, increased bile acid cortex levels and induced neurological decline, accentuated by CA and DCA chow. Lipid lowering drug fed mice and the (Cyp7A1(-/-)) reduced and delayed the effects.	(319)
Atherosclerosis	apoA-I transgenic and C57BL mice	1% supplemented chow	CA	CA reduced high-density lipoprotein cholesterol, and reduced apoA-I transcription and synthesis in apoA-I expressing mice	(309)
Nonalcoholic steatohepatitis	Human subjects	UDCA 15 mg/kg/day for 6 months	UDCA	High-density lipoprotein cholesterol and apoA-I increased, reduced carotid intima media thickness.	(315)
Vasorelaxation	Sprague-Dawley rats' abdominal aortas	100 μM for 1 hour, and/or in combination with 10 mM cholesterol	CA, CDCA	CDCA induced vasorelaxation. Both CDCA and methyl-β-cyclodextrin reduce abdominal aorta endothelial cell caveolae formations, effects partially restored by incorporating cholesterol	(274)

Table 2.3.

Literature references of bile acids and their impact on tissues, cells or organism used as disease model other than the inner ear. A description of the target and type of insult used to model the experiments. The bile acid type, dose and delivery route are presented at which effects were observed. Abbreviations; unfolded protein response, UPR; endoplasmic reticulum, ER; intra peritoneal, I.P.; knock-out, KO; tumour necrosis factor alpha, TNF-α; interleukin 1 beta, IL-1β; interferon gamma, IFN-ϒ; interleukin 6, IL-6; inositol-requiring transmembrane kinase/endoribonuclease 1α, IRE1α; multidrug resistance protein 1a, mrd1a; multidrug resistance-associated protein 2, mrp2; zonula occludens-1/2, ZO-1/2.

Chapter 3

Ursodeoxycholic Acid and Probucol Spray Dried Formulations

3.1. Publications

The manuscript has been published in the Journal of Pharmaceutical Sciences

3. **Corina M Ionescu**, Bozica Kovacevic, Melissa A Jones, Susbin R Wagle, Thomas Foster, Momir Mikov, Armin Mooranian and Hani Al-Salami - Probucol-Ursodeoxycholic Acid Otic Formulations: Stability and In Vitro Assessments for Hearing Loss Treatment. *Journal of Pharmaceutical Sciences*, 2024, 10:S0022-3549(24)00159-X. DOI: 10.1016/j.xphs.2024.04.032.

3.2. Introduction

This Chapter focuses on UDCA as an excipient for probucol-based spray dried microparticles. Since the conjugated T-UDCA is readily used and regarded for its protective effects against ototoxicity, this Chapter will explore in part the safety of the unconjugated UDCA and its effects on HEI-OC1 cells. Probucol as an active pharmaceutical ingredient for drug delivery applications requires pre-formulation processing in order to increase water mixability, that can be achieved through the addition of polymers and polysaccharides. The pre-formulation in the Chapter composes of polyethylene glycol (PEG) and polyvinyl acetate (PVA) as well as β-CD to increase probucol mixability, and PVP to decrease surface tension of the solution. Pre-formulations require further processing before application, for example by spray drying and formation of solid dispersions. There are few publications that use either UDCA or probucol for solid dispersion through spray drying. However, in this chapter both UDCA and probucol are used in pre-formulation to spray dry, and to assess UDCA influence on particle shape, size, drug loading changes, and drug degradation. Besides characterising the spray dried solid dispersions, it is important to determine the use of probucol (F6), probucol-UDCA (F5) and UDCA (F7) dispersions on HEI-OC1 and limitations against cisplatin-challenged HEI-OC1 groups ($F5^+$, $F6^+$, $F7^+$). Cisplatin inhibitory concentration (IC50) was calculated and can be found in Appendix II.

3.3. Summary

Compared to other pre-formulations spray dried and presented in Appendix III, spray dried probucol in combination with PEG, PVA, β-CD, and PVP result in spherical particles that have minimal surface imperfections. The addition of UDCA with or without probucol does not impact pre-formulation spray drying, and although drug encapsulation efficacy percentage is increased by ~2% for probucol-UDCA particles, the probucol content percentage minimally varies. Probucol can degrade to diphenoquinone, spiroquinone and bisphenol that have known beneficial effects as well. Since probucol degradation happens in oxidising condition, forced degradation on probucol and probucol-UDCA particles was investigated as well (Appendix III for chromatograms). UDCA and probucol-UDCA particles show high viability when applied as treatment. However, the cisplatin-challenged groups decrease in viability especially for HEI-OC1 treated with UDCA particles. The combination of probucol-UDCA can restore cisplatin-induced cell loss, as well as it maintains ROS levels closer to untreated cells. Lastly, to better understand the impact on spray dried probucol particle formation, Appendix III includes an extended pre-formulation list incorporating other bile acids and investigates the *in vitro* dissolution on HEI-OC1.

Publication 3

Abstract

Targeted drug delivery is an ongoing aspect of scientific research that is expanding through the design of micro- and nanoparticles. In this paper, we focus on spray dried microparticles as carriers for a lipophilic repurposed antioxidant (probucol). We characterise the microparticles and quantify probucol prior to assessing cytotoxicity on both control and cisplatin-treated immortalised auditory hair cells (HEI-OC1). The addition of water-soluble polymers to 2% β-CD resulted in a stable formulation to encapsulate probucol. UDCA was used as a formulation excipient to increase probucol miscibility and microparticle drug content. Formulation characterisations reveal spray drying suitable to obtain spherical UDCA-drug and probucol microparticles with a mean size distribution of ~5-12 μm. Probucol microparticles show stable short-term drug storage conditions accounting for only ~10% loss over seven days. By mimicking cell culture conditions, both UDCA enriched (67%) and probucol only (82%)

microparticles had probucol release observed within the first two hours. Furthermore, probucol formulations with or without UDCA preserve cell viability and reduce cisplatin-induced oxidative stress more so than UDCA containing microparticles. Mitochondrial bioenergetics were assessed as well resulting in lower basal respiration and non-mitochondrial respiration, and higher maximal respiration, spare capacity, ATP production and proton leak within cisplatin microparticle co-treatments. Overall, we present a facile method for incorporating lipophilic antioxidant carriers in polymer-based particles that are tolerated by HEI-OC1 cells and show stable drug release, sufficient in reducing cisplatin-induced reactive oxygen species accumulation.

Key words: cyclodextrin, probucol, HEI-OC1, cisplatin, hearing loss, UDCA, drug delivery.

Highlights

- CD, PVP, PVA and PEG can increase probucol solubility
- Spray drying represents a simple method to prepare probucol microparticles.
- Probucol-based microparticles can be dispersed in water solutions, allowing for slow probucol release from the particle matrix.
- UDCA stabilises probucol microparticles and delays probucol release.
- Probucol-based microparticles show no cytotoxicity in permissive HEI-OC1 cells.
- UDCA in combination with probucol enhances probucol's protective effects *in vitro* against cisplatin.

3.4.1. Introduction

Cisplatin as a chemotherapeutic agent is used for treating multiple types of cancers *e.g.,* testicular cancer and ovarian cancer. Although with great efficacy against neoplasms, cisplatin's side effects include neurotoxicity, nephrotoxicity, and ototoxicity leading to hearing loss in many patients (320). Mechanosensory hair cells located in the organ of Corti are specialised in transducing and transmitting sound pressure waves and are a critical target for insults associated with age-related, noise-induced trauma or ototoxic drug exposures. Cisplatin cellular entry may be facilitated by passive diffusion or by direct interaction with metal transporting membrane

proteins (321). Once in the cytosolic compartment, cisplatin can form a non-diffusible toxic cation that binds to DNA leading to cancerous cell apoptosis via mitochondrial-mediated ROS damage. However, the production of ROS and subsequent apoptosis observed in auditory cells may be independent of DNA damage (59, 320, 322, 323). ROS accumulate in the cell depleting cellular antioxidant levels. Subsequent organelle calcium release, endoplasmic reticulum degradation, lipid peroxidation, and nuclear membrane dilation further aggravate cisplatin's side effects (324). With cisplatin being effective in clinical anti-cancer treatments, there is a growing need in finding therapeutic strategies to reduce associated side effects including ototoxicity. Several compounds have been tested pre-clinically, including sodium thiosulphate that actively chelate cisplatin thus improving its excretion. Although efficient, sodium thiosulphate could potentially interfere with cisplatin's potency therefore it is administered 1-6 hours after chemotherapy (325). Other active compounds with thiol-groups (R-SH) show promise in neutralising cisplatin's side effects (326) and antioxidants to reduce ROS cellular accumulation (327). Delivery strategies may improve tissue-associated drug availability and decrease toxicity. There is growing evidence in both nano- and microparticle to protect inner ear by using dexamethasone (31), curcumin (328), ROS-sensing polymers (329), pH sensitive polymers (330) and gene delivery (331) strategies for hearing-loss treatments. Particle toxicity studies are generally undertaken on HEI-OC1 cell cultures or organ of Corti explants and reflect well drug tolerable concentrations (59). However *in vivo* access to the inner ear can be reached by trans-tympanic injections that can limit the amount of drug administrated. A study shows that particles are successful in reaching vestibular and cochlear structures by surpassing the oval and round window (332). Overall, permeability is greatly influence by the particle's physical-chemical properties including size, surface charge and surface composition such as polymers or proteins.

An active API can be incorporated into formulations such as solid dispersions produced by spray drying technique. To the best of our knowledge, our group show interest in spray dried probucol-bile acids solid dispersions in the context of *in vitro* applications on HEI-OC1 cells (333). The use of polymers in the spray drying of feed-stock such as PVP, PVA and PEG increases APIs dissolution (334). Spray drying protocols developed for probucol or bile acids involve polymer-drug mixtures in alcohol-solvent feed-stock solutions (335-337). Here we will explore the use of water-based probucol-bile acid polymer mixtures for spray drying. Probucol (bisphenabid)

is a bis-phenol antioxidant, anti-inflammatory compound used in some countries as a cholesterol lowering treatment. Probucol's application have branched out in the last decade showing impressive effects as a neuroprotector (7) as well as conferring antidiabetic benefits (338). Probucol treatment may lower lipid peroxidation levels and increase antioxidant reserves, glutathione, catalase and SOD activity following ischemic reperfusion (9). Probucol shows protective effects against oxidative stress (339), decreasing levels of pro-apoptotic p53 protein and Bcl-2-associated X protein, and increasing anti-apoptotic Bcl-2 (340) Furthermore, probucol derivatives such as succinobucol and oxidised products hold similar results (341, 342). Bile acids are endogenous molecules produced by the liver to aid digestion. Many references provide evidence that bile acids are great antioxidants, however the dose-dependent tissue damaging effects are well acknowledged. There is limited information on bile acids and their otoprotective effects. For example, T-UDCA acid is found to reduce ER stress (95, 134) and activate Nrf2 (94, 98). T-UDCA has been used to protect auditory cell morphology after electrode implant (316) and ameliorates hearing loss (101) caused by gentamicin and cisplatin-induced toxicity (94, 95, 103, 133). UDCA reduces pro-apoptotic caspase-3 and p53 levels (187), two important proteins that if imbalanced are associated with mechanosensory hair cell stress. Unconjugated UDCA confers integrity to the blood-retina-barrier promoting pericyte cell survival in a diabetic model (245), and could strongly modulate inflammation (247) and apoptotic markers (150).

Throughout this paper, the authors aimed to produce stable probucol-loaded microparticles that have potential beneficial effects in reducing oxidative stress in HEI-OC1 cells. For this aim, a cisplatin model representative for ototoxicity was investigated. β-CD, PEG 6000, PVP and PVA were used to increase probucol formulation water mixability prior to obtaining spray dried microparticles. Formulation feed-stock rheology and surface tension was characterised before spray-drying as well. Microparticles collected were characterised for zeta potential, particle size distribution and surface morphology. Additionally, probucol functional groups as well as the drug's concentration, stability and degradation results are presented. The addition of UDCA in formulations was evaluated by the effects observed on probucol's drug content and microparticle dissolution. Lastly, we tested the combination of water-soluble polymers with β-CD to facilitate probucol *in vitro* applications in HEI-OC1 cells by cell proliferation, and mitochondrial energy production assays.

3.4.2. Materials and Methods

β-CD (molecular weight 1134.98 (MW g/mol)), PEG (MW 5000-7000), PVP (MW 111.14), PVA (MW 14000), cisplatin (>98%), DMSO (99.7%, sterile), 2′,7′-dichlorofluorescin diacetate (DCF-DA; ≥97%), paraformaldehyde (PFA), and Hoechst 33258 were purchase from Sigma-Aldrich (Merck, Darmstadt, DE). Probucol powder (≥97%; MW 516) supplied from Beijing Natural-Med Biotechnology Co Ltd (Beijing, China) and UDCA (≥99%; MW 392) from Qingdao Yuanrun Chemical Co., Ltd (Qingdao, Shandong, China). 3-(4,5-dimethylthiazol-2-yl)-2,5-diphenyltetrazolium bromide (MTT; 98%) were purchased from Thermo Fisher Scientific (MA, USA). DMEM, trypsin-ethylenediaminetetraacetic acid (trypsin-EDTA; 0.25%) from Biosciences, Gibco™, Dublin, IE). Phosphate buffer saline (PBS) from Fisher biotech (WA, AU). Foetal bovine serum (FBS) from Serana (Brandenburg, DE). Seahorse XF cell mito stress tests, and plates XFe/XF96 purchased from Agilent Technologies (Santa Clara, CA, USA). Acetonitrile HPLC grade purchased from ChemSupply (Gillman, SA, AU).

Caution: the following chemicals are hazardous and should be handled and disposed appropriately; cisplatin, PFA, DMSO, DCF-DA, MTT.

Formulation Design

Powder components (2% *β*-CD, 2.3% PEG, 1.3% PVP, 0.8% PVA) were mixed with either UDCA (0.3%), probucol (0.6%) or both in milli-Q water. The solutions were stirred at ~500 rpm for 6 hours, then kept in a water bath at 50°C to fully dissolve *β*-CD. Spray drying was done by passing the formulation solution through a 0.7 μm nozzle on a Büchi Mini Spray Dryer (B-290 model, Flawil, CH). Inlet temperature set at 150 ± 2°C, 80% aspirator power, and 15% pump flow. Freshly spray dried formulations were kept in glass vials at room temperature until further analysis.

Rheology, Surface Tension, and Zeta Potential

Prior to spray drying, the formulation's rheological properties, zeta potential and surface tension were analysed at room temperature (22 ± 2°C) on a tensiometer (Sigma 703D, Biolin Scientific, Stockholm, SE) and viscometer (Visco-88, Malvern Instruments, Malvern, UK). Viscosity, torque, shear stress and shear rate

measurements were recorded using a parallel-plate system (30 mm) at 20, 35, 61, 107, 187, 327, 572 and 1000 rpm speed. Both spray drying feed-stock and post-spray dried microparticle's zeta potential was recorded using a zetasizer (3000HS, Malvern Instruments, Malvern, UK). Serum-free cell culture media (reflective index 1.34) was used as dispersant liquid for microparticles (1.25 mg/mL), and formulation feed-stock remained undiluted. Analysis was carried at 25°C in a disposable folded capillary cell.

Particle Size Distribution

To determine the size distributions of the solid dispersions, samples were dispersed in DMEM and analysed on a Mastersizer 2000 (Malvern Instruments, Malvern, UK). The Hydro 2000SM model was used with dH_2O as dispersion fluid agitated at 1890 rpm. Recordings consisted of 12 seconds measurements with 12000 snaps per measurement to generate 4 reports per sample (n = 3). Mean sample obstruction of 12.44 ± 2.7%. The average particle size distribution in micrometres (d0.1, d0.5 and d0.9) was recorded from the integrated software.

Probucol Concentration

Based on our previous protocol (33) probucol concentration from microparticles was analysed on the Shimadzu HPLC instrument (SIL-20A model UV detector 245 nm detection wavelength, Kyoto, JP) using a Jupiter 5 µm C18, 300 Å, 250 x 4.60 mm 5 µ diameter (Phenomenex, Torrance, CA, USA). Samples consisted of UDCA-probucol (F5), probucol (F6) and control UDCA (F7) microparticles as well as acetonitrile blanks. Probucol were extracted from the microparticle matrix (1.25 mg/mL) with acetonitrile, sonicated for 5 minutes and filtered through a 0.22 µm Millex-GP syringe filter (Sigma-Aldrich, Merck, Darmstadt, DE) to remove matrix precipitate. Filtered samples and standards were placed in glass vials and 20 µL were injected into the HPLC. Probucol peaks detected at ~7 minutes were integrated against a probucol standard curve (1 – 0.03 mg/mL; R^2 = 0.99998). Final drug concentration is presented as probucol percentage.

Probucol Stability and Forced Degradation

To assess probucol within spray dried microparticles we performed temperature stability and pH dependent studies. F5-6 microparticles were dispersed in 0.2 M HCl,

NaOH or Na_2O_2 solutions and incubated at 37°C for up to 48 hours. Short term shelf-life stability was assessed for 1, 3 and 7 days at 22°C, 37°C or -20 ± 2°C. Lastly, to mimic probucol *in vitro* availability, 1.25 mg/mL of F5 and F6 were incorporated in DMEM and continuously stirred at 140 rpm and 37 ± 1°C. At different time intervals (0.25, 0.5, 1, 2, 3, 24 or 48 hours) aliquots were spun at 10^4 rpm for 5 minutes, sample supernatant was collected and processed for HPLC analysis as described. Room temperature samples were kept on the bench away from light (22°C), in a hot room at 37°C, or in the freezer to reach -20°C. Results were plotted as cumulative percentage.

Scanning Electron Microscopy

Spray dried particle surface topography/morphology was investigated via the use of a field emission scanning electron microscope (SEM; Clara model, Tescan, Brno, CZ). Small amounts of freshly spray dried microparticles were placed on carbon adhesive tape and sputter coated with 5 nm platinum before analysing at 15 mm working distance, 2 kV and 100 pÅ beam current.

Fourier Transform Infrared Spectrometry

The attenuated total reflection accessory (UATR; PerkinElmer, MA, USA) was used to analyse spray dried microparticles. Small amounts of spray dried microparticle or bulk probucol powder samples were used to register the absorbance spectra. ATR spectrum generated on the fitted equipment software were normalised and converted to Fourier-transform infrared (FT-IR) for interpretation (32).

Cell Culture

Model HEI-OC1 cells were kindly received from Prof. Federico Kalinec (University of California at Los Angeles, CA, USA), and Dr. Young Joon Seo (Yonsei University, Korea). Cultures were kept and tested in permissive conditions at 33°C and 10% CO_2 levels. Cells were grown with DMEM supplemented with 10% FBS. For experiments, cells were detached from flasks using trypsin-EDTA, then seeded at a density of 2 x 10^5 cells/mL in 96 well plates. Seeded plates were grown overnight and treated for 24 or 48 hours in FBS enriched DMEM unless otherwise mentioned. Treatment consisted of F1-F7 dispersed in DMEM with or without cisplatin 13–35 μM. Corresponding blanks, cisplatin and healthy controls were prepared for each plate. Microparticles F1-

F7 were sterilised using a UV lamp for 20 minutes. Probucol quality remains unaffected after sterilisation.

Cell Proliferation Assay

All spray dried microparticle were dispersed in DMEM and tested at 5, 2.5 and 1.25 mg/mL on permissive HEI-OC1 cells. F5-7 microparticles showed good tolerability on HEI-OC1 at 1.25 mg/mL for 48 hours, thus this concentration was used for further experiments.

For cisplatin co-treatment, a 3.3 mM cisplatin-PBS stock solution was used to prepare 13–35 μM dilutions in DMEM without FBS. Microparticle F5-F7 treatments were applied 6 hour pre-incubation prior to 24 hours cisplatin exposure. We will refer to 24 hours cisplatin-treated groups as $F5^{+}$-$F7^{+}$. MTT solution was prepared according to manufacturer's protocol at 0.25 mg/mL PBS. At the end of each time point, cell plates were rinsed twice with 200 μL PBS and replaced with MTT-DMEM. Plates were kept at 33°C for 2.5 hours. The supernatant was removed, and formazan crystals were dissolved with isopropanol by agitating the plates on a rotary shaker for 5 minutes. Absorbance for each well was measured at 560 nm on a Multimode plate reader (EnSight, PerkinElmer, MA, USA). Results were normalised against healthy control (100%) and blank wells (0%).

Cellular Antioxidant Assay

A modified version of the previously described antioxidant assay (343) was used to determine cellular ROS accumulation. In sum, to assess probucol's antioxidant effects on cisplatin-treated HEI-OC1 cells, microparticles were used at a concentration of 1.25 mg/mL. In this instance, F7 was set as a negative control, while F5 and F6 formulations represented the experimental groups. Briefly, cells were treated with microparticles for 6 hours, media was then replaced with 35 μM cisplatin and kept for 24 hours at permissive conditions. Cells were then incubated with 10 μM DCF-DA in DMEM without FBS for 20 minutes. Cells were washed with PBS and immediately imaged on an inverted Nikon epi-fluorescent microscope at 485 nm excitation and 535 nm emission, 200 microseconds exposure time with 250 ISO. Fluorescence intensity was quantified using ImageJ (344) based on multiple images from each group (n = 3). Results were normalised against total cell numbers stained with Hoechst nuclear dye.

Oxygen Consumption Rates and Extracellular Acidification Rates

Cells were seeded on 96 well plates (XFe96 FluxPak) and treated with 1.25 mg/mL F5-7 microparticles dispersed in FBS rich DMEM for 6 hours. Treatment medium was replaced with fresh DMEM or 35 mM cisplatin. After 24 hours, the plate was washed with 200 µL phenol red free DMEM twice. Seahorse reagents were diluted as follows – oligomycin (OMY; 100 µM), rotenone antimycin A (ROT/AA; 50 µM), and carbonyl cyanide-4 (trifluoromethoxy) phenylhydrazone (FCCP; 100 µM) were dissolved in phenol red free DMEM. Seahorse cartridges (XFe96 FluxPak) contained 20 µL OMY, 22 µL ROT and 25 µL FCCP equilibrated for one hour. After analysis, each cell population was recorded. Cells were fixed with 4% PFA for 10 minutes, stained with nuclear Hoechst dye, and analysed in ImageJ. Seahorse results were normalised against cell counts corresponding to each well using the inbuilt Wave 2.6.3 software.

Statistical Analysis

Statistical analysis as area under the curve, *t test,* one-way ANOVA, normalization, and graph representation was done on GraphPad Prism v.9 (GraphPad Software, San Diego, CA, USA). Significant results were considered if $p < 0.05$ (*) and $p < 0.01$ (**). Each assay was performed in triplicate ($n = 3$). Error bars represent standard error of the mean.

3.4.3. Results and Discussion

Formulation Characteristics; Rheology, Surface Tension

Regarding surface tension (**figure 3.1.C**), the addition of PVA (F4) to formulations significantly decrease surface tension compared with control formulations (F1-F3, $p < 0.0001$). Rheological analysis (**figure 3.1**) shows viscosity reduces with increased speed, suggesting that all formulations perform as non-Newtonian liquids. All formulations present speed dependent rheological behaviour however this analysis does not consider time-depended structural decomposition and regeneration to confirm thixotropy. Shear stress increases in F5 opposed to F6 and F7 at 1000 rpm. Taking into consideration the rheological data and reduced surface tension results showing appropriate fluid conditions to be applied for spray drying.

Particle characterisation analyses

SEM analysis shows that microparticles are round and smooth with no deposits (**figure 3.3**) Spray drying outlet temperature remained high around 58-65 ± 3.61°C. Mastersizer particle analysis shows a bimodal size distribution which is part may corroborate SEM size variation findings. The overall span values relate to broad sample distributions with an average 23.60 ± 15.49 μm and with only F2, F4, F5, F6 show a narrower size distribution. Half of the size distribution for F5-7 consists of 5-43 μm (**table 3.1**) and show similarity with other reports (335). Our results require further validation as we observed a high weight residual percentage of 23.6 ± 15.49. Zeta size analysis was performed in DMEM as dispersion fluid to better reflect *in vitro* applications. Pre-formulation feed-stock zeta potential was recorded without dilution. The results presented in table 3.2 show that spray drying feed-stock and microparticles have weak negative charge reflective of the poor stability in solution and predictive of particle aggregation. FT-IR peaks are summarised in figure 3.2; corresponding probucol peaks around the 3631 cm^{-1}, 2950 cm^{-1}, 1422 cm^{-1} bands are not present in the final microparticles, perhaps due to limited probucol content within the particles.

Drug Content, Release and Stability

HPLC was used to detect probucol concentrations within spray dried microparticles. From a 10 mg sample size we calculated a probucol percentage of 6.49 % in F5, and 5.38 % for F6, respectively (**table 3.3.iii**). Consistent with our previous findings (345), the addition of bile acids to formulations enhance drug encapsulation capacity (**table 3.3.iv**). In the current example, UDCA incorporated to F5 formulation resulted in higher, non-significant encapsulation capacity compared to F6. In terms of probucol's stability once encapsulated, results suggest no clear significant degradation and drug breakdown patterns over the study period at three temperature settings (-20, 22 and 37°C; **figure 3.4.A**). To note that after seven days probucol sample percentage reached ~90% for both F5 at -20°C and F6 at 37°C. We then performed forced degradation and probucol microparticle release studies to replicate the *in vivo* environment. Microparticles F5 and F6 show potential probucol degradation over a 24 hour period in the presence of 0.2 M HCl, NaOH and Na_2O_2 (**figure 3.4.C**). Acidic conditions suggest increased degradation by ~5% for both formulations; however, it is possibly more significant for F5 (p = 0.004) compared to baseline. Similarly, basic condition

account for ~10% and 13% degradation increase for F5 and F6, respectively. This would indicate that probucol's *in vitro* availability is possibly limited by the microenvironmental pH, and intra-cellular degradation conditions, which can influence and dictate treatment dosage. Microparticles dispersed at 1.25 mg/mL in DMEM were used to measure probucol dissolution (**figure 3.4.b**). Probucol release was likely for F6 and F5 in the first 3 hours. A significant amount of probucol release from microparticles within the first 2 hour marked by a 15% difference between F4 and F5.

Cell Viability

All formulations were dispersed in DMEM at a concentration of 5 mg/mL and appropriate dilutions were made at 2.5 and 1.25 mg/mL. Treatments were applied on HEI-OC1 cell cultures for 48 hours to assess viability using MTT assay (**figure 3.5.a**). For cisplatin 24 hours exposure, probucol-UDCA (F5), probucol (F6) or UDCA (F7) microparticles were used at 1.25 mg/mL for 6 hours prior to the addition of cisplatin (**figure 3.5.b**). F5 microparticle treatment presents the strongest protective effects against cisplatin insult. HEI-OC1 cell survival after cisplatin exposure is significantly increased for $F6^{+}$ and more so for $F5^{+}$. F7 UDCA microparticles are tolerated by HEI-OC1 cells, yet at the current tested dose fail to prevent cellular survival after cisplatin.

Cellular Antioxidant Assay

The cellular antioxidant assay principle is based on the proportional conversion of a non-florescent dye precursor to fluorescent DCF in the presence of intracellular ROS; the higher the stressor the more intense the DCF signal. Cells were pre-treated with F5-7 for 6 hours prior to cisplatin application. ROS intracellular accumulation occurs due to cisplatin toxicity (322). Cisplatin-treated cells for 24 hours seem to show a significant increase in DCF signal compared to control (**figure 3.6.a**). The increase in fluorescence signal and ROS accumulation reduces with probucol-microparticles addition in culture. In fact, ROS is likely to be present in $F5^{+}$-7^{+} treatments but with less intensity than cisplatin control. F5 microparticles performed better than F6 in reducing ROS levels. The DFC increase for $F7^{+}$ might reflect the previously discussed MTT findings where F7 treatment alone cannot fully restore cellular proliferation after cisplatin. Microparticles containing UDCA and probucol (F5) applied for 6 hours are

probably sufficient to lower ROS accumulation in HEI-OC1 cells after cisplatin exposure.

Measurement of Oxygen Consumption Rates and Extracellular Acidification Rates

Following Seahorse analysis, cisplatin-treated HEI-OC1 cells exhibited compromised baseline mitochondrial respiration (**figure 3.7**), with limited maximal capacity and non-mitochondrial respiration (**figure 3.7.E, F**). F6 and F7 treated cells followed by $F6^{+}$, and F5 appear to have higher oxygen consumption rates (OCR) than control (**figure 3.7.B**). Seahorse extracellular acidification rates (ECAR) reveal higher levels in the cisplatin group compared to control and $F5^{+}$-7^{+} treatments groups (**figure 3.7.A**). From plotting ECAR together with OCR (**figure 3.7.B**), there seems to be a notable incline for HEI-OC1 cells to function in anaerobic conditions when treated with cisplatin. A significant increase in ATP production is noted between F5 and F6 groups, and F6 and $F7^{+}$, respectively (**figure 3.7.H**). In terms of energetic percentage profile, ATP production (**figure 3.7.C**) increases for cisplatin, F6 and F7. Proton leak (H^{+}) is significantly higher in the control group (control, F5, F6, F7;) compared to cisplatin treatments (**figure 3.7.I**). The similar ATP production between control and cisplatin groups with a slight decrease for $F5^{+}$-7^{+}, along with no significance in maximal respiration (**figure 3.7.E**) may possibly reflect minimal damage to mitochondria during cisplatin treatment in the first 24 hours of exposure.

3.4.4. Discussions

In this paper we present spray dried solid dispersions composed of probucol-bile acid-polymer water-based formulations that can produce spherical smooth microparticles consistent with literature findings (335, 336). The surface imperfections (grooves and depressions) seen in F1-F7 microparticles could be attributed to higher formulation concentration rather than the drying rate since our outlet temperature showed minimal variation (58-65 ± 3.61°C) (346). Pre-formulation feed-stock varies in zeta potential depending on formulation type showing slight negative particle charge. Although our analysis is qualitative, the close to neutral zeta potential as well as the feed-stock turbidity point to unstable pre-formulation. PVP as well as PVA and PEG are common spray dried polymer ingredient for APIs to increase drug solubility (334). Viscosity, sheer thinning behaviour, surface tension and polymer solvent mixability are important

factors in spray drying droplet formation and filament diameter evolution (347). High surface tension requires more energy to form particles, and the addition of PVA is anticipated to reduce solutions surface tension (348). We note a significantly decreases in F4 surface tension by ~11 units compared to F3 and maintained similar values with addition of probucol or bile acids into the pre-formulation.

All microparticles showed broad FT-IR peaks between 3200 – 3500 cm^{-1}, consistent with hydroxyl group bond stretching. Such groups are also found in *β*-CD, PVA, and PVP dry powders. All formulations also showed a sharp peak around 2880-2900 cm^{-1}. This is characteristic of alkane C-H bond stretching. This bond stretching is also noted in all the dry, separate powders. F3-7 show a sharp peak at 1650 – 1750 cm^{-1}. This is consistent with a peak at a similar position in UDCA, PVA, and PVP and suggests C=O bond stretching, consistent with aldehydes, ketones, and carboxylic acid functions groups found in these chemicals. Interestingly, the sharp probucol peak at 3550 cm^{-1} was not detected in any of the probucol containing formulations. This may suggest that probucol may be incorporated within the *β*-CD-polymer matrix. Consistent with previous findings from our group (345), the addition of bile acids to formulations enhances drug encapsulation. Furthermore, UDCA may have influence on polymer-drug ratio, formulation mixability, particle wettability and could decrease drug aggregation thus impacting API dissolution (335, 336). Our results show that UDCA potentially delayed probucol release from microparticles by ~14% *in vitro* in the first 2 hours of treatment. This might be accounted by UDCA ability to maintain stable APIs. It is known that under oxidising conditions probucol has the potential to degrade to spiroquinone and diphenoquinone (342), with impurities detected in our dissolution and forced degradation analysis. It is beyond the scope of the paper to analyse probucol impurities, yet the question of whether spiroquinone and diphenoquinone may hold the same beneficial effects *in vitro* or *in vivo* against cisplatin as probucol remains an open question.

Cytotoxicity, was observed in F1 microparticles containing only 2% *β*-CD, leading to approximatively 50% proliferation compared to controls. Cyclodextrins are known to interfere with cholesterol, which in turn affect the stability of mechano-protein prestin in cochlear hair cells (271). However drug delivery strategies that include *β*-CD in combination with drugs and other molecules can maintain treatment efficacy (349). The addition of polymers such as PEG (F2-F7) was sufficient to reduce *β*-CD negative effects. At 1.25 mg/mL F3, F4 show high viability, F5 peaking at 2.5 mg/mL whilst F2

viability remains at roughly the same levels. F7 maximum viability was observed at higher concentration (2.5 mg/mL). Probucol-UDCA microparticles (F5) show a slight decline in growth after 48 hours at 1.25 mg/mL compared to 2.5 mg/mL (**figure 3.5.A**). F5 and F6 show promising results *in vitro* in preserving cell proliferation after cisplatin treatment ($F5^+$, $F6^+$).

While there is a slight increase in spare respiratory capacity for cisplatin control and cisplatin treatments, significant changes relate to F5 and F7, and F7 to $F6^+$ (**figure 3.7.F**). The increased trend might not be completely consistent with other findings where spare reserve capacity decreases upon chemotherapy treatment (temozolomide for U251 and UTMZ cells) (350). The cells' ability to respond to stress corresponds with an increased reserve capacity as well as an increase in ATP production and use. ATP depletion in these reserves can potentially lead to cellular death. This correlation can be better observed in figure 3.6.D where most of the bioenergetics profile for cisplatin, co-treatments (F5-$F7^+$) and F5 show increased percentage values for spare respiratory capacity. Group profile percentage (**figure 3.7.C**) for non-mitochondrial respiration and relative values (**figure 3.7.G**) are different to published studies (351). Moreover, the decrease in $F5^+$-7^+ may be cross-referenced with the previously described low CAA results within these groups. Perhaps taken in consideration along with the CAA analysis; higher ROS levels (**figure 3.6**), and higher spare respiratory capacity (**figure 3.7.F**) combined with low non-mitochondrial respiration (**figure 3.7.G**) values might potentially reflect a better chance of cellular HEI-OC1 survival against cisplatin insult.

3.4.5. Conclusions

In conclusion, the presented formulations are suitable for spray drying purposes, which represents a facile method to incorporate the lipophilic antioxidant probucol into aqueous suspensions. Formulations based on *β*-CD, PEG, PVP and PVA improve probucol's mixability. UDCA added as an excipient minimally increased probucol retention in microparticles and improved probucol release *in vitro.* Our observations show that the formulation concentration and the spray drying conditions are favourable to obtain probucol solid dispersions with minimal surface imperfections. The total drug content is quantifiable by HPLC, with no degradation observed post-spray drying thus ensuring probucol stability (see Supplementary III.5 and III6). Addition of UDCA in formulation with probucol (F5) increased drug load and delayed probucol release. The

slower yet higher drug release to HEI-OC1 cells enhanced their survival and reduced ROS cellular-accumulation ensuring the positive effects of probucol-based therapy. In terms of HEI-OC1 mitochondrial oxygen consumption observed through Seahorse analysis, control and microparticle treated cells have similar or higher basal respiration, spare respiratory capacity, and maximal respiration levels. Probucol microparticle treatments promoted HEI-OC1 energy-producing capabilities even under cisplatin-induced stress by increasing the cell's higher maximal respiration, spare capacity, and lower proton leak and non-mitochondrial respiration. Survivability of F5 treatments and combinations with cisplatin ($F5^{+}$-$F7^{+}$) follows the overall spare respiratory capacity increase. More research is required to assess probucol-loaded microparticle effects *in vivo* against cisplatin and other ototoxic insults alike.

Acknowledgments

The authors acknowledge the Australian Postgraduate Award and the Curtin Research Scholarship for their support. We would address our gratitude to the Curtin University staff members who provided inductions and access to the laboratories based in the Pharmacy Building, the microscopy and cell culture suite at Curtin Health Innovation Research Institute and the scanning electron microscope at the John de Laeter Research Centre. We are grateful to use the House Ear Institute-Organ of Corti 1 cells provided by Prof. Federico Kalinec and appreciate the knowledge of working with these cells to Dr. Young Joon Seo.

Funding

The work is partially supported by the European Union Horizon 2020 research project and innovation program under the Marie Skłodowska-Curie Grant Agreement No 872370. Curtin Faculty ORS-WAHAI Consortium, the Australian National Health and Medical Research (APP9000597).

Conflicts of interest

Al-Salami H. has been and is currently receiving of funding from Beijing Nat-Med Biotechnology Co. Ltd. and Glanis PTY Ltd. All other authors have no completing interest to declare.

Data Availability

The data that support the findings of this study are available from the corresponding author, Al-Salami H., upon reasonable request.

Author contribution

CMI, MM, AM and HAS conceptualised and designed the project. The main draft of the manuscript was prepared and assisted by all authors, who contributed effectively to the final draft.

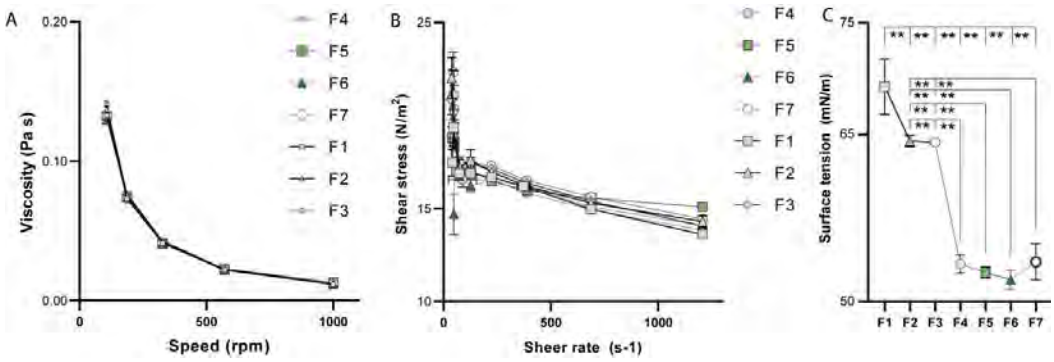

Figure 3.1.

Rheology and surface tension of pre-formulation mixture. (A, B) Rheological results for F1-F7 feed-stock solutions, showing consistency between formulations in viscosity with increased speed, and shear rate over sheer rate. (C) The formulation surface tension significantly decreases with the addition of PVA starting with F4 to F7. Error bars represent standard error of the mean; $n = 3$, ($p <$

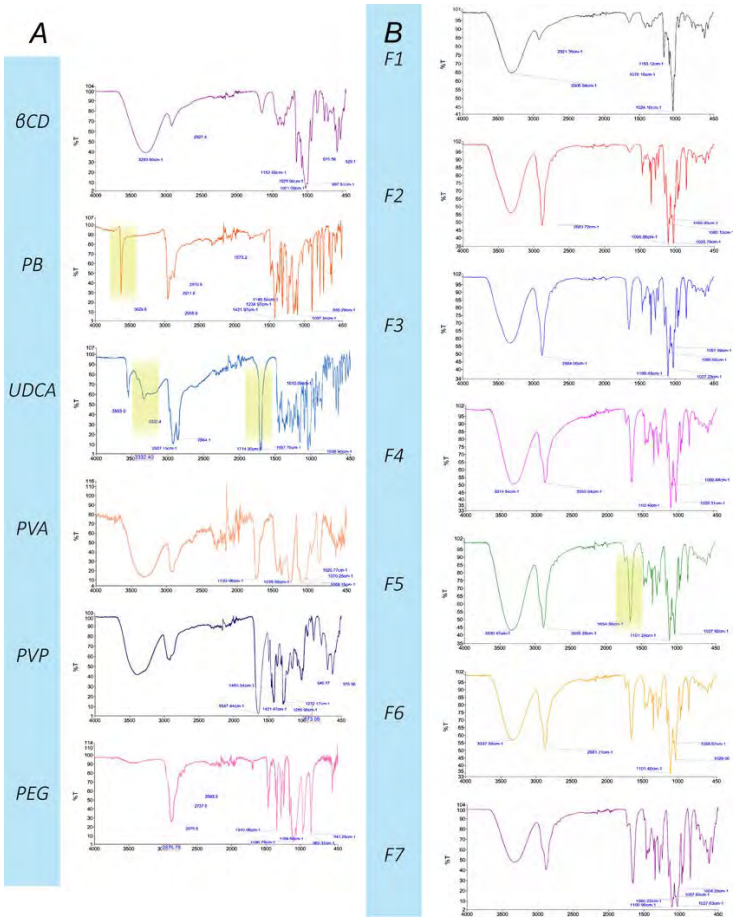

Figure 3.2.

Normalised FT-IR spectra cover the range of 4000-400 cm^{-1} at room temperature. (A) powder formulation ingredients, including probucol (PB) where probucol-specific bands peak at 3632 and 2957 cm-1. (B) Corresponding FT-IR spectra from spray dried microparticles. Probucol specific bands are not present in F5 and F6. This indicates that probucol may be present in quantities below the detection limit or, the drug is well incorporated within the formulation matrix (no crystalline drug structure – see figure 3.3 and Supplementary III.12).

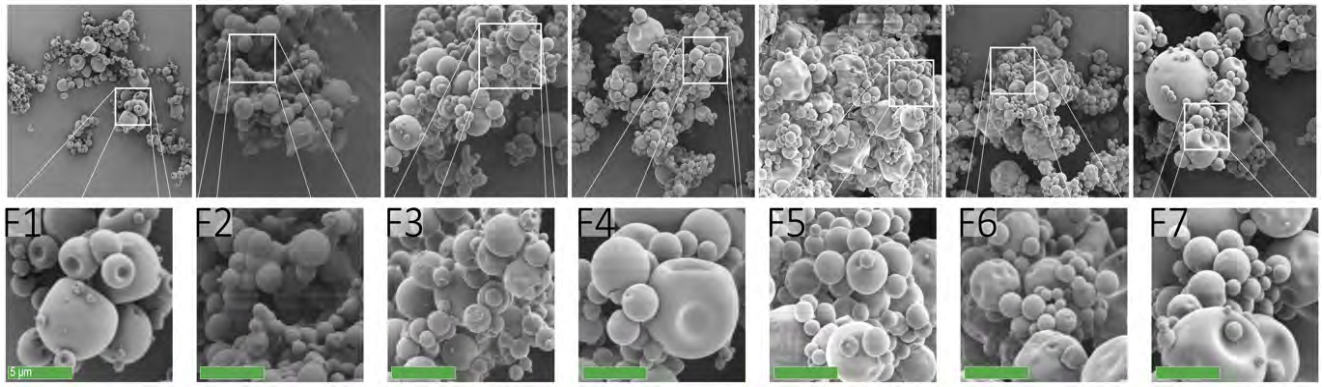

Figure 3.3.

Scanning electron micrographs of solid dispersions post-spray drying. Particle surface is smooth with no surface deposits reflective of well-optimised components with no presence of drug crystallisation. The limited outlet temperature variation (58-65 ± 3.61°C) prevented particle deformities and ensured efficient drying; scale bar 5 µm. Supplementary III.3 shows particle shape uniformity regardless of the bile acid used. For compresence, Supplementary III.8-III.11 contains more spray dried solid dispersion formulations that present coalesced particles.

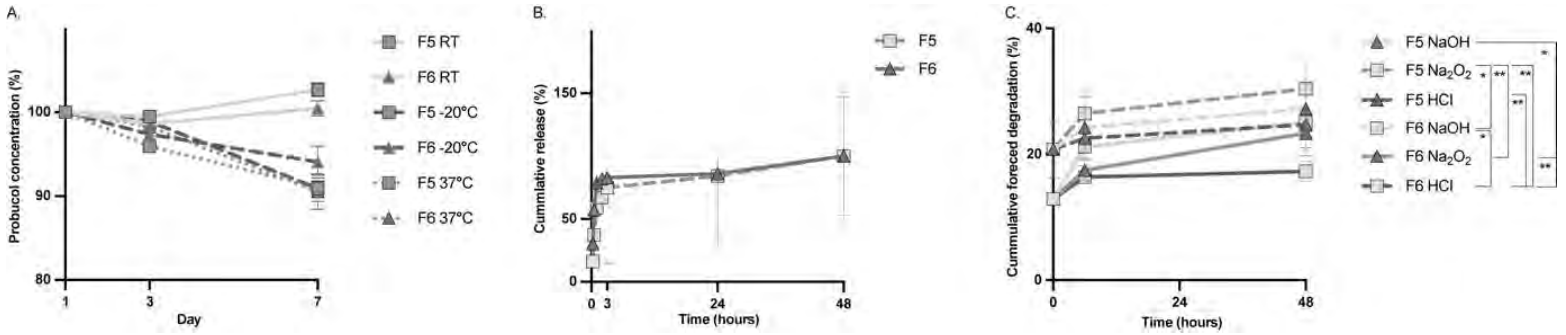

Figure 3.4.

HPLC quantification of F5 and F6 probucol content from post-spray dried microparticles. (A) Probucol shelf-life percentage availability decreases insignificantly over the duration of one-week at room temperature (RT) 22°C, -20°C or 37°C. (B) Probucol relative release (dissolution) shown as total percentage from 0.25, 0.5, 1, 2, 3, 24 and 48 hour time points at 37°C. Both formulations follow a similar release pattern, however F6 has an increased release in the first 3 hours. (C) Cumulative forced degradation of F6 and F5 in 0.2 M HCl, NaOH or N_2O_2 for 6 and 48 hours at 37°C. This shows an increased probucol degradation in acidic solutions. Error bars represent standard error of the mean, $n = 3$; *$p < 0.05$, **$p < 0.0$. Supplementary III.4 and III.7 shows the effect of different bile acids on probucol microparticle content as well as the variation in drug release patterns.

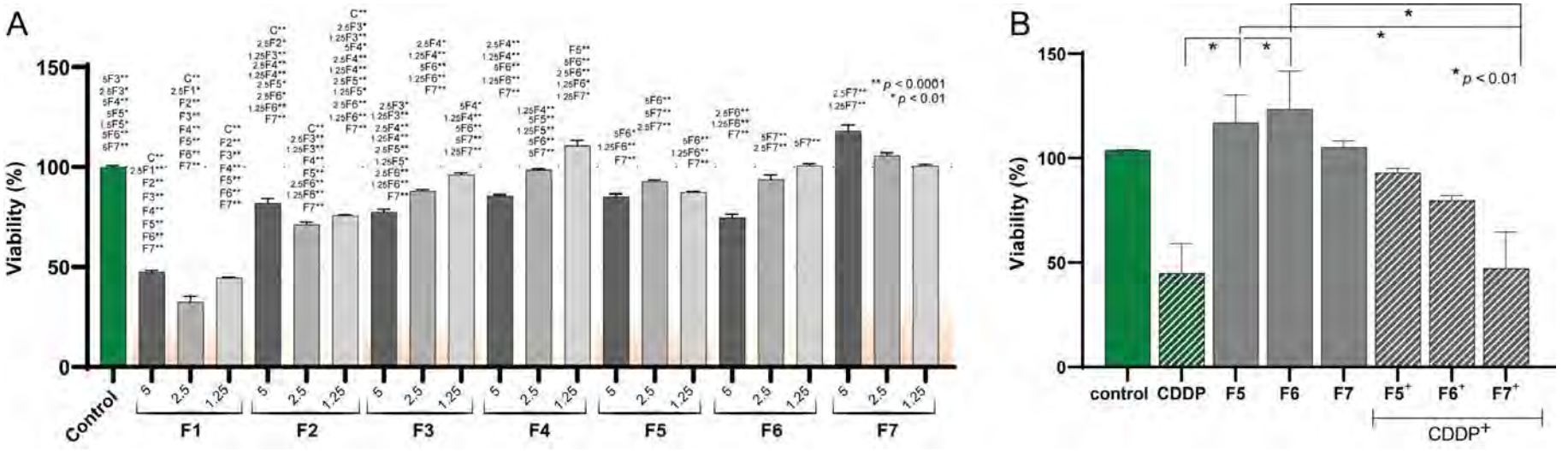

Figure 3.5.

Solid dispersion microparticles *in vitro* application on HEI-OC1 for 24 and 48 hours. (A) MTT assay results following F1-F7 treatments 48 hours at three different concentrations (5, 2.5 and 1.25 mg/mL). Microparticle safety benefits from the inclusion of multiple formulation components. Lower (1.25 mg/mL) probucol, yet higher (5 mg/mL) microparticle amounts are well tolerated by HEI-OC1 cells; (B) 6 hours pre-treatment with 1.25 mg/mL F5-7 without or with cisplatin (35 μM as $F5^{+}$-7^{+}) for 24 hours ($p < 0.01$). The probucol load within microparticles is successfully released in culture and protects cells against cisplatin damage. Control (green), CDDP: cisplatin (stripe green), F5-7 without CDDP (grey), F5-7^{+} with CDDP (stripe green). Error bars represent standard error of the mean, $n = 3$, *$p < 0.05$, **$p < 0.01$.

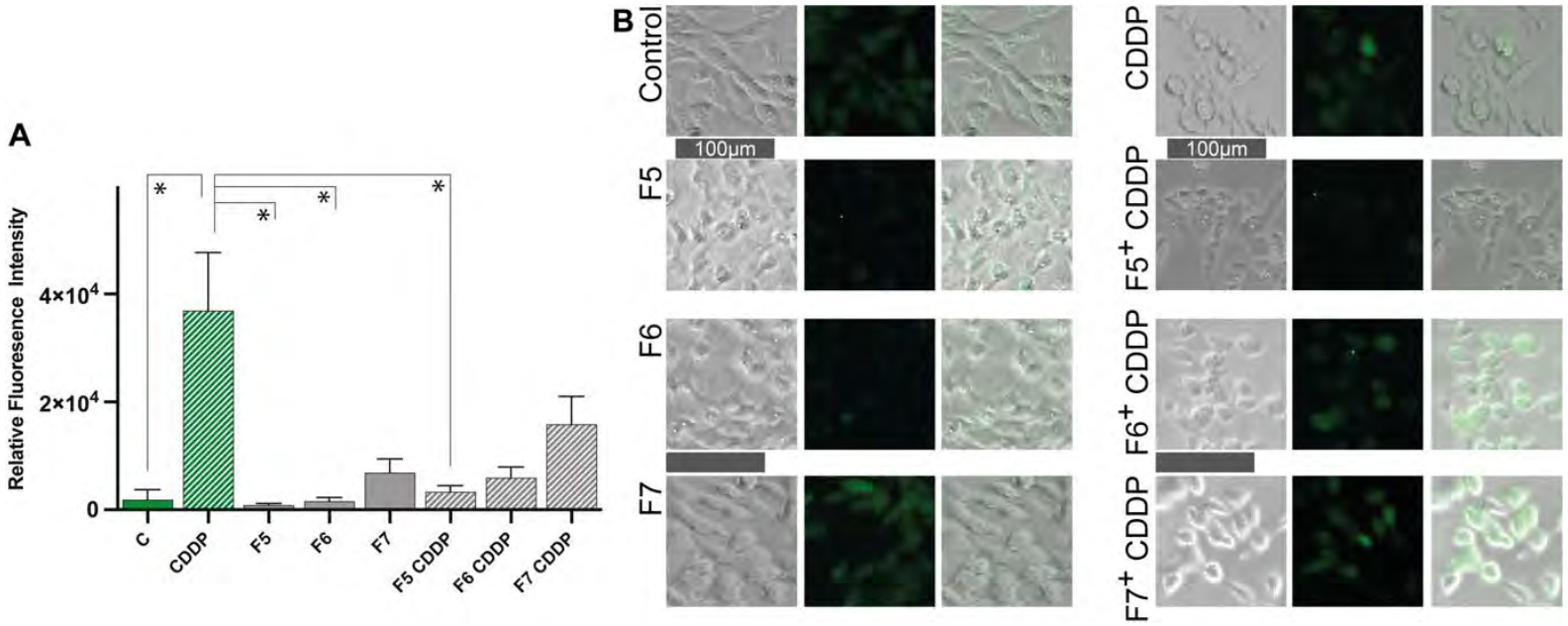

Figure 3.6:

Cellular ROS accumulation detected after 24 hours *via* dichlorofluorescein signal (DCF); cells were pre-treated with 1.25 mg/mL microparticle formulations for 6 hours, followed by cisplatin exposure. (A) Cell-normalised DCF quantified signal of (B) bright field and fluorescence micrographs. Cisplatin increases ROS accumulation as seen through the increase in DCF signal. Probucol-loaded microparticles significantly reduces DCF signal and ROS accumulation in HEI-OC1 cells. Control (green bars), CDDP: cisplatin (stripe green bars), F5-7 without CDDP (grey bars), F5-7^{+} with CDDP (stripe green bars), scale bar 100 µm, error bars represent standard error of the mean, $n = 3$, $*p < 0.05$.

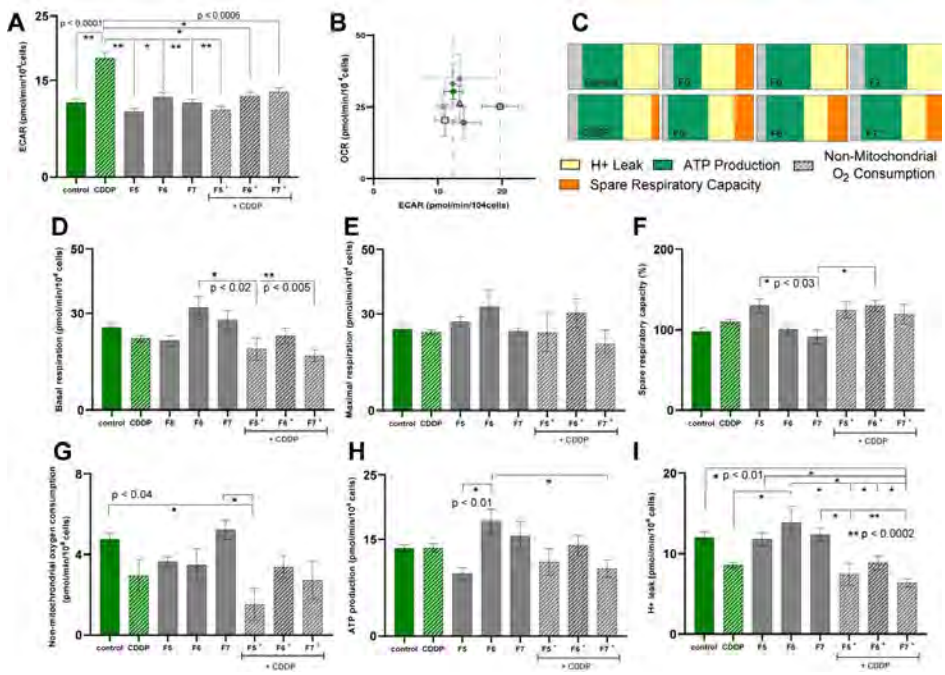

Figure 3.7.

HEI-OC1 bioenergetics profile. (A) Extracellular acidification (ECAR) values. Treatments show significant lower ECAR values similar to control, reflecting normal metabolic activity and mitochondrial respiration. (B) Baseline respiration OCR and ECAR correlation; dotted vertical lines mark control and cisplatin groups. The cisplatin-treated group higher ECAR reflects an increased glycolysis for energy production. (C) Bioenergetic profile representation for each group; non-mitochondrial O_2 consumption (striped light grey), ATP production (green), H+ (proton) leak (yellow) and spare capacity (orange). (D) Basal respiration reflects the cell's normal energy requirements. The F6 probucol formulation show elevated energy levels. (E) Maximal respiration and (F) spare respiratory capacity reflect the cell's ability to respond to an increase energy demand such as stress. (G) Non-mitochondrial respiration reflects cellular energy consumption during high-demand cellular processes such as ROS production. (H) ATP production reflective of mitochondria function and activity. (I) Proton (H^+) leak across the mitochondrial membrane that is not contributing to ATP production. Lower values reflect more oxygen contributing to ATP production, higher values suggest mitochondrial disfunction. Control (green bars), CDDP: cisplatin (stripe green bars), F5-7 without CDDP (grey bars), F5-7$^+$ with CDDP (stripe green bars). Normalised per 10^4 cells. Error bars represent standard error of the mean, $n = 4$, $*p < 0.05$, $**p < 0.01$.

Formulation	d(0.1) (µm)	d(0.5) (µm)	d(0.9) (µm)	Span
F1	0.095 ± 0.001	8.92 ± 1.08	694.26 ± 187.67	77.48
F2	1047.64 ± 10.01	1357.49 ± 9.06	1675.063 ± 7.63	0.46
F3	2.16 ± 1.31	4.22 ± 2.52	10.82 ± 2.00	6.76
F4	130.65 ± 2.79	226.60 ± 4.03	421.53 ± 25.05	1.28
F5	0.58 ± 0.04	5.64 ± 2.22	121.37 ± 116.25	17.69
F6	0.62 ± 0.008	12.02 ± 0.06	28.67 ± 0.35	2.33
F7	0.97 ± 0.05	43.72 ± 44.15	257.50 ±1 3.95	17.95

Table 3.1.

Mastersizer size distribution of post-spray dried microparticles. Size distributions are divided into three populations corresponding to less than 10% - d(0.1), 50% - d(0.5) and more than 90% - d(0.9) sizes. For F5, the majority of particles (50%) fit within the 5.64 µm and more than 90% are over 100 µm. The varied distribution corroborates SEM observations (figure 3.3); ± standard error of the mean.

Formulation	*Pre-spray drying feed-stock (mV)*	*Post-spray drying – microparticles (mV)*
F1	-4.21 ± -3.27	-3.67 ± 0.66
F2	6.19 ± 0.41	-2.65 ± 0.40
F3	4.57 ± 0.69	-2.77 ± 0.29
F4	0.37 ± 0.27	-1.49 ± 0.38
F5	-0.41 ± 0.16	-1.41 ± 0.34
F6	-0.22 ± 0.09	-1.33 ± 0.23
F7	0.56 ± 2.07	-3.80 ± 0.95

Table 3.2.

Zeta potential values for pre-formulation and post-spray dried microparticles. For microparticles, the dispersant liquid represents cell culture media. The more neutral values recorded for the feed-stock zeta potential reflects poor particle stability within these mixtures and a tendency to precipitate. In contrast, the negative values of the post-spray dried microparticles improves particulate repulsion in liquids. Pre-formulations feed-stock and microparticle dispersions required an average of 19.08 ± 21.58 respectively 69 ± 25 zeta acquisition runs; table values represent millivolts ± standard error of the mean.

	i. Formulation	ii. Production Yield (%)	iii. Probucol Content (%)	iv. Encapsulation Efficacy (%)
F1	β-CD	56.35		
F2	β-CD + PEG	38.13		
F3	β-CD + PEG + PVP	19.21		
F4	β-CD + PEG + PVP + PVA	64.71		
F5	β-CD + PEG + PVP + PVA + UDCA + probucol	33.47	6.49	10.82
F6	β-CD + PEG + PVP + PVA + probucol	28.04	5.38	8.97
F7	β-CD + PEG + PVP + PVA + UDCA	18.51		

Table 3.3.

Formulation components, production yield calculations, and probucol content and encapsulation efficiency; i. Formulation ingredients follow a set of controls (F1-F4 and F7) as well as the experimental probucol and probucol-bile acid mixtures; ii. Percentage yield following spray-drying; HPLC quantified probucol is used to calculate iii. drug content and iv. encapsulation efficacy from 1.5 mg/mL microparticle weight.

Chapter 4

Deoxycholic Acid as Excipient for Chitosan-Probucol Formulation Films

4.1. Publications

The work in this chapter is developed for publication as:

4. **Corina M Ionescu**, Bozica Kovacevic, Susbin R Wagle, Thomas P Foster, Armin Mooranian and Hani Al-Salami - Secondary Bile Acid-Polymer Based Micro-Films for Ear-Targeted Delivery of The Drug Probucol: Applications for Treating Hearing Loss.

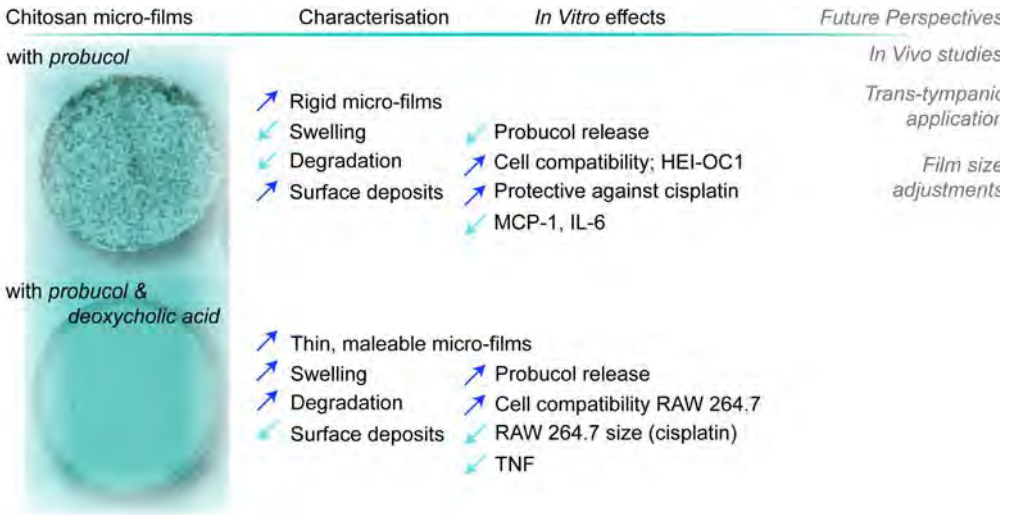

Graphical abstract 2. Chitosan-probucol and bile acids formulation.

Optical visualisation of chitosan-based membranes (films) containing micro sized probucol crystalline deposits (micro-films) compared to chitosan, probucol and deoxycholic acid (DCA) micro-films. The addition of DCA changes micro-film swelling behaviour, decomposition patters and affect differently cell cultures. Chitosan biocompatibility may have great advantages for future studies involving micro-film middle ear delivery.

4.2. Introduction

Chapter 4 continues exploring the use of probucol on HEI-OC1 with a different bile acid formulation. Previously discussed in Chapter II, DCA is regarded in literatures as pro-apoptotic, proinflammatory, and can disturb membrane integrity. This Chapter focus is on chitosan as the main pre-formulation component and takes in consideration DCA's known effects. DCA membrane permeation properties are paired with chitosan because of the polysaccharide's mucoadhesive and biocompatible properties. The use of spray dried chitosan-probucol-DCA particles is however limited by poor formulation dispersion into liquids (Appendix IV.2), therefore Chapter 4 characterises micro-film formulations. The use of micro-films is advantageous for middle ear drug targeting favouring prolonged drug exposure and improving drug release passage through the round window membrane. Thus, the importance of micro-film properties such as swelling, degradation and drug release are important and form the main points of Chapter 4. The pre-formulation addition of ethanol containing transonic gel (TGel) as well as *β*-CD were chosen to improve probucol mixability, and polypropylene glycol (PG) for its humectant properties. Chitosan micro-film swelling was tested in three aqueous conditions, as well as in direct contact cell culture with metabolites and enzymes. Experiments are carried out on *in vitro* HEI-OC1 cells gown in co-culture conditions with a macrophage cell line (RAW 264.7). Cisplatin induces HEI-OC1 proinflammatory cytokine production (TNF-*α*, interleukine-1*β,* and interleukin-6 (IL-6)) (352) subsequently aggravating cytotoxicity by macrophages recruitment. Macrophage activation is reported as a possible means for noise and age-related hearing loss, not only ototoxicity. Since probucol's anti-inflammatory effects were previously explored on macrophages, the Chapter investigates cytokine production of co-cultured HEI-OC1 and macrophages together with probucol (F4), DCA (F5) and probucol-DCA (F6) micro-films and their effects against cisplatin. Co-culture conditions are more stressful for cells and can lead to an increase in cytokine production even in control untreated cells, however it may better represent the cells' reaction to the addition of both cisplatin and micro-films. For these experimental conditions micro-films were placed on Transwell inserts in contact with the two cells lines (Appendix IV). This approach, in part, limits *in vivo* application similarly to how the round window would limit drug entry.

4.3. Summary

The graphical abstract 2 summarise this Chapter's findings. Firstly, the addition of DCA increases probucol retention within chitosan films. Incorporating PG to chitosan pre-formulation improves micro-film swelling. As a result, in combination with DCA swelling is significantly increased for DCA and probucol-DCA micro-films. The increase in swelling is marked by faster micro-film degradation *in vitro*, however probucol release remains similar and extends for ~3 days for both micro-films. Chitosan requires acetic solution to dissolve. The formulation homogenate dried as micro-films were hydrated with PBS prior to *in vitro* application, however this crucial step might minimise micro-film shelf storage (Appendix IV). Both cell types tolerate micro-films in culture, with RAW 264.7 showing preferable proliferation condition for DCA, and a decrease in macrophage size for probucol-DCA formulations. Unlike the results presented Chapter III, the HEI-OC1 cells tolerate probucol better than DCA or probucol-DCA-containing micro-films especially when challenged with cisplatin. Although the cisplatin conditions were previously optimised on HEI-OC1 (Appendix IV), the same concentration of cisplatin leads a decline in cell population in co-cultures. Appendix IV presents a variation to the micro-film pre-formulations production by adding an additional step (ingredients ground mixing) to evaluate the difference in micro-film drug content, appearance and swelling.

Publication 4

Abstract

Hearing loss is a serious medical condition with an increasing prevalence worldwide. Ongoing research aims to develop safer therapies that can either prevent, treat, or reverse hearing loss.

This study investigates DCA's suitability in designing new micro-films that can be used to deliver the lipophilic drug – probucol, into the middle ear by first assessing an *in vitro* model representative for ototoxicity, and inflammation.

Probucol-chitosan formulation gels were prepared by homogenisation and dried to form thin films (micro-films). Micro-film characterisation of polymer-matrix interaction, surface analysis, swelling, and probucol release were recorded using high-pressure liquid chromatography. *In vitro* compatibility was carried out by applying the

micro-films in culture with hearing representative cells (HEI-OC1), and a macrophage cell line (RAW 264.7).

Probucol-chitosan-based films show micron-sized surface deposits when dried, and after hydration. The probucol deposits appear well incorporated into the chitosan matrix. DCA used as an excipient increased probucol's formulation mixability, micro-film swelling, drug release and matrix degradation. Probucol-only micro-films performed better against cisplatin-challenged co-cultured cells in terms of viability and showed a reduction of the interleukin-6 marker.

Key words: *chitosan, bile acids, probucol, micro-films, ear delivery*

Highlights:

- Probucol can be used together with chitosan to form malleable micro-films.
- The addition of DCA to the formulation increases micro-film swelling and probucol release.
- Both probucol-chitosan micro-films with DCA are safe when applied to HEI-OC1 cells.
- Micro-films provide limited effects against the ototoxic agent, cisplatin; however, may prove useful in reducing inflammatory cytokines *in vitro.*
- The use of chitosan-based films may prove stable and advantageous to deliver probucol to the middle ear.

4.4.1. Introduction

Hearing loss is an ongoing social and economic burden primarily caused by age, noise-exposure, certain diseases, genetic factors, ototoxic medication, and injury. Hearing loss is classified as either sensorineural, conductive, mixed, or as auditory neuropathy spectrum disorder. Side effects from an anti-neoplastic medication, cisplatin (CDDP), used to treat an array of cancer types can lead to sensorineural hearing loss (SNHL) in paediatric and adult patients during and after chemotherapy treatment (353, 354). Cisplatin results in cellular stress and subsequent apoptosis. Research strategies that focus on maintaining the non-regenerative sensory organ of Corti and spiral ganglion cells are therefore required to combat hearing loss.

Probucol is a lipophilic bis-phenol molecule containing two sulphur atoms traditionally used as an antilipidemic drug. Poor water solubility yet high permeability properties place probucol as class II drug in the BCS. Probucol has also demonstrated useful antioxidant properties in both the kidney (8) and brain (7). The following review (10) discusses more of probucol's effects and its suitability for hearing loss research. Probucol has a low water solubility of < 5 ng/mL and requires the addition of excipients to improve *in vitro* and *in vivo* delivery (355). Studies show that oral bioavailability is significantly increased once crystalline probucol is mechanically reduced to an amorphous drug through ground mixture methods (15, 356) (see Supplementary IV.11-15). The addition of polymers (356) further increases probucol's solubility and improves the drug's pharmaceutical targeting potential. Previous studies from our laboratory have used bile acids as pre-formulation excipients for probucol as it increases particle rigidity and surface smoothness (32). Chitosan is a cationic polysaccharide formed from alkaline *N*-deacetylation of chitin, the second most abundant polymer in nature. Chitosan can be degraded by lysozymes and glycosidases and has been widely used for its anti-inflammatory properties (357), antimicrobial activity (358), low toxicity, mucoadhesive (359) and increased absorption properties (360). Chitosan, in combination with methylated β-CD and sodium caprate, show enhanced metformin (class III, BCS) and furosemide (class IV, BCS) permeation to intestinal cells (361). Trans-tympanic application of the steroid dexamethasone (class II or I/III, BCS) in combination with sodium caprate significantly increases round window membrane permeation, thus increasing dexamethasone accumulation in cochlear tissue (76). Chitosan, as well as the use of non-steroidal drugs-based strategies for inner ear delivery show great promise and require further attention.

Trans-tympanic and intra-bullar injections are two common procedures used for the delivery of drugs to the cochlea. Both techniques are considered routine and have reduced long-term impact on hearing ability (362). Short term for example, there is evidence of temporary conductive hearing loss, however the majority of treatments are removed through the Eustachian tube allowing recovery (363). The round window membrane is one of the primary physiological barriers for trans-tympanic or intra-bullar drug applications to enter the inner ear. Both nanoparticles derived from chitosan and chitosan solution downregulate tight junction proteins of the round window membrane, thus improving permeability (77, 364). Therapeutic applications can increase the thickness of the round window membrane without affecting basilar

hair cell numbers (365). It is important to consider that saline injections alone could alter the normal histology of the round window membrane to such extent as thickening the membrane and mobilising inflammatory cells (366). As opposed to traditional trans-tympanic approaches, residue fragments of chitosan placed in the middle ear cavity can persist *in vivo* for days or weeks (365, 367, 368). It is therefore important to balance formulation preparations, as they may either persist without clearance and cause toxicity, or clear faster than the time required for the APIs to pass the round window membrane. Chitosan enzyme degradation could accelerate clearing, minimise prolonged formulation-tissue contact, and favour controlled drug release during the clearing process (369). Commercially available chitosan has several variations. These include high, medium, and low molecular weight products. There are also water-soluble chitosan derivatives that can be considered (367, 368, 370), however the deacetylation degree of chitosan generally requires acidic conditions to dissolve. Multiple studies show that nanoparticle (371), liposome stability (369) and more importantly overall drug availability (372) is increased with the addition of chitosan in formulation. Furthermore, middle ear chitosan applications provided otoprotection against cisplatin *in vivo* (372). Cisplatin's effects can aggravate in acidic conditions. It is therefore important to consider how chitosan formulations pH changes and may affect hearing thresholds (373).

Based on their critical micellar concentration, bile acids can self-assemble and form nanosized particles in combination with chitosan (374, 375). DCA is a secondary bile acid produced by gut bacteria through 7α-dehydroxylation of the primary bile acid, cholic acid (201). Besides its importance in digestion and nutrient absorption, in excess DCA can significantly increase intestinal permeability (376), increase blood-barrier permeability (55), and negatively promote Golgi disassembly and induce endoplasmic reticulum stress (139). The bile acid concentrations utilised as excipients is often less than that found at physiological levels, thus reducing the chance of encountering significant side-effects. The impact of formulations on cochlear resident macrophages are crucial, as studies point to the negative effects of prolonged inflammation in aggravating cisplatin, noise and age-induced hearing loss (377-379). Therefore, it is important to observe the biocompatibility of drug formulations with macrophages. For example, DCA can induce nitric oxide and macrophage polarization *in vitro* and *in vivo* (145), thus requiring controlled concentration-dependent applications. The degree of chitin deacetylation, as well as chitosan concentration, appear to influence

macrophage phagocytosis, with previous research showing that chitosan microparticles are internalised by RAW 264.7 cells and impact the pro-inflammation signal response (380).

The following article aims to develop chitosan and probucol formulations for future middle ear delivery application by first assessing probucol micro-film biocompatibility *in vitro*. Two cell types (established auditory cell and macrophages cell lines) grown in non-contact paracrine co-culture were used to assess proliferation, morphology, and cytokine levels. Micro-film characteristics such as swelling potential, drug loading capacity, probucol stability and dissolution were recorded as well.

4.4.2. Materials and Methods

Medium molecular weight chitosan, *β*-CD, PFA, trypsin-EDTA (0.25%), cell proliferation reagent based on water-soluble tetrazolium salt, (WST-1), were acquired from Sigma-Aldrich (Darmstadt, DE). Polypropylene glycol (PG; molecular weight 76.09) was purchased from PCCA (Matraville, AU). Transonic gel (TGel) was purchased from Telic Group (Barcelona, ES). Acetic acid glacial was procured from Ajax Finechem, (Sydney, Australia). Probucol powder is supplied by Beijing Natural-Med Biotechnology Co Ltd (Beijing, China). DCA is supplied from Qingdao Yuanrun Chemical Co., Ltd (Qingdao, Shandong, China). DMEM purchased from Biosciences, (Dublin, IE). PBS acquired from Fisher biotech (WA, AU). FBS acquired Serana (Brandenburg, DE). Hoechst 33342 (H1399) and Pierce bicinchoninic acid protein assay kit (BCA) from ThermoFisher (Waltham, MA, USA). CytoPainter Cell Plasma Membrane Staining Kit Deep Red Fluorescence (Abcam, Cambridge, UK). Cytometric Bead Array flex kits for mouse monocyte chemoattractant protein-1 (MCP-1), tumour necrosis factor (TNF) and interleukin-6 (IL-6) were acquired from BD Biosciences (North Ryde, AU).

Micro-Film Preparation

Formulations were homogenised for 3 minutes in Milli-Q with 1% acetic acid. Each of the 6 formulations were prepared as follows: control F1 with *β*-CD only; control F2 with *β*-CD, TGel and chitosan; control F3 with *β*-CD, TGel, chitosan and PG; F4 with all control component and probucol; F5 with all control components and DCA; F6 with all control components, DCA and probucol. Homogenised formulations were

dried in 50 µL aliquots at room temperature (micro-films). The dried micro-films were used for characterisation and *in vitro* studies. Cellular compatibility was performed by coating the bottom outside surface of 6.5 mm Corning Costar Transwell cell culture insert (Sigma-Aldrich, Merck, Darmstadt, DE) with F4, F5 and F6 formulation.

Infrared Spectroscopy

To investigate the intramolecular interactions of probucol and the formulation components, we performed UATR (PerkinElmer, MA, USA) analysis on probucol powder, a mixture of F6 powder component as well as dry micro-films. Generated ATR spectra were normalised and converted to FT-IR spectra for interpretation utilising the in-built software (32).

In Vitro Studies

RAW 264.7 (ATCC®, TIB-71™) purchased from ATCC (Manassas, VA, USA) and HEI-OC1, from Prof. Federico Kalinec and Dr. Young Joon Seo, were used for experiments. HEI-OC1 were grown in non-contact co-culture with RAW 264.7 macrophages in permissive conditions (33°C). Bottom side of Transwell inserts were pre-coated with F4-F6 formulations. HEI-OC1 were seeded on inserts and RAW cells were seeded on Transwell wells. Micro-films were UV treated and hydrated with PBS 20 minutes prior to *in vitro* culture seeding. Experimental groups consist of F4, F5 and F6 formulations co-treated cells with or without cisplatin 3 µM (challenged). Control cells remained untreated.

Micro-Film Swelling Measurements

F2-F6 micro-films were immersed in various aqueous solutions for 20 minutes. Micro-film area was recorded using a stereo microscope (Nikon SMZ 745T, Tokyo, JP), before and after 20 minute hydration. Milli-Q water, PBS, and DMEM were used as hydration medium. Filtered DMEM media was obtained from HEI-OC1 routine passaging to better assess the swelling effects *in vitro.* Each sample was prepared in four technical replicates in triplicate (n = 3). ImageJ (344) was used to contour and measure micro-film area. For consistent imaging, dry and hydrated films were place between two glass slides when imaged.

Scanning Electron Microscopy and Elemental Analysis

Dry micro-films were adhered to carbon taped aluminium stubs and sputter coated with carbon or platinum at 5 nm thickness. Micrographs were acquired at 2 kV, 10 mm working distance and 100 Å current beam using a field emission SEM (Clara model, Tescan, Brno, CZ). Energy Dispersive Spectroscopy (EDS) was performed using (Oxford Instruments, Abingdon, UK) detector at 10 kV to acquire Kα sulphur peaks and 20 kV for Mα peaks platinum characteristic for probucol and cisplatin, respectively. Spectra were processed using the Aztec v.5.1 software (Oxford Instruments, Abingdon, UK). EDS was acquired on dry micro-films and cell culture media pre-hydrated micro-films.

High Pressure Liquid Chromatography

After formulation homogenisation, 50 µL of F4 and F6 homogenate as well as dried micro-films were resuspended in acetonitrile to extract probucol. To compere the accuracy of this extraction, dry micro-films were hydrated with Milli-Q water for 20 minutes followed by acetonitrile extraction (10:90). Suspensions were sonicated for 5 minutes and filtered prior to analysis on a 150 x 4.6 mm column (Luna 5 µm, 100 Å, Phenomenex, Torrance, CA, USA) HPLC (SIL-20A model UV detector, Kyoto, JP). For probucol dissolution studies, micro-films were incubated with HEI-OC1 in complete DMEM prior to probucol extractions. Injection volumes were 20 µL for both samples and standards (standard curve; 1 – 0.015 mg/mL, $R^2 = 0.99998$), $n = 3$.

Cell Density and Size

Three-day HEI-OC1 and RAW 264.7 cells co-cultures were washed with PBS prior to 4% PFA fixation. Cells were stained with nuclear (Hoechst) and plasma membrane (CytoPainter) dyes to determine morphological phenotype changes associated with macrophage activation, and to facilitate cell counting. After multiple PBS washes, the cells on the insets and in wells were stained with Hoechst and CytoPainter Cell Plasma Membrane Staining Kit in assay buffer according to manufacturer's protocol. Inserts were detached and mounted on glass slides with HEI-OC1 facing the coverslip. Slides and wells were imaged with the Andor Dragonfly High Speed Confocal Microscope System (Oxford Instruments, Abingdon, UK). Images were acquired on Imaris analysis software (Oxford Instruments, Abingdon, UK). Cell population for each group

was based on nuclei recordings and normalised against the control group (100%). RAW 264.7 cell area contours were traced and recorded. Final measurements were prepared in ImageJ.

Inflammatory Markers Assay

Before preparing the cells for imaging, culture supernatant from three-day HEI-OC1 and RAW 264.7 cells in co-cultures were collected and placed on ice. Cell supernatant was used to determine inflammatory markers using the Cytometric Bead Array Mouse TNF, IL-6 and MCP-1 Flex Kits. Following reagent protocols, capture and detection bead dilutions were mixed with 50 µL samples and analysed with the BD FACSCanto Clinical Flow Cytometry System (Franklin Lakes, NJ, USA). For each standard and samples 1500 fluorescent events were counted. Multiplexed samples were integrated using kit standards from 2500-20 pg/mL. Results were normalised against total protein concentration to account for cellular viability difference between groups. Total protein concentration from cell culture supernatant were integrated using a 2000-25 µg/mL standard curve following the Pierce BCA Protein Assay Kit. The cytokine ratio to total protein was then calculated and expressed as [pg of cytokines]/[mg of total protein].

Statistical analysis

Data analysis was done using GraphPad Prism v.10 (GraphPad Software San Diego, CA, USA). Graph representation, one-way ANOVA, normalisation, or t test were prepared on the same software.

4.4.3. Results

Chitosan Micro-Film Characterisation

Except for F1, all chitosan-containing formulations formed thin malleable films that were cut and analysed for surface deposits. F2 and F3 present similar crystalline deposits that may represent undissolved *β*-CD. Mid-sections of F3 hold well defined groves with uneven deposit patterns (**figure 4.1-F3-a**). F2, F5, F6 show smooth, well-incorporated, dense layers, and probucol F4 micro-films appear thinner. Surrounding the micro-films and around edges are uneven clusters including probucol crystals. On the surface (**figure 4.1-F4-c**) as well as superficially embedded in the matrix (**figure**

4.1-F4-d), these structures are likely probucol and *β*-CD. DCA containing micro-films (**figure 4.1-F5**) are smooth-transparent, with minimal surface deposits.

To distinguish between probucol and other surface deposits, EDS was performed at 10 kV to detect sulphur Kα peaks. Results show (**figure 4.2**) that probucol is present on the surface of F4 and F6 micro-films as expected, unlike F3 and F5 that do not contain probucol. Large crystalline deposits characteristic for unhomogenised *β*-CD on F3 are not present after hydration (**figure 4.2-E, I**). Probucol crystals embedded within the film matrix are still visible in less abundancy, even after hydration within F4 and F6 micro-films (**figure 4.2-F, H, J, L**).

Cisplatin adsorption from media culture was investigated at 20 kV to detect platinum Mα peaks present form cisplatin. No conclusive results were made (**figure 4.2-I-L**) possibly due to the low cisplatin concentration or the limited detection capacity of the instrument (381). Interestingly, the micro-films cultured with HEI-OC1 show trace elements adsorbed on the matrix surface from the short exposure (**figure 4.2-E-L**) revealing sodium, potassium, or chlorine peaks.

FT-IR stretching vibration at the 3631 cm^{-1} band (**table 4.1**) is likely to correspond with free hydroxyl groups (382). In addition, medium bond C-H stretching at 2950 cm^{-1} band, as well as medium O-H bending band at 1422 cm^{-1} are further likely to be associated with probucol. In the F6 powder mixture, and bulk probucol, these bonds are distinctive. The addition of formulation excipients in both F4 and F6, and the homogenisation time seem sufficient to incorporate probucol well without possible interference from the chitosan matrix.

Micro-Film Swelling

Figure 4.3 depicts micro-films before and after hydration in PBS for 20 minutes. Micro-film diameters were measured before and after hydration in three different solutions. There are small to moderate variations between the formulations when hydrated with PBS suggesting micro-film integrity is formulation-dependant (**table 4.2**). The addition of PG in F3 increases the film's ability to absorb water compared to hydrated F2 by ~130%. This pattern is also observed for DCA containing micro-films (F5 and F6), with minimal impact on F4 probucol (~32%) compared to F2. Dry probucol F4 micro-films seem rigid when handled and the reduced swelling could be explained in part by probucol's hydrophobic nature. Two-day old HEI-OC1 media discarded from routine passaging was used to better asses the swelling effects *in vitro*.

Minimal swelling changes appear when micro-films are immersed in DMEM or PBS for 20 minutes (**table 4.2**). However, after a three-day exposure to DMEM, micro-films underwent intense degradation and thinning (**figure 4.3-F5*, F6***). This shows that *in vitro* exposure to cellular metabolites is crucial for designing chitosan-based films, and that the addition of DCA reduces micro-film integrity.

Probucol Retention and Quantification

To quantify probucol from F4 (probucol only) and F6 (probucol-DCA) micro-films, HPLC was performed. Firstly, it was important to establish the probucol content within formulation homogenate prior to drying. Extracting probucol from micro-films with acetonitrile is significantly inefficient ($p < 0.001$) for quantifying the total amount of probucol in micro-films compared to F4 (**figure 4.4-A**) or F6 (**figure 4.4-B**) homogenate. An additional step of hydrating the micro-films prior to acetonitrile extraction is required to facilitate probucol release from the matrix and improve drug loading and content as well as the release kinetics measurements. **Figure 4.4-C** represents probucol release *in vitro* over a period of three days, with sample micro-films collected at 3, 6, 24, 48 and 72 hours. Consistent with the degradation (**figure 4.3-F6***) and swelling pattern in Milli-Q water of DCA micro-films (**table 4.2**) F6 micro-films show faster probucol release in the first 6 hours (50%). The final time point in **figure 4.4-C** reveals less probucol for F6 relative to F4 can be explained from the degraded stage at which the films were collected at.

Chitosan-Probucol Micro-Films and Cellular Compatibility

Cisplatin has known toxicity profiles against HEI-OC1 cells and represents a known ototoxic compound that promotes hearing loss (383). Research has also shown that macrophage inflammation could potentiate cisplatin toxicity *in vivo* (378). Although there are more ideal co-culture round window models in literature, this experiment represents a simplified method to establish preliminary conclusions (384). Images acquired from the top insert (HEI-OC1 cell layer – **figure 4.5**) and bottom wells (RAW 264.7 cell layer – **figure 4.6**) reveal that both cell types have been affected by cisplatin (**table 4.3**). Cell population declined for both cell lines in presence of cisplatin, with formulations providing little protection against the insult. Micro-film treatments alone had minimal negative impact in cell culture with probucol showing substantial effects

in preserving HEI-OC1 cells, while probucol-DCA showed better effects on RAW 264.7. Cisplatin is detrimental for both cell populations, however F4 appears to promote viability for both HEI-OC1 and RAW 264.7 by ~12% and ~6%, respectively (**table 4.3**). RAW 264.7 macrophage stimulation is highlighted by morphological changes, such as increased cytoplasm size and the appearance of multiple cytoplasmatic processes, with subsequent release of cytokines (385). If stimulated by cisplatin, RAW 264.7 cells increase in size by ~300% compared to controls, regardless of probucol and chitosan-based micro-films applications (**table 4.4**).

Cytokine Cellular In Vitro Release

To better evaluate the effects of chitosan-probucol micro-films on co-cultured HEI-OC1 and RAW 264.7 cells, three cytokine markers were measured (**table 4.5**). Probucol micro-film F4, showed a decrease by ~15% of MCP-1 levels compared to control. In terms of cisplatin-challenged cells, the trend favours cisplatin groups with lower TNF levels by ~35% while MCP-1 is reduced by ~22% compared to control. Besides the difference in cell population that might account for higher levels, it is important to consider that the increased control levels could be due to the co-cultured conditions. The literature shows that contact *versus* non-contact RAW 264.7 cell growth accounted for a similar trend, with higher cytokine levels in controls (386). The addition of micro-films in culture minimally impacts the cells, importantly F6 appears to lower TNF (~3%) and MCP-1 (~15%) release. However, $F6^{+}$ cisplatin-challenge increases MCP-1 by ~45% ($F6^{+}$), compared to cisplatin alone. Probucol micro-films F6 (~12%), and $F4^{+}$ (~42%) treatments have lower IL-6 than control, although cisplatin shows a decrease in IL-6 as well. The decrease in IL-6 might account for cell proliferation, and although not significant, there is a ~8% difference between cisplatin and $F4^{+}$ treatments.

4.4.4. Discussions

Given that no band characteristic to probucol was detected in micro-films *via* FT-IR analysis, it is likely that probucol is incorporated into the matrix (**table 4.1**). This can be confirmed by SEM, EDS, and by HPLC. From SEM analysis there are noticeable probucol crystals on the surface of F6 *versus* F4 surface that suggests DCA improves probucol micro-film smoothness (**figure 4.1** and **figure 4.2**). After three days

hydration in DMEM, the films have a uniform yet rough appearance with small and more distinct probucol deposits present on both F4 and F6 (**figure 4.2**) and could explain, in part, the incomplete *in vitro* dissolution at 48 hours (**figure 4.4-C**; ~90% for F6 and ~92% for F4). In terms of micro-film stability, probucol provides rigidity, and limited chitosan film swelling (**table 4.2**). The addition of PG (F3) significantly increases micro-film swelling in Milli-Q water in agreement with literature where increased swelling properties highly influence construct degradation (387, 388).

Faster drug release from formulations could benefit poor soluble drugs for middle ear delivery (29). Our DCA films show both slow release and degradation that require further testing *in vivo* to determine the absorption patten when applied to the round window niche. Another important element to consider, is that acidic conditions could amplify cisplatin's effects (373). Although the type of chitosan used for this study requires acid to dissolve, rehydrating the micro-films in neutral buffers allows in part *in vitro* and *in vivo* application that can be further improved by using water-soluble chitosan derivatives (*e.g. N*-hexanoyl glycol chitosan (367)).

From the HEI-OC1 and RAW 264.7 cells co-culture, results suggest that HEI-OC1 cells are more tolerant to F4 > F5 > F6 while the opposite pattern is valid for macrophages (**table 4.3**). Cisplatin is known to reduce cell viability and increase cellular oxidative stress (389, 390), that represents a possible protective mechanism for probucol and could explain our observations, however, requires validation. Furthermore, the morphological appearance of RAW 264.7 resembles controls when exposed to chitosan micro-films, with few cytoplasmic processes and reduced cell bodies (**table 4.4**). Typically, M1 pro-inflammatory macrophages are stimulated by lipopolysaccharides or IFN-gamma cytokines, and can produce TNF-α, while M2 activated cells are stimulated by IL-4 and IL-10 to have anti-inflammatory effects (391). Activated RAW 264.7 present a different morphology than cultured primary macrophages or naïve cells (392). Once RAW 264.7 are activated, the cells' cytoplasm expands and forms multiple processes, and cytokines are released (393). The developed probucol micro-film in combination with an ototoxic stressor, such as cisplatin is not sufficient to alleviate cisplatin's effects. However, probucol ($F4^{+}$) appears to protect HEI-OC1 the most (~12% difference from cisplatin control; not significant). Cisplatin reduces cell population in both cell lines and increases RAW 264.7 activated morphology (**figure 4.6-B**). Cisplatin also activates inflammatory caspases and leads to apoptosis in RAW 264.7 (394). Although minimal, chitosan-

probucol-DCA micro-films ($F6^+$; **table 4.4**) show a slight improvement against cisplatin (~20% difference), this could explain the beneficial effect both chitosan and probucol share. The literature shows that probucol exhibits anti-inflammatory effects including reduced inflammatory markers (TNF-α, IL-6, IL-1β) after RAW 264.7 lipopolysaccharide exposure (395). Similarly, chitosan-based microspheres and chitosan solution can reduce both TNF-α and IL-1β (357, 396). *In vivo,* cisplatin activates macrophages in a mixed population (M1 and M2) predominantly outside the organ Corti leading to local neuroinflammation and a temporal shift in hearing thresholds (378). In regards to hearing, macrophage activation after noise-exposure is detrimental (379, 397, 398), and is associated with inflammation associated age-related hearing loss (399). Both IL-6 and MCP-1 (better known as chemokine (C-C motif) ligand 2; CCL2) are dominant cytokines associated with the inner ear. Studies show that excessive inflammation, secondary to excess noise-exposure, and oxidative stress can potentiate cochlear tissue to produce IL-6 and MCP-1 (400). IL-6 is a pro-inflammatory cytokine produced by lateral wall cells, the stria vascularis, the spiral ligament and spiral ganglion neurons. MCP-1 is a recruiter of monocytes to inflamed regions and can further induce IL-6 production (401). Both cytokines are expressed *in vivo* (402, 403), and *in vitro* in HEI-OC1 cells (383). Although there is some discrepancy in its persistence after short term noise-exposure, cisplatin increases both IL-6 and MCP-1 expression (404). Our results show that probucol micro-films (F4) may decrease IL-6 and MCP-1 in co-culture, while DCA micro-films (F5) could decrease TNF production during cisplatin exposure.

4.4.5. Conclusions

Medium molecular weight chitosan gels are useful to incorporate the hydrophobic drug probucol into malleable films. As an excipient, DCA proves useful in thinning chitosan films and improves component miscibility and retention within the chitosan matrix. Probucol increases micro-film matrix rigidity reflected through the minimal swelling properties in Milli-Q water, and during prolonged *in vitro* exposure. In practice, a decrease in swelling prolongs probucol's availability so that the F4 probucol micro-film matrix requires more than 72 hours to degrade. In hindsight, the addition of DCA to the formulation increases micro-film degradation and probucol release. By adjusting DCA's concentration, enhanced probucol release can be optimised to produce better time-sensitive chitosan-probucol gels and films. Both cell lines proliferate well in

presence of micro-films. Probucol F4 micro-films are more compatible with HEI-OC1 cells than with RAW 264.7 and maintain the cell's population similar to control values. Although RAW 264.7 cells thrive in presence of probucol-DCA F6 micro-films, probucol as F4 promoted cellular survival after cisplatin-treatment, and although minimal, reduces MCP-1 and IL-6 cytokine levels in co-culture. Further research is required in testing the compatibility of probucol-chitosan micro-films *in vivo* in combination with other bile acids, where impact on the round window morphology as well as hearing thresholds can be further assessed.

Acknowledgments

The authors acknowledge the Australian Postgraduate Award and the Curtin Research Scholarship for their support. The authors also acknowledge the use of laboratory equipment, and the scientific and technical assistance of the John de Laeter Centre Electron Microscope Facility Curtin University, which has been partially funded by the University, State and Commonwealth Governments. Confocal microscopy analysis was performed using the Curtin Health Innovation Research Institute Microscopy and Histology Shared Resources Laboratory with the assistance for the Andor Dragonfly funded by the Australian Research Council under the grant LE200100122. Much appreciation goes for training and sample instrument operations performed at the Flow Cytometry Suite, Curtin Health Innovation Research Institute. We are grateful to use the HEI-OC1 cells provided from Prof. Federico Kalinec and appreciate the knowledge of working with these cells from Dr. Young Joon Seo.

Funding

This work is also partially funded by the Curtin Faculty ORS-WAHAI Consortium, the Australian National Health and Medical Research Fund (APP9000597). The authors want to acknowledge the Australian Postgraduate Award (APA) and Curtin Research Scholarship (CRS).

Conflicts of Interest

Al-Salami Hani is currently receiving funding from Austin Biotec Pty, Ltd and Glanis PTY Ltd. All other authors have no completing interest to declare.

Data Availability

The data that support the findings of this study are available from the corresponding author upon reasonable request.

Author contributions

CMI, AM and HAS conceptualised and designed the project. The main draft of the manuscript was prepared and assisted by all authors, who contributed effectively to the final draft.

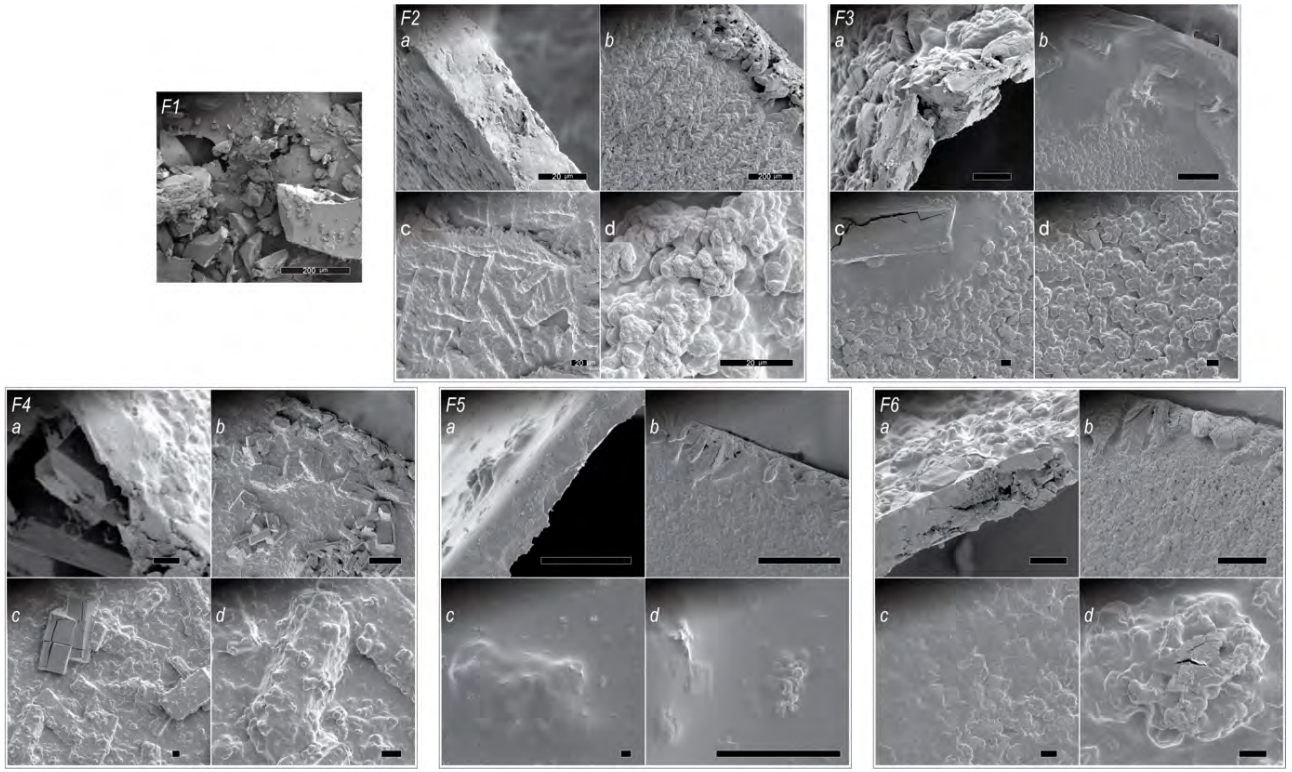

Figure 4.1.

Scanning electron micrographs of dry micro-film surfaces. F1 cyclodextrin control and chitosan formulations F2 to F6 with (a) cross-section of micro-films, (b) edges, and (c, d) close-up view of deposits. The addition of DCA to F6 reduces surface deposit abundancy. Incorporating DCA into micro-films (F5) improves the matrix uniformity. Scale bars (a, c, d) 20 µm, (b) and F1 200 µm.

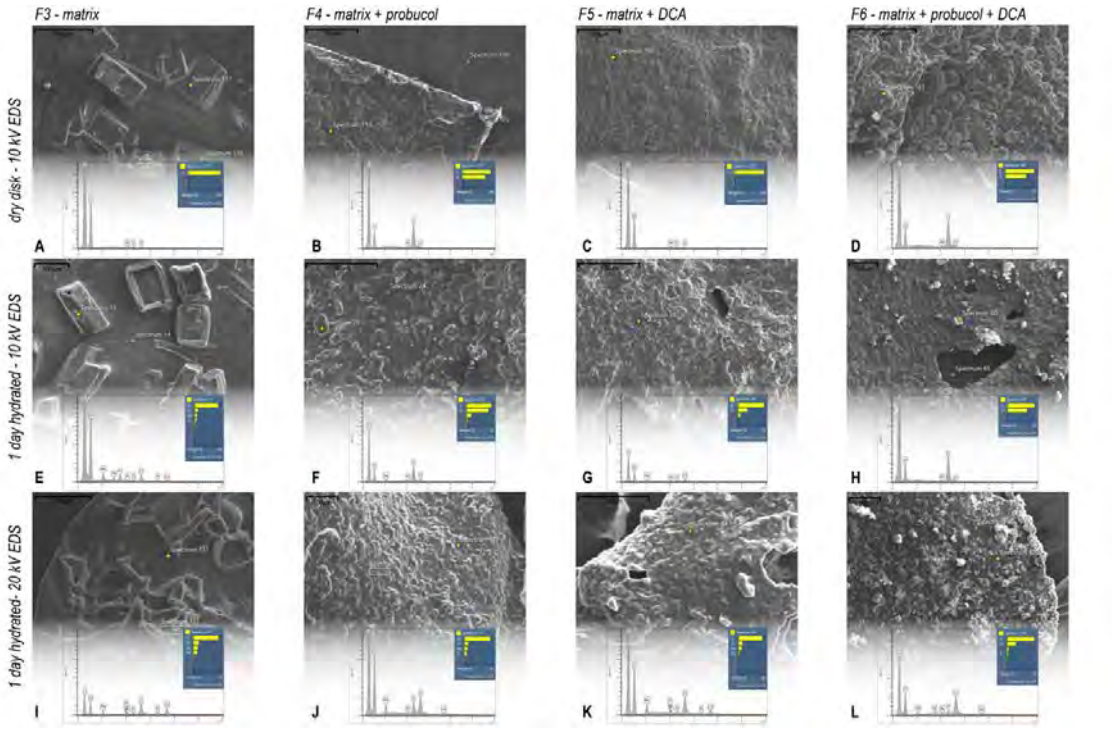

Figure 4.2.

Scanning electron micrographs and EDS spectra. (A-D) Dry F3 to F6 formulation and elemental analysis showing sulphur peaks. (E-H) Micro-films pre-hydrated one day in cell culture media without and (I-L) with cisplatin. Component deposits appear to decrease/detach in abundancy after hydration. Unlike F3 which consists of water-soluble components, probucol sulphur rich deposits persist on the surface of F4 and F6. No platinum peaks were detected. Scale bars 100 µm, 10 kV for probucol (sulphur EDS spectra) and 20 kV for cisplatin (platinum EDS spectra).

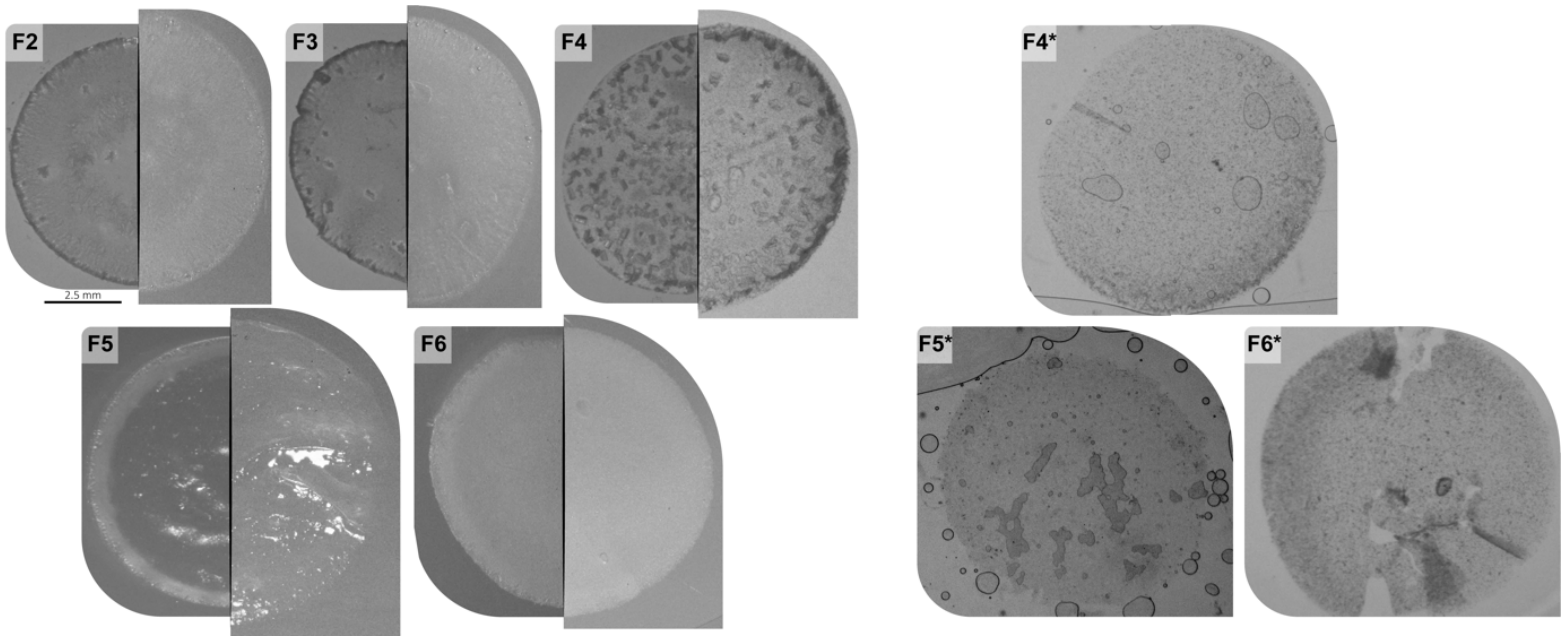

Figure 4.3.

Representative dry micro-films F2-F6 before (left) and after (right) hydration in PBS. Right side of figure reveals degree of micro-film degradation from cell media on F4*, F5* and F6* after three-days (hydration at 33°C). The micro-film degradation correlate with an enhanced sustained probucol release *in vitro.* Scale bar 2.5 mm.

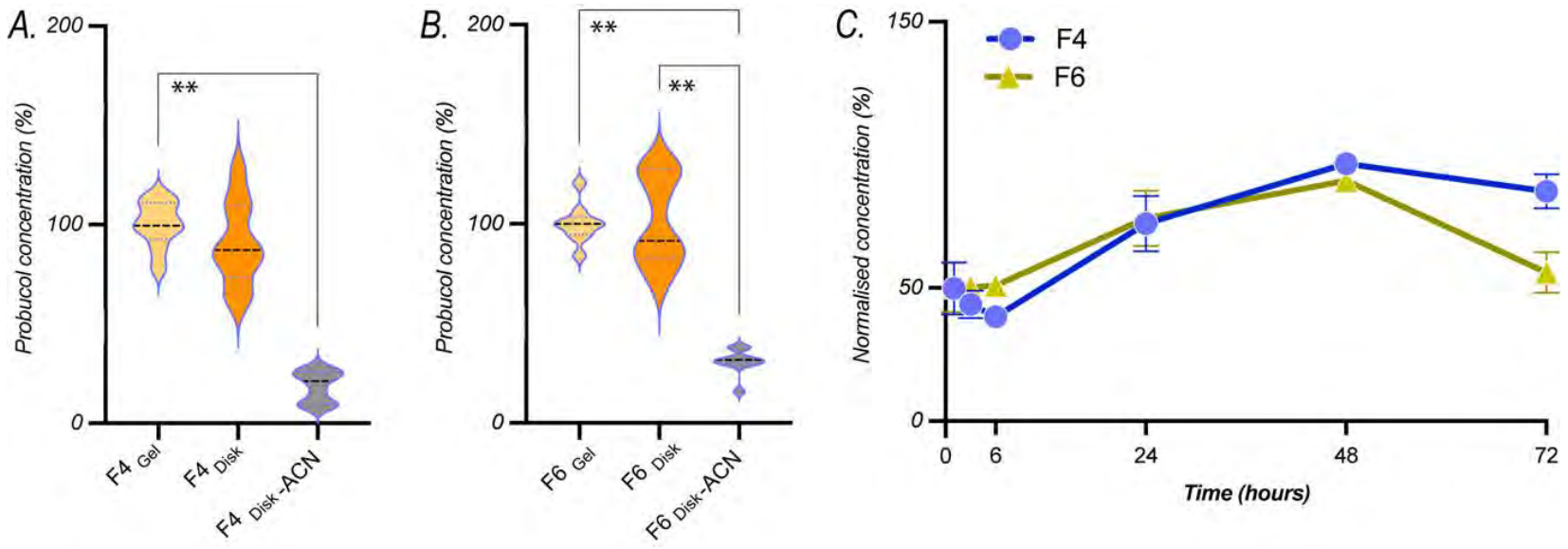

Figure 4.4.

Probucol quantification and drug release *in vitro*. (A, B) Normalised probucol percentage content from homogenate (yellow), micro-films hydrated with dH_2O and extracted with acetonitrile (disk; orange), and micro-films extracted with acetonitrile only (disk-ACN; grey). (C) Probucol's percentage from *in vitro* cumulative dissolution on HEI-OC1 cells over a 72 hour period. Hydrated probucol-DCA (F6) micro-films exposed to HEI-OC1 cells show increased probucol release in the first 6 hours followed by a sharp probucol availability due to the accelerated micro-film degradation (as seen in figure 4.3); Percentage results are normalised against F4 and F6 homogenate (100%); Error bars represent standard error of the mean, $n = 3$ in four repeats; $p < 0.001$ (**).

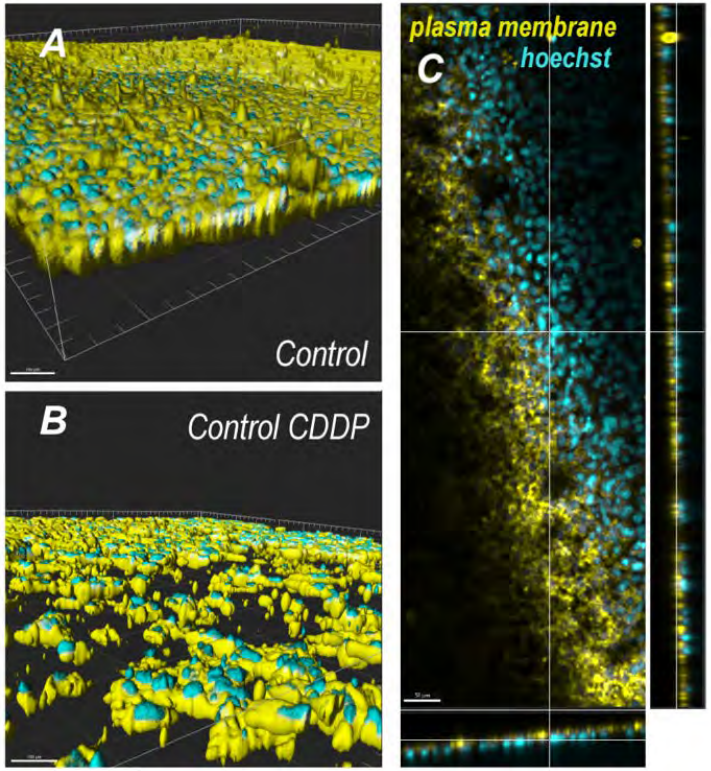

Figure 4.5.

Micro-film compatibility of HEI-OC1 co-cultures in Transwell plates at 33°C. The bottom insert membranes contains a thin layer of formulations (F4, F5, F6). (A) Volume representation of HEI-OC1 grown on the top insert membrane treated without or (B) with cisplatin (CDDP). (C) Cross-sectional view of insert membrane. Scale bars 100 µm; nuclei (blue), plasma membrane (yellow). Complementary to Supplementary IV.5 – IV.8.

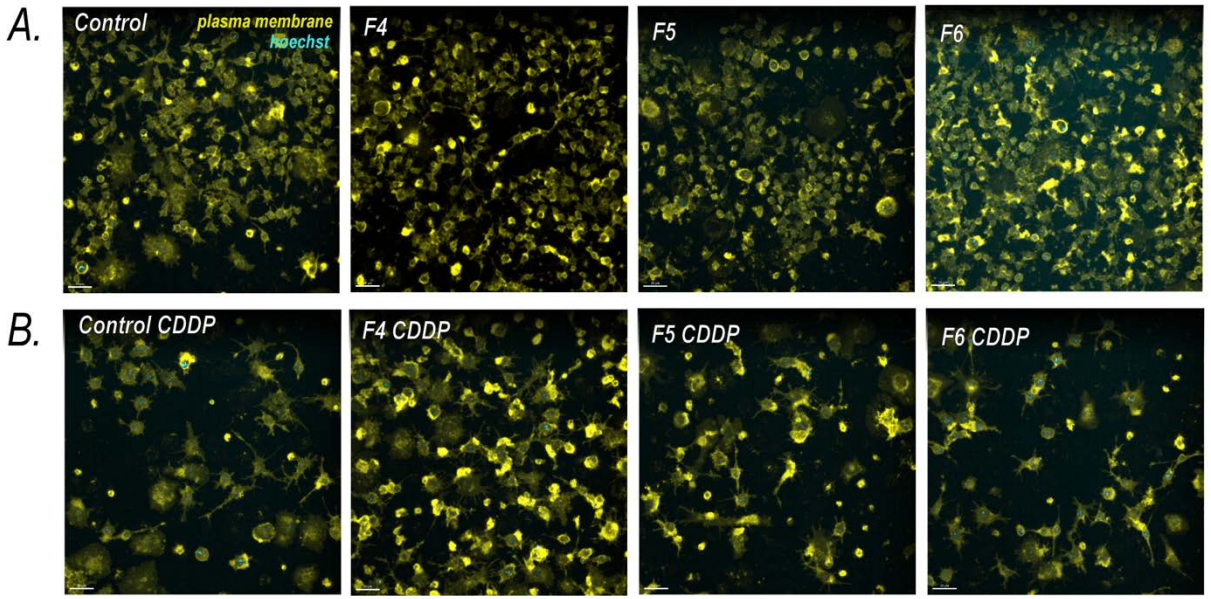

Figure 4.6.

Micro-film compatibility of RAW 264.7 cells co-cultures in Transwell plates at 33°C. The bottom insert membrane contains a thin layer of formulations (F4, F5, F6). RAW 264.7 cells were grown in the bottom wells. (A) Confocal images of RAW 264.7 cells treatments without or (B) challenged with cisplatin (CDDP) showing an increase in macrophage-activated-like morphology (enlarged cell size and cytoplasm processes). Scale bars 50 μm; nuclei (blue), plasma membrane (yellow).

Formulation	Main peak bands detected (cm^{-1})				
Probucol	3631.15	2957.85	1422.02	1234.77	1097.31
Powder mix	3633.00	3305.72	2958.14	1150.51	1023.13
F1	3300.80	1152.40	1022.70		
F2	3275.39	2925.38	1556.63	1151.55	1076.88
F3	3288.98	2923.76	1152.49	1077.24	1024.43
F4	3294.03	2923.91	1152.45	1077.34	1024.15
F5	3283.87	2923.69	1556.70	1077.32	1025.31
F6	3283.43	2924.63	1151.95	1078.05	1025.08

Table 4.1.

Normalised FT-IR peaks of probucol bulk powder, F6 powder mix, and dry micro-films post-homogenisation (F1-F6). Spectra are presented in Supplementary IV.12.

Micro-films	Area before hydration (μm)	Area after hydration in Milli-Q water (%)	Area after hydration in PBS (%)	Area after hydration in DMEM (%)
F2	35.79 ± 0.42	*122 ± 2.02	**138 ± 7.86	**138 ± 5.30
F3	32.56 ± 0.88	**256 ± 44.44	139 ± 3.63	136 ± 3.02
F4	31.10 ± 0.68	**154 ± 7.98	**133 ± 1.54	**142 ± 1.58
F5	37.38 ± 0.65	**261 ± 57.86	133 ± 3.29	128 ± 2.07
F6	38.55 ± 0.52	*221 ± 33.65	130 ± 1.74	127 ± 2.71

Table 4.2.

Micro-film swelling measurements before and after hydration in Milli-Q water, PBS, and DMEM obtained from cell culture. The addition of PG in F3 significantly increase the micro-film's overall water absorption (> 250%). Although significant compared to the initial dry state, the probucol F4 micro-films are more rigid in appearance and adsorb less water (> 150%); significance stars correspond to each formulation against its area before hydration (100%), $n = 3$, $p < 0.05$ (*), $p < 0.001$ (**) ± standard error of mean.

Treatment	HEI-OC1 cell count (%)	HEI-OC1 significant results
Control	100 ± 15.06	**CDDP, **F4^{+}, **F5^{+}, **F6^{+}
F4	106 ± 16.77	**CDDP, *F4^{+}, *F4, **F6^{+}
F5	98± 17.54	**CDDP, **F4^{+}, *F5^{+}, *F6^{+}
F6	83 ± 17.50	*CDDP, *F5^{+}, *F6^{+}
CDDP	27 ± 2.07	
F4^{+}	39 ± 4.85	
F5^{+}	27 ± 6.70	
F6^{+}	19 ± 3.92	
Treatment	**RAW 264.7 cell count (%)**	**RAW 264.7 significant results**
Control	100 ± 6.78	**CDDP, **F4^{+}, **F5^{+}, **F6^{+}
F4	76 ± 8.20	*F5, **F6, **CDDP, **F4^{+}, **F5^{+}, **F6^{+}
F5	109 ± 8.02	**CDDP, **F4^{+}, **F5^{+}, **F6^{+}
F6	120 ± 9.43	**CDDP, **F4^{+}, **F5^{+}, **F6^{+}
CDDP	29 ± 4.93	
F4^{+}	35 ± 4.97	
F5^{+}	29 ± 4.48	
F6^{+}	26 ± 2.32	

Table 4.3.

Relative HEI-OC1 cell populations represented as percentage. Micro-film formulation groups and controls are treated without or challenged with cisplatin (CDDP, F4^{+}, F5^{+}, F6^{+}). Both cell populations decline in presence of cisplatin. Probucol F4 negatively impacts RAW 264.7 population, while HEI-OC1 F4-treated cells remain similar to control (~100%). Treatments with cisplatin in F4^{+} groups slightly improve cell population density. Significance is represented in the column adjacent and considers only the same cell type; Control (C), $n = 3$ in triplicates, $p < 0.05$ (*) $p < 0.001$ (**) ± standard error of mean.

Treatment	Area (μm^2)	Area (%)
Control	224.07 ± 10.13	100 ± 4.52
F4	266.73 ± 32.50	119 ± 14.50
F5	218.49 ± 13.97	97 ± 6.24
F6	218.84 ± 22.57	98 ± 10.10
CDDP	927.26 ± 76.23	414 ± 34.00
F4$^+$	936.68 ± 76. 92	418 ± 34.30
F5$^+$	978.59 ± 95.18	437 ± 42.50
F6$^+$	879.07 ± 64.25	392 ± 28.70

Table 4.4.

Macrophage-activated-like phenotype based on cell area (μm^2) measurements in RAW 264.7 cell. Cisplatin increases cell area regardless of treatments. Groups were treated with and without cisplatin (CDDP, F4$^+$, F5$^+$, F6$^+$) and normalised against control untreated cells (100 %); *n* = 3 in triplicates, ± standard error of mean.

Treatment	TNF (pg/mL)	MCP-1 (pg/mL)	IL-6 (pg/mL)
Control	1212 ± 98.59	3322 ± 295.96	153 ± 14.61
F4	1495 ± 366.23	2839 ± 753.51	145 ± 23.74
F5	1246 ± 206.93	3170 ± 412.08	161 ± 24.92
F6	1177 ± 251.94	2816 ± 432.10	134 ± 20.28
CDDP	790 ± 128.78	2601 ± 384.89	101 ± 7.77
F4$^+$	1250 ± 355.41	2696 ± 238.56	89 ± 7.87
F5$^+$	1027 ± 138.92	3463 ± 376.83	157 ± 21.05
F6$^+$	1276 ± 127.36	4112 ± 121.80	158 ± 11.05

Table 4.5.

Cytokine markers release for HEI-OC1 and RAW 264.7 analysed from co-culture supernatant. Cells were treated with F4-F6 microfilms without and challenged with cisplatin (CDDP, F4$^+$, F5$^+$, F6$^+$). Although not significant, F6 and F4$^+$-cisplatin micro-film treatments slightly reduce TNF and IL-6, respectively. Cytokine results (pg/mL) are normalised against total sample protein levels (mg/mL); *n* = 3, ± standard error of mean.

Chapter 5

Bile acids Self-Assembled Cyclodextrin Particles for Probucol Delivery

5.1. Publications

The work in this chapter is developed for publication as:

5. **Corina M Ionescu**, Thomas P Foster, Bozica Kovacevic, Susbin R Wagle, Armin Mooranian and Hani Al-Salami - Cyclodextrin Probucol Bile Acid Particles and Their Effects on HEI-OC1 Cells.

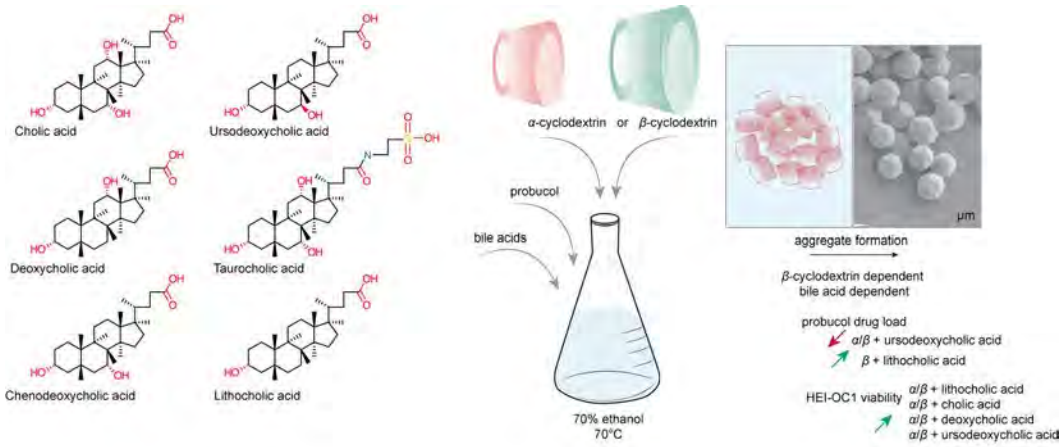

Graphical abstract 3. Cyclodextrin complexation with probucol and bile acids.

Cyclodextrin complexation with bile acids is well-known in literature and better described for *β*-cyclodextrin. The effects of probucol and *α*/*β*-cyclodextrin inclusions are explored using scanning electron microscopy. The addition of bile acids to the probucol-cyclodextrin mixtures is crucial for obtaining aggregates. Both aggregate formation, drug retention and *in vitro* viability effects are reflective of the bile acid type and their concentration used in formulation.

5.2. Introduction

Chapter 5 will focus on CD as the main formulation ingredient. The polysaccharide can form inclusion complexes with organic and bioactive molecules including BSC class II drugs, and can self-assemble into particles and aggregate (1). There is limited or no information on probucol, probucol metabolites and other phenol-like molecules' interaction with CD in terms of the complexation mechanism and thermodynamics. Besides the knowledge lacuna in complexation, this chapter will discuss the morphological differences and uses of CD-probucol aggregates. Since probucol is a small highly lipophilic molecule it may interact with cyclodextrin's core. The addition of bile acids will be used to assess probucol-CD self-assembled/aggregate formation. Particle optimisation variables are detailed in Appendix V. Four cyclodextrins in combination with six bile acids were used (CA, DCA, CDCA, UDCA, TCA, LCA) to assess probucol-CD complexation aggregates.

5.3. Summary

Aggregate formation is limited for probucol and CD. Both CD and bile acid types are important to determine aggregate formation. As α-CD forms less aggregates compared to β-CD, the same drug-bile acid ratio is not sufficient for gamma-CD (γ-CD) nor hydroxy-propyl-β-CD aggregation (Supplementary V.6). After drying the formulations, both α-CD and β-CD aggregates can be resuspended in liquids showing strong negative zeta potentials. Nonetheless, the aggregates applied on HEI-OC1 cells shows little variation between the CD type, but rather are affected by the bile acid type. Minor HEI-OC1 viability was observed when aggregates were applied in culture with an oxidative stressor.

5.4. Development

Chapter V formulations based on CD, probucol and bile acids aggregates can be further optimised in preparation for *in vivo* applications. In appendix V (Supplementary V.7), a fluorescently conjugated β-CD inclusion complex with probucol and bile acids is presented. Appendix VI describes a patent for the organic synthesis of conjugated bile acids and probucol filed by supervisor Dr Hani Al-Salmi, Dr Amin Mooranian, Dr Giuseppe Luna *et al*. Newly synthetised molecules according to the patent – HA1, HA2 and HA3 (LCA, CDCA and UDCA probucol conjugates), were used in the same

complexation formulation with *β*-CD. Similar to Chapter V results where *β*LCA-PB shows the smallest aggregate formation, the new HA1 molecule (LCA-probucol conjugate; Supplementary VI.6) result in nano-sized particles that can be used to test probucol's therapeutic use *in vitro* and *in vivo*.

Publication 5

Abstract

Drug delivery to the inner ear requires formulation development strategies that improve both safety and efficacy. Here we develop formulations based on *α* and *β* cyclodextrin for the antioxidant drug probucol. Bile acids were used as excipients to improve probucol aggregate formation. Formulations were tested on auditory representative cells – HEI-OC1.

We assessed complexation conditions to determine particle formation using six bile acid excipients. Particle size, morphology and zeta potential were determined using Malvern Zetasizer and scanning electron microscopy. Probucol drug concentration was determined *via* HPLC prior *in vitro* viability measurements.

Our results show that 0.36-2% cyclodextrin and 0.04% probucol requires the addition of bile acids to form hollow particles in 70% ethanol at high temperatures. Particles vary in size and have negative charge. *β*-cyclodextrin results in abundant particle formation compared to *α*-cyclodextrin. Significantly higher probucol drug content is retained with *β*-lithocholic acid, compared to *α*/*β*-chenodeoxycholic acid, *α*/*β*-ursodeoxycholic acid and *α*/*β*-deoxycholic. *In vitro* viability form 24/48 hours show varied results for all particles - *α*/*β*-chenodeoxycholic acid, *α*/*β*-ursodeoxycholic acid and *α*/*β*-lithocholic negatively influence HEI-OC1 survival. Against hydrogen peroxide-induced oxidative stress, *α*/*β*-cholic acid, *α*/*β*-deoxycholic acid, and *α*-lithocholic acid show minimal protective results. The combination of probucol and bile acids with *α*/*β*-cyclodextrins proves advantageous for drug delivery, requiring further optimisation in improving drug loading to maximise viability in oxidative stress conditions.

Key words: bile acids; drug delivery; self-assembled particles; cyclodextrin; probucol; HEI-OC1

Highlights:

- Cyclodextrin complexation with probucol remains unknown
- Cyclodextrin complexation of probucol in presence of bile acids allows for larger particle/aggregate formation in relation to the bile acid type and concentration.
- Ursodeoxycholic acid shows the lowest aggregate probucol loading effect.
- Lithocholic acid has the highest drug loading in presence of β-cyclodextrin, and show the smallest aggregate formations.
- Particle zeta potential remains negative regardless of bile acid and cyclodextrin type used in formulation.
- HEI-OC1 cell viability is positively influenced by higher probucol concentration.

5.5.1. Introduction

CD is a toroidal shaped cyclic oligomer consisting of six (α-CD), seven (β-CD), or eight (γ-CD) glucose units. Because of the molecule's hydroxyl groups, CDs are useful agents to form complex inclusions with hydrophobic drugs. The complexes hold several uses including compound separation (405), are used in food industry and the advancement of drug-delivery formulation (406). Bile acids have been widely researched for their affinity to certain CDs as the guest-host interactions are dependent on non-covalent bonds to form stable complexes. For example, most bile acid-host complexes designed for oral delivery are useful in part for sequestrating bile acids and cholesterol alike. The use of a drug-CD complex is favoured by the bile acids' ability to displace molecules from the CD cavity, and represents a strategic method for drug delivery to the gastro-intestinal track (407). CDs can also increase drug solubility and formulation shelf-life by reducing precipitation (408). Formulation complexation can be enhanced by prior mechanical milling of components (409). Not all drugs show core interaction with CDs, and other phenomena may aid in the solubilisation effects (410). As the guest-host interaction starts with the exclusion of water molecules from the CD cavity, this phenomena is part dependent on CD's moiety, ring conformation, and size (411), and is governed by exothermic enthalpy that enhances with temperature increase (412). For example, the strong inclusion complex attributed to LCA depends on the bile ring structure and the absence of C7 and C12 hydroxyl groups (**figure 2.3**),

in comparison, CA interacts with CD though the aliphatic chain (413). Bile salts-conjugated with taurine and glycine, such as T-CDCA, G-CDCA and T-βMC show stronger affinity to β-CD than TCA and T-DCA, further emphasising the importance of core interaction with bile acids at the steroid D-ring (C12 hydroxyl group) or C-ring (hydrogen) (414, 415). Regarding affinity, bile acids display week interaction towards α-CD compared to modified hydroxypropyl-α-CD or even to β-CD demonstrated by minimal cavity displacement (416).

Several commercially available drug formulations incorporate CDs. Inclusion complexation favours interaction with BCS class II and class IV drugs (1). Although probucol's anti-hyperlipidemic use is commercially unavailable in many countries, the drug gained research interest for its antioxidant properties (7-9). For this reason, probucol may serve as a possible drug delivery candidate to ameliorate several forms of hearing loss, primarily those with an oxidative stress-induced mechanisms (155, 162, 169, 340, 417). As probucol is highly lipophilic, strategies that can increase its solubility are required and include the use of mechanical milling and polysaccharides use (355). There are however no notable references that could describe probucol-CD inclusion complexes, and how the molecular interaction occurs. With no direct interaction mechanisms, the probucol derivative succinobuccol together with modified β-CD have been used to form ~110 nm particles that ameliorate metastatic cancer phenotype (418). Previous papers from our group (including this thesis Chapter 3 & 4) focusing on bile acids as pre-formulation excipients show promising results in terms of increasing dissolution, drug stability and water mixability for probucol formulations (32). However, CDs especially 2-hydroxpropyl-β-CD have demonstrated toxicity within the inner ear as it is shown to interact with lipid rafts and remove cholesterol from the hair cell's stereocilia, affecting hearing function (271). There is limited research regarding CD delivery to the inner ear; one paper explores the use of modified Na-carboxymethyl-β-CD for delivery of genes that proved to enhance dendrimer-delivery to the inner ear (419). Other examples include dexamethasone - a corticosteroid drug model against hearing loss – the drug's complexation with CDs through various methods can result in monodispersed (~105 nm; (420)) and polydisperse (~20 nm - 60 µm, ~400-900 nm; (421, 422)) particles.

In terms of particle formation and stability, β-CD can self-assemble in water and form secondary aggregate structures. Class II drugs are unable to form hydrogen bonds in water thus hindering solubilisation, and require entropy to break the water layer

surrounding the molecule (412). By adjusting the solution temperature, solvent type, mixing time, drug type, molar ratio, plus the addition of surfactants (423) or polymers, all contribute to drug-CD interaction, and ultimately solubilisation, particle and aggregate formation. Polymers, as well as alcohols, aid drug-CD solubility by increasing the polarity and the dielectric constant of the complexation media. Increasing the temperature, solvent concentration, and selecting the right solvent can reduce aggregate formation (424, 425). Most aggregate formations are dependent on the guest molecule properties, for example drug lipophilicity can increase the formation of aggregates due to micelle-like structures (426). Sonicating the CD solutions at room temperature increases complexation and secondary aggregate formation (427). From self-assembled, dense or hollow aggregates, not all *β*-CD-drug complexes form spherical particles; for example, oxadiazole-CD conjugates form multi-stacked rod-shaped structures, with the disadvantage of retaining less drug after filtration (428). The use of cross-linked chitosan CD can affect particle formation, and one study recorded the formation of hollow spheres with a positive charged inner cavity to be advantageous for entrapping specific drugs (429). Cross-linked CDs can negatively affect bile acid absorption allowing for more drug-complexation, however may pose a disadvantage by increasing aggregate size (430).

With this paper we explore a non-steroidal approach for inner ear therapeutic delivery based on probucol. The antioxidant probucol in combination with *α/β*-CD and bile acids particles were developed and characterised based on morphology, size, drug loading and zeta potential. Scanning electron microscopy analysis was used to determine particle formation, shape and size. We compare probucol particle formation in presence of *α*- and *β*-CD with UDCA, CA, DCA, CDCA, TCA and LCA. We further evaluate particle *in vitro* compatibility by metabolic activity as a measure of cellular proliferation using a water-soluble tetrazolium salt assay (WST-1). For the *in vitro* assessment we used the two culture stages of HEI-OC1 cells; proliferative permissive conditions (33°C, 24-48 hours), and differentiated non-permissive (39°C, 24-48 hours) conditions challenged with or without mild oxidative stress by adding hydrogen peroxide to cultures at 39°C for 48 hours.

5.5.2. Materials and Methods

Probucol powder is supplied by Beijing Natural-Med Biotechnology Co Ltd (Beijing, China). CA, DCA, CDCA, UDCA, TCA were supplied from Qingdao Yuanrun

Chemical Co., Ltd (Qingdao, Shandong, China). LCA (<95%) was purchased from Cayman Chemicals (Ann Arbor, MI, USA). PFA, CDs (*α*-CD, *β*-CD), Cell Proliferation Reagent (WST-1), trypsin-EDTA 0.25% and hydrogen peroxide 30% (H_2O_2) were purchase from Sigma-Aldrich (Merck, Melbourne, AU). DMEM was purchased from Biosciences, (GibcoTM, Dublin, IE), PBS from Fisher biotech (WA, AU). FBS was from Serana (Brandenburg, DE). Hoechst 33342 (H1399; Thermo Fisher, Waltham, MA, USA). Acetonitrile, HPLC grade, was purchased from ChemSupply (Gillman, SA, AU).

Cyclodextrin Probucol-Bile Formulations

Probucol and bile acid concentration as well as the solution conditions were adapted based on the literature (431-433). Formulation components (**table 5.1**) were solubilised in 0, 50 or 70% volume per volume (v/v %) dH_2O and ethanol, and mixed at 1300 rpm for one hour at 37°C, 50°C or 70°C. The solution was kept on ice for another hour followed by filtration using a 0.22 μm syringe filter (Sigma-Aldrich, Merck, Darmstadt, DE). The filtrate was dried using a concentrator (Thermo Savant's ISS110 Integrated SpeedVac, Thermo Fisher, Waltham, MA, USA) as 1 mL aliquots that were later used for assays. Abbreviations are used for formulations as *α/β*-CD-probucol (*α/β*CD-PB) and *α/β*-CD-bile acid type-probucol (*e.g. α/β*CA-PB).

Scanning Electron Microscopy and Elemental Analysis

After drying, samples were collected and placed on adhesive carbon taped aluminium stubs. Samples were sputter coated with 5 nm platinum and imaged on a field emission SEM (Clara model, Tescan, Brno, CZ). EDS (Oxford Instruments, UK) sulphur spectra was acquired simultaneously, to confirm probucol presence on particle surfaces and core. Both SEM and EDS was performed at 10 mm working distance, 2 kV (SEM) or 10 kV (for EDS) and 100 Å current beam. EDS spectra created using AZtec v 5.1 software (Oxford Instruments, UK).

Particle Size and Charge Analysis

Multiple SEM images acquired were used to measure relative particle size using ImageJ (344). Dynamic light scattering technique was implemented to measure particle size distributions using the Zetasizer (Malvern Instruments, Malvern, UK).

Zeta potential was also acquired using the Zetasizer. Dry particle samples were dispersed in 1 mL distilled water, vortexed for 15 seconds and spun down for 10 seconds prior to analysis in disposable green capillary cells.

High Pressure Liquid Chromatography

Dried samples were extracted with 1 mL acetonitrile to quantify probucol. HPLC (SIL-20A model UV detector, Kyoto, JP) was utilised to detect and quantify probucol within samples and solvent blanks on a C18 column (Luna 5 µm, 100 Å, 150 x 4.6 mm, Phenomenex, Torrance, CA, USA), 1 mL/minute flow rate and ~13 minutes retention time. Samples were sonicated for 10 minutes prior to filtration and 20 µL was injected and analysed against a probucol standard curve (0.015 – 1 mg/mL, $R^2 = 0.99998$). The overall HPLC analysis as well as the production yield, drug content and encapsulation efficiency calculations followed our previous publication (33).

Cell Culture

The HEI-OC1 cells were kindly received from Prof. Federico Kalinec (University of California, CA, USA), and Dr. Young Joon Seo (Yonsei University, Korea). Cultures were kept in permissive conditions at 33°C and 10% CO_2 levels. Cells were grown with DMEM supplemented with 10% FBS. For experiments in 96 well plates, cells were detached from flasks using trypsin-EDTA, then seeded at 2 x 10^5 cells/mL. Seeded plates were grown overnight and treated for 6 hours in FBS-free media, followed by 24 or 48 hours in FBS rich DMEM. Experimental groups consisted of treated (1.25 mg/mL for 6 hours) and treated-challenged cells (6 hours particles proceeded by 1 hour 1 mM H_2O_2). Experimental groups and appropriate controls (unchallenged or challenged with 1 mM H_2O_2 only) were tested at both permissive (treatment applied next day from seeding; 33°C/10% CO_2) and non-permissive (treatment applied after two weeks from seeding; 33°C/5% CO_2) conditions. For challenged groups, cells were exposed to H_2O_2 to mimic oxidative stress conditions (434), H_2O_2 represents another stressor model for HEI-OC1 representative for age-related senescence and hearing loss (435).

WST-1 Assay

24/48 post-treatment, cells were incubated with 10% (v/v) WST-1 for 3 hours as per manufacture protocol. Absorbance was determined at 420 nm on a Multimode plate reader (EnSight, PerkinElmer, MA, USA). Results were normalised against healthy control (100%) and blank wells (0%).

Statistical Analysis

Statistical analysis, *t test,* one-way ANOVA with Tukey test correction, normalization, and graph representation were done on GraphPad Prism v.9 (GraphPad Software San Diego, CA, USA). Significance was reported as follows; *$p < 0.05$, and **$p < 0.01$. Assays performed in three particle replicates in triplicate ($n = 3$). Graph mean error bars represent ± standard mean error.

5.5.3. Results

Particle Formation Conditions

The addition of probucol in 70% ethanol with 2% β-CD results in few small aggregates. At the same probucol 0.04% concentration with 0.137% DCA or CA, complexation is dependent on CD type with β-CD resulting in particle formation (**figure 5.1.A**). Probucol and 0.6% DCA at 37°C in water shows numerous β-CD deposits, with minimal aggregate formation. With the increase in ethanol, the β-CD deposits are still presents, although spherical uniform particles are more abundant at 70% ethanol (**figure 5.1.B**). Increasing solvent conditions to 70% ethanol and 70°C further promotes particle formation at 0.6% or 0.36% β-CD. Even at 2% β-CD (**figure 5.1. C, DCA**), particles are formed with less abundancy and tend to coalesce (**figure 5.1.C**).

Bile Acids and Particle Formation

As 0.36% β-CD, probucol and DCA result in well-defined particles. We tested six bile acids (**table 5.1**) in combination with either β-CD and α-CD. Bile acids such as TCA > UDCA > CDCA > DCA result in spherical particles when combined with α-CD and probucol. However spherical particle formation is not successful for αCA-PB nor αLCA-PB, with more CD deposits visible through SEM. All bile acids tested in combination with β-CD and probucol form particles (**figure 5.2**) and have a smooth

appearance except for βCDCA-PB particles that have a rugose surface. While the smaller particles from βTCA-PB appear to coalesce, βLCA-PB has relative less abundant, yet smaller particle.

Particle Size and Zeta Potential

We performed two sets of size measurements based on the collected SEM images and the Zetasizer. The relative results are presented in **table 5.2** for α-CD particles, and **table 5.3** for β-CD particles. Based on the high polydispersity index (PDI ≥ 0.3), and the difference between peak and average Zetasizer measurements, we can conclude that the generated particles are all polydisperse. There is a noticeable size discrepancy between measurements obtained from micrographs and zeta size, however both indicate an uneven size distribution. Although there were no identifiable spherical particles formed form αCA-CD and αLCA-CD (**figure 5.2**), zeta size distributions were recorded and may reflect the smaller irregular sample deposits.

Based on the relative particle size acquired from SEM, α-CD particles ranged from ~1-2 µm size and β-CD showed larger particles of about ~1.8-4 µm. As SEM requires sample coating, the true size of the particles (436) is not in accordance with the zeta size measurements. The smallest particles recorded for αDCA-PB and βLCA-PB averaged at 0.97 µm and 1.18 µm respectively. The largest particles were recorded for αUDCA-PB at 1.84 µm and βCA-PB at 3.96 µm, followed by βTCA-PB and βUDCA-PB. The average size reflective of the hydrodynamic size was low at ~0.8-2 µm for α-CD and 0.8-3.3 µm for β-CD.

On average, α-CD samples required 12 ± 0.11 zeta runs, respectively 13 ± 0.41 runs for β-CD to acquire good zeta potential reports (**figure 5.3**). Particles containing α-CD; αCDCA-PB, αUDCA-PB and αTCA-PB show strong negative zeta-potential of -33.12, -33.75, -32.71 mV, respectively. Significant values ($p < 0.01$) appear for αDCA-PB (-24.48 mV), as well as αLCA-PB (-25.32 mV) compared to αCDCA, αUDCA and αTCA-PB (~ -30 mV). Except for βUDCA-PB (-11.89 mV), all β-CD particles present significant ($p < 0.05$) negative zeta-potential.

Probucol Concentration

All α-CD and β-CD particles had probucol peaks detected by EDS and quantified using HPLC (Appendix V, Supplementary V.1 and V.2). Both types of CD formulations had

a production yield ranging from 54 to 71% (**table 5.4 and 5.5**). Probucol encapsulation efficiency showed little variation ~5-7%, however there were significant differences in drug content recorded for *α*CA-PB against *α*CDCA-PB ($p < 0.02$), *α*UDCA-PB ($p < 0.0001$), *α*TCA-PB ($p < 0.002$). A similar significance difference is observed for *α*DCA-PB compared to *α*CDCA-PB ($p < 0.02$), *α*UDCA-PB ($p < 0.0001$) and *α*TCA-PB ($p < 0.003$) as well as *α*LCA-PB compared to *α*UDCA-PB ($p < 0.003$) and *α*TCA-PB ($p < 0.002$). Although *α*CA-PB and *α*DCA-PB have abundant particle formations, the higher probucol content could be the result of precipitate material after filtration, that included free probucol that crystallised from the ethanol solution. From table 5.5 both *β*LCA-PB *β*CA-PB show significant ~0.7-0.8% increase in drug content compared to *β*DCA-PB ($p < 0.04$), *β*CDCA-PB ($p < 0.001$), *β*UDCA-PB ($p < 0.0006$) and *β*TCA ($p < 0.002$), respectively.

HEI-OC1 and Particle Toxicity

We tested the ototoxicity of both *α*-CD and *β*-CD particles *in vitro* on a HEI-OC1 murine cell model with and without H_2O_2-induced oxidative stress. After the 24 and 48 hours incubation post-treatment at 33°C, both *α*-CD and *β*-CD particle formulations follow a similar trend. HEI-OC1 cells treated with *α*/*β*CA-PB, *α*LCA-PB, *α*/*β*DCA-PB or *β*DCA-PB show the highest viability at 24 hours (~80%; **figure 5.4.A**) with a slight increase over the next 24 hours (**figure 5.5.B**). After 24 hours, *α*/*β*CDCA-PB, *α*/*β*UDCA-PB and *α*TCA-PB showed negative effects on HEI-OC1 cells. However, in permissive conditions (33°C) in the 48 hours timeframe, only some treatments showed a minimal increase by ~7% (*α*UDCA-PB and *β*TCA-PB), 10% (*α*TCA-PB), and 22% (*β*UDCA-PB). To mention that after 48 hours *β*LCA-PB treated cells recover in viability by 20% compared with the initial 24 hours of treatment.

The 24 hours at 39°C after pre-treatment shows similar results to untreated cells for control *α*/*β*-CDs, and formulations *α*/*β*CD-PB, *α*/*β*DCA-PB, *α*/*β*UDCA-PB, *α*/*β*LCA-PB with more than 80% viability (**figure 5.5**). The addition of *α*/*β*TCA-PB in culture decreased cell viability by ~60-70%, with *α*/*β*CDCA-PB showing the most negative effects, similar to results in permissive conditions. Although there is no clear significance between CDs in cell culture, the permissive and non-permissive conditions show a slight viability variation for *α*/*β*DCA-PB and *α*/βCDCA-PB.

After 48 hours there is a difference in viability between control untreated, *α*/*β*-CDs control and *α*/*β*-CD formulation groups and challenged H_2O_2. The control challenged

with 1 mM H_2O_2 reached 77.5% viability compared to control untreated cells. *α/β*-CDs pre-treatments show minimal efficacy after H_2O_2-conditioning, expect for *α/β*CA-PB that maintains the highest viability (95/80%; **figure 5.6**). While at 24 and 48 hours bile acid treatments show similarities in effects, αDCA-PB, *α*UDCA-PB and *α*LCA-PB treatments are significantly ($p < 0.01$) less affected than challenged *α*CA-PB, *α*UDCA-PB and *α*TCA-PB. Non-permissive conditioned HEI-OC1 cells were less affected by *α/β*CA-PB, *α/β*DCA-PB, *α*UDCA-PB and *α*LCA-PB treatments showing more than 80% viability.

5.5.4. Discussion

In the present work, we have demonstrated that *β*-CD and probucol formulations result in few undefined structures. However, upon the addition of DCA these structures form spherical supramolecular aggregates. All CD samples contain various degrees of CD residue sheets that the particles separated from. In fact, filtering the reacted CD solution appears to form similar sheets, observed alongside CD particle aggregates (437). Probucol's high lipophilicity might explain the presence of large aggregates, or even micelle-like structures according with previous reports on lipophilic drugs (426). We first investigated 0.137% DCA or CA with *α/β*-CDs and determined that bile acid concentration, CD type, and CD concentration are important for particle formation. Similar to other reports (423, 424), particle formation increases with the addition of ethanol (70%) and an increase in temperature (70°C). Low particle formation for *α*-CDs (*α*CDCA-PB < *α*DCA-PB < *α*UDCA-PB and *α*TCA-PB), may be reflect in part the smaller CD cavity that allows for weak bile acid complexation (416). The overall particle size appears larger than other studies reported on various drug-CD combinations (349, 419, 420).

Positively charged dexamethasone-CD nanoparticles have been shown to pass the round and oval window to reach the cochlea and increase protection against streptomycin (349). Although our particles show negative charge, the effects *in vivo* might still be substantial. Better described in a review, particles that are around ~500-700 nm with negative charge are more successful in reaching the inner ear after round window applications. Based on SEM measurements, *α*-CD shows smaller particles than *β*-CD, however the values are not consistent with the Zetasizer data. From the elevated PDI (~0.5-0.7) all formulations appear to have a broad size distribution (438), that is in part reflected by SEM. Particles, alongside CD sheets and clusters, might

account for the higher PDI values considering the lower resolution power of Zetasize in differentiating between shapes (439). In part, this may explain *α*CA-PB and *α*LCA-PB's average distribution size and PDI readings similar to the rest of the samples even though no aggregates were detected in these samples. The low PDI (~0.5) for *β*LCA-PB could be explained by LCA's affinity to *β*-CD and complexation even at small concentrations (0.05-0.5 mM) in aqueous water-solvent mixtures (440).

Although *α*CA-PB and *α*LCA-PB samples do not show particle formation, probucol was quantified and samples are dispersed well in medium for *in vitro* application. The HPLC content of all formulations shows similar encapsulation efficiencies, the total drug content is significantly lower for *α*/*β*CDCA, *α*/*β*UDCA and *α*/*β*TCA. Curiously, the same formulations show less *in vitro* viability, perhaps due to an increase in CD-bile acid interaction. Further analysis is therefore required to determine the bile acid content and complexation efficiency and how it affects inclusion size in presence of probucol. Previous reports by Mohamed H. *et al.,* (2017) found that a stronger guest-host interaction is shown by increased CD cross-linking, leading to less bile acid absorption. Moreover, they show that larger particles occur with the increase in cross-linking (430), that is also seen in our results in relation to *β*-CD compared to *α*-CD size differences. If for example the drug complexation occurs, it should be prior to bile acid displacement (441), therefore influencing the relationship between the type of bile acid ratio to probucol required for particle stability. Unfortunately, there are no available references observing the guest inclusion complex of probucol nor its metabolites with CD, let alone how the complex inclusion changes in the presence of bile acids. Probucol is metabolised to bisphenol (4,4'-bis(2'6-di-*tert*-butyl-phenol) (442) which is similar in structure to the pollutant bisphenol A and linear 4,4'-biphenol. Stronger aqueous *β*-CD inclusions occur for the bent bisphenol A rather than the linear 4,4'-bisphenol studied before (443, 444). Although these compounds are smaller than probucol and lack the probucol's characteristic *tert*-butyl groups, it is important to note that molecules containing the *tert*-butyl moieties interact with the CD cavity and form inclusions (445, 446).

As 2-hydroxypropyl-*β*-CD is regarded as an ototoxic compound (271), we therefore assessed the effects of *α*/*β*-CD rich samples, with appropriate controls on HEI-OC1 cells. It is important to note that bile acids at higher concentration could show similar effects in removing cholesterol – however the precise mechanism is outside the scope of this paper. Although *α*/*β*CDCA, *α*/*β*UDCA and *α*/*β*TCA present negative effects on

cell viability at both 33°C and 39°C, this could possibly be explained by the bile acids' concentrations and effects observed on other models. For example, CDCA similarly to methyl-*β*-CD and unlike CA, can affect caveolae formation (274). T-UDCA has received attention for reducing endoplasmic reticulum stress associated with ototoxic gentamicin in HEI-OC1 cells at 200 μM concentration (103). UDCA (10 μM) has also shown the ability to reduce age-related autophagy in miR-34a-induced HEI-OC1 cells (168). However, DCA (>100 μM) can induce apoptosis is some cells (447), and the more hydrophobic LCA (50 μM) is reported to restore intestinal cells integrity by modulating SIRT1, Nrf2 and HO-1 proteins in relation to oxidative stress (317). The aforementioned proteins are modulated by probucol in various models (338, 417), and further relate to age (155), noise (162) and diabetes-induced (169) hearing loss. Therefore, the low bile acid complexation by *α*CD could possibly explain the significant increased viability difference between *α*DCA, *α*UDCA and *α*LCA compared to the H_2O_2-treated group (*α*DCA, *α*UDCA and *α*LCA). Although the stressor used was chosen based on a previous report on oxidative stress-induced senescence model for HEI-OC1 cells (434), the suboptimal H_2O_2 concentration had significant impact on some of the particle treatments by further reducing viability compared to H_2O_2 control ($p < 0.01$). The possibility for better CD-bile-probucol constructs remains open for further analysis that can overlook probucol dissolution patterns and tissue permeability for improved probucol drug delivery outcomes in HEI-OC1.

5.5.5. Conclusions

In summary, this chapter shows that CD complexation with probucol is possible, although aggregate formation is dependent on the addition of bile acids. CA, DCA, CDCA, UDCA, TCA and LCA were used to assess probucol-CD particle construct and their compatibility *in vitro.* First, we determined that the bile acid type and their concentration is crucial for particle formation. For example, the same concentration of CA or DCA shows particle aggregation and formation only for DCA. Moreover, higher temperature and an increase in ethanol concentration improves particle formation. All six bile acids added to *β*-CD-probucol formulations formed particles, and only four were successful for *α*-CD. As expected, due to the smaller *α*-CD cavity, less abundant and smaller particle aggregates formed compared to *β*-CD. The zeta particle charge is mostly consistent through samples (negative ~ -30 mV) except for *β*UDCA-PB (-11

mV). In terms of *in vitro* responses from HEI-OC1 cells, the low probucol loading for *α*/*β*CDCA, *α*/*β*UDCA and *α*/*β*TCA related to a decline in cell viability. In general, *α*/*β*CA, *α*/*β*DCA and *α*/*β*LCA did not affect HEI-OC1 cells at permissive (prolific stage) or non-permissive (differentiated stage) conditions. *α*UDCA proves more useful in non-permissive cells especially against mild oxidative stress conditions along with *α*DCA and *α*LCA. Overall, further research is required to optimise particle size for better *in vivo* applications and asses probucol-CD ability against other ototoxic compounds *in vitro* and *in vivo*.

Acknowledgments

We would address our gratitude to the Curtin University staff members who provided inductions and access to the laboratories based in the Pharmacy Building, the Scanning Electron Microscope at the John de Laeter Research Centre, and the Curtin Health Innovation Research Institute, Faculty of Health Sciences, Curtin University, W.A., Australia. We are grateful to use the House Ear Institute-Organ of Corti 1 cells provided from Prof. Federico Kalinec and Dr. Young Joon Seo. The authors want to further acknowledge the Australian Postgraduate Award (APA) and Curtin Research Scholarship (CRS).

Funding

Curtin Faculty ORS-WAHAI Consortium, the Australian National Health and Medical Research (APP9000597).

Conflicts of interest

Al-Salami H is currently receiving funding from Austin Biotec Pty, Ltd and Glanis PTY Ltd. All other authors have no completing interest to declare.

Author contributions

CMI, AM and HAS conceptualised and designed the project. The main draft of the manuscript was prepared and assisted by all authors, who contributed effectively to the final draft.

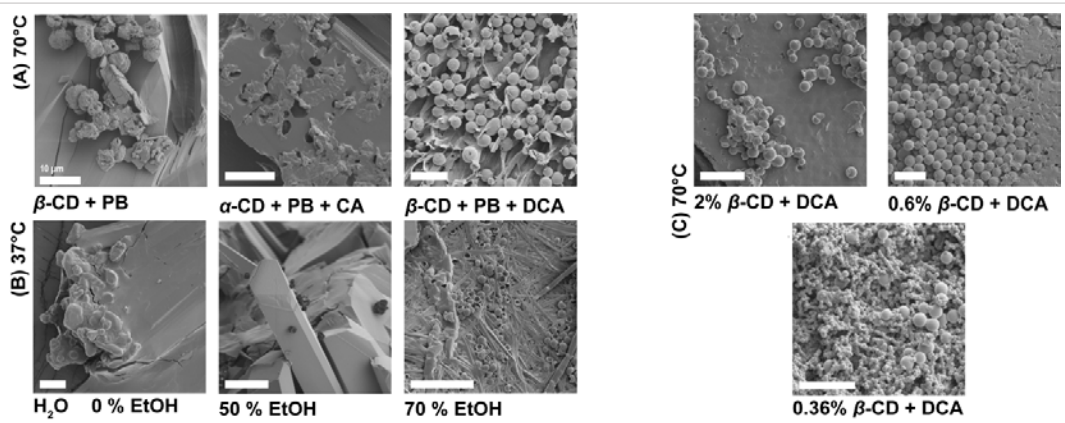

Figure 5.1.

Scanning electron micrographs of probucol (PB) particle formation in different conditions. Particle formation depends on temperature, probucol, CD, and ethanol (EtOH) concentrations. (A) Probucol 0.04% with β-CD compared to 0.137% CA α-CD, and 0.137% DCA (70°C, 70% EtOH). Complexation undergone at (B) 37°C in 0, 50 or 70% ethanol (EtOH) impacts 0.137% DCA + β-CD particle formation. (C) With higher 70°C EtOH β-CD and lower CD concentrations (0.36-0.6%), particles appear more abundant with well-defined spherical shapes. Scale bars 10

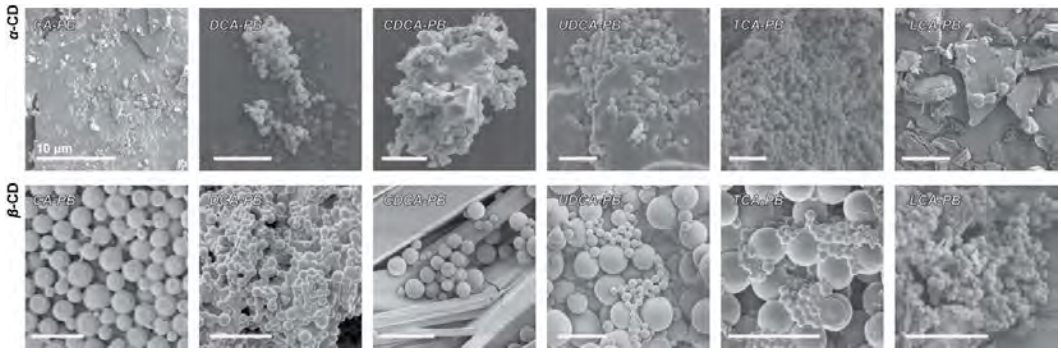

Figure 5.2.

Scanning electron micrographs of bile acid-probucol particle morphology. From left to right are cyclodextrin-bile acid and probucol (PB) particles; *α*/*β*CA-PB, *α*/*β*DCA-PB, *α*/*β*CDCA-PB, *α*/*β*UDCA-PB, *α*/*β*TCA-PB, *α*/*β*LCA-PB. Most combinations formed spherical and abundant particulates except for *α*-CD mixtures - especially *α*CA-PB and *α*LCA-PB. This reflects the higher complexation ability of *β*-CD with lipophilic molecules such as probucol and bile acids. First row represents particles obtained from *α*-CD, and second row *β*-CD particles, respectively. Scale bars 10 µm.

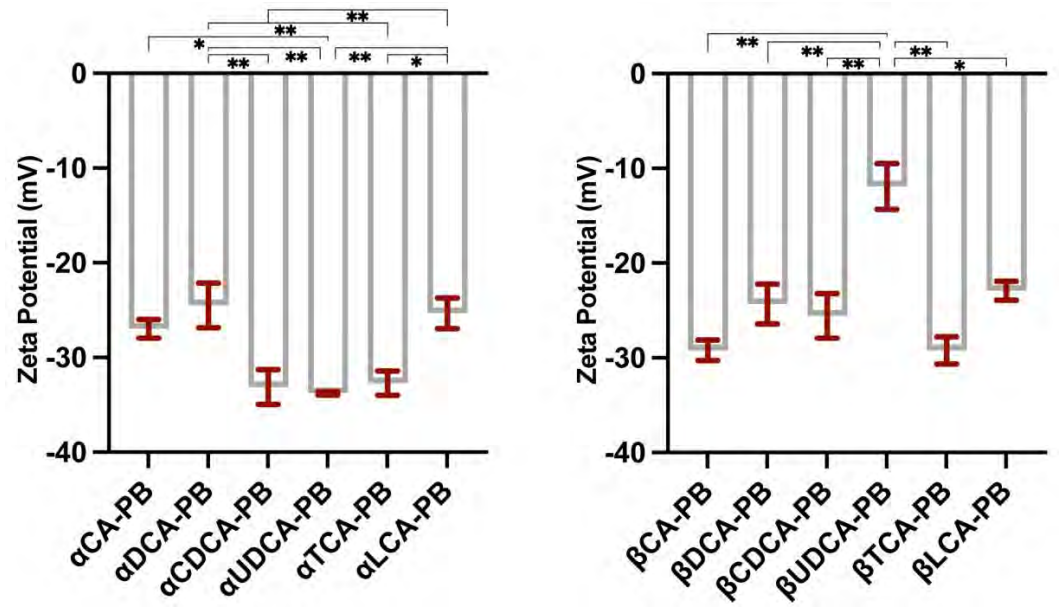

Figure 5.3.

Zeta potential measurements of *α*-CD (left graph) and *β*-CD (right graph) bile acid-probucol (PB) particles. All formulation combinations show strong negative zeta potential, expect for *β*UDCA-PB. Significance value *$p < 0.05$, and **$p < 0.01$; error bars represent standard error of the mean, $n = 3$.

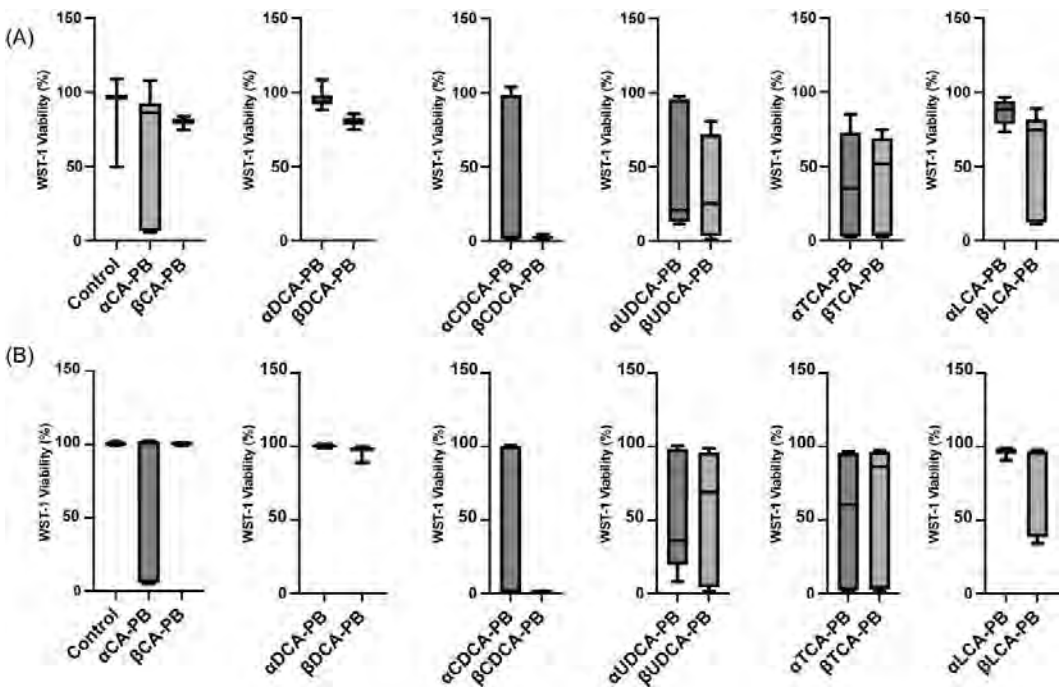

Figure 5.4.

WST-1 viability intensity results from (A) 24 hours and (B) 48 hours. Control untreated cells and α-CD or β-CD particles 6 hour pre-incubation with HEI-OC1 cell cultures in permissive conditions (33°C). Although group mean results vary greatly, the effects between α-CD or β-CD remain similar and do not affect viability. Bile acid type appears to influence cell viability the most as α/βCDCA-PB > α/βUDCA-PB > α/βTCA-PB show lower viability values than control; Error bars represent standard error of the mean, n = 3.

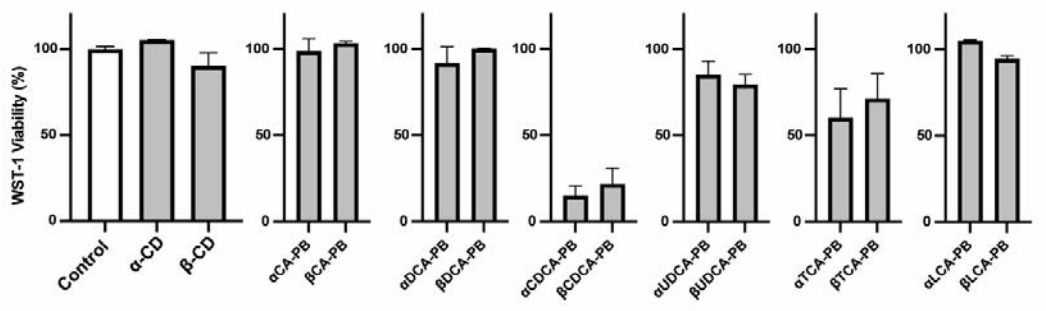

Figure 5.5.

WST-1 viability intensity results from 24 hours following a 6 hour pre-treatment with α-CD and β-CD particles on HEI-OC1 cells in non-permissive conditions (39°C). Similar to the permissive conditions results from figure 5.4, α/βCDCA-PB and α/βTCA-PB show the least viability revealing to the importance of bile acid type on HEI-OC1 cells. Control α/β-CD show minimal variation and similarities to control untreated. Groups represent control untreated cells, control treated with α/β-CDs (0.35%) and particle formulations. Error bars represent standard error of the mean, $n = 3$.

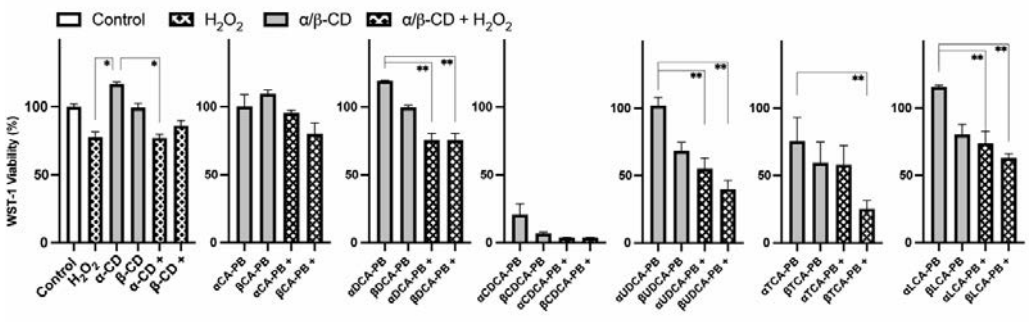

Figure 5.6.

WST-1 viability intensity results from 48 hours following a 6 hour pre-treatment with *α*-CD and *β*-CD particles and 1 hour stressor (1 mM H_2O_2) on HEI-OC1 cells in non-permissive conditions (39°C). Some *α*-CD treatment groups (*α*DCA-PB, *α*UDCA-PB, *α*LCA-PB) conditioned with H_2O_2 show a significant decrease in viability compared to the starting conditions. The variation might be attributed to the difference in probucol drug load (see table 5.4). The lower viability observed for *β*-CD may be reflective of the stronger interaction between these bile acids and cyclodextrin. Groups represent control untreated cells, control treated with *α/β*-CDs (0.35%) and particle formulations unchallenged or challenged ($^+$) with H_2O_2. Significance value *$p < 0.05$, and **$p < 0.01$; Error bars represent standard error of the mean, $n = 3$.

α-CD and β-CD formulations				
Formulation abbreviation	Cyclodextrin (%)	Probucol (%)	Bile acid (%)	Bile acid type
CA-PB	0.36	0.04	0.081	CA
DCA-PB	0.36	0.04	0.137	DCA
CDCA-PB	0.36	0.04	0.176	CDCA
UDCA-PB	0.36	0.04	0.371	UDCA
TCA-PB	0.36	0.04	0.257	TCA
LCA-PB	0.36	0.04	0.076	LCA
Optimisation steps				
Formulation abbreviation	Cyclodextrin (%)	Probucol (%)	Bile acid (%)	Bile acid type
PB	0.6	0.04	0	n/a
αCA-PB	0.6 (α-CD)	0.04	0.137	CA
αDCA-PB	0.6 (α-CD)	0.04	0.137	DCA
βDCA-PB	0.36 (β-CD)	0.04	0.137	DCA
βDCA-PB	2 (β-CD)	0.04	0.137	DCA

Table 5.1.

Formulation ingredients and ratios. Bile acid, cyclodextrins (α/β) and probucol concentrations as percentage weight per volume concentrations (w/v %). The mixtures optimisation corresponds with figure 5.1 and Supplementary V.4-V6.

Formulation	*SEM size (µm)*	*Zetasize average (µm)*	*Zetasize peak (µm)*	*PDI*
*α*CA-PB	NA	0.80 ± 0.04	0.61 ± 0.05	0.57 ± 0.03
*α*DCA-PB	0.97 ± 0.01	1.68 ± 0.33	0.30 ± 0.06	0.70 ± 0.09
*α*CDCA-PB	1.61 ± 0.02	0.72 ± 0.03	0.45 ± 0.03	0.61 ± 0.03
*α*UDCA-PB	1.84 ± 0.02	0.85 ± 0.03	0.41 ± 0.02	0.64 ± 0.03
*α*TCA-PB	1.11 ± 0.01	2.27 ± 0.65	0.32 ± 0.07	0.79 ± 0.06
*α*LCA-PB	NA	0.70 ± 0.96	0.53 ± 0.05	0.58 ± 0.07
α-CD probucol particle size				

Table 5.2.

Size measurements obtained from micrographs and dynamic light scattering Zetasize recordings of *α*-CD-based bile acid-probucol (PB) formulation; SEM size, zeta size with the first peak measurements and PDI. High PDI and the variable size recordings corroborate with the SEM observations from figure 5.2 where aggregate formations appear to vary in size. The lower PDI in *α*CA-PB and *α*LCA-PB is contradicts the SEM recordings, showing no spherical particles present within these samples. SEM total count; *α*DCA-PB = 392, *α*CDCA-PB =158, *α*UDCA-PB = 565, *α*TCA-PB = 920. Values represent µm, *n* = 3, ± standard error of the mean.

Formulation	*SEM size (µm)*	*Zetasize average (µm)*	*Zetasize peak (µm)*	*PDI*
*β*CA-PB	3.96 ± 0.24	3.32 ± 0.53	0.67 ± 0.04	0.91 ± 0.06
*β*DCA-PB	2.53 ± 0.31	1.40 ± 0.28	0.43 ± 0.04	0.75 ± 0.06
*β*CDCA-PB	2.43 ± 0.13	0.80 ± 0.08	0.48 ± 0.13	0.60 ± 0.06
*β*UDCA-PB	3.85 ± 0.58	1.23 ± 0.17	0.51 ± 0.08	0.65 ± 0.04
*β*TCA-PB	3.62 ± 0.14	1.36 ± 0.78	0.31 ± 0.03	0.81 ± 0.03
*β*LCA-PB	1.18 ± 0.01	0.48 ± 0.27	0.45 ± 0.04	0.50 ± 0.02
β-CD probucol particle size				

Table 5.3.

Size measurements from micrographs and dynamic light scattering Zetasize recordings of *β*-CD-based bile acid-probucol (PB) particles; SEM size, zeta size and the first peak and PDI. High PDI and the variable size recordings corroborate with the SEM observations from figure 5.2 where aggregate formation appears to vary in size. The smallest size measurements attributed to *β*LCA-PB reflects on LCA's interaction with *β*-CD, and the formation of a stronger inclusion complexation. SEM total count; *β*CA-PB = 972, *β*DCA-PB = 1171, *β*CDCA-PB = 2273, *β*UDCA-PB = 1820, *β*TCA-PB = 417, *β*LCA-PB = 374. Values represent µm, *n* = 3, ± standard error of mean.

Formulation	*EDS sulphur spectra*	*Production yield (%)*	*Drug Content (%)*	*Drug encapsulation efficacy (%)*
*α*CA-PB	Yes	71.98 ± 3.28	[a]1.28 ± 0.09	7.03 ± 0.65
*α*DCA-PB	Yes	60.69 ± 6.22	[b]1.27 ± 0.17	6.31 ± 0.39
*α*CDCA-PB	Yes	60.47 ± 1.65	[ab*]0.90 ± 0.02	5.38 ± 0.16
*α*UDCA-PB	Yes	60.82 ± 2.75	[abc**]0.64 ± 0.02	5.80 ± 0.38
*α*TCA-PB	Yes	58.93 ± 2.23	[ab**c*]0.81 ± 0.03	5.75 ± 0.37
*α*LCA-PB	Yes	60.99 ± 3.29	[c]1.20 ± 0.06	5.57 ± 0.50
probucol concentrations from *α*-CD particles				

Table 5.4.

Particles yield, probucol content and encapsulation efficacy of *α*-CD represented as percentages. Confirmation of EDS spectra for sulphur (S) energy peak (~2.3 keV) in probucol (PB) particle surfaces. EDS spectra can be observed in Supplementary V.1 and V.3. Drug quantification values for *α*DCA-PB, *α*CDCA-PB, *α*UDCA-PB, *α*TCA-PB and *α*LCA-PB correspond to 563 ± 50, 505 ± 31, 430 ± 10, 464 ± 30, 460 ± 30, 446 ± 40 µg/mL, probucol concentration respectively. Probucol peaks are quantifiable by HPLC and show minimal degradation occurring during the formulation development method (see Supplementary V.9). Significance pairs are denoted by [a], [b], [c] and the significance value are *$p < 0.05$ and **$p < 0.01$; $n = 3$, ± standard error of mean.

Formulation	*EDS sulphur spectra*	*Production yield (%)*	*Drug Content (%)*	*Drug encapsulation efficacy (%)*
*β*CA-PB	Yes	56.29 ± 1.64	1.21 ± 0.07	5.09 ± 0.27
*β*DCA-PB	Yes	54.00 ± 2.02	[a*]0.97 ± 0.07	6.31 ± 0.39
*β*CDCA-PB	Yes	64.11 ± 3.77	[a**]0.74 ± 0.04	5.97 ± 0.38
*β*UDCA-PB	Yes	56.12 ± 1.08	[a**]0.68 ± 0.07	6.17 ± 0.38
*β*TCA-PB	Yes	60.21 ± 3.43	[a**]0.76 ± 0.04	5.59 ± 0.56
*β*LCA-PB	Yes	64.31 ± 16.19	[a]1.56 ± 0.31	6.03 ± 0.69
probucol formulation concentrations from *β*-CD particles				

Table 5.5.

Particles yield, probucol content and encapsulation efficacy of *β*-CD represented as percentages. Confirmation of EDS spectra for sulphur (S) energy peak (~2.3 keV) in probucol (PB) on particle surfaces. EDS spectra can be observed in Supplementary V.2 and V.3. Drug quantification values for *β*CA-PB, *β*DCA-PB, *β*CDCA-PB, *β*UDCA-PB, *β*TCA and *β*LCA-PB probucol corresponds to 407 ± 22, 367 ± 19, 478 ± 30, 494 ± 30, 448 ± 45, 482 ± 55 µg/mL, probucol concentration respectively. Drug content percentage significance pairs are denoted by [a] and the significance value are *$p < 0.05$ and **$p < 0.01$; $n = 3$, ± standard error of mean.

Chapter 6

General discussion, conclusions, limitations and future perspectives

6.1. Discussion and Conclusions

Probucol as a lipophilic antioxidant could represent a strong candidate for inner ear drug delivery. However, the drug requires formulation preparation to improve therapeutic efficacy. In general, formulation application improves drug delivery compared to drug solution applications. This thesis presents three different formulations that prove useful to maintain probucol stability and allow for a slow drug release. The use of bile acids as excipients enhances probucol content retention within formulations and allows for sustained drug release.

The type of bile acid however determines the effects observed during formulation characterisation and can act as viability modulators *in vitro*. Although the bile acid ratio to probucol is low, an effort was made to understand the extent bile acids may have on the inner ear. The review outcome is presented in Chapter 2 and reflects a lack of resources describing bile acids applications to the inner ear, however, possible bile acids targets that should be considered for future research. The literature review provides useful information on the previous applications of T-UDCA and UDCA to the inner ear. Within the same review, DCA is referenced highly for its cytotoxicity, however these effects depend on the type of tissue and concentration at which the bile acids are applied *in vitro* or *in vivo.* For this reason, Chapter III and Chapter IV focuses on UDCA and DCA formulation stability.

Spray drying probucol from a water-based polymer with UDCA proves efficient in obtaining solid dispersions. Upon visual inspection, these probucol-UDCA and probucol particles vary in size yet appear similar to control formulations. Drug retention, encapsulation efficiency and drug release are slightly improved for probucol-UDCA compared to probucol particles. The beneficial effect of probucol-UDCA is more noticeable and significant against cisplatin-induced ROS accumulation in HEI-OC1 cells. Cell culture viability and increased mitochondrial bioenergetics improved as well.

In terms of probucol-chitosan homogenate dried as films, the addition of DCA to the homogenate improves film stability, probucol incorporation and allows for sustained drug release patters by improving film water adsorption and allowing for

chitosan degradation. Regardless, probucol formulation films slightly improved *in vitro* HEI-OC1 against cisplatin-induced toxicity.

Reducing probucol particulate size is essential for improving dissolution, regardless of formulation composition (448-450). A minimal formulation consisting of CDs, probucol and bile acids was thus optimised. *α/β*CD-probucol particle formation requires bile acid at various concentrations to form stable aggregates. Probucol is retained within the particles, and the construct is suitable for *in vitro* applications on HEI-OC1 cells. Regardless of CD type, the CDCA, UDCA, TCA with CD-probucol particles show a negative effect on HEI-OC1 cells viability.

6.2. Summary Findings

- Probucol's antioxidant effects are maintained irrespective of drug formulation as seen in Chapter III.
- Probucol's slower release from the formulation matrix improves the drug's protective effect *in vitro.*
- Probucol formulations are stable (no degradation) if homogenised in acidic conditions (23°C), spray dried from water suspensions (150°C) or exposed to ethanol (70°C).
- Bile acids and their effects are not fully explored for inner ear therapeutics.
- Bile acids as excipients for probucol enhance formulation outcomes.
    - Improve probucol content, drug encapsulation and forced degradation for spray dried solid dispersions.
    - Increase chitosan micro-film malleability, water adsorption, and probucol retention within the matrix.
    - DCA increases chitosan micro-film sustained drug release (3 days after cell culture).
    - Drug lipophilicity (LCA) is optimal to reduce CD-based aggregate particle size.
    - Improve CD-probucol particle formation and drug retention.
    - Ensure viability for HEI-OC1 cells exposed to cisplatin (UDCA).
    - Significantly reduce reactive oxygen species accumulation in HEI-OC1 after cisplatin exposure (UDCA).
- Bile acid limitations on formulation outcomes.

- Bile acid type and concentration may affect HEI-OC1 viability and require thorough screening.
- Probucol-DCA chitosan films do not improve cell viability.
- Drug release is influenced by bile acid lipophilicity rather than concentration.

6.3. Limitations

The current study limitations are three-fold. Firstly, the lack of permeation testing using *in vivo* or *in vitro* models. Secondly, the absence of probucol powder controls for experiments. Lastly, lack of prolonged formulation characterisation. Additionally for each chapter a subset of limitations are discussed and open for further research.

Drug permeability results from *in vivo* models through the round window membrane offer a better understanding on drug permeation and tests should consider the following variables (microenvironmental pH, formulation degradation, tissue metabolite, tight junction expression). In an attempt to understand probucol inner ear permeability, Appendix VI contains permeation predictions for probucol, bile acids and CDs compared to dexamethasone. Readers can observe the Brain Or IntestinaL EstimateD permeation method (BOILED-Egg) (451) based on the SwissADME (452) online platform, as well as FluidSim V5 (453) inner ear drug entry predictions developed by Dr Alec Salts (454).

Another limitation present is not adequately testing probucol powder in cell culture as dissolution control. As probucol remains trapped on the surface tension barrier in culture media, drug availability to the cellular layer is limited, and formulation design is crucial to maintain probucol suspension in water. Appendix VI contains HEI-OC1 viability graph for probucol, and some metabolite solutions dissolved in DMSO.

Formulation characterisation as FT-IR, DSC, and HPLC drug degradation are important to determine formulation stability. Since all formulations were prepared, characterised and tested *in vitro* within a week of production, important long-term stability data is lacking (six months). This aspect is important not only for commercialisation purposes but also for transportation.

Chapter 2 provides future research directions to test bile acids. The literature review revealed possible molecular targets for bile acids within the inner ear.

Chapter 3 requires a better design for assessing *in vitro* outcomes. Spray dried solid dispersions were resuspended in culture media to maximise probucol contact with cells, however it is not reflective of inner ear applications. The study could benefit from prolonged contact to probucol, and different cisplatin-induced stress exposure time-points. Although all spray dried formulations are dispersed in aqueous solutions, the formulation might be prone to clearing from the middle ear if applied *in vivo*. However, the neutral particle zeta potential could provide better particle agglomeration on round window membrane surface thus delaying the clearing process.

Chapter 4 investigates DCA only. Other bile acids required testing to assess micro-film degradation patterns *in vitro.* Rather than co-culturing macrophages and HEI-OC1, a different culture exposure model should be considered. For example, media collected from macrophages challenged with cisplatin for different days should be used to grow HEI-OC1 cells. In this fashion, probucol treated HEI-OC1 excludes stress from direct co-culture, and both cytokine production stress irrespective of cisplatin can be assessed.

Chapter 5 lacks information on bile acid concentration retained within the particulate CD-probucol. More SEM information is required to assess aggerate stability over time. Transmission electron microscopy can be implemented to understand probucol-bile nanoaggregates formation within the initial hour of preparation and before and after filtration or sonication. Additional information should focus on molecular docking, both for probucol, probucol and bile acids, and future synthetic molecules (HA1, HA2, HA3). Drug stability and degradation patters require further testing for this chapters and represents the main design limitations. Drug loading and viability could be correlated with the bile acid loading concentrations. To quantify bile acid loading concentration, a mass spectrometry method should be developed. As for *in vitro* testing, a viability gradient based on bile acid loading and probucol loading is required.

6.4. Future perspectives

The methods presented can be combined to form long-term stable formulations for *in vivo* application. For example, chitosan films would be better retained at the round window membrane. Therefore, an increase in probucol concentration can be obtained by incorporating solid dispersions rather than probucol powder into the chitosan homogenate. This could improve controlled release by further delaying probucol release from the CD-probucol-bile particles and the chitosan films.

To continue the study theme, the following formulations would be used *in vivo*; *β*UDCA-PB, *β*LCA-PB, *β*CD-HA1, and probucol powder all in absence or in combination with chitosan. The low drug loading of *β*UDCA-PB has larger particle aggregates, while *β*LCA-PB shows high drug loading and small particles and can be compared to determine particle transport, cellular uptake and toxicity levels. The smallest particles are obtained for *β*CD-HA1 mixtures (Appendix V). Probucol powder should be considered the baseline for permeation to compare all particle aggregates. Chitosan film formulation should be used and compared for its ability to enhance and prologue drug permeation. Besides the round window membrane permeability *in vitro* model, a BLB permeability *in vitro* model (455) could be considered as well for nanoaggregates (*β*CD-HA1) as an alternative delivery route.

A future direction for bile acid-probucol interaction would focus on obtaining synergistic effects from probucol and bile solutions. Synergy refers to the dynamic increase in treatment potency conferred by the two or more drugs in combination. *In vitro* synergy studies on HEI-OC1 cultures are limited to the type of solvent used for drug solutions, requiring a different cell culture or *ex vivo* model to better understand synergistic probucol-bile effects.

Cellular uptake studies that follow dissolution patterns may be important to determine drug toxicity levels. Cells can be subjected to either drugs in solution or in formulations to assess the cellular uptake concentration – assessed through HPLC by quantifying probucol from the cell culture layers. Drug uptake can then be compared with direct (in media) or indirect membrane permeability.

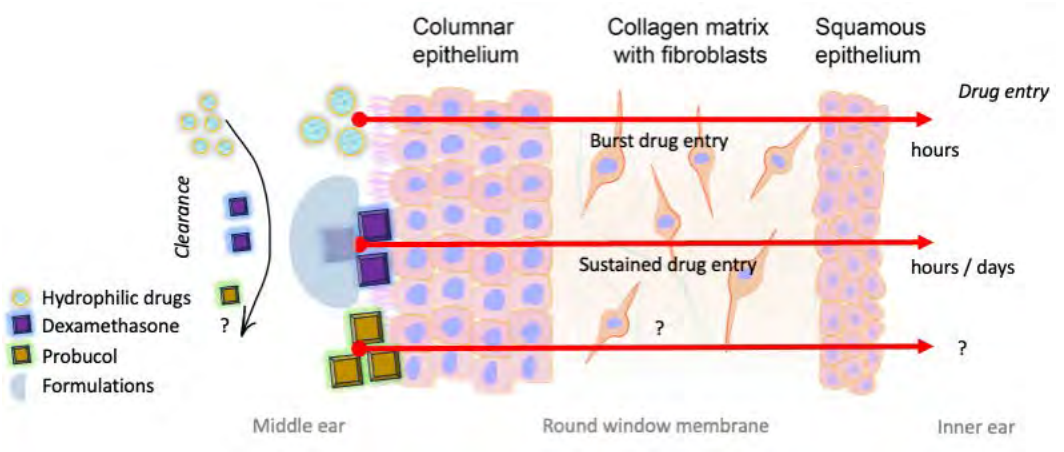

Graphical abstract 4. Future perspectives.

Drug entry for formulations applied to the middle ear could enter the inner ear through the round window membrane (composed of three cellular layers). Formulation clearing from the middle ear exerts pressure in developing drug delivery strategies that improve drug entry. Hydrophilic compounds in the form of drug solutions applications show a burst drug entry lasting for hours. Lipophilic drugs such as dexamethasone can remain in contact for longer with the round window membrane allowing for sustained release and drug entry. With the addition of dexamethasone in formulations, drug entry is further prolonged. Probucol's lipophilic nature may allow the drug to remain in contact with the round window membrane. However, the permeation and entry pattern, as well as the clearing rate of probucol solution or in formulation remain unknown. Within this thesis, three methods for obtaining probucol formulation in combination with bile acids as stabilisers are presented. The use of polymers, polysaccharides and bile acids in formulation can increase probucol solubilisation, influence formulation stability, and increase drug loading and release patterns. Formulation behaviour and drug release are important factors that influence drug absorption. The thesis results show that probucol-bile acid formulations present limited toxicity *in vitro* on auditory hair cells (in normal or in oxidative stress condition) and could be used in the future to determine drug tissue permeation *in vivo.*

Appendix I

Copyright clearance and licences has been obtained for the following Publication 1 from chapters 2, and publication 3 from chapter 3.

Corina M. Ionescu, Melissa A. Jones, Susbin R. Wagle, Bozica Kovacevic, Thomas Foster, Momir Mikov, Armin Mooranian and Hani Al-Salami - Bile Acid Application in Cell-Targeting for Molecular Receptors in Relation to Hearing: A Comprehensive Review. *Current Drug Targets*, Volume 25, Issue 3, 2024, Page 158 – 170. DOI:10.2174/0113894501278292231223035733

Corina M Ionescu, Bozica Kovacevic, Melissa A Jones, Susbin R Wagle, Thomas Foster, Momir Mikov, Armin Mooranian and Hani Al-Salami - Probucol-Ursodeoxycholic Acid Otic Formulations: Stability and In Vitro Assessments for Hearing Loss Treatment. *Journal of Pharmaceutical Sciences*, 2024, 10:S0022-3549(24)00159-X. DOI: 10.1016/j.xphs.2024.04.032.

Publication 1

CCC Marketplace

This is a License Agreement between Corina M Ionescu ("User") and Copyright Clearance Center, Inc. ("CCC") on behalf of the Rightsholder identified in the order details below. The license consists of the order details, the Marketplace Permissions General Terms and Conditions below, and any Rightsholder Terms and Conditions which are included below.

All payments must be made in full to CCC in accordance with the Marketplace Permissions General Terms and Conditions below.

Order Date	06-Feb-2024	Type of Use	Republish in a thesis/dissertation
Order License ID	1447221-1		
ISSN	1389-4501	Publisher	BENTHAM SCIENCE PUBLISHERS LTD.
		Portion	Chapter/article

LICENSED CONTENT

Publication Title	CURRENT DRUG TARGETS	Country	Netherlands
Date	01/01/2000	Rightsholder	EUREKA SCIENCE (FZC)
Language	English	Publication Type	Journal

REQUEST DETAILS

Portion Type	Chapter/article	Rights Requested	Main product, any product related to main product, and other compilations/derivative products
Page Range(s)	all		
Total Number of Pages	13		
Format (select all that apply)	Electronic	Distribution	Worldwide
Who Will Republish the Content?	Academic institution	Translation	Original language of publication
Duration of Use	Life of current and all future editions	Copies for the Disabled?	Yes
		Minor Editing Privileges?	No
Lifetime Unit Quantity	Up to 499	Incidental Promotional Use?	No
		Currency	USD

NEW WORK DETAILS

Title	Thesis	Institution Name	Curtin University
Instructor Name	Corina M Ionescu	Expected Presentation Date	2024-02-24

ADDITIONAL DETAILS

Order Reference Number	N/A	The Requesting Person / Organization to Appear on the License	Corina M Ionescu

REQUESTED CONTENT DETAILS

Title, Description or Numeric Reference of the Portion(s)	Bile Acid Application in Cell-Targeting for Molecular Receptors in Relation to Hearing: A Comprehensive Review	**Title of the Article / Chapter the Portion Is From**	Bile Acid Application in Cell-Targeting for Molecular Receptors in Relation to Hearing: A Comprehensive Review
Editor of Portion(s)	N/A	**Author of Portion(s)**	Corina M. Ionescu, Melissa A. Jones, Susbin R Wagle, Bozica Kovacevic, Thomas Foster, Momir Mikov, Armin Mooranian* and Hani Al-Salami*
Volume / Edition	N/A		
Page or Page Range of Portion	1-13	**Issue, if Republishing an Article From a Serial**	N/A
		Publication Date of Portion	2000-01-01

RIGHTSHOLDER TERMS AND CONDITIONS

If your permission request relates to Open Access content, published under the CC BY 4.0 license, you don't need to take permission from Bentham Science for reuse, as long as the original publication and Bentham Science are correctly credited.

Marketplace Permissions General Terms and Conditions

The following terms and conditions ("General Terms"), together with any applicable Publisher Terms and Conditions, govern User's use of Works pursuant to the Licenses granted by Copyright Clearance Center, Inc. ("CCC") on behalf of the applicable Rightsholders of such Works through CCC's applicable Marketplace transactional licensing services (each, a "Service").

1) **Definitions.** For purposes of these General Terms, the following definitions apply:

"License" is the licensed use the User obtains via the Marketplace platform in a particular licensing transaction, as set forth in the Order Confirmation.

"Order Confirmation" is the confirmation CCC provides to the User at the conclusion of each Marketplace transaction. "Order Confirmation Terms" are additional terms set forth on specific Order Confirmations not set forth in the General Terms that can include terms applicable to a particular CCC transactional licensing service and/or any Rightsholder-specific terms.

"Rightsholder(s)" are the holders of copyright rights in the Works for which a User obtains licenses via the Marketplace platform, which are displayed on specific Order Confirmations.

"Terms" means the terms and conditions set forth in these General Terms and any additional Order Confirmation Terms collectively.

"User" or "you" is the person or entity making the use granted under the relevant License. Where the person accepting the Terms on behalf of a User is a freelancer or other third party who the User authorized to accept the General Terms on the User's behalf, such person shall be deemed jointly a User for purposes of such Terms.

"Work(s)" are the copyright protected works described in relevant Order Confirmations.

2) **Description of Service.** CCC's Marketplace enables Users to obtain Licenses to use one or more Works in accordance with all relevant Terms. CCC grants Licenses as an agent on behalf of the copyright rightsholder identified in the relevant Order Confirmation.

3) **Applicability of Terms.** The Terms govern User's use of Works in connection with the relevant License. In the event of

any conflict between General Terms and Order Confirmation Terms, the latter shall govern. User acknowledges that Rightsholders have complete discretion whether to grant any permission, and whether to place any limitations on any grant, and that CCC has no right to supersede or to modify any such discretionary act by a Rightsholder.

4) **Representations; Acceptance.** By using the Service, User represents and warrants that User has been duly authorized by the User to accept, and hereby does accept, all Terms.

5) **Scope of License; Limitations and Obligations.** All Works and all rights therein, including copyright rights, remain the sole and exclusive property of the Rightsholder. The License provides only those rights expressly set forth in the terms and conveys no other rights in any Works

6) **General Payment Terms.** User may pay at time of checkout by credit card or choose to be invoiced. If the User chooses to be invoiced, the User shall: (i) remit payments in the manner identified on specific invoices, (ii) unless otherwise specifically stated in an Order Confirmation or separate written agreement, Users shall remit payments upon receipt of the relevant invoice from CCC, either by delivery or notification of availability of the invoice via the Marketplace platform, and (iii) if the User does not pay the invoice within 30 days of receipt, the User may incur a service charge of 1.5% per month or the maximum rate allowed by applicable law, whichever is less. While User may exercise the rights in the License immediately upon receiving the Order Confirmation, the License is automatically revoked and is null and void, as if it had never been issued, if CCC does not receive complete payment on a timely basis.

7) **General Limits on Use.** Unless otherwise provided in the Order Confirmation, any grant of rights to User (i) involves only the rights set forth in the Terms and does not include subsequent or additional uses, (ii) is non-exclusive and non-transferable, and (iii) is subject to any and all limitations and restrictions (such as, but not limited to, limitations on duration of use or circulation) included in the Terms. Upon completion of the licensed use as set forth in the Order Confirmation, User shall either secure a new permission for further use of the Work(s) or immediately cease any new use of the Work(s) and shall render inaccessible (such as by deleting or by removing or severing links or other locators) any further copies of the Work. User may only make alterations to the Work if and as expressly set forth in the Order Confirmation. No Work may be used in any way that is unlawful, including without limitation if such use would violate applicable sanctions laws or regulations, would be defamatory, violate the rights of third parties (including such third parties' rights of copyright, privacy, publicity, or other tangible or intangible property), or is otherwise illegal, sexually explicit, or obscene. In addition, User may not conjoin a Work with any other material that may result in damage to the reputation of the Rightsholder. Any unlawful use will render any licenses hereunder null and void. User agrees to inform CCC if it becomes aware of any infringement of any rights in a Work and to cooperate with any reasonable request of CCC or the Rightsholder in connection therewith.

8) **Third Party Materials.** In the event that the material for which a License is sought includes third party materials (such as photographs, illustrations, graphs, inserts and similar materials) that are identified in such material as having been used by permission (or a similar indicator), User is responsible for identifying, and seeking separate licenses (under this Service, if available, or otherwise) for any of such third party materials; without a separate license, User may not use such third party materials via the License.

9) **Copyright Notice.** Use of proper copyright notice for a Work is required as a condition of any License granted under the Service. Unless otherwise provided in the Order Confirmation, a proper copyright notice will read substantially as follows: "Used with permission of [Rightsholder's name], from [Work's title, author, volume, edition number and year of copyright]; permission conveyed through Copyright Clearance Center, Inc." Such notice must be provided in a reasonably legible font size and must be placed either on a cover page or in another location that any person, upon gaining access to the material which is the subject of a permission, shall see, or in the case of republication Licenses, immediately adjacent to the Work as used (for example, as part of a by-line or footnote) or in the place where substantially all other credits or notices for the new work containing the republished Work are located. Failure to include the required notice results in loss to the Rightsholder and CCC, and the User shall be liable to pay liquidated damages for each such failure equal to twice the use fee specified in the Order Confirmation, in addition to the use fee itself and any other fees and charges specified.

10) **Indemnity.** User hereby indemnifies and agrees to defend the Rightsholder and CCC, and their respective employees and directors, against all claims, liability, damages, costs, and expenses, including legal fees and expenses, arising out of any use of a Work beyond the scope of the rights granted herein and in the Order Confirmation, or any use of a Work which has been altered in any unauthorized way by User, including claims of defamation or infringement of rights of copyright, publicity, privacy, or other tangible or intangible property.

11) **Limitation of Liability.** UNDER NO CIRCUMSTANCES WILL CCC OR THE RIGHTSHOLDER BE LIABLE FOR ANY DIRECT, INDIRECT, CONSEQUENTIAL, OR INCIDENTAL DAMAGES (INCLUDING WITHOUT LIMITATION DAMAGES FOR LOSS OF BUSINESS PROFITS OR INFORMATION, OR FOR BUSINESS INTERRUPTION) ARISING OUT OF THE USE OR INABILITY TO USE A WORK, EVEN IF ONE OR BOTH OF THEM HAS BEEN ADVISED OF THE POSSIBILITY OF SUCH DAMAGES. In any event, the total liability of the Rightsholder and CCC (including their respective employees and directors) shall not exceed the total amount actually paid by User for the relevant License. User assumes full liability for the actions and omissions of its principals, employees, agents, affiliates, successors, and assigns.

12) **Limited Warranties.** THE WORK(S) AND RIGHT(S) ARE PROVIDED "AS IS." CCC HAS THE RIGHT TO GRANT TO USER THE RIGHTS GRANTED IN THE ORDER CONFIRMATION DOCUMENT. CCC AND THE RIGHTSHOLDER DISCLAIM ALL OTHER WARRANTIES RELATING TO THE WORK(S) AND RIGHT(S), EITHER EXPRESS OR IMPLIED, INCLUDING WITHOUT LIMITATION IMPLIED WARRANTIES OF MERCHANTABILITY OR FITNESS FOR A PARTICULAR PURPOSE. ADDITIONAL RIGHTS MAY BE REQUIRED TO USE ILLUSTRATIONS, GRAPHS, PHOTOGRAPHS, ABSTRACTS, INSERTS, OR OTHER PORTIONS OF THE WORK (AS OPPOSED TO THE ENTIRE WORK) IN A MANNER CONTEMPLATED BY USER; USER UNDERSTANDS AND AGREES THAT NEITHER CCC NOR THE RIGHTSHOLDER MAY HAVE SUCH ADDITIONAL RIGHTS TO GRANT.

13) **Effect of Breach.** Any failure by User to pay any amount when due, or any use by User of a Work beyond the scope of the License set forth in the Order Confirmation and/or the Terms, shall be a material breach of such License. Any breach not cured within 10 days of written notice thereof shall result in immediate termination of such License without further notice. Any unauthorized (but licensable) use of a Work that is terminated immediately upon notice thereof may be liquidated by payment of the Rightsholder's ordinary license price therefor; any unauthorized (and unlicensable) use that is not terminated immediately for any reason (including, for example, because materials containing the Work cannot reasonably be recalled) will be subject to all remedies available at law or in equity, but in no event to a payment of less than three times the Rightsholder's ordinary license price for the most closely analogous licensable use plus Rightsholder's and/or CCC's costs and expenses incurred in collecting such payment.

14) **Additional Terms for Specific Products and Services.** If a User is making one of the uses described in this Section 14, the additional terms and conditions apply:

a) ***Print Uses of Academic Course Content and Materials (photocopies for academic coursepacks or classroom handouts).*** For photocopies for academic coursepacks or classroom handouts the following additional terms apply:

i) The copies and anthologies created under this License may be made and assembled by faculty members individually or at their request by on-campus bookstores or copy centers, or by off-campus copy shops and other similar entities.

ii) No License granted shall in any way: (i) include any right by User to create a substantively non-identical copy of the Work or to edit or in any other way modify the Work (except by means of deleting material immediately preceding or following the entire portion of the Work copied) (ii) permit "publishing ventures" where any particular anthology would be systematically marketed at multiple institutions.

iii) Subject to any Publisher Terms (and notwithstanding any apparent contradiction in the Order Confirmation arising from data provided by User), any use authorized under the academic pay-per-use service is limited as follows:

A) any License granted shall apply to only one class (bearing a unique identifier as assigned by the institution, and thereby including all sections or other subparts of the class) at one institution;

B) use is limited to not more than 25% of the text of a book or of the items in a published collection of essays, poems or articles;

C) use is limited to no more than the greater of (a) 25% of the text of an issue of a journal or other periodical or (b) two articles from such an issue;

D) no User may sell or distribute any particular anthology, whether photocopied or electronic, at more than one institution of learning;

E) in the case of a photocopy permission, no materials may be entered into electronic memory by User except in order to produce an identical copy of a Work before or during the academic term (or analogous period) as to which any particular permission is granted. In the event that User shall choose to retain materials that are the subject of a photocopy permission in electronic memory for purposes of producing identical copies more

than one day after such retention (but still within the scope of any permission granted), User must notify CCC of such fact in the applicable permission request and such retention shall constitute one copy actually sold for purposes of calculating permission fees due; and

F) any permission granted shall expire at the end of the class. No permission granted shall in any way include any right by User to create a substantively non-identical copy of the Work or to edit or in any other way modify the Work (except by means of deleting material immediately preceding or following the entire portion of the Work copied).

iv) Books and Records; Right to Audit. As to each permission granted under the academic pay-per-use Service, User shall maintain for at least four full calendar years books and records sufficient for CCC to determine the numbers of copies made by User under such permission. CCC and any representatives it may designate shall have the right to audit such books and records at any time during User's ordinary business hours, upon two days' prior notice. If any such audit shall determine that User shall have underpaid for, or underreported, any photocopies sold or by three percent (3%) or more, then User shall bear all the costs of any such audit; otherwise, CCC shall bear the costs of any such audit. Any amount determined by such audit to have been underpaid by User shall immediately be paid to CCC by User, together with interest thereon at the rate of 10% per annum from the date such amount was originally due. The provisions of this paragraph shall survive the termination of this License for any reason.

b) ***Digital Pay-Per-Uses of Academic Course Content and Materials (e-coursepacks, electronic reserves, learning management systems, academic institution intranets).*** For uses in e-coursepacks, posts in electronic reserves, posts in learning management systems, or posts on academic institution intranets, the following additional terms apply:

i) The pay-per-uses subject to this Section 14(b) include:

A) **Posting e-reserves, course management systems, e-coursepacks for text-based content,** which grants authorizations to import requested material in electronic format, and allows electronic access to this material to members of a designated college or university class, under the direction of an instructor designated by the college or university, accessible only under appropriate electronic controls (e.g., password);

B) **Posting e-reserves, course management systems, e-coursepacks for material consisting of photographs or other still images not embedded in text,** which grants not only the authorizations described in Section 14(b)(i)(A) above, but also the following authorization: to include the requested material in course materials for use consistent with Section 14(b)(i)(A) above, including any necessary resizing, reformatting or modification of the resolution of such requested material (provided that such modification does not alter the underlying editorial content or meaning of the requested material, and provided that the resulting modified content is used solely within the scope of, and in a manner consistent with, the particular authorization described in the Order Confirmation and the Terms), but not including any other form of manipulation, alteration or editing of the requested material;

C) **Posting e-reserves, course management systems, e-coursepacks or other academic distribution for audiovisual content,** which grants not only the authorizations described in Section 14(b)(i)(A) above, but also the following authorizations: (i) to include the requested material in course materials for use consistent with Section 14(b)(i)(A) above; (ii) to display and perform the requested material to such members of such class in the physical classroom or remotely by means of streaming media or other video formats; and (iii) to "clip" or reformat the requested material for purposes of time or content management or ease of delivery, provided that such "clipping" or reformatting does not alter the underlying editorial content or meaning of the requested material and that the resulting material is used solely within the scope of, and in a manner consistent with, the particular authorization described in the Order Confirmation and the Terms. Unless expressly set forth in the relevant Order Conformation, the License does not authorize any other form of manipulation, alteration or editing of the requested material.

ii) Unless expressly set forth in the relevant Order Confirmation, no License granted shall in any way: (i) include any right by User to create a substantively non-identical copy of the Work or to edit or in any other way modify the Work (except by means of deleting material immediately preceding or following the entire portion of the Work copied or, in the case of Works subject to Sections 14(b)(1)(B) or (C) above, as described in such Sections) (ii) permit "publishing ventures" where any particular course materials would be systematically marketed at multiple institutions.

iii) Subject to any further limitations determined in the Rightsholder Terms (and notwithstanding any apparent contradiction in the Order Confirmation arising from data provided by User), any use authorized under the electronic course content pay-per-use service is limited as follows:

A) any License granted shall apply to only one class (bearing a unique identifier as assigned by the institution, and thereby including all sections or other subparts of the class) at one institution;

B) use is limited to not more than 25% of the text of a book or of the items in a published collection of essays, poems or articles;

C) use is limited to not more than the greater of (a) 25% of the text of an issue of a journal or other periodical or (b) two articles from such an issue;

D) no User may sell or distribute any particular materials, whether photocopied or electronic, at more than one institution of learning;

E) electronic access to material which is the subject of an electronic-use permission must be limited by means of electronic password, student identification or other control permitting access solely to students and instructors in the class;

F) User must ensure (through use of an electronic cover page or other appropriate means) that any person, upon gaining electronic access to the material, which is the subject of a permission, shall see:

- a proper copyright notice, identifying the Rightsholder in whose name CCC has granted permission,
- a statement to the effect that such copy was made pursuant to permission,
- a statement identifying the class to which the material applies and notifying the reader that the material has been made available electronically solely for use in the class, and
- a statement to the effect that the material may not be further distributed to any person outside the class, whether by copying or by transmission and whether electronically or in paper form, and User must also ensure that such cover page or other means will print out in the event that the person accessing the material chooses to print out the material or any part thereof.

G) any permission granted shall expire at the end of the class and, absent some other form of authorization, User is thereupon required to delete the applicable material from any electronic storage or to block electronic access to the applicable material.

iv) Uses of separate portions of a Work, even if they are to be included in the same course material or the same university or college class, require separate permissions under the electronic course content pay-per-use Service. Unless otherwise provided in the Order Confirmation, any grant of rights to User is limited to use completed no later than the end of the academic term (or analogous period) as to which any particular permission is granted.

v) Books and Records; Right to Audit. As to each permission granted under the electronic course content Service, User shall maintain for at least four full calendar years books and records sufficient for CCC to determine the numbers of copies made by User under such permission. CCC and any representatives it may designate shall have the right to audit such books and records at any time during User's ordinary business hours, upon two days' prior notice. If any such audit shall determine that User shall have underpaid for, or underreported, any electronic copies used by three percent (3%) or more, then User shall bear all the costs of any such audit; otherwise, CCC shall bear the costs of any such audit. Any amount determined by such audit to have been underpaid by User shall immediately be paid to CCC by User, together with interest thereon at the rate of 10% per annum from the date such amount was originally due. The provisions of this paragraph shall survive the termination of this license for any reason.

c) ***Pay-Per-Use Permissions for Certain Reproductions (Academic photocopies for library reserves and interlibrary loan reporting) (Non-academic internal/external business uses and commercial document delivery).*** The License expressly excludes the uses listed in Section (c)(i)-(v) below (which must be subject to separate license from the applicable Rightsholder) for: academic photocopies for library reserves and interlibrary loan reporting; and non-academic internal/external business uses and commercial document delivery.

i) electronic storage of any reproduction (whether in plain-text, PDF, or any other format) other than on a transitory basis;

ii) the input of Works or reproductions thereof into any computerized database;

iii) reproduction of an entire Work (cover-to-cover copying) except where the Work is a single article;

iv) reproduction for resale to anyone other than a specific customer of User;

v) republication in any different form. Please obtain authorizations for these uses through other CCC services or directly from the rightsholder.

Any license granted is further limited as set forth in any restrictions included in the Order Confirmation and/or in these Terms.

d) ***Electronic Reproductions in Online Environments (Non-Academic-email, intranet, internet and extranet).*** For "electronic reproductions", which generally includes e-mail use (including instant messaging or other electronic transmission to a defined group of recipients) or posting on an intranet, extranet or Intranet site (including any display or performance incidental thereto), the following additional terms apply:

i) Unless otherwise set forth in the Order Confirmation, the License is limited to use completed within 30 days for any use on the Internet, 60 days for any use on an intranet or extranet and one year for any other use, all as measured from the "republication date" as identified in the Order Confirmation, if any, and otherwise from the date of the Order Confirmation.

ii) User may not make or permit any alterations to the Work, unless expressly set forth in the Order Confirmation (after request by User and approval by Rightsholder); provided, however, that a Work consisting of photographs or other still images not embedded in text may, if necessary, be resized, reformatted or have its resolution modified without additional express permission, and a Work consisting of audiovisual content may, if necessary, be "clipped" or reformatted for purposes of time or content management or ease of delivery (provided that any such resizing, reformatting, resolution modification or "clipping" does not alter the underlying editorial content or meaning of the Work used, and that the resulting material is used solely within the scope of, and in a manner consistent with, the particular License described in the Order Confirmation and the Terms.

15) **Miscellaneous.**

a) User acknowledges that CCC may, from time to time, make changes or additions to the Service or to the Terms, and that Rightsholder may make changes or additions to the Rightsholder Terms. Such updated Terms will replace the prior terms and conditions in the order workflow and shall be effective as to any subsequent Licenses but shall not apply to Licenses already granted and paid for under a prior set of terms.

b) Use of User-related information collected through the Service is governed by CCC's privacy policy, available online at www.copyright.com/about/privacy-policy/.

c) The License is personal to User. Therefore, User may not assign or transfer to any other person (whether a natural person or an organization of any kind) the License or any rights granted thereunder; provided, however, that, where applicable, User may assign such License in its entirety on written notice to CCC in the event of a transfer of all or substantially all of User's rights in any new material which includes the Work(s) licensed under this Service.

d) No amendment or waiver of any Terms is binding unless set forth in writing and signed by the appropriate parties, including, where applicable, the Rightsholder. The Rightsholder and CCC hereby object to any terms contained in any writing prepared by or on behalf of the User or its principals, employees, agents or affiliates and purporting to govern or otherwise relate to the License described in the Order Confirmation, which terms are in any way inconsistent with any Terms set forth in the Order Confirmation, and/or in CCC's standard operating procedures, whether such writing is prepared prior to, simultaneously with or subsequent to the Order Confirmation, and whether such writing appears on a copy of the Order Confirmation or in a separate instrument.

e) The License described in the Order Confirmation shall be governed by and construed under the law of the State of New York, USA, without regard to the principles thereof of conflicts of law. Any case, controversy, suit, action, or proceeding arising out of, in connection with, or related to such License shall be brought, at CCC's sole discretion, in

any federal or state court located in the County of New York, State of New York, USA, or in any federal or state court whose geographical jurisdiction covers the location of the Rightsholder set forth in the Order Confirmation. The parties expressly submit to the personal jurisdiction and venue of each such federal or state court.

Last updated October 2022

Publication 3

RightsLink

Sign in/Register

Probucol-Ursodeoxycholic Acid Otic Formulations: Stability and In Vitro Assessments for Hearing Loss Treatment

Author:
Corina M. Ionescu,Bozica Kovacevic,Melissa A. Jones,Susbin R. Wagle,Thomas Foster,Momir Mikov,Armin Mooranian,Hani Al-Salami

Publication: Journal of Pharmaceutical Sciences
Publisher: Elsevier
Date: Available online 10 May 2024

Journal Author Rights

Please note that, as the author of this Elsevier article, you retain the right to include it in a thesis or dissertation, provided it is not published commercially. Permission is not required, but please ensure that you reference the journal as the original source. For more information on this and on your other retained rights, please visit: https://www.elsevier.com/about/our-business/policies/copyright#Author-rights

BACK CLOSE WINDOW

Appendix II

The Appendix contains Primary Publication Attribution statements.

I, Corina Mihaela Ionescu, as the author of this thesis, contributed to the following publications as outlined below. Co-author signed authorship forms approved by Curtin University with attributed contributions (including myself for secondary publications) are available upon request from the primary supervisor and the corresponding author – Dr Hani Al-Salami (Tel: +61 8 9266 9816; E-mail: hani.al-salami@curtin.edu.au)

Publication 1 & Publication 2 (Chapter 2)

Conception and design of the project, comprehensive literature search, analysis and drafting of the reviews, generating figures, editing and reviewing the manuscript for publication.

Publication 3 (Chapter 3)

Conception and design of the project, comprehensive literature search, data analysis and interpretation, drafting of the paper, generating figures, editing and reviewing the manuscript for publication.

Publication 4 (Chapter 4)

Conception and design of the project, comprehensive literature search, data analysis and interpretation, drafting of the paper, generating figures, editing and reviewing the manuscript for publication.

Publication 5 (Chapter 5)

Conception and design of the project, comprehensive literature search, data analysis and interpretation, drafting of the paper, generating figures, editing and reviewing the manuscript for publication.

Signature: 

Data: 25.08.2024

Appendix III

The Appendix is an extension of Chapter 3 and contains Supplementary figures.

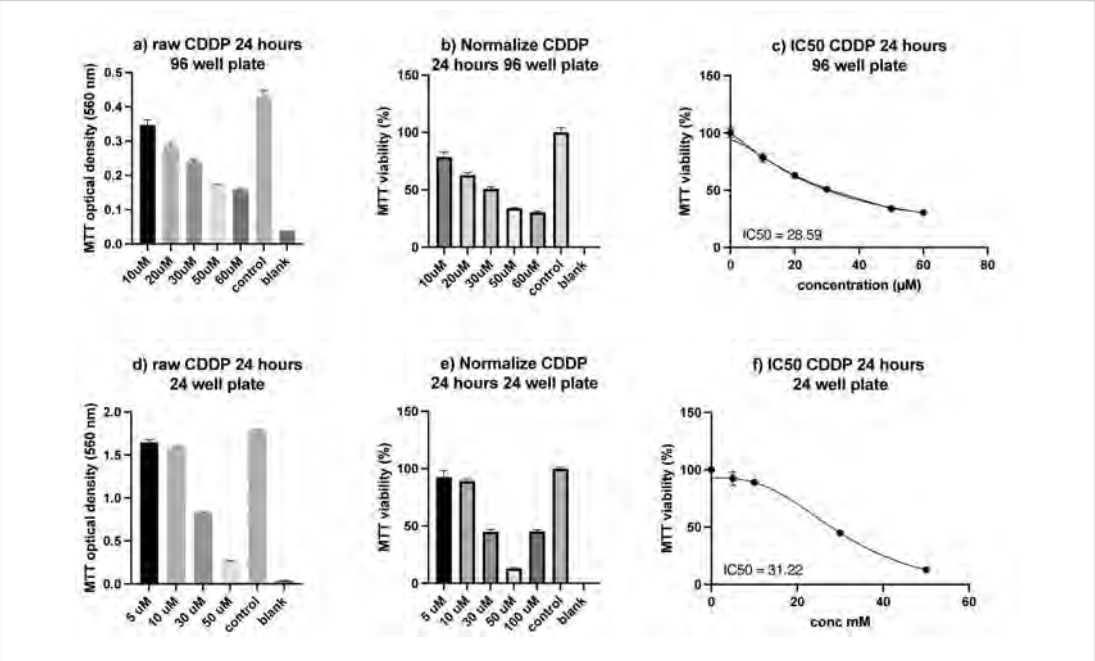

Supplementary III.1.

Cisplatin inhibitory concentration (IC50) for HEI-OC1 at 24 hours grown on 96 well plates or 24 well plates. MTT results with a,d) raw data collected from the multimode plate reader (560 nm). Normalised results were calculated from raw readings in GraphPad Prism using control mean as 100%, and blank mean as 0%. The IC50 curve c,f) for cisplatin was calculated using the nonlinear regression (curve fit) with dose-response inhibition equation on GraphPad Prism. Cisplatin stock solutions were prepared at 1 mg/mL (3.3 mM) in PBS and filtered with syringe filters (456). Stock solutions are stable for approximatively a month at 4°C (457). Appropriate dilutions were prepared from stock solution in DMEM for experiments. Cisplatin instability was recorded on some optimisation experiments examples within the later Appendixes. This was observed by higher than 50% viability in CDDP groups. Viability variation for CDDP can also be influenced by cellular seeding density. HEI-OC1 were seeded at 2 x 10^5 cells/mL density according to protocol (59).

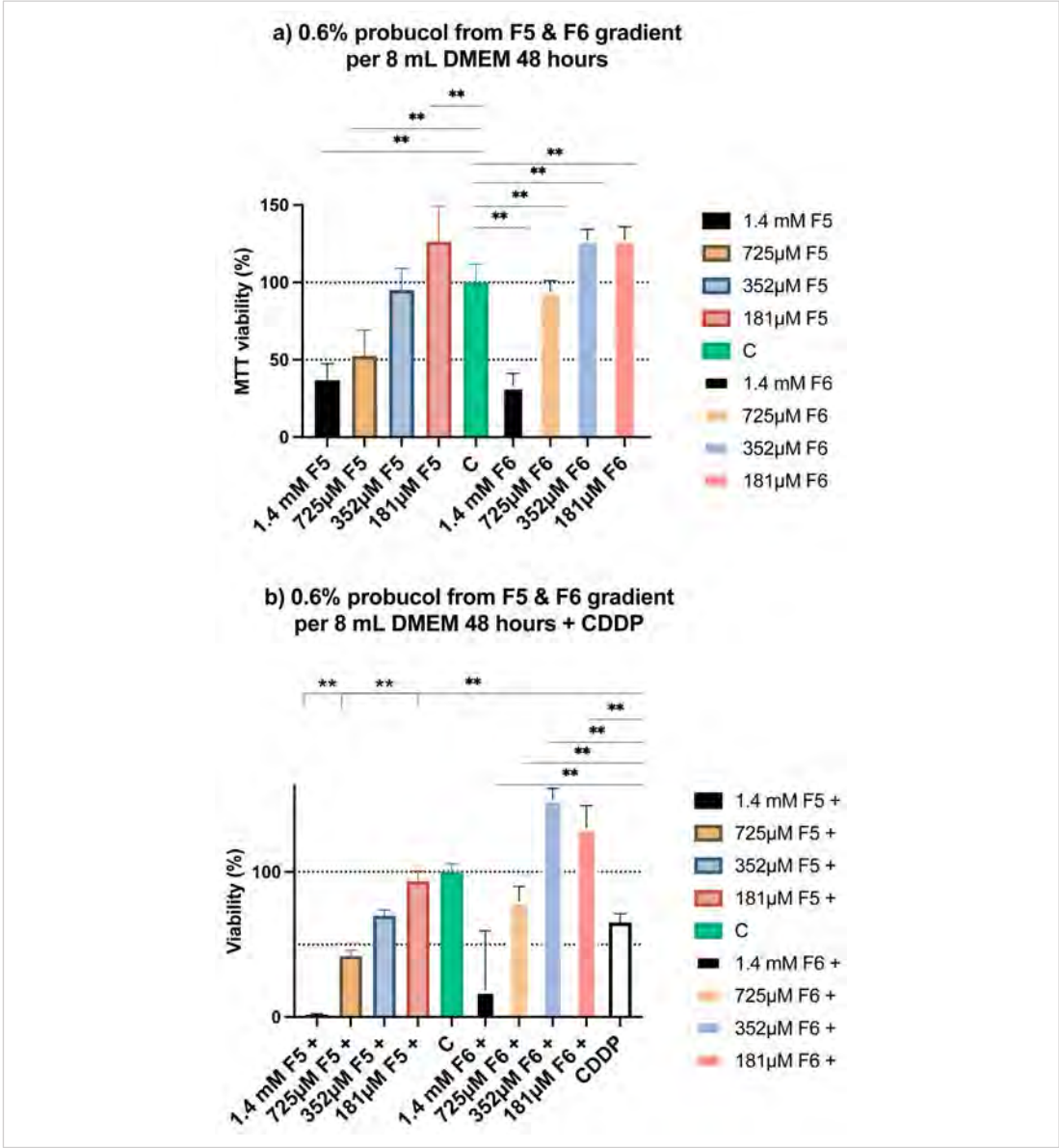

Supplementary III.2.

Probucol formulations improve HEI-OC1 viability against cisplatin. Spray dried solid dispersion F5 (probucol-UDCA) and F6 (probucol) gradient dilutions as treatments on HEI-OC1 cells after 48 hours culture (complementary for figure 3.5). Based on previous HPLC drug quantification from F5 and F6, spray dried solid dispersions were weight and dispersed in 8 mL DMEM at a set drug concentration of 1.4 mM (representing the spray-dried feed-stock concentration of 0.6%). a) F5 and F6 treatments and control untreated cells. b) F5 and F6 treatments and cisplatin (CDDP; F5+, F6+) in cell culture. Treatments at 181 µM (F5) and 352 µM and 181 µM (F6) show significant increased viability (<95%) in relation to control untreated and control CDDP. Error bards represent standard error of the mean, $n = 1$, $^{**}p < 0.002$.

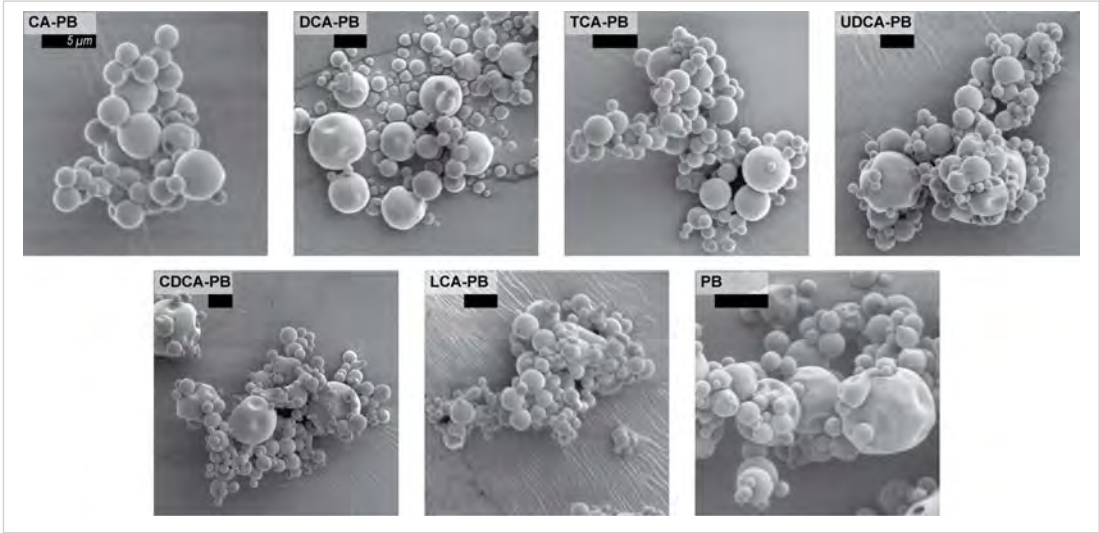

Supplementary III.3.

Scanning electron micrographs of spray dried solid dispersions containing probucol (PB) in combination with CA, DCA, TCA, UDCA, CDCA, LCA. Formulation components are presented in Chapter 3 (2% β-CD, 2.3% PEG, 1.3% PVP, 0.8% PVA, 0.3% bile acids, 0.6% probucol mixed in milli-Q water) are spray dried at the same conditions; 150°C inlet and 58-65°C outlet temperature with 80% aspirator power. Scale bars 5 µm.

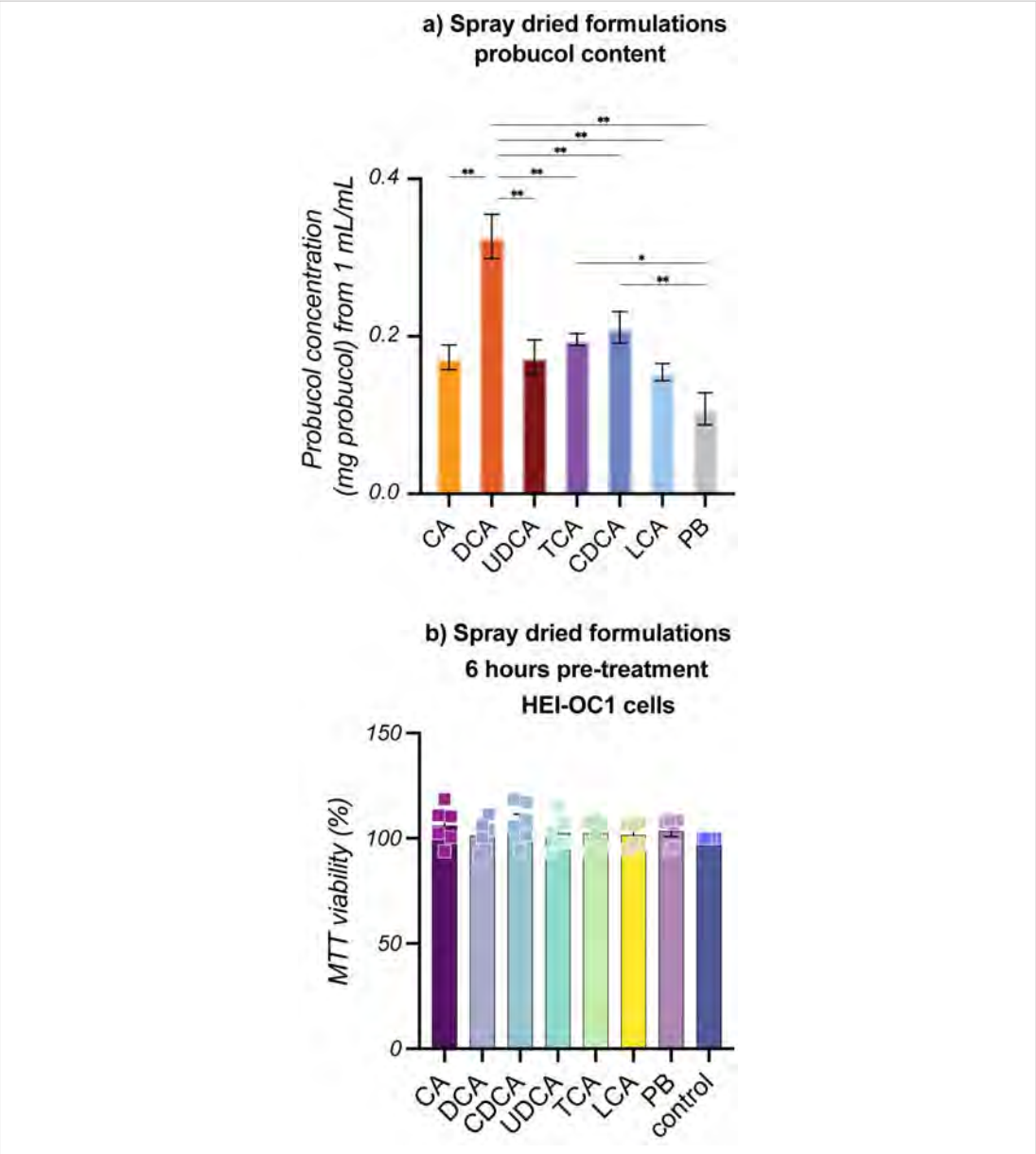

Supplementary III.4.

Probucol-bile acid drug content and *in vitro* treatments. a) Drug content from probucol-bile acid (CA, DCA, CDCA, UDCA, TCA and LCA) and probucol only (PB) solid dispersions (as seen in Supplementary III.3). HPLC (SIL-20A model UV detector, Kyoto, JP) solid dispersions samples were extracted with 100% acetonitrile at 1 mg/mL. Analysed using a C18 column (Luna 5 µm, 100 Å, 150 x 4.6 mm, Phenomenex, Torrance, CA, USA) at 1 mL/minute flow rate and ~13 minutes retention time, $n = 3$. b) HEI-OC1 viability after six hours pre-treatment with solid dispersion followed by 24 hours culture at 33°C. Spray dried probucol solid dispersions drug loading variation does not affect HEI-OC1 survival. Error bars represent standard error of the mean, $n = 2$*$p < 0.03$, **$p < 0.002$.

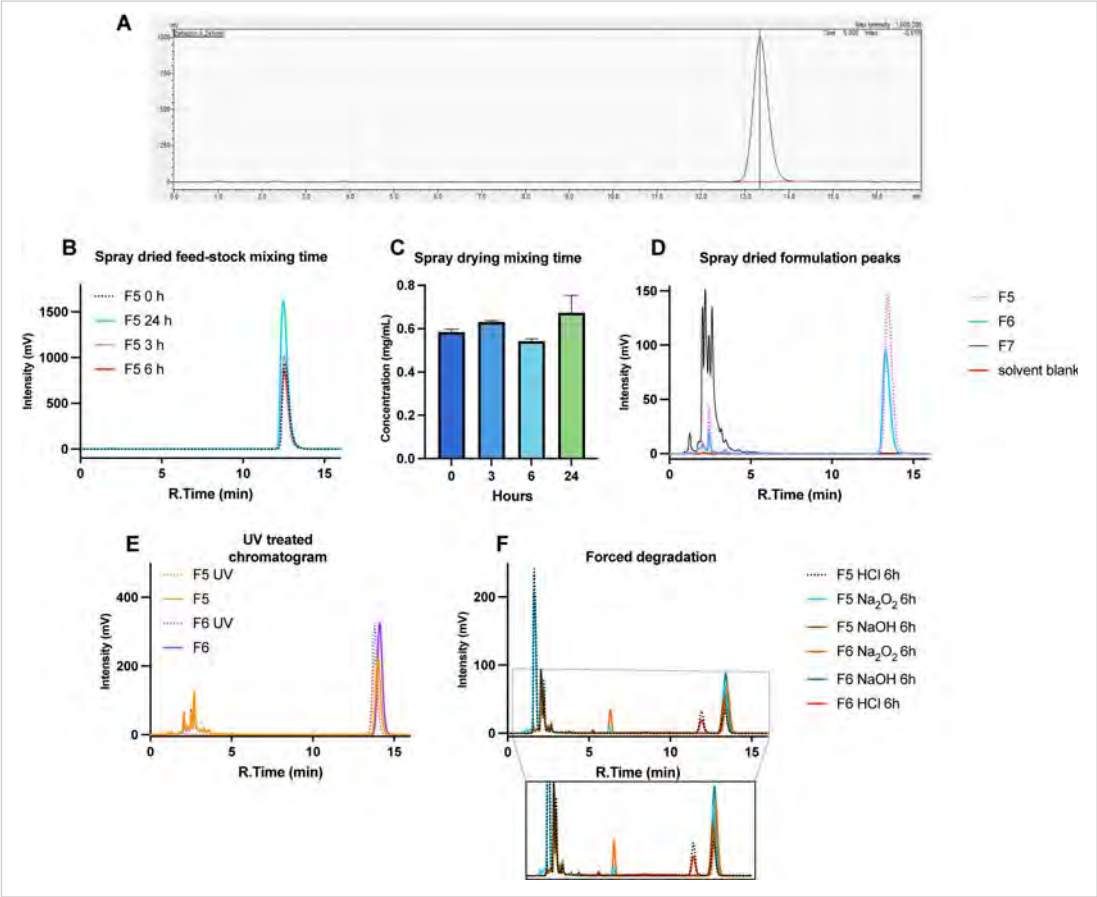

Supplementary III.5.

Probucol chromatograms, drug intensity and degradation (complementary to figure 3.4, table 3.3). A) Probucol peak integration (red line), retention time ~13.4 minutes. B) Probucol chromatogram from F5 feed-stock solutions after homogenisation (0 hours) or stirring for 3, 6 and 24 hours, and associated C) drug concentration showing drug content variation, but no significance in probucol after spray drying ($n = 2$ in four technical replicates). D) Solid dispersions of probucol F5, F6 and control F7 (DCA only). Chromatogram intensity differs for F5 and F6 and formulations show different concentrations. Control F7 shows that the initial peak intensities around 2-5 minutes correspond with formulation matrix ingredients. E) Solid dispersion chromatograms before and after 20 minute UV exposure. F) Probucol forced degradation from F5 and F6 solid dispersions in HCl, Na_2O_2 and NaOH solutions after 6 hours. Probucol impurity/metabolite peaks are at ~11 minutes after HCl degradation, and at ~7 minutes for Na_2O_2 degradation. The additional peaks do not interfere with probucol integration.

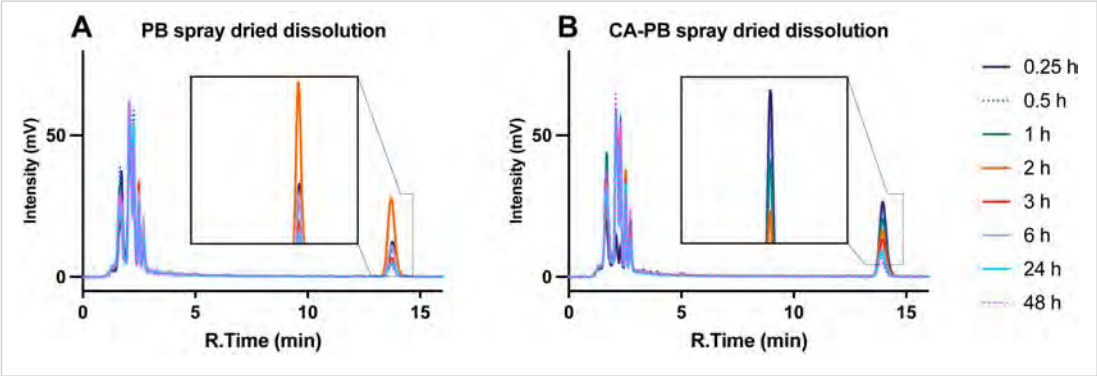

Supplementary III.6.

Probucol chromatograms from spray dried solid dispersions (complementary for Supplementary III.3 and Supplementary III.7.). A) Probucol (PB) spray dried solid dispersions and B) CA-PB solid dispersion dissolution chromatograms for 0.25, 0.5, 1, 2, 3, 6, 24 and 48 hours. Probucol retention time ~13 minutes. Peak intensity decreases with dissolution time and differs for both formulations.

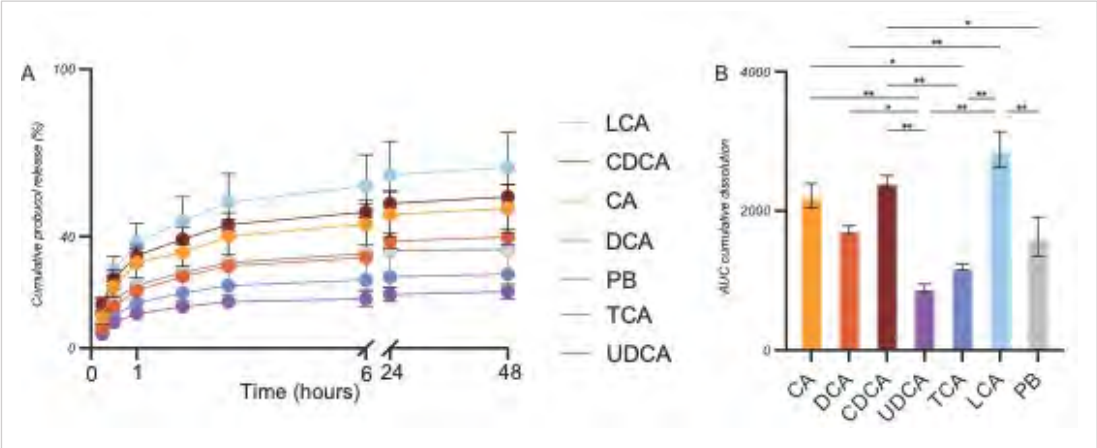

Supplementary III.7.

Probucol-bile acid (CA, DCA, CDCA, UDCA, TCA, LCA) and probucol (PB) solid dispersion dissolution patterns. A. Percentage values of cumulative release over time (48 hours). Spray dried particles were kept in co-treatment culture with HEI-OC1 cells. Particles were resuspended in DMEM at 20 mg/mL. At each time point (0.25, 0.5, 1, 3, 6, 24, 48 and 72 hours), 1 mL aliquots were collected, spun at 10^4 rmp for 5 minutes, then supernatant was processed for HPLC by acetonitrile extraction (1:1). 1 mL DMEM was added to cell culture for each aliquot collected. Samples were filtrated prior to analysis on HPLC (SIL-20A model UV detector, Kyoto, JP) using a C18 column (Luna 5 µm, 100 Å, 150 x 4.6 mm, Phenomenex, Torrance, CA, USA) at 1 mL/minute flow rate and ~13 minutes retention time. B. Area under the curve calculated from the cumulative probucol release (A). This shows that the more lipophilic bile acid (LCA > CDCA > CA) formulations have a significantly higher probucol release compared to probucol-UDCA (F5 formulation presented in Chapter III). Values represent mg/mL probucol, error bars represent standard error of the mean, $n = 2$ in three technical replicates. *$p < 0.05$, **$p < 0.01$.

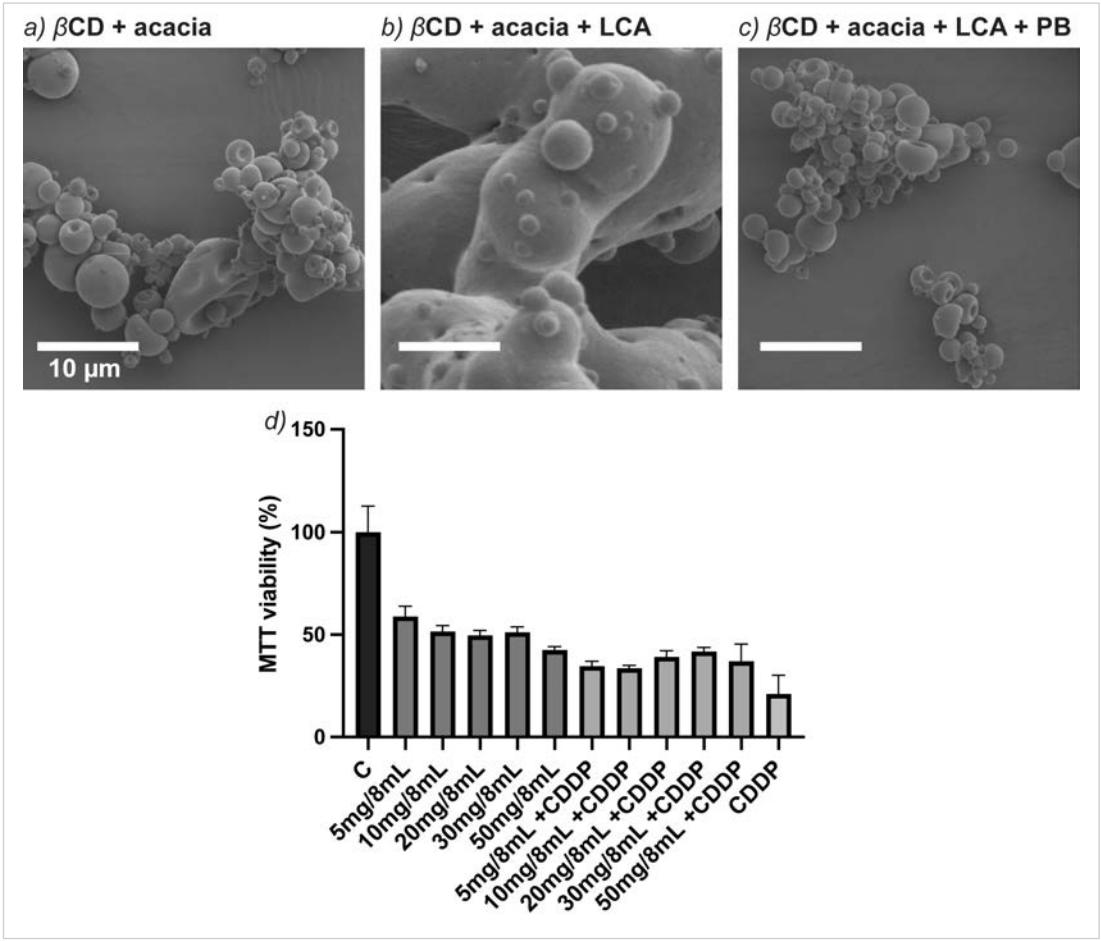

Supplementary III.8.

Spray dried solid dispersion formulation optimisation using [#]acacia polymer. Scanning electron micrographs of formulations, a) containing *β*-CD 2% acacia 1.5%, b) with LCA 0.05% or c) LCA 0.05% and probucol (PB 0.1%). d) Solid dispersions at 50 mg, 20 mg, 10 mg, and 5 mg in 8 mL DMEM applied as treatment on HEI-OC1 cells for 24 hours, with or without cisplatin (+CDDP). Error bars represent standard error of the mean, $n = 1$ in eight technical replicates. Scale bars 10 µm. [#]Purchased from Sigma Aldrich, AU

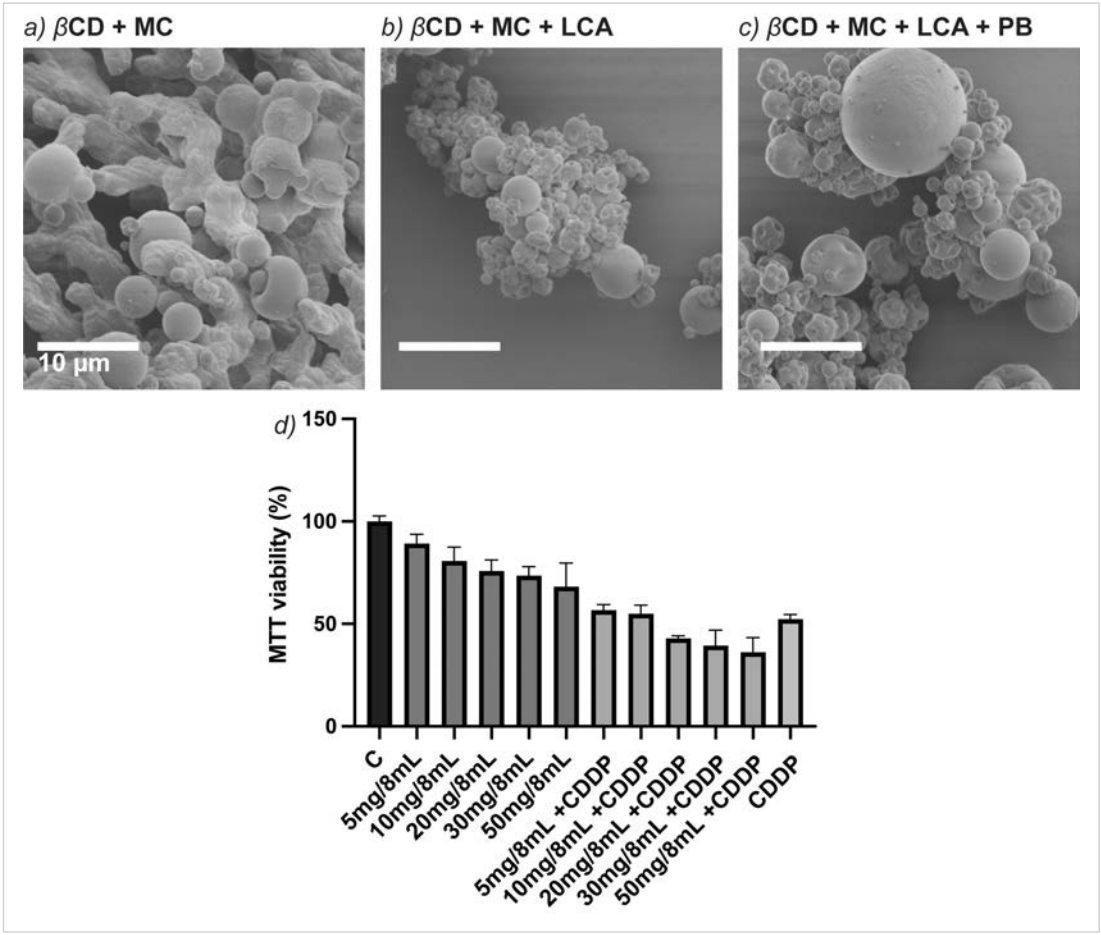

Supplementary III.9.

Spray dried solid dispersion formulation optimisation using [#]methyl cellulose polymer (MC). Scanning electron micrographs of formulations, a) containing *β*-CD 2% MC 1.5%, b) with LCA 0.05% or c) LCA 0.05% and probucol (PB 0.1%). d) Solid dispersions at 50 mg, 20 mg, 10 mg, and 5 mg in 8 mL DMEM applied as treatment for HEI-OC1 cells for 24 hours, with or without cisplatin (+CDDP). Error bars represent standard error of the mean, $n = 1$ in eight technical replicates. Scale bars 10 µm. [#]Purchased from Sigma-Aldrich, AU.

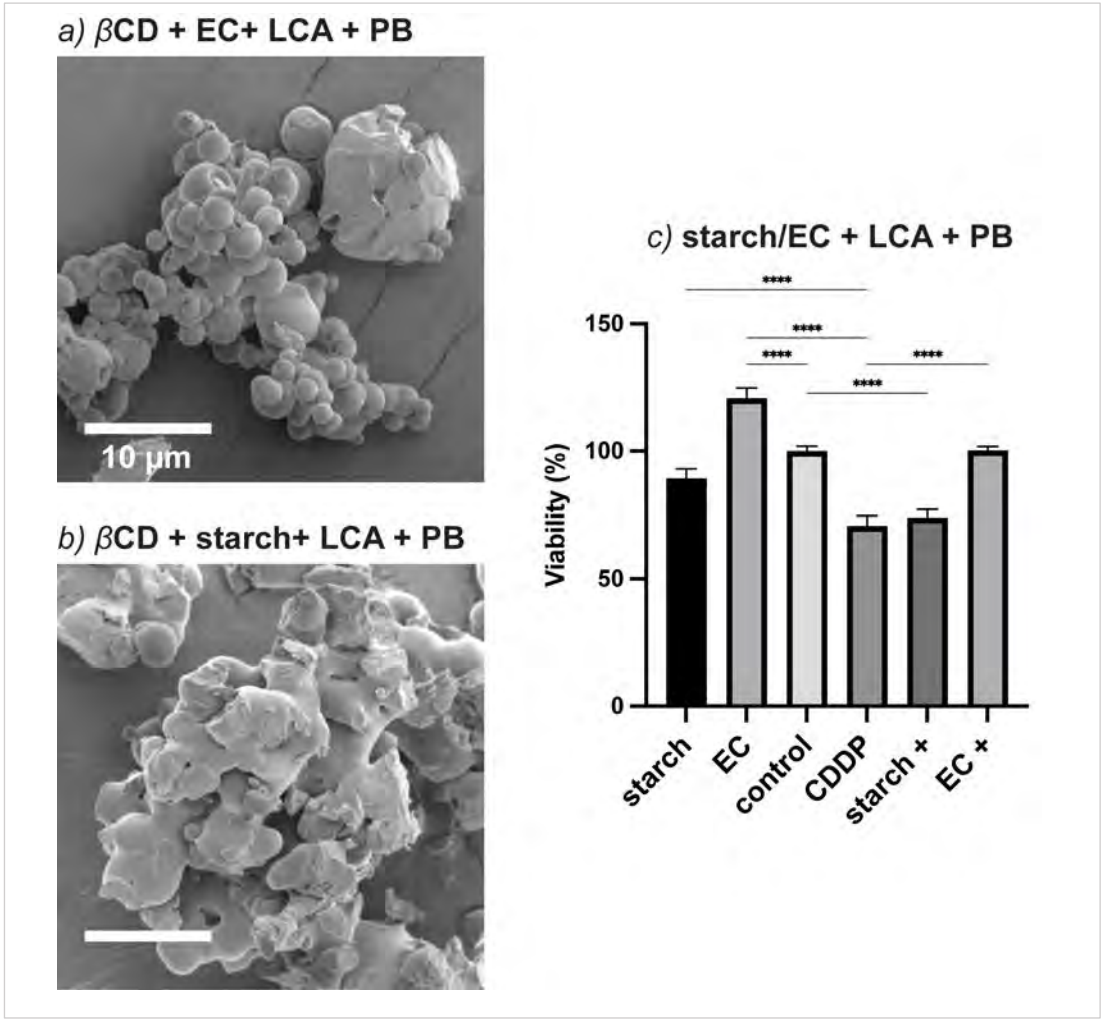

Supplementary III.10.

Spray dried solid dispersion formulation optimisation using ethyl cellulose polymer (EC) or starch (Sigma-Aldrich, AU). Scanning electron micrographs of spray dried a) formulation containing *β*-CD 2% EC 1.5% with LCA 0.05% and probucol (PB 0.1%) and b) *β*-CD 2% starch 1.5% with LCA 0.05% and PB 0.1%. c) Solid dispersions at 10 mg in 8 mL DMEM applied as treatment for HEI-OC1 cells for 24 hours, with or without cisplatin (CDDP; +). Error bars represent standard error of the mean, $n = 1$ in eight technical replicates, ***$p < 0.0002$. Scale bars 10 µm. [#]Purchased from Sigma-Aldrich, AU.

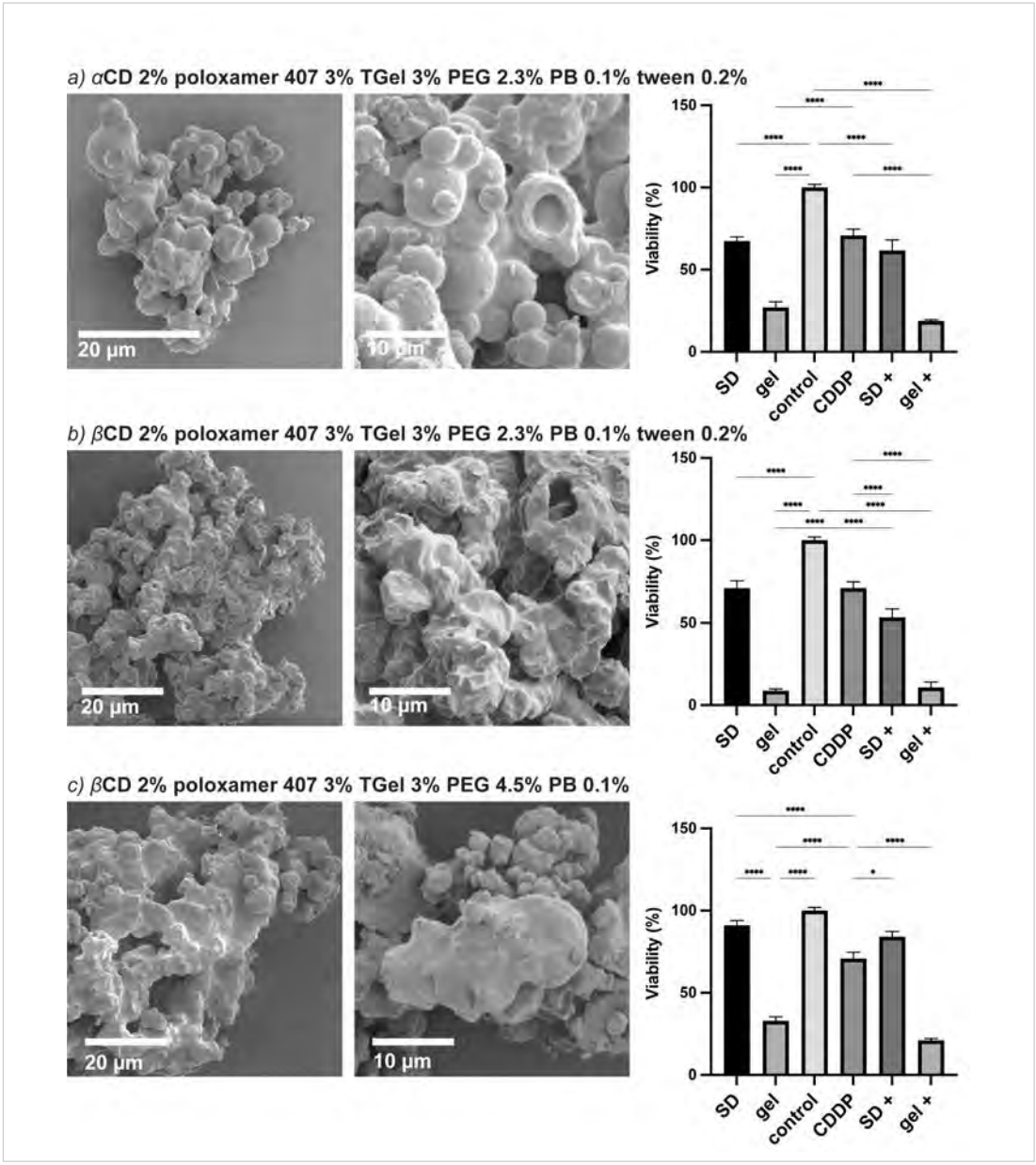

Supplementary III.11.

Scanning electron micrographs of spray dried solid dispersion formulation optimisation and *in vitro* viability results of suspensions (SD) and feed-stock (gel). a) *α*-CD 2%, [#]poloxamer 407 3%, TGel 3%, PEG 2.3%, [#]tween 0.2% and PB 0.1%. b) *β*-CD 2%, poloxamer 407 3%, TGel 3%, PEG 2.3%, [#]tween 0.2% and PB 0.1%. c) *β*-CD 2%, poloxamer 407 3%, TGel 3%, PEG 2.3%, [#]tween 0.2% and PB 0.1%. *In vitro* HEI-OC1 cell treatments for 24 hours, with or without cisplatin (CDDP; +). Error bars represent standard error of the mean, $n = 1$ in eight technical replicates, $*p < 0.03$, $****p < 0.0001$. Scale bars 20 µM (left) and 10 µM (right). [#]Pruchased from Sigma Aldrich, AU.

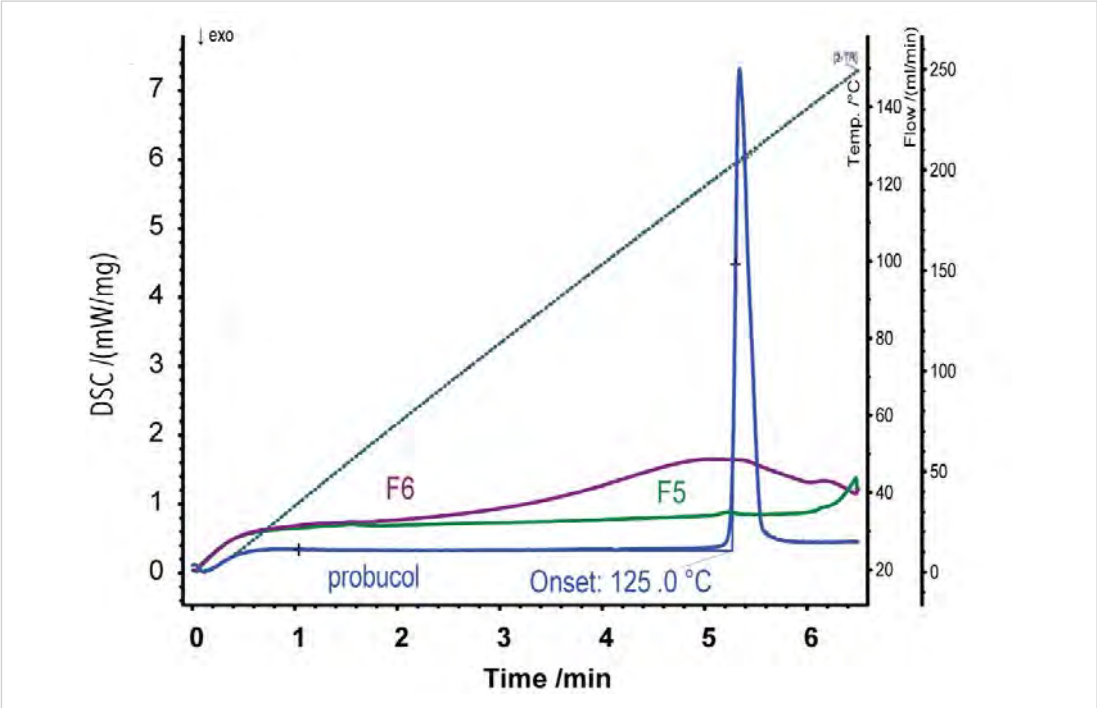

Supplementary III.12.

Differential scanning calorimetry (DSC) for F5 and F6 spray dried solid dispersions in relation to powdered probucol (PB). Dry nitrogen was used as inert gas at 20 mL/min flow rate. Measurements were carried out on a Netzsch instrument (3500 Sirius, Netzsch, Selb, Germany) from 20-160°C at a heating rate of 20°C/min. Probucol powder and samples were placed in pierced aluminium pans for measurements. DSC thermogram for probucol powder (blue) show an endothermic peak at 125°C. The lack of endothermic peaks for F5 (green) and F6 (purple) could either results from insufficient drug within the samples or may represent a transition of the drug from crystalline (endothermic peak) to amorphous state (F4, no peak), and a higher interaction with the polymeric matrix.

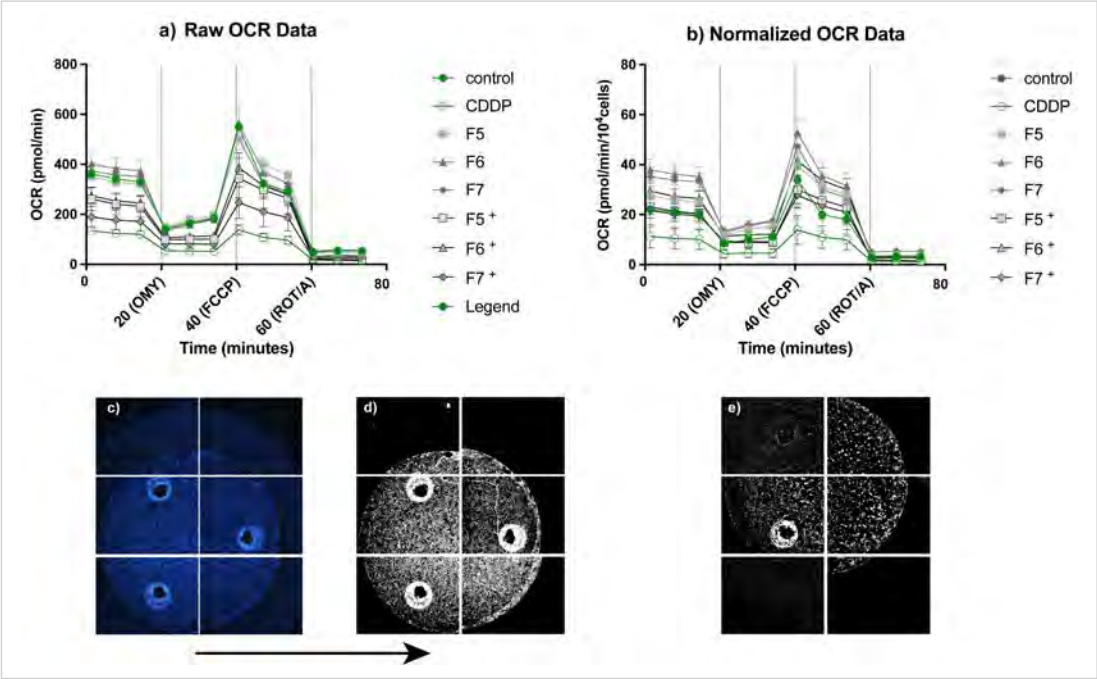

Supplementary III.13.

Seahorse normalisation process (complementary for figure 3.7). As per the assay instructions, seahorse results should be normalised against cell count or total protein concentration for each well. a) Obtained Seahorse raw results were b) normalised per 10^4 cells. At the end of the assay, experimental plates were fixed with 4% PFA and stained with Hoechst dye (blue) 2 µL/mL (from 10 µg/mL stock) and c) imaged using an inverted microscope in six frames to capture the full plate. d) Using ImageJ, the nuclei contour was masked to count cells. Step c) and d) were repeated for each well and results were input in the analysis Wave 2.6.3 software to obtain the b) graphs. Image c) represents a control well, and image e) a cisplatin-challenged well. The three equidistance circles within the wells (characteristic to the Seahorse plates) were excluded from cell counting analysis.

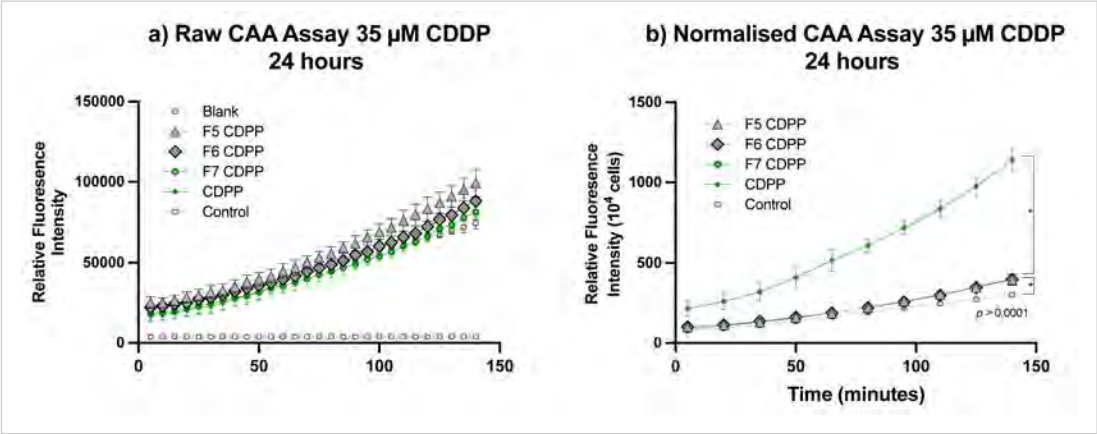

Supplementary III.14.

Cellular antioxidant assay (CAA) curve based on DCF fluorescence measured every 10 minutes for 2 hours (complementary for figure 3.6). The protocol is based on Wolfe and Liu's (2017) method (343). a) In a 96 well plate HEI-OC1 were pre-treated with F5, F6 or F7 formulations dispersed in DMEM, washed, incubated with 10 µM DCF-DA for 10 minutes and then washed again. PBS was added to each well to minimise fluorescence reading, and cisplatin (CDDP) was added to each well except control. The conversion of DCF-DA to DCF was recorded on the multiplate reader for 2 hours at 485 nm. DCF-DA conversation to DCF is proportional to ROS cellular accumulation after an insult (*e.g.* CDDP). To avoid inter-well fluorescence signal leaching, cells were grown on Corning® 96 well black microplates (Sigma Aldrich, AU). Cell viability and cell count is similar to control untreated within the first 6 hours pre-treatment for each group. Following the same counting steps described in Supplementary III.13., at the end of the CAA reading, plates were fixed with 4% PFA, stained with nuclear dye and counted. Cell counts from each well were used to b) normalise CAA results against 10^4 cells to better reflect DCF intensity values per group cell population. Blank wells contained PBS with DCF-DA and no cells. Control wells contained cells and PBS only. Area under the curve for b) was calculated using GraphPad Prism for each group for statistic comparison. Error bars represent standard error of the mean, $n = 1$ in six technical replicates, $*p < 0.03$.

Appendix IV

The Appendix is an extension of Chapter 4 and contains Supplementary figures.

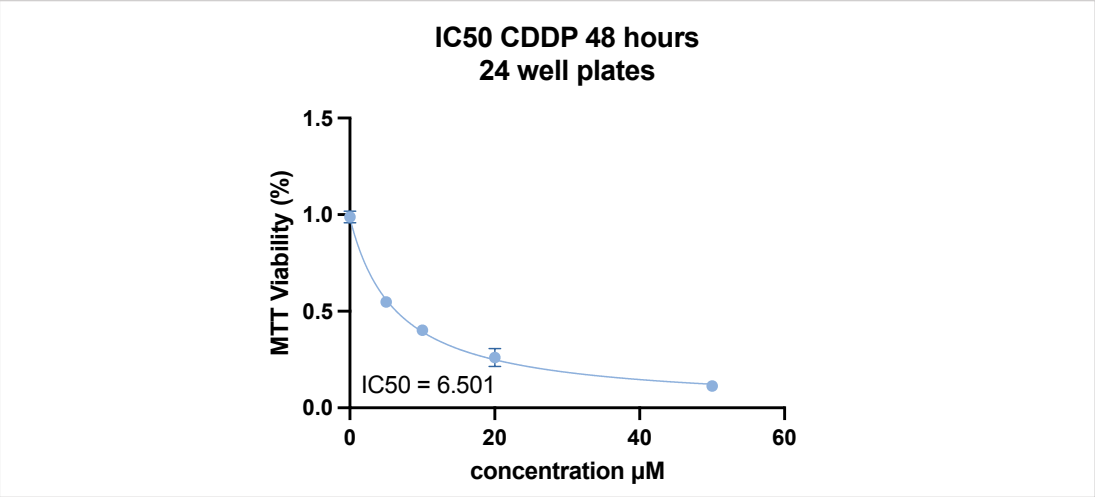

Supplementary IV.1.

Cisplatin inhibitory concentration (IC50) for HEI-OC1 at 48 hours grown on 24 well plates. In practice, cisplatin concentration varied greatly, and the working concentration was adjusted to be below the IC50 in order to obtain 50% viability after 48 hours (~5 µM) and 3 µM for extending the assay at 72 hours.

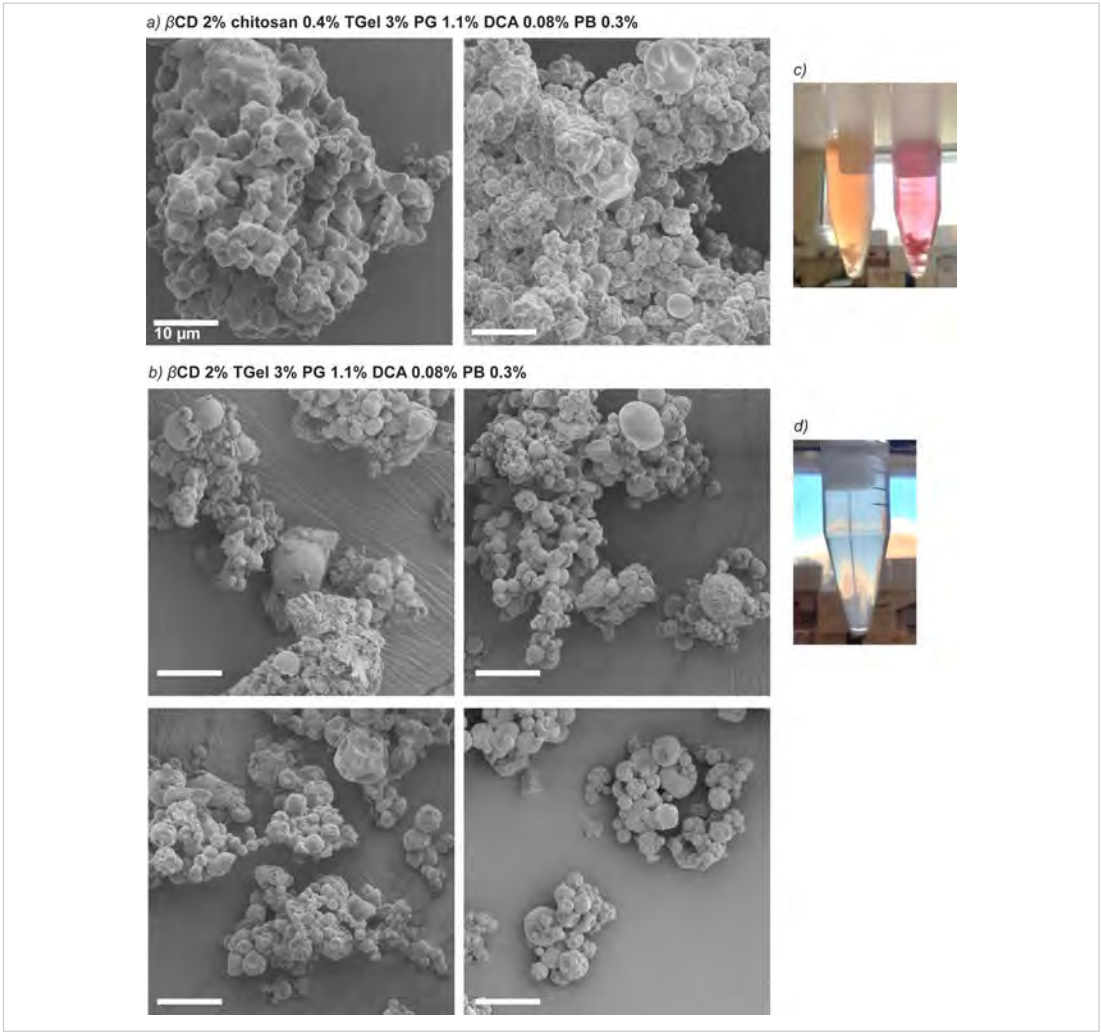

Supplementary IV.2.

Scanning electron micrographs of spray dried solid dispersions based on the formulations presented in (Chapter IV). a) Chitosan 0.4% was dissolved in 1% acetic acid prior to mixing in *β*-CD 2%, TGel 3%, PG 1.1%, DCA 0.08%, probucol (PB) 0.3% to form the spray drying feed-stock solution. b) The same formulation components were used to spray dry without the addition of chitosan nor acetic acid. c) The chitosan solid dispersions were resuspended in DMEM at 10 mg/mL and mixed. Because of the chitosan in formulation, solid dispersions swell and precipitate upon DMEM resuspension. The phenol red pH indicator present in DMEM reveals a rapid change in colour reflective of acetic conditions (red > pink > yellow). In cell culture, an acidic environment can aggravate cisplatin effects *in vivo* (373). d) Solid dispersions without chitosan nor acetic acid dispersed in PBS (10 mg/mL) do not precipitate immediately. Scale bar 10 µm.

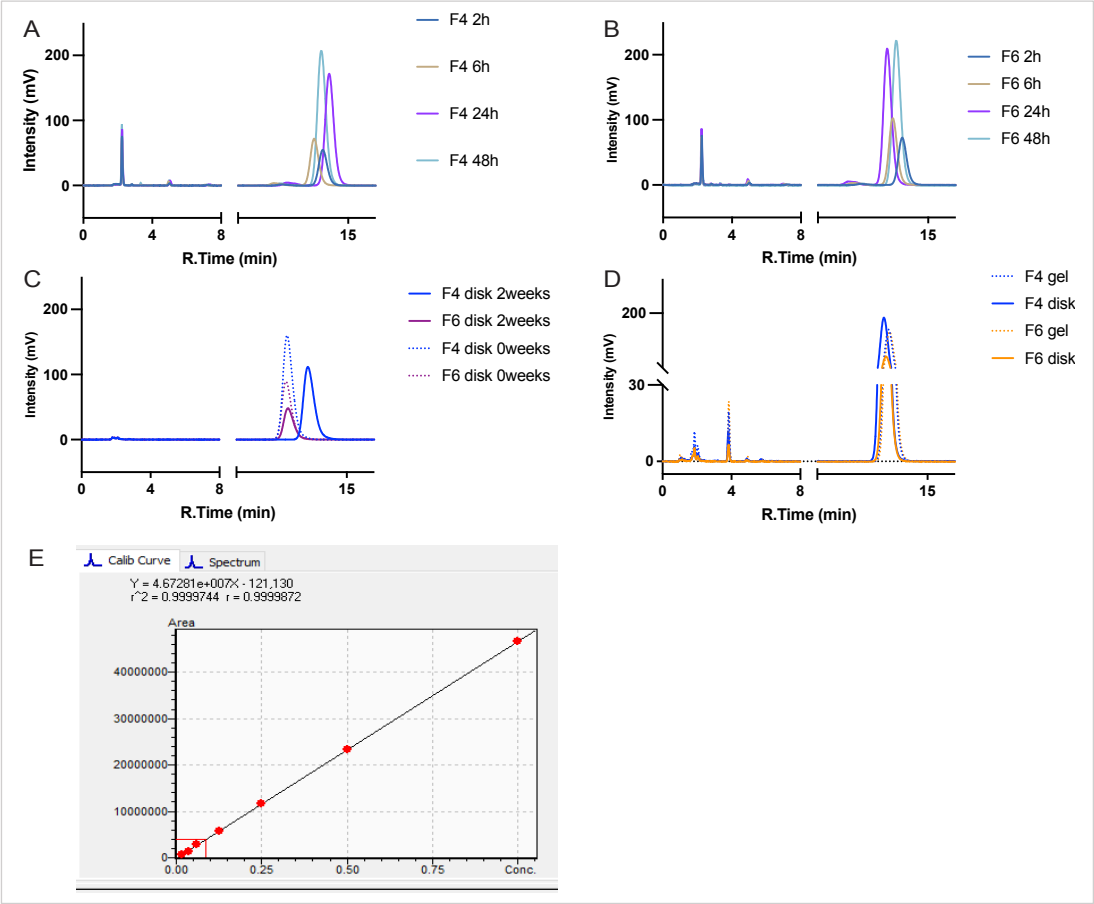

Supplementary IV.3.

HPLC probucol chromatograms from F4 and F6 micro-films formulations (complementary for figure 4.4.). Chromatograms for detecting probucol peak intensity from A) F4 and B) F6 dissolution at 2, 6, 24 and 48 hour time points showing an increase in probucol detection with time. C) F4 and F6 probucol stability from dry micro-films kept at room temperature at day-0 from drying, and after two weeks from drying; drug peaks decrease with increased storage time and may be accelerated by the 1% acetic acid added to the formulation. D) Probucol chromatograms from gel (fresh homogenised formulation) and hydrated micro-films (disk); the gel and hydrated mico-film drug peak is similar, showing little variation. E) Standard calibration curve for probucol at 1 mg/mL (top standard point) and 0.00115 mg/mL (lowest standard), $R^2 = 0.99997$, probucol retention time ~13 minutes.

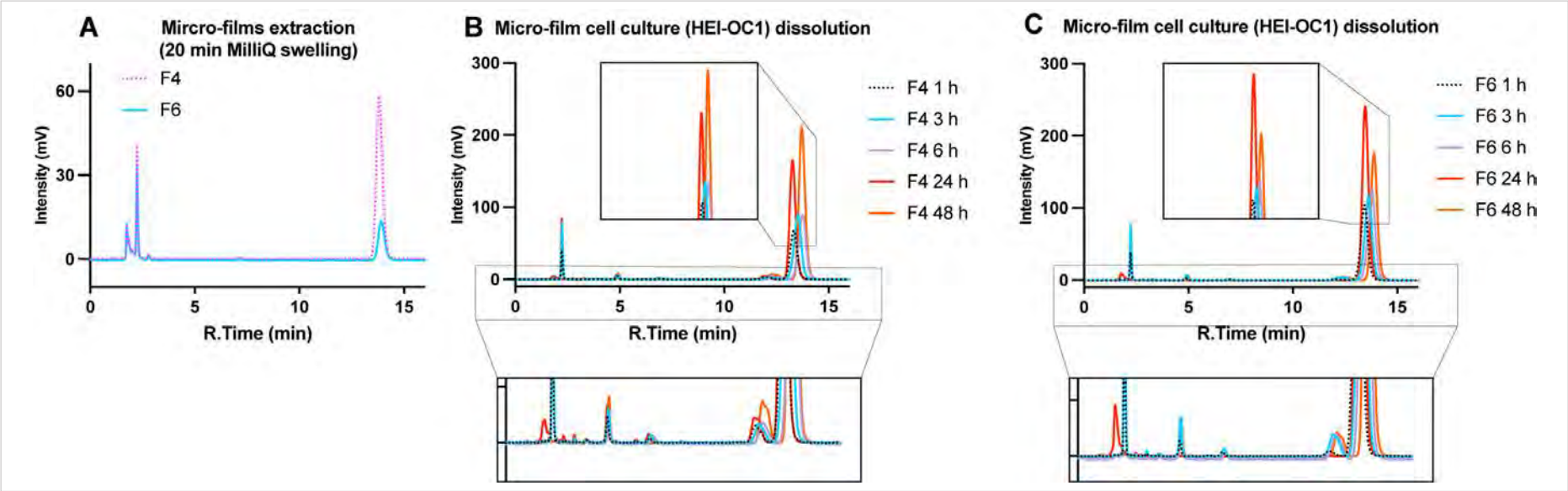

Supplementary IV.4.

Probucol chromatograms form micro-film extractions (complementary for figure 4.4). A) Probucol peaks from hydrated F4 and F6 micro-films showing different intensities. Probucol chromatograms as seen from B) F4 and C) F6 *in vitro* dissolution over 1, 3, 6, 24 and 48 hours. The impurity/degradation peaks with retention times of ~ 5, 7 and 11 minutes do not interfere with probucol integration at ~13 minutes.

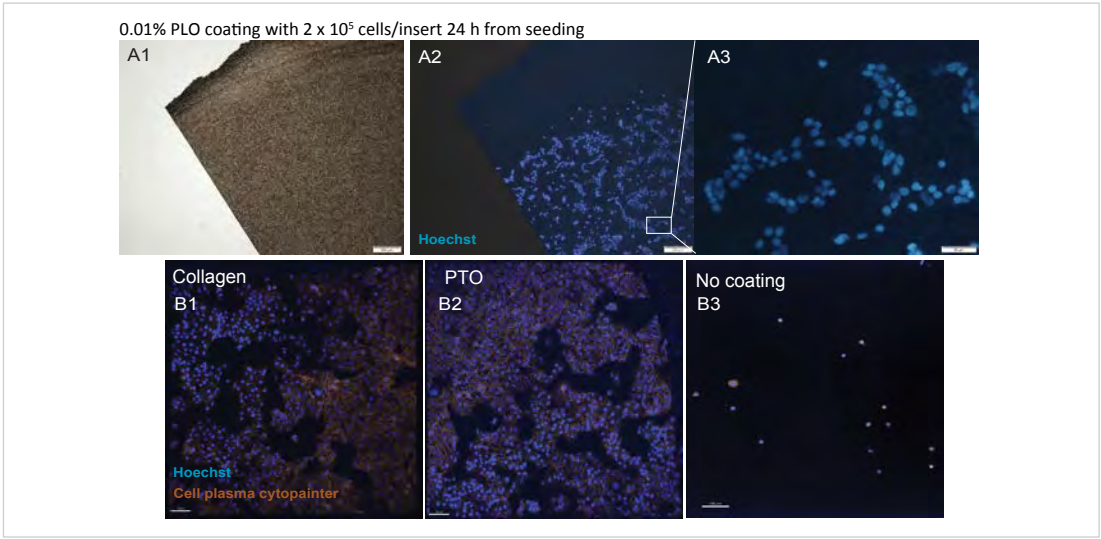

Supplementary IV.5.

Cell culture inserts coating condition to facilitate cell growth (complementary for figure 4.5). Cell culture inserts required coating to promote cellular attachment on the plastic surfaces. Culture inserts (see Supplementary IV.8) were treated with A1) 0.01% #poly(L-ornithine) (PLO) for 1 hour at 33°C. After drying, the inserts were washed 3 times for 10 minutes with PBS to remove excess polymer. HEI-OC1 cells were then seeded at the standard density per each insert (2 x 10^5 cells as 100 µL per insert/well). After growing for 24 hours the cells on inserts were fixed with 4% PFA for 10 minutes then washed 3 times for 10 minutes with PBS, stained with Hoechst 2 µL/mL before detaching the insert membrane using a scalpel blade, rinsed with PBS 3 times 10 minutes. Panel A1) shows the cut insert membrane placed on a coverslip (4x objective) with A2) cell nuclei as seen through the inverted microscope and A3) close-up on the 40x objective. B1) #Rat collagen coating solution was compared with B2) 0.01% PLO and show similar attachment. B3) Without pre-coating there are few cells attached to the insert membrane. B) micrographs were procured using the Dragonfly confocal microscope to facilitate the Cell Plasma Cytopainter detection (ab219942; Abcam Cambridge, UK). After multiple PBS washes, both attached cells on insets and wells were stained with a mixture of 10 µg/mL Hoechst and 2 µL/mL the CytoPainter Cell Plasma Membrane Staining Kit in manufactures assay buffer for 20 minutes, then washed three times with PBS. Inserts were detached and mounted on glass slides with HEI-OC1 facing the coverslip. #Pruchased from Sigma Aldrich, AU. Scale bars A1,2) 200 µm, A3) 50 µm, B) 100 µm.

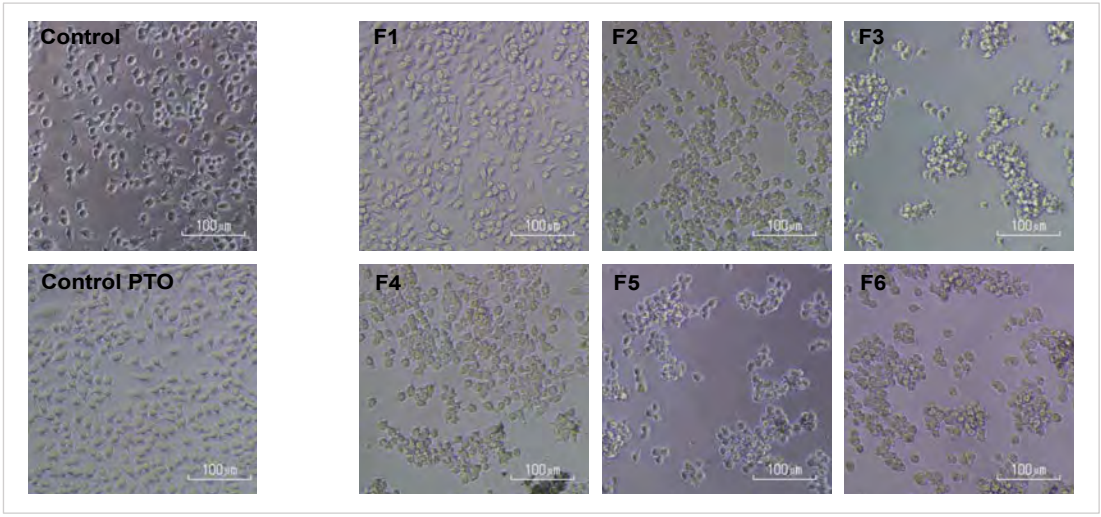

Supplementary IV.6.

Cellular attachment and growth of RAW 264.7 macrophages on control uncoated, and PTO coated wells with F1-F6 gel formulations. After homogenisation, 10 µL formulation homogenate (as described in Chapter 4) were dried on 96 well plates. Plate wells were hydrated for 20 minutes in PBS then coated with 0.01% PTO for 1 hour at 33°C, then washed 3 times x10 minutes. Cellular attachment is inhibited by all formulations except F1 (β-CD 2% in 1% acetic acid homogenate). Chitosan formulations (F2-F3) minimise cellular attachment, which is more evident for F5, F6 containing 0.08% DCA. Scale bars 100 µm.

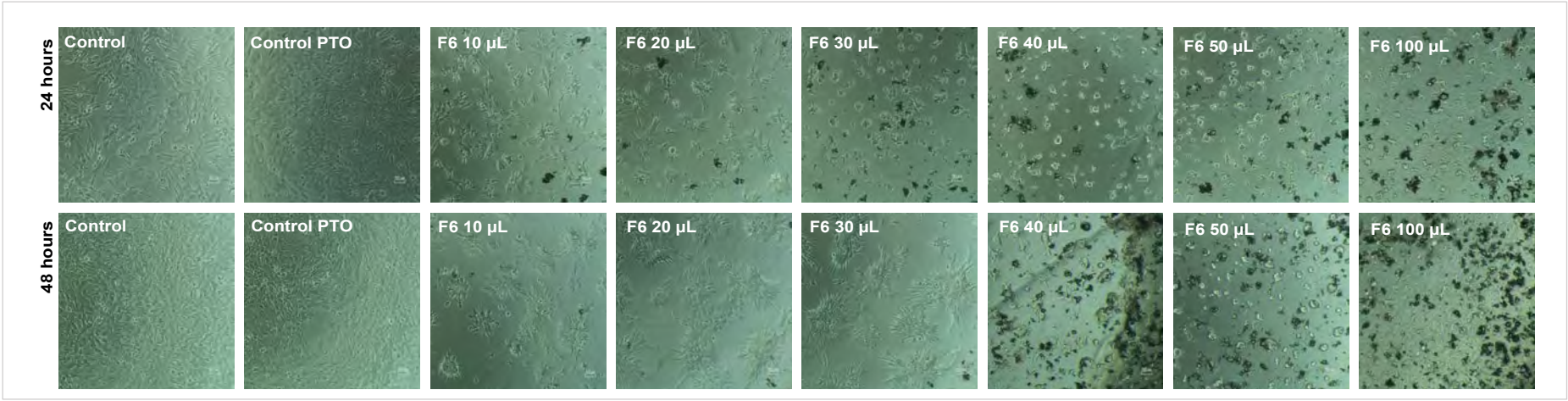

Supplementary IV.7.

Cellular attachment and growth of HEI-OC1 cells on control uncoated, and PTO coated wells with F1-F6 gel formulations. After homogenisation, 10, 20, 30, 40, 50 and 100 µL formulation homogenate (as described in Chapter 4) were dried on 96 well plates. Plate wells were hydrated for 20 minutes in PBS then coated with 0.01% PTO for 1 hour at 33°C, then washed 3 times x10 minutes. This type of formulation contact is not physiologically possible, but rather shows the formulation concentrate the cells can sustain. For HEI-OC1 grown on a F6 formulations base, cell attachment is possible at 10 and 20 µL homogenate in the first 24 hours from seeding. After 48 hours, cells proliferate in presence of 10, 20 and 30 µL homogenate. Cellular morphology is affected, and confluency is not reached after 48 hours. Scale. bars 50 µm, inverted brightfield micrographs at 10x objective.

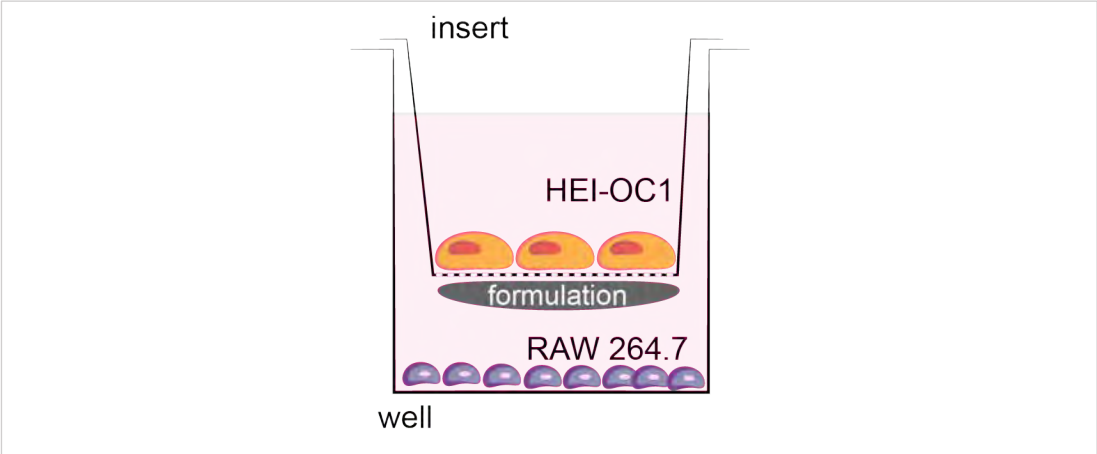

Supplementary IV.8.

Corning® Transwell® 6.5mm with 3.0 µm pore polycarbonate membrane inserts, 24 well plate detail (complementary for figure 4.5. and 4.6). Well inserts remain suspended in cell culture media without reaching the bottom of the well. Prior to cell seeding, F2-F6 formulations were dried on the bottom side of the insert, then hydrated in PBS for 20 minutes. HEI-OC1 cells were added to the insert, and RAW 264.7 were seeded in the well compartment, and grown in co-culture at 33°C.

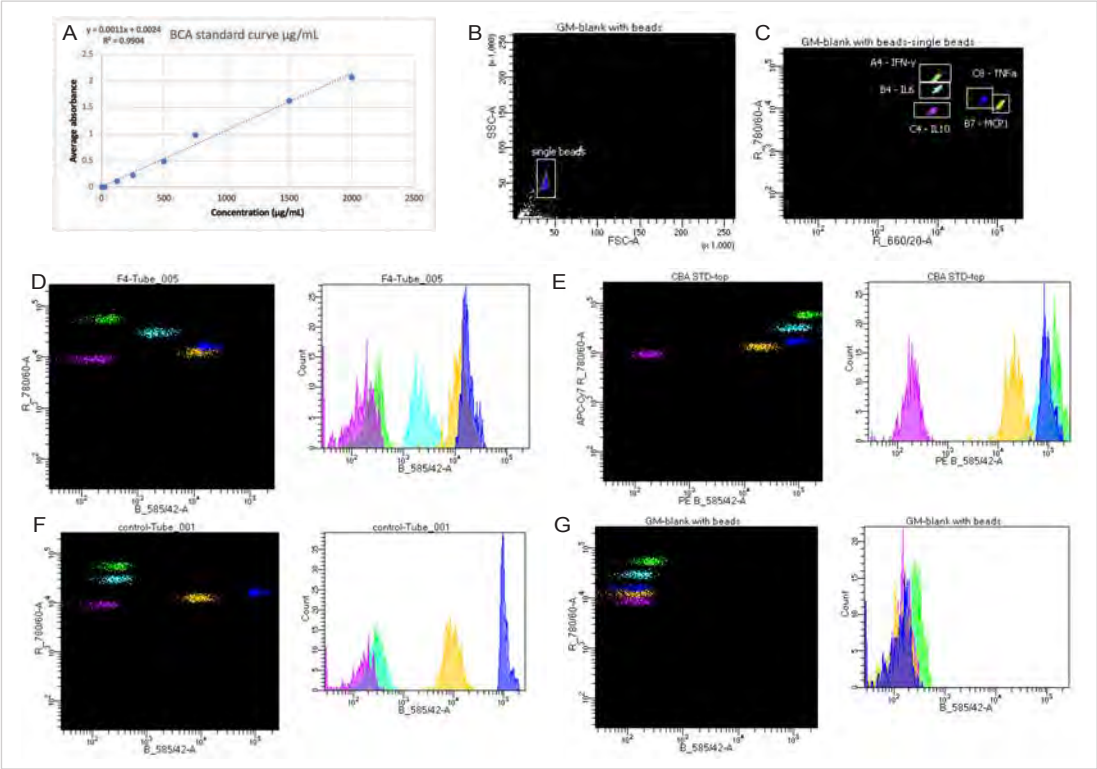

Supplementary IV.9.

Flow cytometry gating strategy and fluorescent bead signal (complementary for table 4.5). A) Standard curve for Pierce bicinchoninic acid protein assay kit (BCA) protein concentration (562 nm) used to normalise cytokine results. B, C) gating strategy. D) Fluorescent bead signal from sample F4 treatment, E) top standard, F) control untreated sample, and G) blank with beads only. IL-10 assays beads fluorescence was not detected in the standards. Interferon-γ (IFN-γ) was not detected in analysed samples.

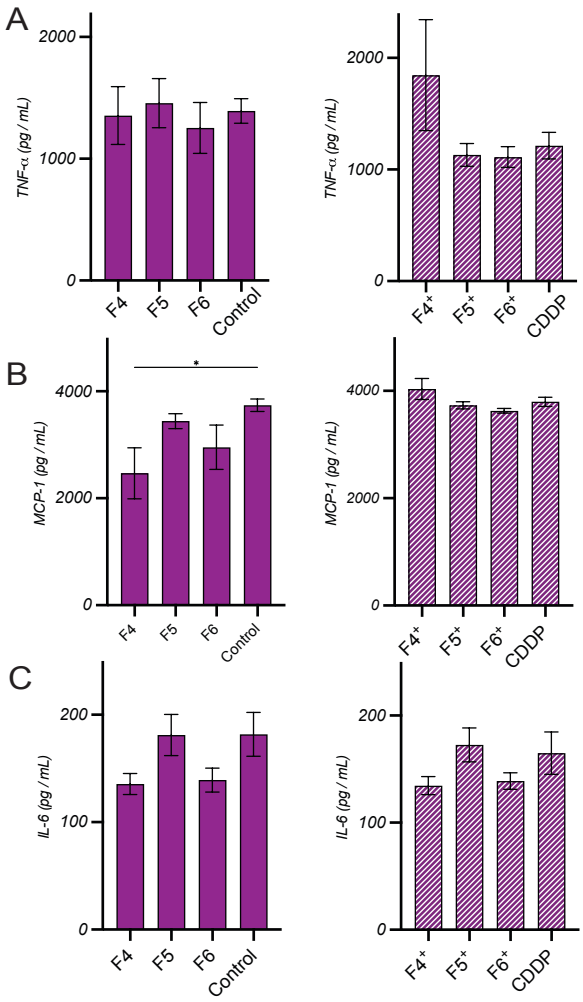

Supplementary IV.10.

Bead Array flex kit quantification for mouse monocyte chemoattractant protein-1 (MCP-1), tumour necrosis factor (TNF) and interleukin-6 (IL-6). Raw quantification results complementary for table 4.5. Error bars represent standard error of the mean, $n = 3$, $*p < 0.03$.

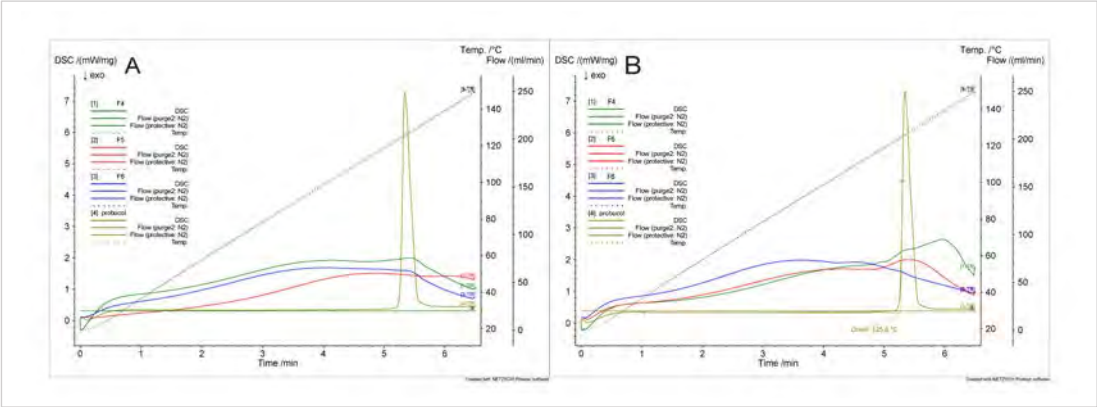

Supplementary IV.11.

DSC for probucol micro-films in relation to powder probucol (PB). Dry nitrogen was used as inert gas at a flow rate of 20 mL/min. Measurements were carried out from 20-160°C at a heating rate of 20°C/min. DSC thermogram with probucol powder (yellow) show an endothermic peak at 125°C. A) Chapter 5 micro-films with probucol (F4, F6) and blanks micro-film (DCA; F5) were analysed. Blank and F4, F6 micro-films lack endothermic peaks, highlighting the probability of having obtained amorphous probucol in F4 and F6 formulations. B) Formulation components were milled using a glass laboratory mortar and pestle to obtain a ground mixture (GM) of probucol-chitosan prior to homogenisation. GM represent a method used to obtain amorphous probucol form and it is referenced in literature to increase drug dissolution and absorption properties (356). We note that both A) and B) formulations do now show the characteristic melting point peak which could either results from insufficient drug within the samples or may represent a transition of the drug from crystalline (endothermic peak) to amorphous state.

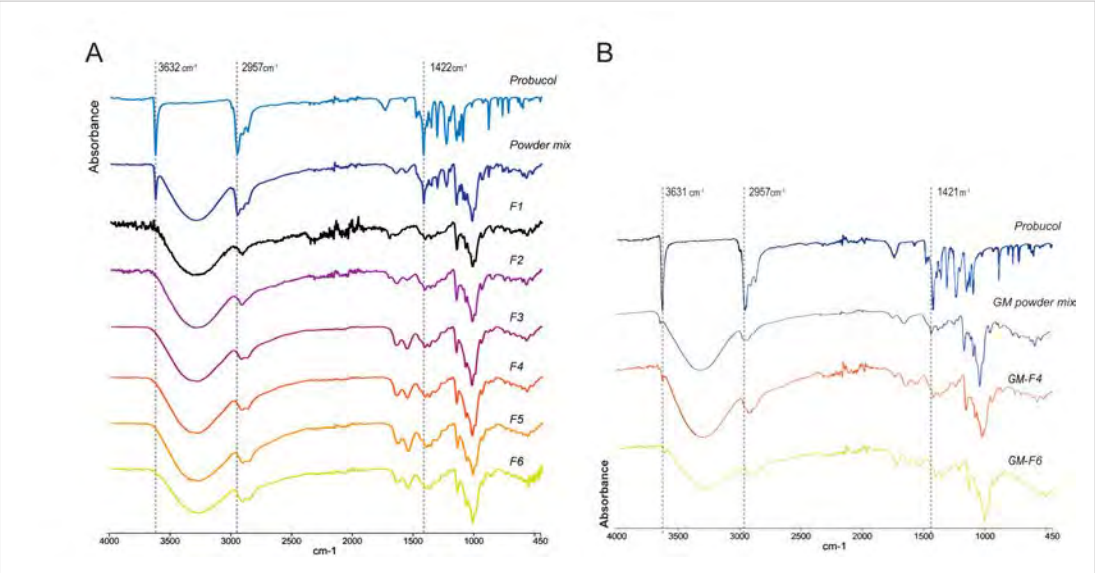

Supplementary IV.12.

Infrared spectroscopy spectra from probucol, probucol mixtures and micro-film formulations (complementary for table 4.1). Marked by dashed lines, the FT-IR free hydroxyl group (OH) stretching vibrations at 3631 cm^{-1} together with the medium C-H stretching at 2957 cm^{-1}, and O-H bending at 1422 cm^{-1} are prominent within the probucol powder. A) By mixing the formulation ingredients with probucol, the probucol characteristic stretching and bending bands are still visible on spectra and are less noticeable once the formulations are homogenised (F4, F6). B). Formulation components were milled using a glass laboratory mortar and pestle to obtain a ground mixture (GM powder mix). Probucol-chitosan prior to homogenisation have less visible probucol characteristic spectra bonds and are similar to the formulations obtained from the GM powder mix (GM-F4, GM- F6). This is to show that both homogenisation, and ground mixing the components before homogenisation has similar impact for probucol-matrix interaction within this chitosan-based formulation.

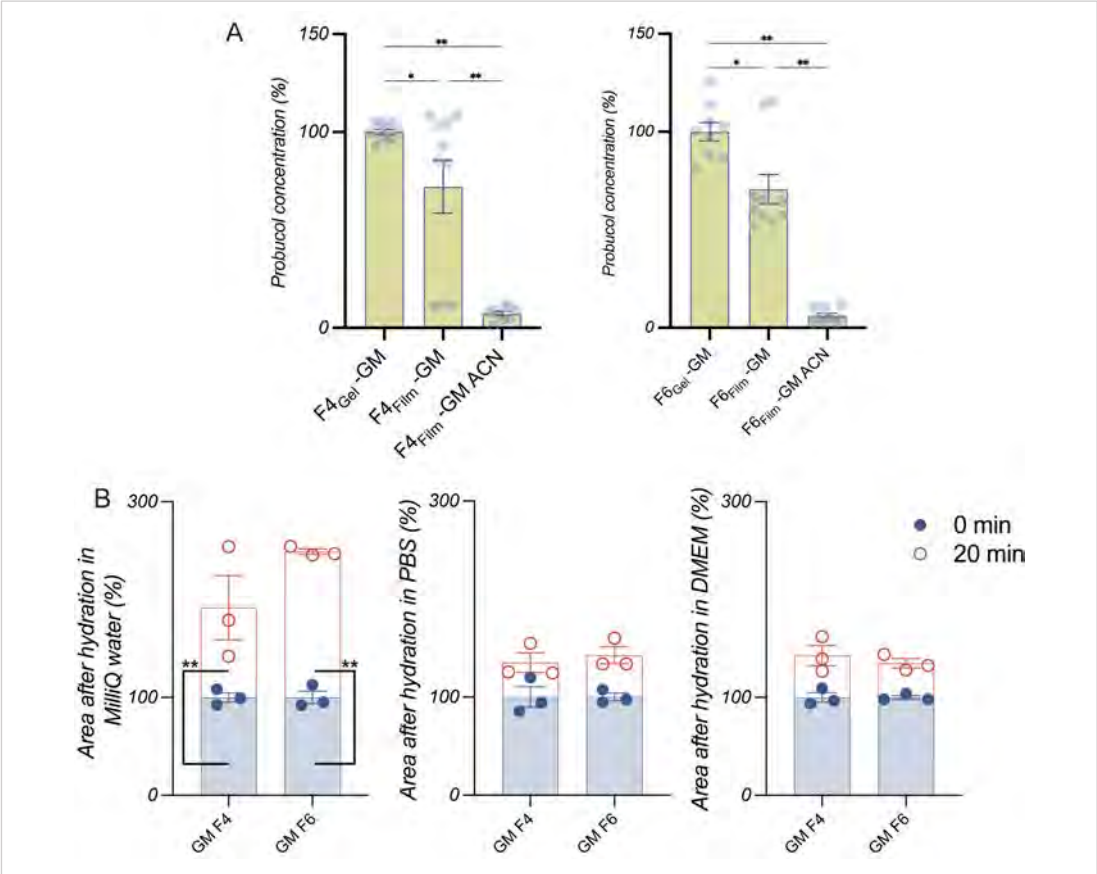

Supplementary IV.13.

Drug content and micro-film swelling of ground mixture (GM) components prior to formulation homogenisation (complementary to figure 4.4 and table 4.2). A) Probucol quantification from GM F4 and B) GM F6 micro-films. Drug concentration from homogenate represents 100% drug content. Probucol extraction is important for quantify the highest amount of drug from micro-films. Significant lower drug content is extracted from dry micro-films using acetonitrile (film-GM ACN), and the total drug increases if the micro-films are allowed to swell in Milli-Q water for 20 minutes (film-GM) prior to acetonitrile extraction. B) Micro-film swelling after 20 minutes hydration in Milli-Q water, PBS and DMEM. Dry films measurements represent 100%; significant swelling for F4 191.57 ± 32.99%, F6 248.99 ± 2.75% in water. Compared to figure 4.4 and table 4.2, the use of probucol-chitosan GM for homogenisation significantly decreases the amount of probucol release from the matrix after 20 minutes hydration (A), and significantly increases swelling for GM F4 (B; by 36%). Error bars represent standard error of the mean, $n = 3$ in three technical replicates, *$p < 0.0005$, **$p < 0.0001$.

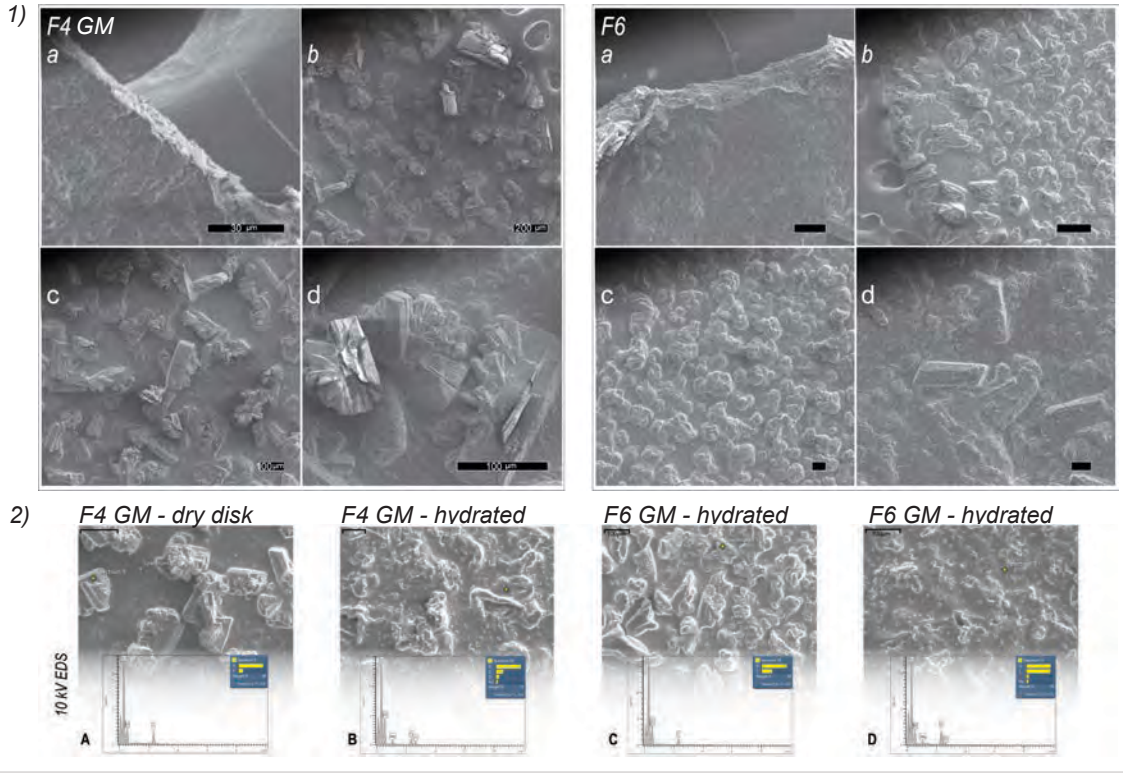

Supplementary IV.14.

Scanning electron micrographs of formulation components milled using a glass laboratory mortar and pestle to obtain a ground mixture (GM) of probucol-chitosan prior to homogenisation (complementary to figure 4.1 and 4.2). 1) Micro-film surface details of F4 GM and F6 GM formulations. 2) Dry (A,C) and hydrated (B,D) (DMEM) micro-film capturing sulphur rich regions characteristic to probucol (~2.3 keV) using EDS analysis. Scale bars a) 30 µm, b) 200 µm, c,d) 100 µm, 2) 100 µm.

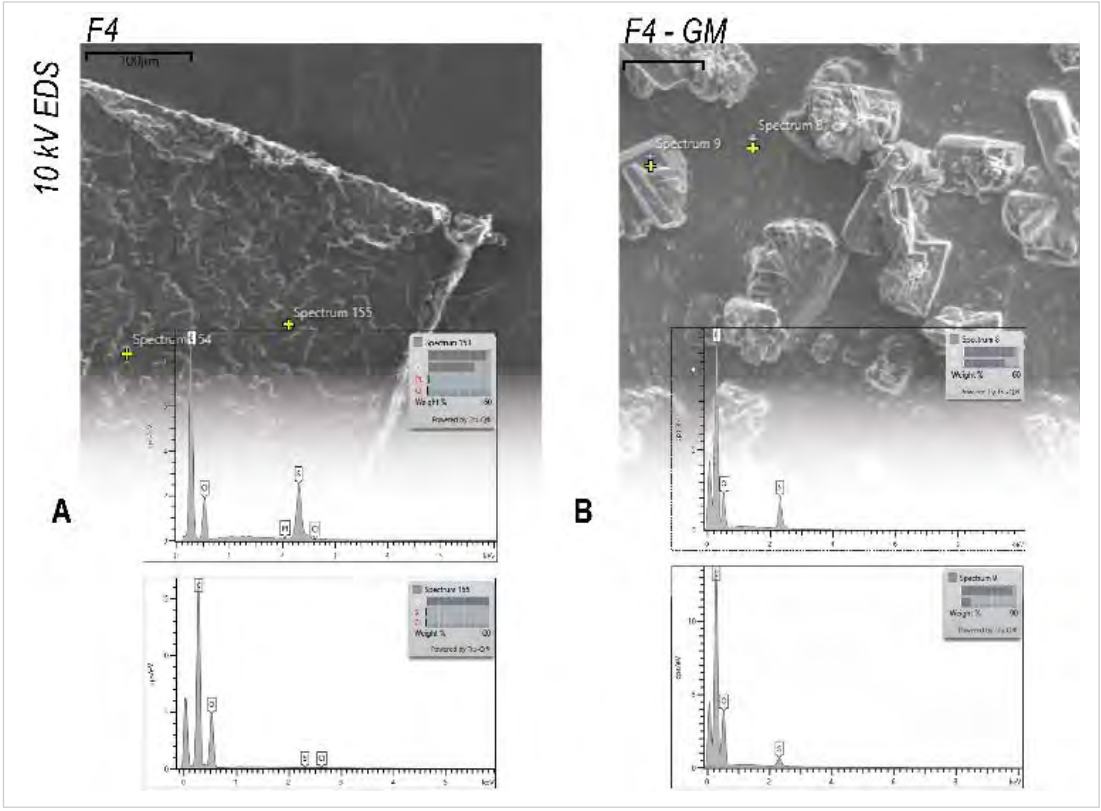

Supplementary IV.15.

EDS spectra analysis from micro-film surface of two F4 formulation combinations (complementary to figure 4.2). A) F4 formulation presented in figure 4.2 with two EDS spectra obtained from the surface deposit (spectrum 154) showing a sulphur peak. The matrix region (spectrum 155) has no sulphur peak detected. B) F4 GM formulation components were milled using a glass laboratory mortar and pestle to obtain a ground mixture (GM) of probucol-chitosan prior to homogenisation. Both spectra collected from the matrix surface (spectrum 8) and from the crystalline surface deposit (spectrum 9) show the characteristic sulphur peak. Probucol peak ~2.3 keV, Scale bars 100 µm.

Appendix V

The Appendix is an extension of Chapter 5 and contains Supplementary figures.

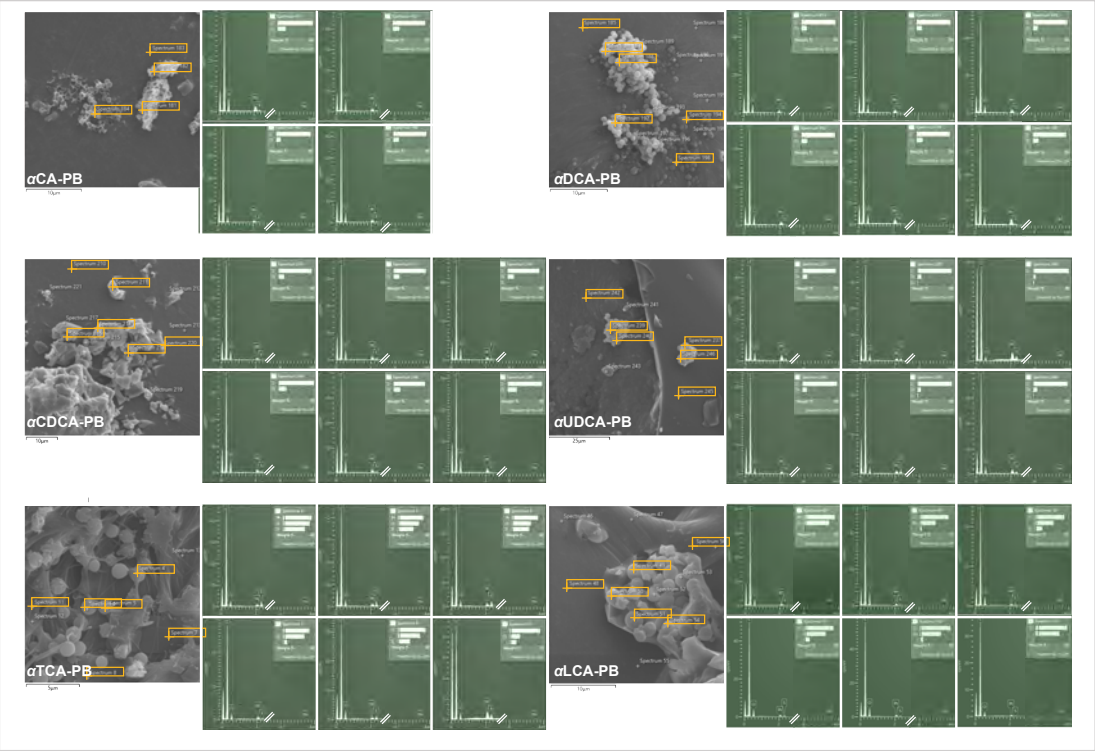

Supplementary V.1.

EDS spectra for *α*CD-PB formulations showing probucol characteristic peaks for sulphur at ~2.3 keV (complementary for figure 5.2). Scale bars 5 µm (*α*TCA-PB), 10 µm (*α*CA-PB, *α*DCA-PB, *α*CDCA-PB), 25 µm (*α*UDCA-PB).

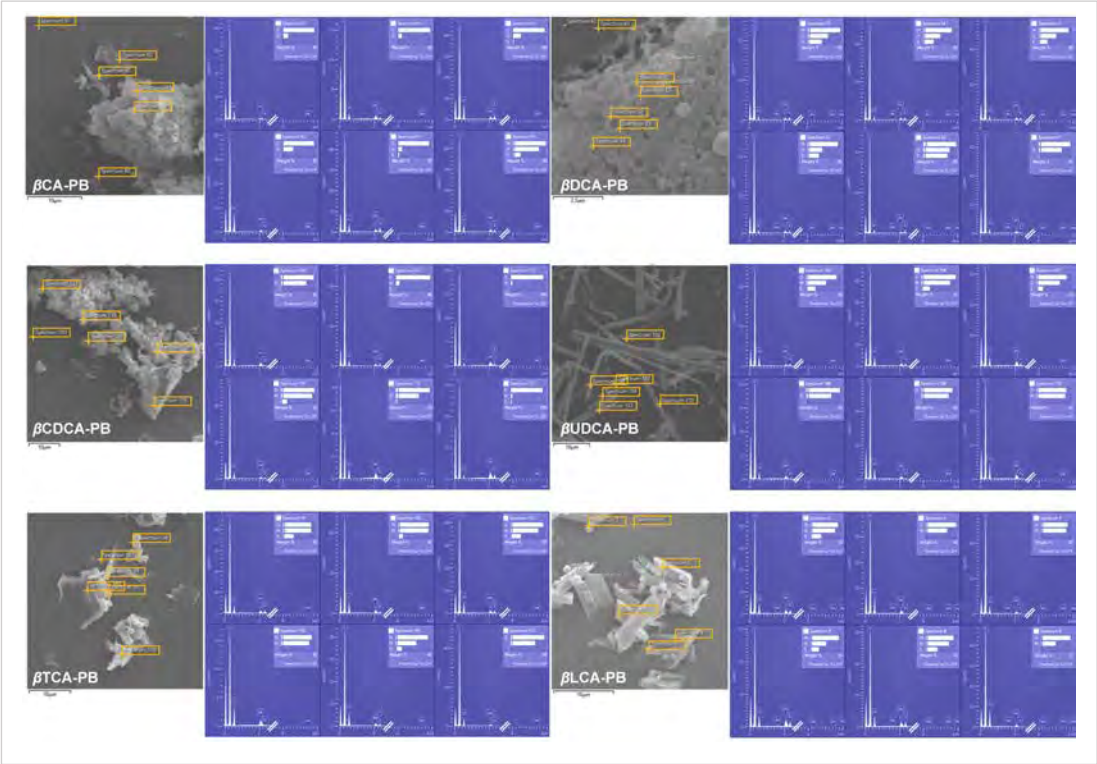

Supplementary V.2.

EDS spectra for *β*CD-PB formulations showing probucol characteristic peaks for sulphur at ~2.3 keV (complementary for figure 5.2). Scale bars 2.5 µm (*β*TCA-PB) and 10 µm.

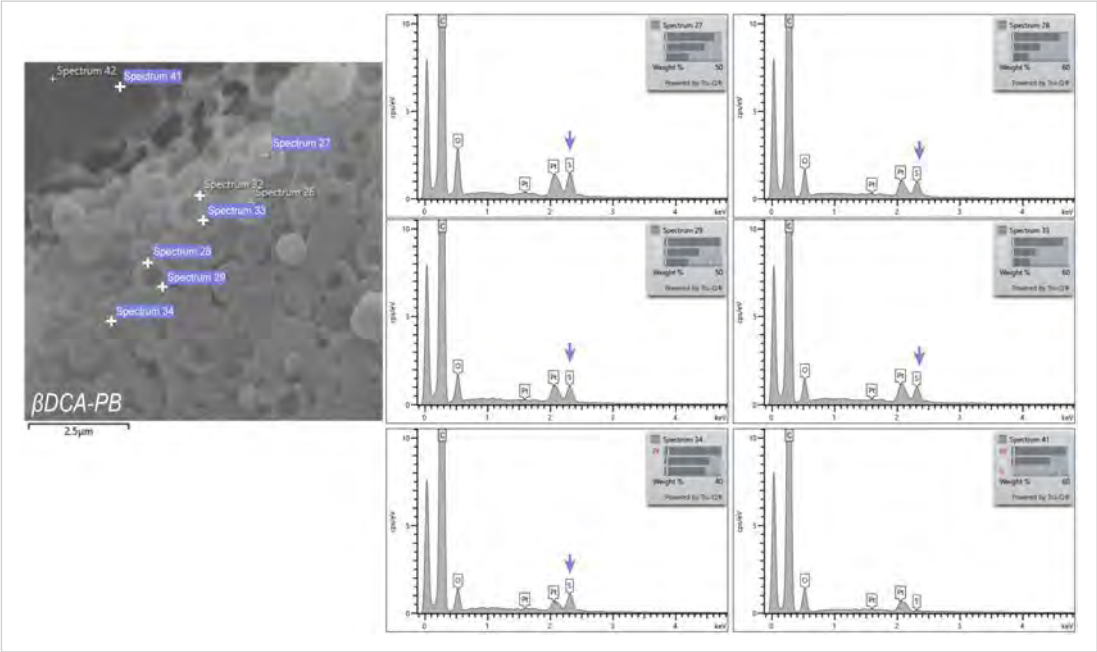

Supplementary V.3.

EDS spectra for sulphur (S) energy peak (~2.3 keV) to confirm probucol (PB) presence within the particle matrix. Point analysis spectra with C, O, Pt and S peaks (arrowhead). Samples were platinum (Pt) sputter coated; background spectrum 41, scale bar 2.5 µm.

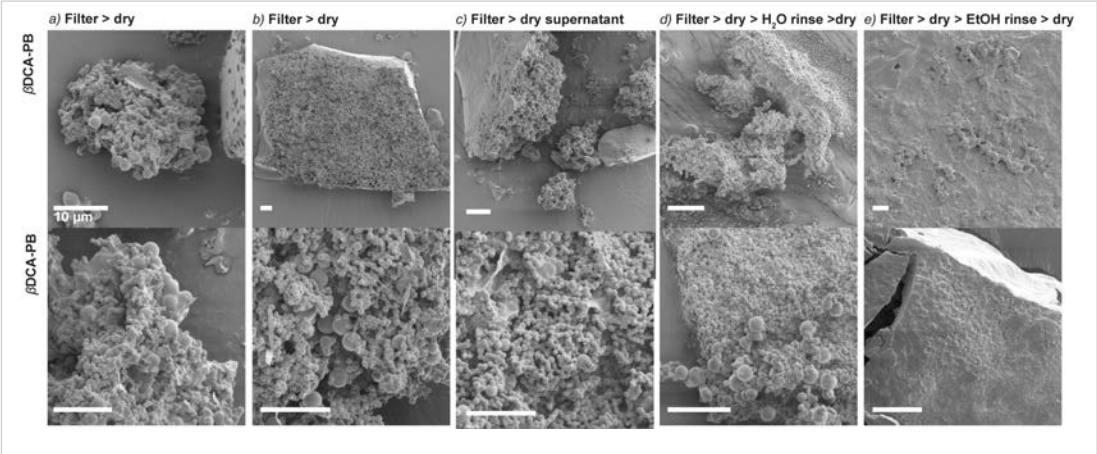

Supplementary V.4.

Scanning electron micrographs of *β*CD-PB formulation aggregates obtained with different drying variations. a, b) Formulations were prepared as described in Chapter V. After filtration, formulations undergone drying in the concentrator. c) Formulation filtrate was spun and dried. d) Formulation filtrate was dried; the precipitate was rinsed with water before drying again. e) Formulation filtrate was dried; the precipitate was rinsed with ethanol before drying again. Except for the ethanol rinse step (e) particle aggregates are visible in abundancy. Scale bars 10 µm.

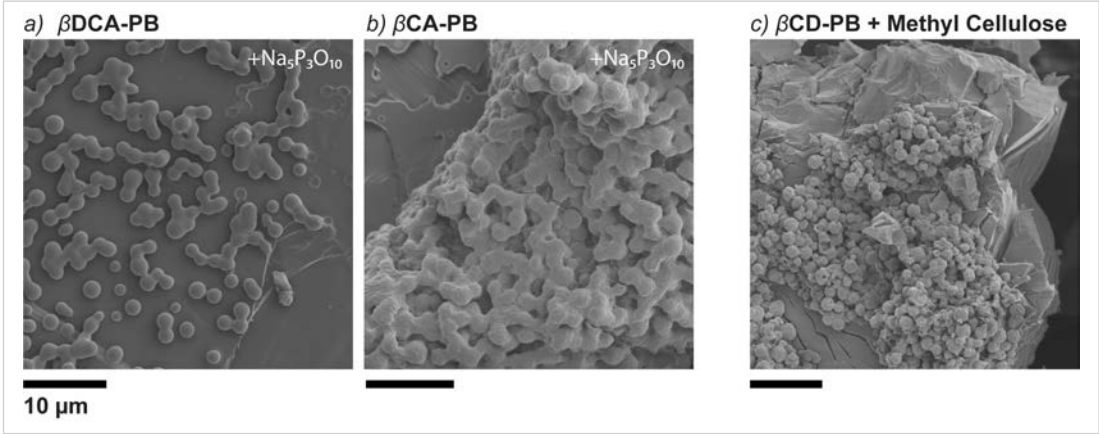

Supplementary V.5.

Scanning electron micrographs of *β*CD-PB formulation optimisation (complementary to figure 5.1). Probucol 0.04% (PB) and the cross-linker sodium tripolyphosphate ($Na_5P_3O_{10}$) were combined with a) 0.137% *β*-CD or b) 0.081% *α*-CD. The cross-linker helps with particle aggregation, however particle tend to coalesce. c) 0.04% PB and 0.137% *β*-CD aggregate formation is possible with the addition of methyl cellulose 3.3%, however the polymer leads to aggregates agglomeration and irregular surface appearance. Scale bars 10 µm.

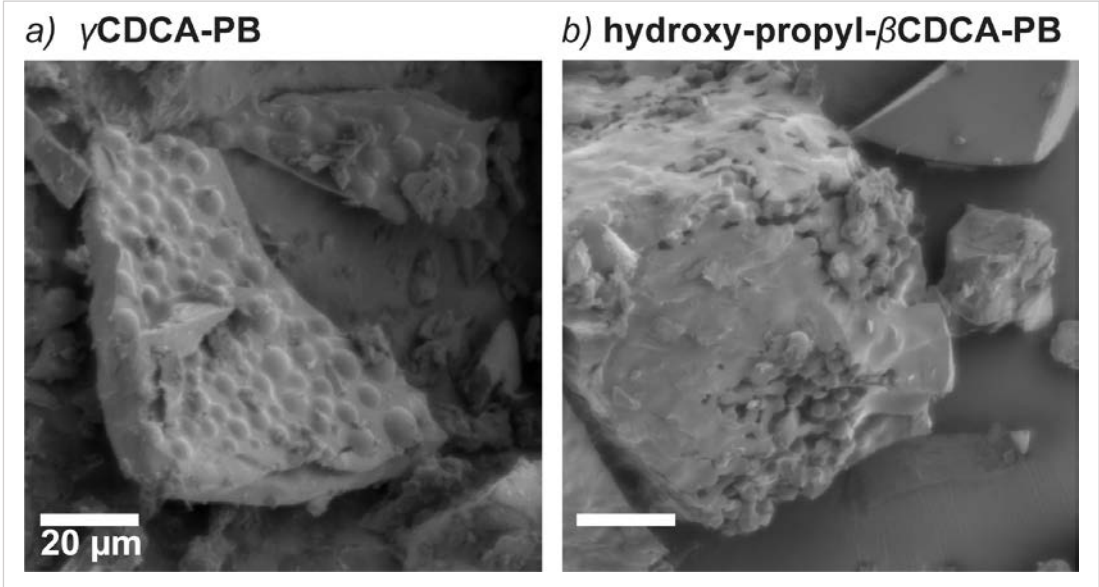

Supplementary V.6.

Scanning electron micrographs of CD-PB formulation optimisation. a) CDCA 0.176% with γ-CD and probucol (PB) results in few larger aggregates that are not fully separated. b) CDCA 0.176% with hydroxy-propyl-*β*-CD and PB shows minimal aggregate formation. Scale bars 20 µm.

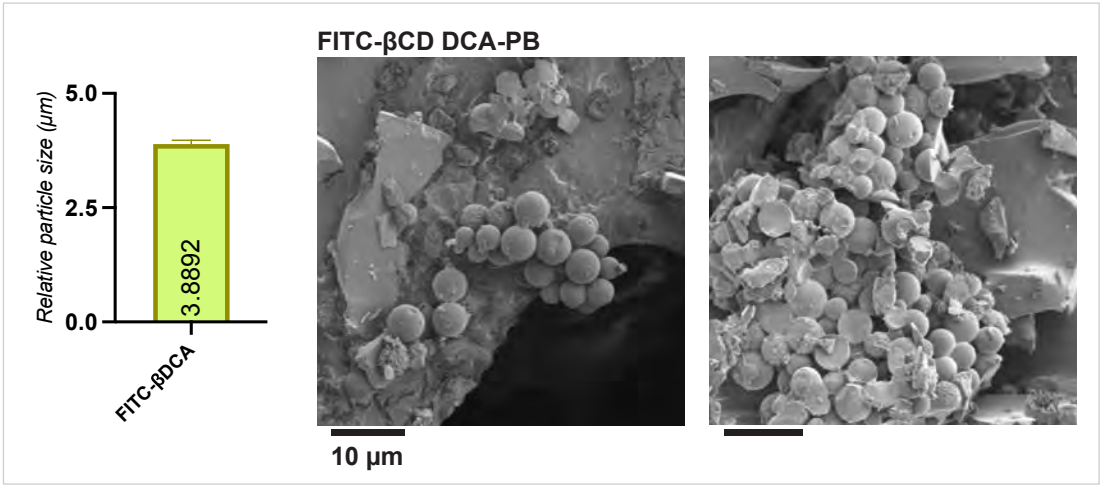

Supplementary V.7.

Scanning electron micrographs of amine-*β*-CD conjugated with fluorescein isothiocyanate (FITC). ^Amine-*β*-CD was conjugated with FITC according to a developed protocol by Chen *et al.,* (2015) (458). Briefly, amine-*β*-CD and FITC were dissolved in anhydrous dimethylformamide for 48 hours at 4°C. The reaction was evaporated using the BÜCHI R-205 rotary evaporator (Flawil, CH), and the precipitate was dissolved in Milli-Q and dialysed for 24 hours. The dialysed fraction was freeze dried (Dynavac FD3, Dynapumps, AU). The freeze-dried material was combined with *β*-CD and DCA as previously described (Chapter V). With a larger aminated-FITC *β*-CD, the addition of DCA results in larger particles compared to *β*DCA-PB (figure 5.1). It is predicted that the functional changes in CDs impact drug inclusion complex formation (415). This is indeed evident through the larger relative particle size (3.88 µm). ^purchased from Cyclolab, Budapest, HU, #purchased from Sigma Aldrich, AU. *n* = 1. Scale bars 10 µm.

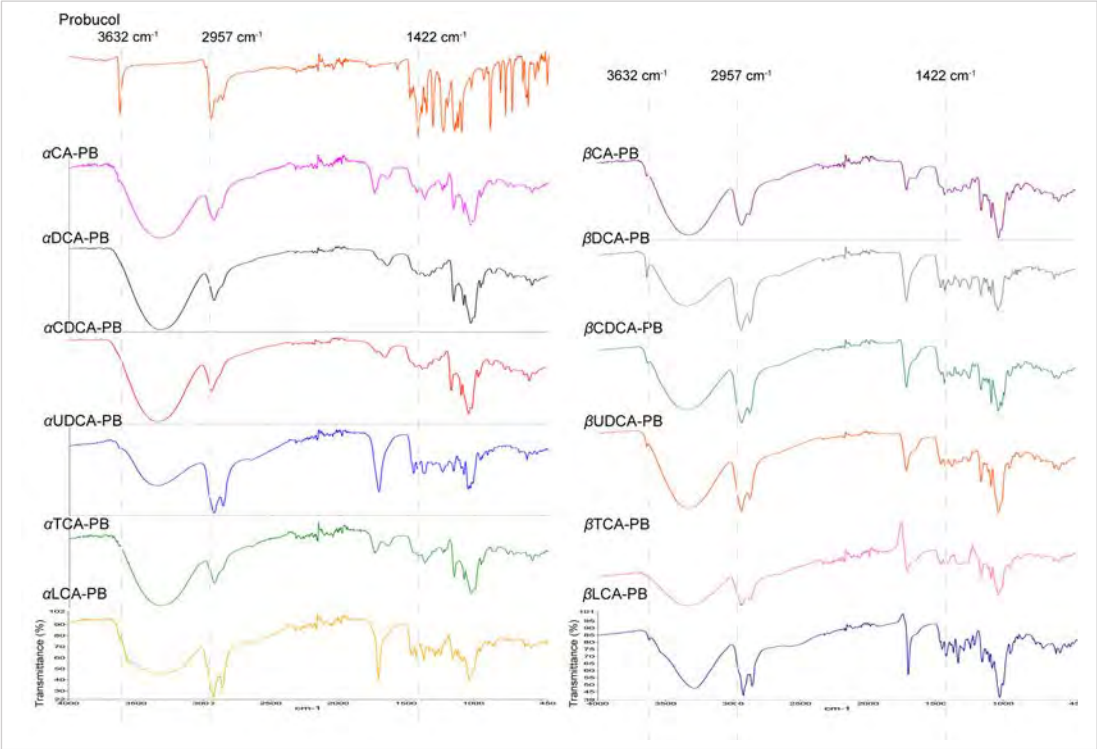

Supplementary V.8.

Infrared spectroscopy spectra from probucol powder and *α*/*β*-bile acid-PB formulations Marked by dashed lines, the FT-IR free hydroxyl group (-OH) stretching vibrations at 3631 cm^{-1} together with the medium C-H stretching at 2957 cm^{-1}, and O-H bending at 1422 cm^{-1} are prominent within probucol powder. Some bonds (3631 cm^{-1}) remain visible within formulations (*α*CA-PB, *β*CA-PB, *β*DCA-PB, *β*UDCA-PB, *β*LCA-PB).

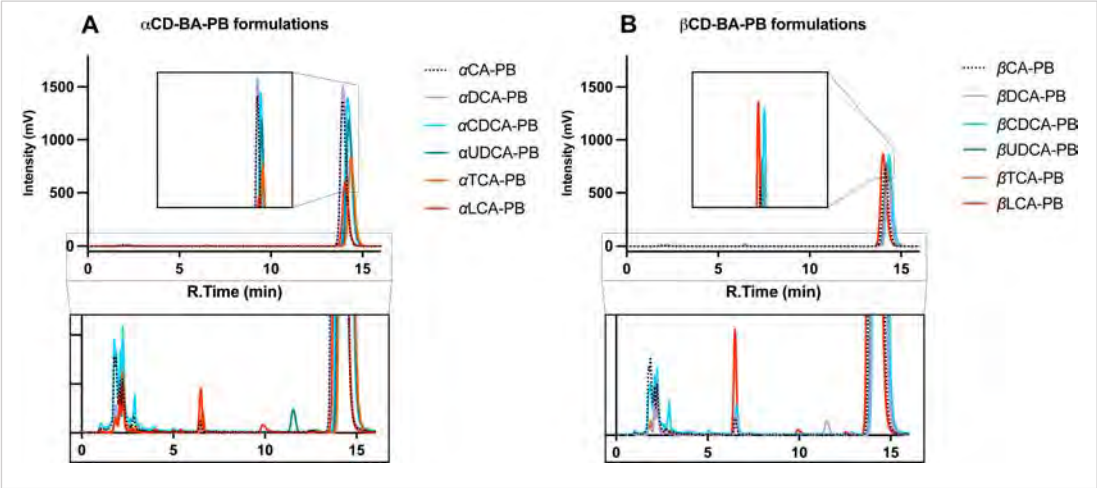

Supplementary V.9.

Probucol chromatograms from *α*/*β*-bile acid-PB formulations. Probucol retention time ~14 minutes. Few impurity peaks occurring before 13 minutes with minimal intensity that do not interfere with probucol integration.

Appendix VI

The Appendix contains Supplementary figures on patented bile-probucol synthesis.

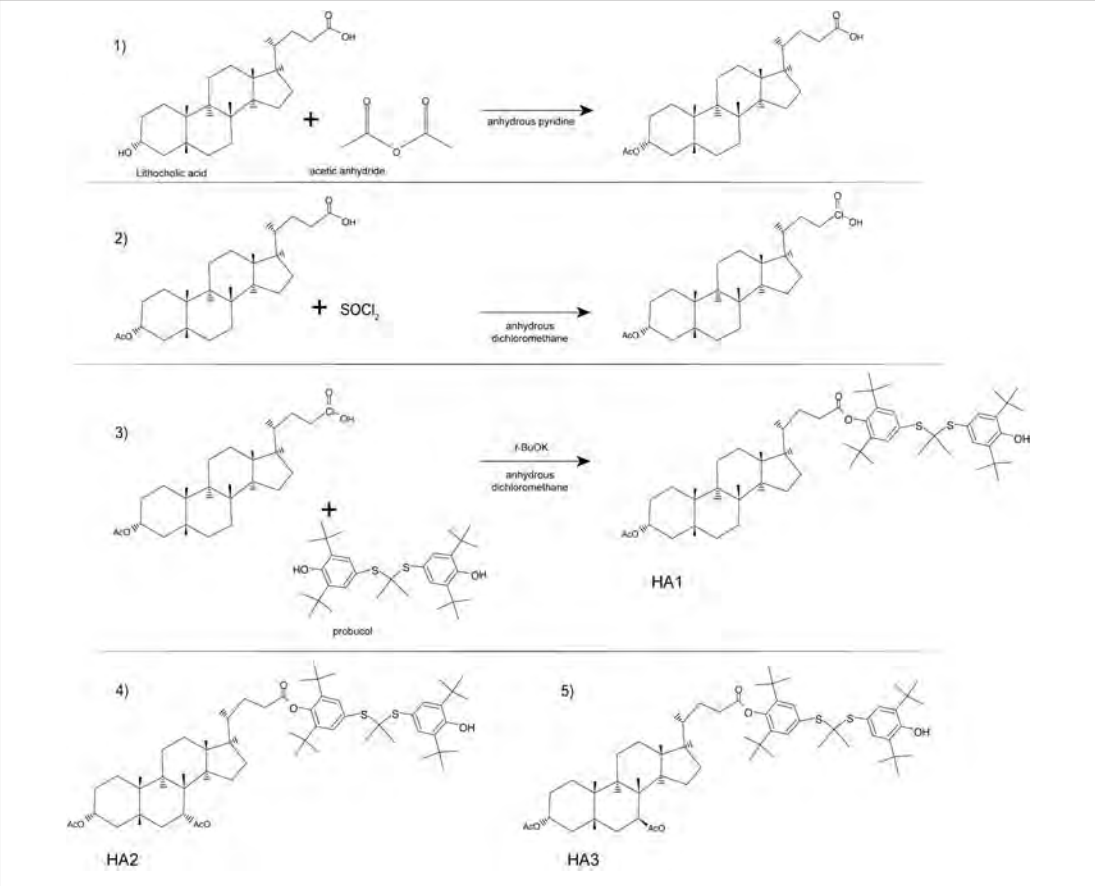

Supplementary VI.1.

HA1, HA2 and HA3 reaction and molecular structure (adapted from the patent filed in December 10th 2021 by Hani Al-Salami, Armin Mooranian, Giuseppe Luna, Anton Dolzhenko, John Mamo, Ryu Takechi, Virginie Lam. Bile acid conjugates. Provisional patent, Australia, 2021904008, P117109.AU).

HA1, HA2 and HA3 are new molecules based on conjugated bile acids with probucol. HA1, HA2 and HA3 were produced according to the patented protocol and used to create *β*-CD aggregates. The steps in obtaining HA1 start with 1) the protection of lithocholic acid (LCA) with anhydrous acetic anhydride. 2) The protected lithocholic acid is chlorinated using $SOCl_2$ and 3) combined with pre-reacted probucol with *t*-BuOK to obtain HA1 (conjugated LCA with probucol). The same 1-3) steps are used to create 4) HA2 (conjugated CDCA with probucol) and 5) HA3 (conjugated UDCA with probucol). Reagents and solvents purchased from Sigma Aldrich or Honeywell Research Chemicals, AU.

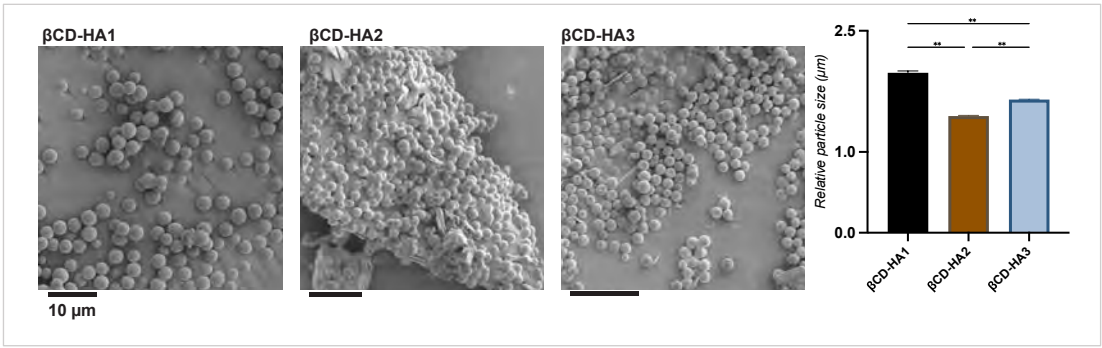

Supplementary VI.2.

Scanning electron micrographs of *β*-CD particle aggregation for HA1, HA2 and HA2. Based on Chapter V method, *β*-CD 0.137% with either 0.3% HA1, HA2 or HA3 were mixed to obtain aggregates. Relative particle size measurements were recorded based on micrographs using ImageJ. Particle size is as follows; 1.98 ± 0.02 µm for *β*CD-HA1, 1.44 ± 0.01 µm for *β*CD-HA2, 1.65 ± 0.004 µm for *β*CD-HA3. Error bars represent standard error of the mean, $n = 1$, $^{**}p < 0.0001$. Scale bars 10 µm.

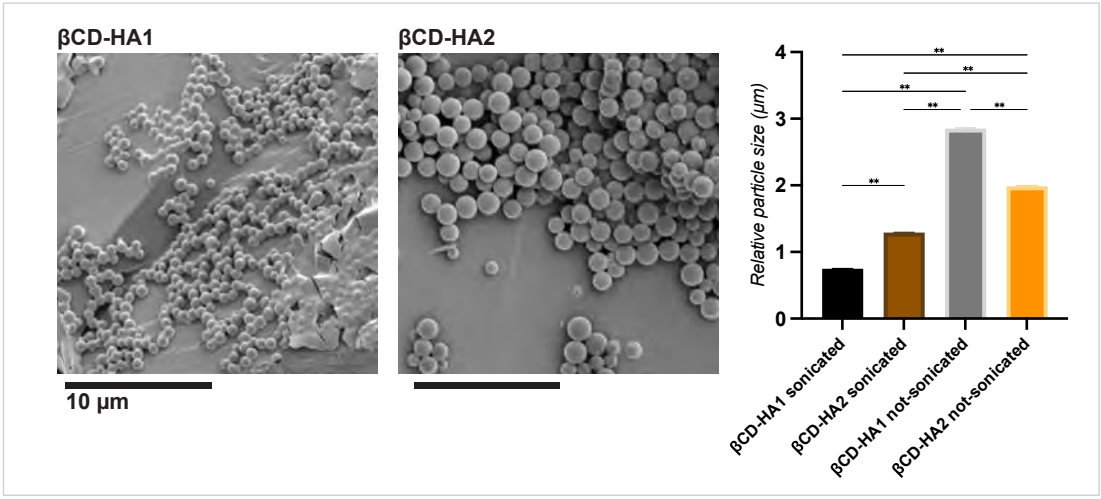

Supplementary VI.3.

Scanning electron micrographs of *β*CD-HA1 and *β*CD-HA2 particle aggregation size optimisation. Based on the method presented in Chapter V to create the *β*CD-HA1 and *β*CD-HA2 presented in Supplementary VI.2. An additional step was added to the method. By sonicating the aggregate mixture prior to filtration allows the guest molecules to interact better with *β*-CD (427). The stronger drug-*β*-CD interaction results in smaller aggregate relative size; from 2.85 ± 0.01 µm to 0.75 ± 0.003 µm for *β*CD-HA1, and form 1.98 ± 0.006 µm to 1.29 ± 0.005 µm for *β*CD-HA3 respectively. Error bars represent standard error of the mean, $n = 1$, $^{**}p < 0.0001$. Scale bars 10 µm.

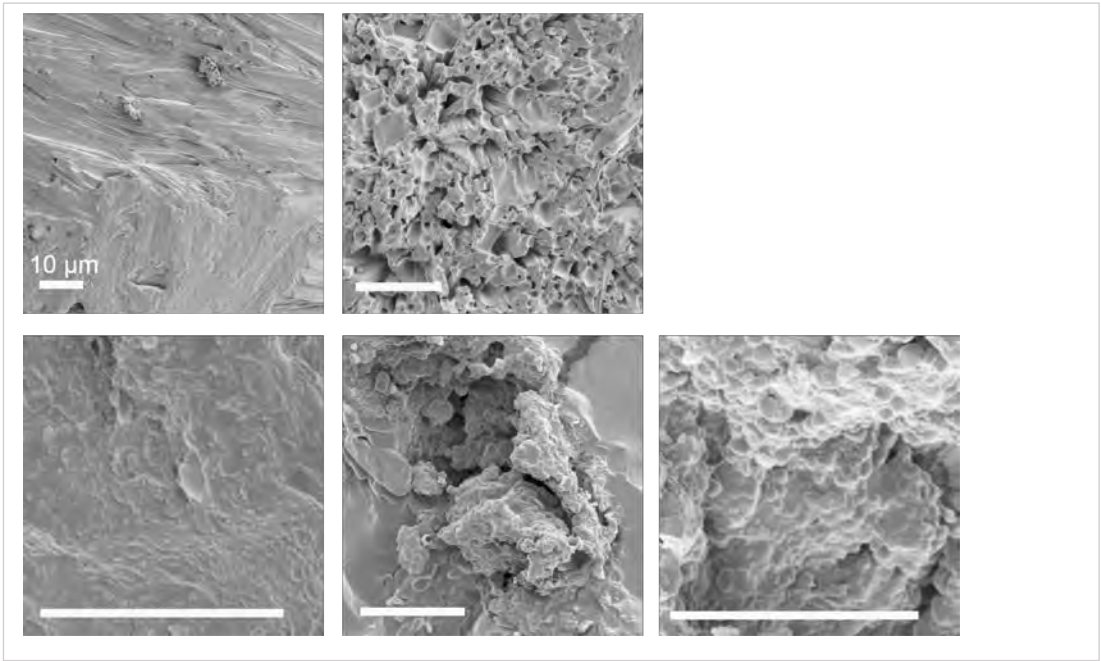

Supplementary VI.4.

Scanning electron micrographs *β*CD-HA1 aggregates incorporated into chitosan matrix (complementary to Supplementary V.2 and Chapter IV micro-films). Chitosan micro-films homogenate (as described in chapter IV) was used to incorporate *β*CD-HA1 aggregates. After drying the homogenate (50 µL), micro-film surface shows various sized round-aggregates uniformly incorporated into the matrix. Scale bar 10 µm.

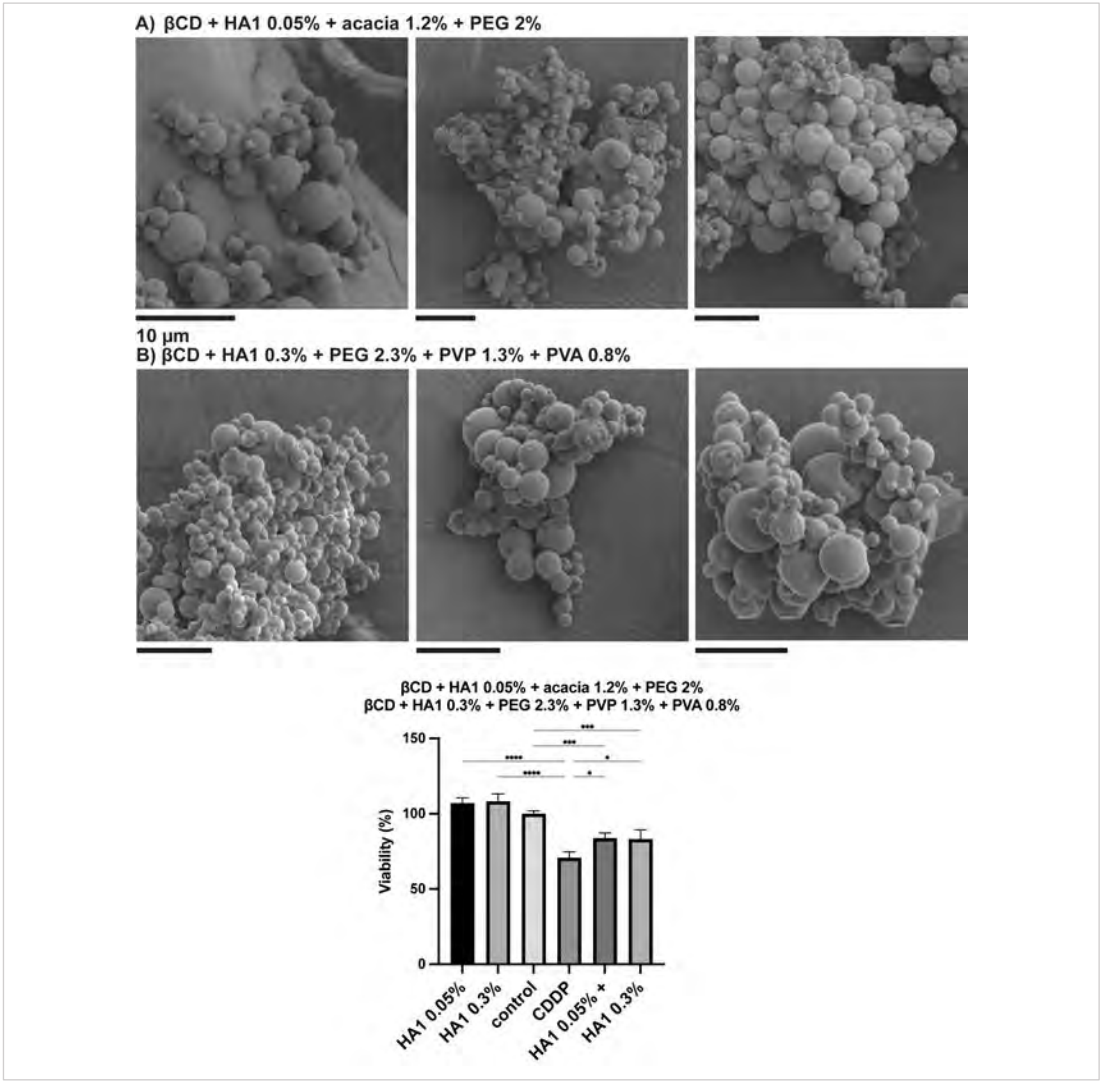

Supplementary VI.5.

Scanning electron micrographs of spray dried solid dispersions containing *β*-CD 2% and HA1. Scale bars 10 µm. a) HA1 0.05%, acacia 1.2% and PEG 2% spray dried suspensions show larger particles with rugous surface appearance. b) HA1 0.3%, PVP 1.3% and PVA 0.8% show better results on particle appearance. Both formulations dispersed into DMEM and applied to HEI-OC1 cells in culture show the HA1 concentration difference is not affecting viability in control formulation treated cells, nor cisplatin (CDDP) treaded groups (+). Error bars represent standard error of the mean, $n = 1$, *$p < 0.03$, ***$p < 0.0002$, ****$p < 0.0001$.

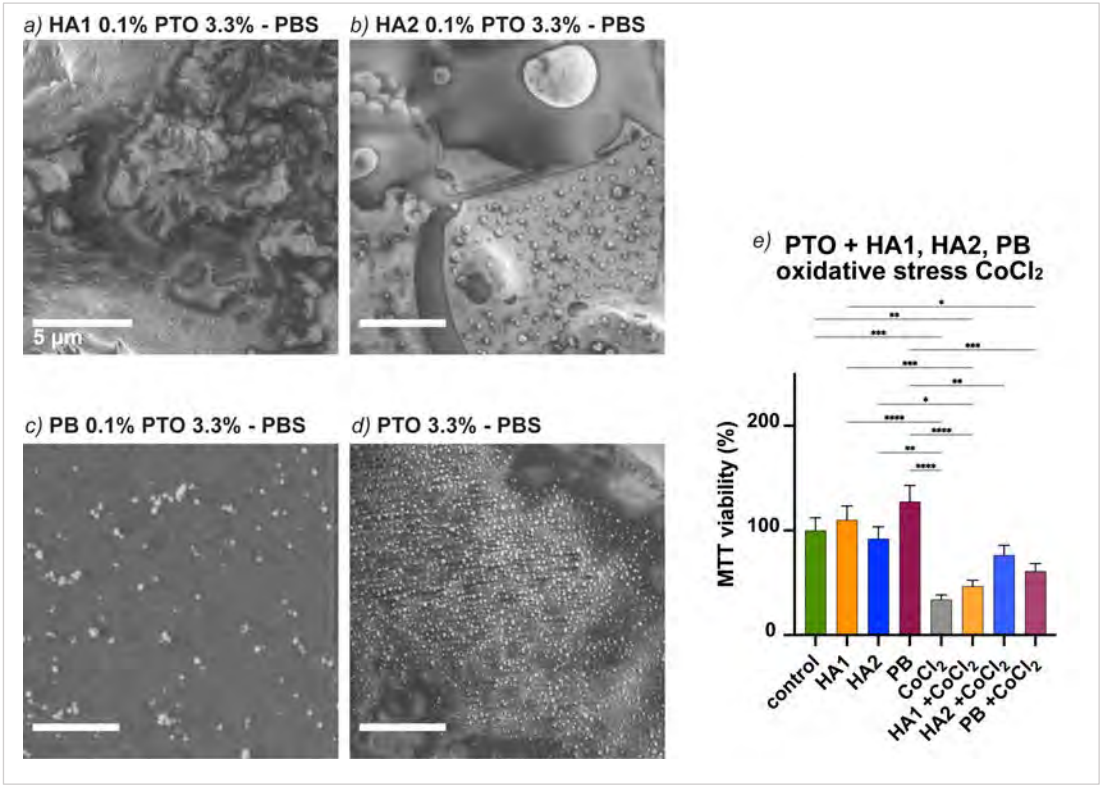

Supplementary VI.6.

Scanning electron micrographs of homogenised emulsions of 0.1% HA1, HA2 and PB and their effects *in vitro*. The aliphatic alcohol phytantriol (PTO) 3.3% and a) HA1, b) HA2, c) probucol (PB) were homogenised with PBS. The resulting formulations were dried on aluminium stubs and imaged using SEM. a-c) Micrographs show nano-sized particulates. e) A volume of 2.5 µL of each formulation was added to HEI-OC1 cell culture, the viability effects are similar to control. With the addition of a stressor ($CoCl_2$; 6 hours pre-treatment 400 mM, (459)), HA1 and PB, but less for HA2 show reduced viability similar to $CoCl_2$ control. Error bars represent standard error of the mean, $n = 1$, $*p < 0.03$, $**p < 0.002$, $***p < 0.0002$, $****p < 0.0001$, $n = 1$, Scale bar 5 µm.

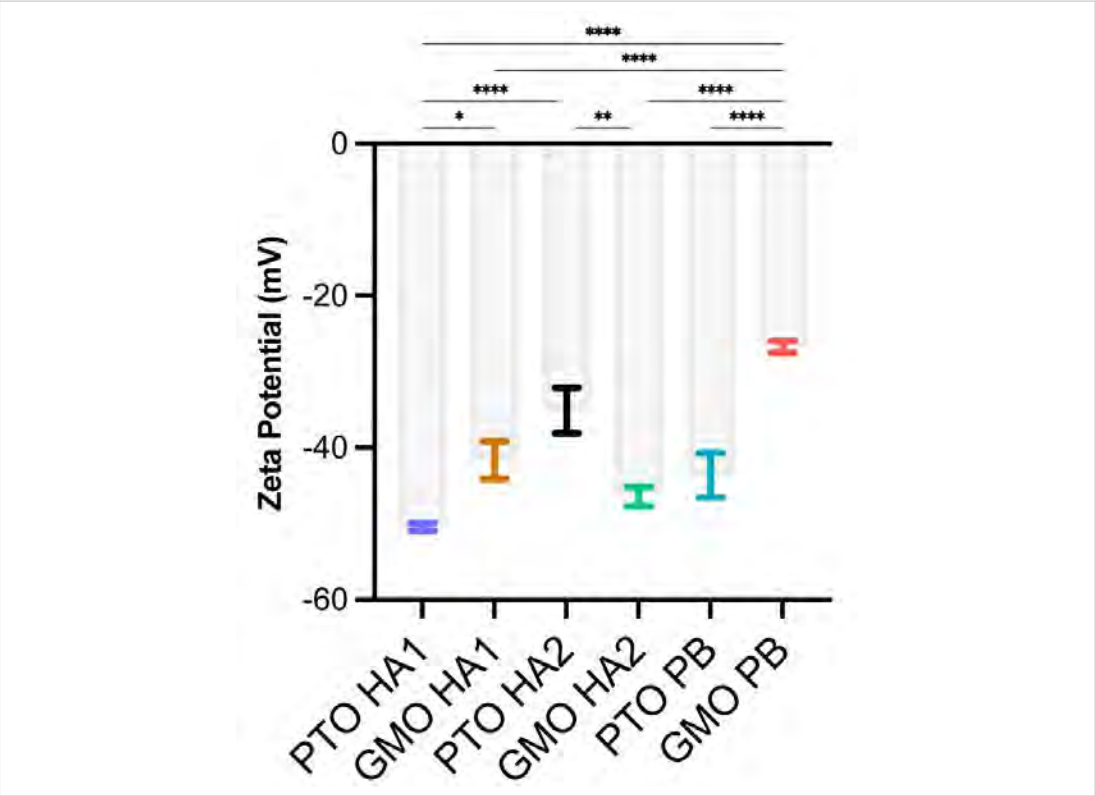

Supplementary VI.7.

Zeta potential measurements for HA1, HA2 and PB emulsions (complementary to Supplementary IV.6). 3.3% phytantriol (PTO) or glycerol monooleate (GMO) were homogenised with HA1, HA2 or probucol (PB) in PBS. The emulsions' zeta potential was measured. Each formulation shows strong negative zeta potential, predictive of a strong particle repulsion within the samples (in part corroborated by the dispersed particles observed through SEM in Supplementary IV.6). The strong negative potential in cell culture allows for less cellular interaction and may contribute to less cellular uptake minimising toxicity (26). Error bars represent standard error of the mean, n = 1, *$p < 0.03$, **$p < 0.002$, ****$p < 0.0001$.

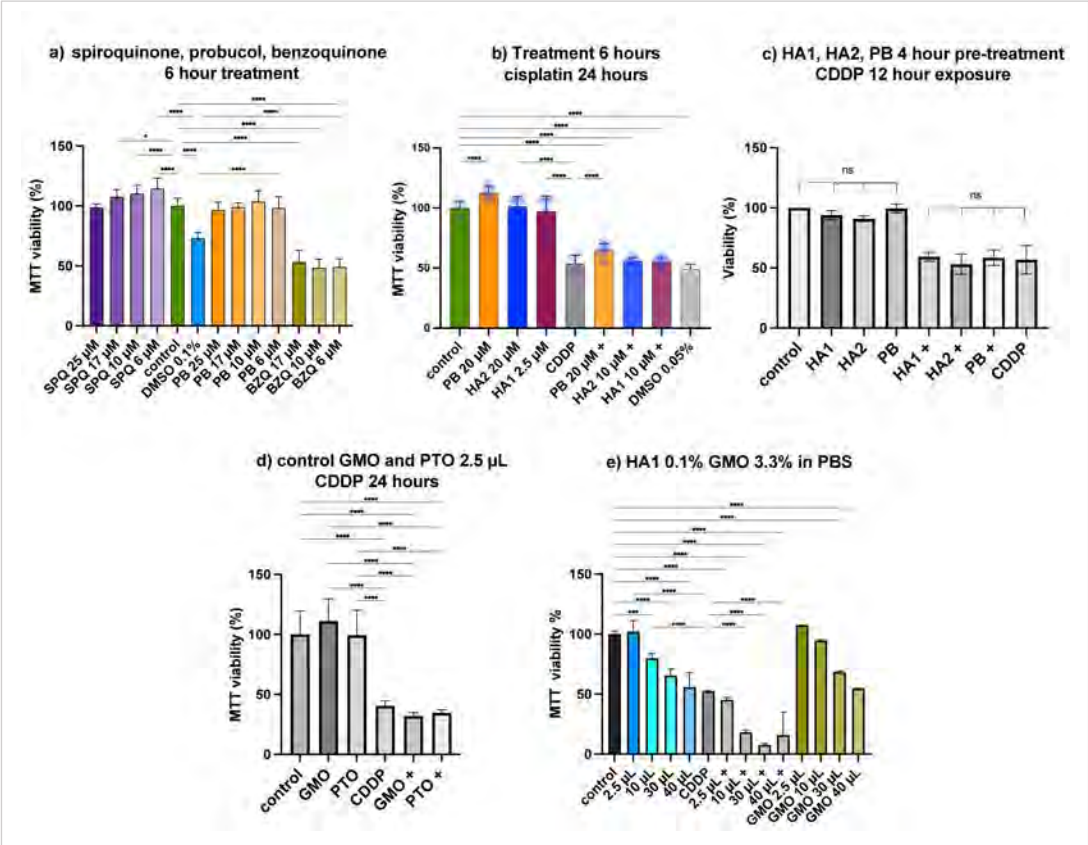

Supplementary VI.8.

Probucol, probucol metabolites, HA1 and HA2 *in vitro* application and optimisation. a) Probucol (PB) and metabolites; spiroquinone (SPQ) and benzoquinone (BZQ) dissolved in DMSO applied as 0.1% solutions at 25, 17, 10 and 6 µM for 6 hours. b) PB, HA1 and HA2 dissolved in DMSO and applied as 0.05% solutions, with or without stressor (cisplatin; CDDP). Cells media was then replaced with fresh DMEM, and cells were grown for another 24 hours. A similar decrease in viability for drug treatments is observed with c) 4 hour drug pre-treatment and 12 hour CDDP exposure. d) 3.3% glycerol monooleate (GMO) and phytantriol (PTO) control-emulsions in PBS with or without CDDP for 24 hours. e) HA1 0.1% GMO emulsion applied as 2.5, 10, 30, 40 µL, and control GMO emulsion with or without CDDP applied in culture for 24 hours. Error bars represent standard error of the mean, $n = 1$, $*p < 0.03$, $****p < 0.0001$.

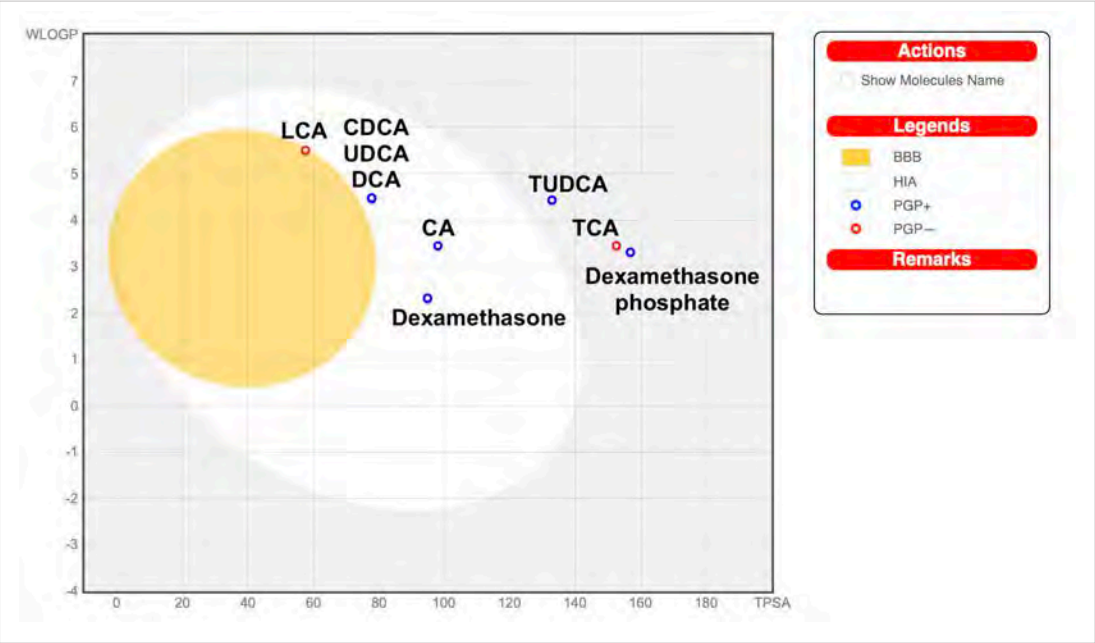

Supplementary VI.9.

SwissADME BOILED-Egg plot (452) drug diffusion. The log *P* method developed by Wildman and Crippen (WLOP) of bile acids and dexamethasone and dexamethasone phosphate are plotted against the topological surface area of the molecules. Drug passive diffusion prediction to the gastrointestinal (white area) and BBB (yellow area) can be estimated. For the inner ear entry through the BLB by systemic drug administration, drugs require a similar WLOGP (~1-6) and TPSA (0-80) to the BBB predictions. Probucol would fit outside of this graph on the WLOGP axis because of the higher value of 9.91.

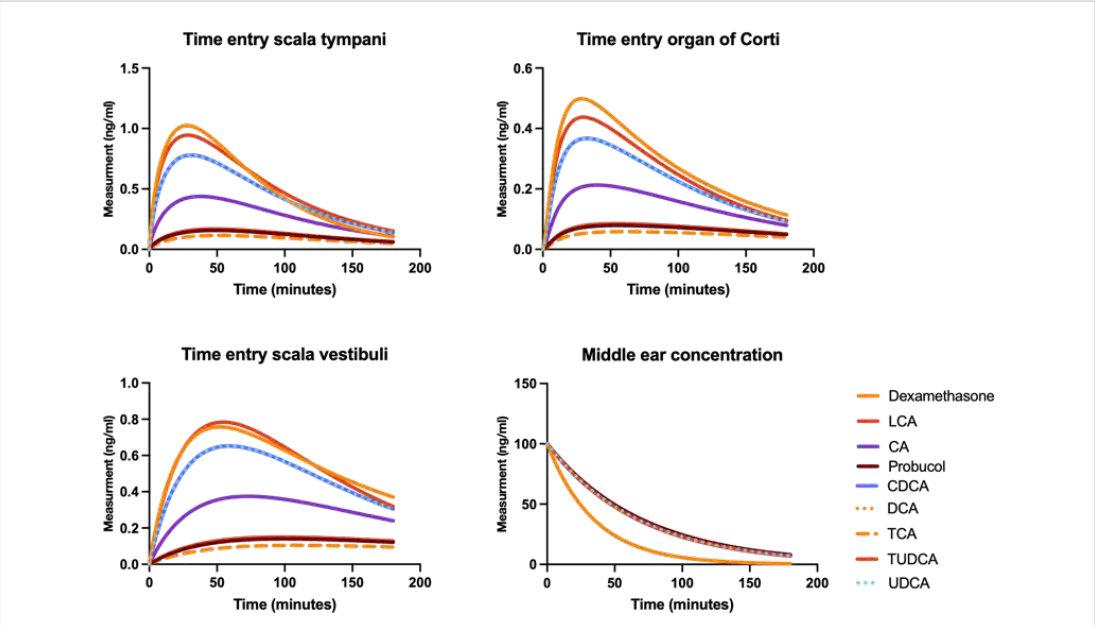

Supplementary VI.10.

FluidSim5 probucol diffusion pattern simulation through the round window membrane. Based on SwissADME EGG-Plot (452), water partition coefficient and drug molecular surface area were input into FluidSim (453, 454). To generate the diffusion patterns through the round window membrane of a known molecule applied as a clinical hearing loss treatment (dexamethasone), the six bile acids used for this thesis as excipients, and probucol were plotted in the graph. Analysis parameters were set for 100 µg/mL drug solutions, round window drug contact time 180 minutes, intratympanic measurement with default settings (elimination, permeation and volume entries) using the guinea pig prediction model. Middle ear concentration prediction decreases for all molecules at a similar rate, unlike dexamethasone (orange line). Drug entry prediction for scala tympani, scala vestibuli, and organ of Corti is higher for dexamethasone, followed by LCA (red line), CDCA (dark blue line), UDCA (dashed blue line), and CA (purple line). Probucol entry prediction is lower, similar to DCA. Round window membrane entry prediction can be associated in part with the molecule's characteristics. The bile acids (low molecular weight, higher lipophilicity) that show similar and higher diffusion rate to dexamethasone are also referenced to cross the BBB. The current FluidSim simulation does not consider the middle ear clearance pattern specific for probucol, thus requires future analysis *in vivo* to allow for better simulations.

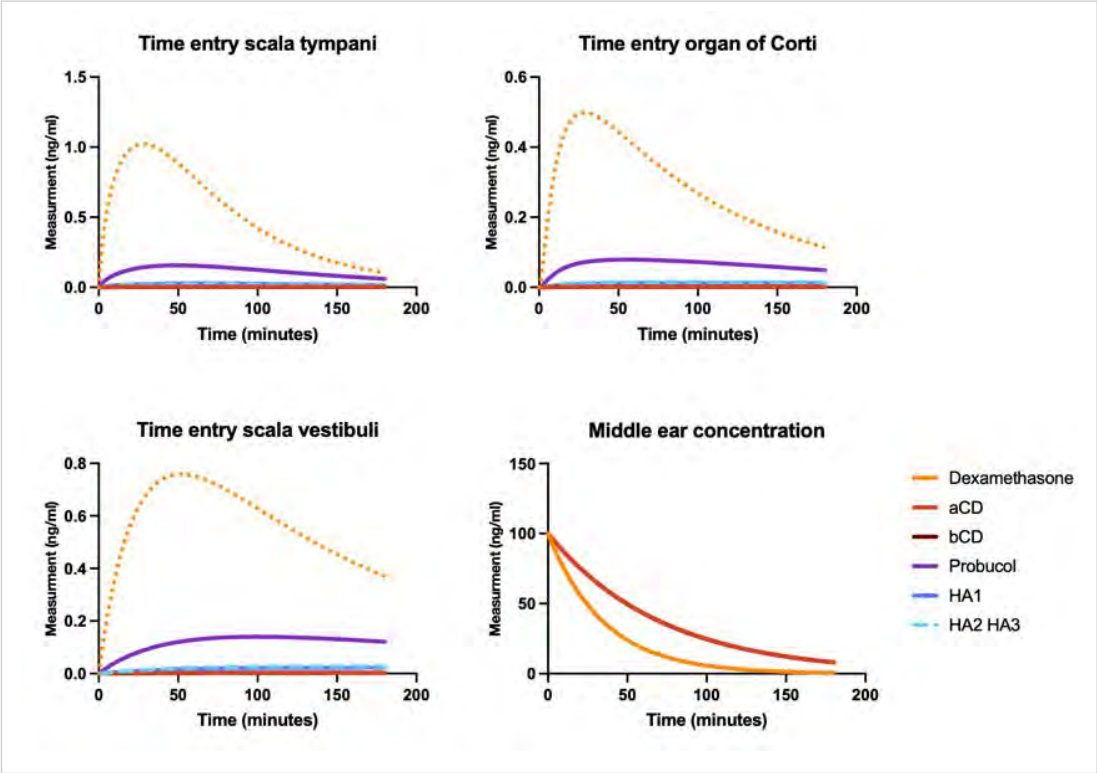

Supplementary VI.11.

FluidSim5 HA1, HA2, HA3 and *α/β*-CD diffusion pattern simulation through the round window membrane. The same parameters set for Supplementary VI.9. were used to generate the prediction pattern for round window membrane permeation and entry to the scala tympani, scala vestibuli and organ of Corti of dexamethasone (orange line), *α*-CD (red line), *β*-CD (brown line), probucol (purple line), HA1 (blue line) HA2, and HA3 (dashed blue line). As expected, due to the larger molecular weight (<1000) the diffusion and permeation prediction of HA1, HA2, HA3 and *α/β*-CD (hydrophilic compound) is very low.

Molecular structures were drawn using ChemSketch v2 (ACD/Labs Toronto, CA)
Graphs were prepared using GraphPad Prism v8-10.
Figures and illustrations were arranged/drawn using Adobe Illustrator (v. 26-28).
Micrographs brightness and contrast were corrected using Photoshop (v. 25).

References

1. Loftsson T, Brewster ME. Pharmaceutical applications of cyclodextrins: basic science and product development. J Pharm Pharmacol. 2010;62(11):1607-21.
2. Wishart DS, Knox C, Guo AC, Shrivastava S, Hassanali M, Stothard P, et al. DrugBank: a comprehensive resource for in silico drug discovery and exploration. Nucleic Acids Res. 2006;34(Database issue):D668-72.
3. Mooranian A, Zamani N, Takechi R, Luna G, Mikov M, Goločorbin-Kon S, et al. An in vivo pharmacological study: Variation in tissue-accumulation for the drug probucol as the result of targeted microtechnology and matrix-acrylic acid optimization and stabilization techniques. PLoS One. 2019;14(4):e0214984.
4. Kubo Y, Terashima Y, Yagi N, Nochi H, Tamoto K, Sekikawa H. Enhanced Bioavailability of Probucol Following the Administration of Solid Dispersion Systems of Probucol–Polyvinylpyrrolidone in Rabbits. Biological and Pharmaceutical Bulletin. 2009;32(11):1880-4.
5. Li F, Li L, Wang S, Yang Y, Li J, Liu D, et al. Improved dissolution and oral absorption by co-grinding active drug probucol and ternary stabilizers mixtures with planetary beads-milling method. Asian Journal of Pharmaceutical Sciences. 2019;14(6):649-57.
6. Lipinski CA, Lombardo F, Dominy BW, Feeney PJ. Experimental and computational approaches to estimate solubility and permeability in drug discovery and development settings. Adv Drug Deliv Rev. 2001;46(1-3):3-26.
7. Colle D, Hartwig JM, Soares FA, Farina M. Probucol modulates oxidative stress and excitotoxicity in Huntington's disease models in vitro. Brain Res Bull. 2012;87(4-5):397-405.
8. Bird JE, Milhoan K, Wilson CB, Young SG, Mundy CA, Parthasarathy S, et al. Ischemic acute renal failure and antioxidant therapy in the rat. The relation between glomerular and tubular dysfunction. J Clin Invest. 1988;81(5):1630-8.
9. Singla DK, Kaur K, Sharma AK, Dhingra S, Singal PK. Probucol promotes endogenous antioxidant reserve and confers protection against reperfusion injury. Can J Physiol Pharmacol. 2007;85(3-4):439-43.

10. Foster T, Ionescu C, Walker D, Jones M, Wagle S, Kovacevic B, et al. Chemotherapy-induced hearing loss: the applications of bio-nanotechnologies and bile acid-based delivery matrices. Ther Deliv. 2021;12(10):723-37.
11. Wanawongthai C, Pongpeerapat A, Higashi K, Tozuka Y, Moribe K, Yamamoto K. Nanoparticle formation from probucol/PVP/sodium alkyl sulfate co-ground mixture. International Journal of Pharmaceutics. 2009;376(1):169-75.
12. Hanada N, Higashi K, Zhao Z, Ueda K, Moribe K. Preparation of a ternary amorphous solid dispersion using hot-melt extrusion for obtaining a stable colloidal dispersion of amorphous probucol nanoparticles. International Journal of Pharmaceutics. 2023;640:122959.
13. Pongpeerapat A, Wanawongthai C, Tozuka Y, Moribe K, Yamamoto K. Formation mechanism of colloidal nanoparticles obtained from probucol/PVP/SDS ternary ground mixture. International Journal of Pharmaceutics. 2008;352(1):309-16.
14. Li J, Yang Y, Zhao M, Xu H, Ma J, Wang S. Improved oral bioavailability of probucol by dry media-milling. Materials Science and Engineering: C. 2017;78:780-6.
15. Zhao Z, Katai H, Higashi K, Ueda K, Kawakami K, Moribe K. Cryo-TEM and AFM Observation of the Time-Dependent Evolution of Amorphous Probucol Nanoparticles Formed by the Aqueous Dispersion of Ternary Solid Dispersions. Mol Pharm. 2019;16(5):2184-98.
16. Zaghloul A, Khattab I, Nada A, Al-Saidan S. Preparation, characterization and optimization of probucol self-emulsified drug delivery system to enhance solubility and dissolution. Pharmazie. 2008;63(9):654-60.
17. Zaghloul A, Lila A, Abd-Allah F, Nada A. Probucol Self-Emulsified Drug Delivery System: Stability Testing and Bioavailability Assessment in Human Volunteers. Current Drug Delivery. 2019;16(4):325-30.
18. Lau M, Giri K, Garcia-Bennett AE. Antioxidant properties of probucol released from mesoporous silica. European Journal of Pharmaceutical Sciences. 2019;138:105038.
19. WHO. Deafness and hearing loss 2024 [cited 2024 05 March]. Available from: https://www.who.int/news-room/fact-sheets/detail/deafness-and-hearing-loss.
20. Department of energy m, industry regulation and safety. Ototoxic chemicals - chemicals that result in hearing loss 2024 [

21. Wang J, Puel J-L. Toward Cochlear Therapies. Physiological Reviews. 2018;98(4):2477-522.
22. Reynard P, Thai-Van H. Drug-induced hearing loss: Listening to the latest advances. Therapies. 2023.
23. Hammill TL, Campbell KC. Protection for medication-induced hearing loss: the state of the science. International Journal of Audiology. 2018;57(sup4):S87-S95.
24. Sheth S, Mukherjea D, Rybak LP, Ramkumar V. Mechanisms of Cisplatin-Induced Ototoxicity and Otoprotection. Front Cell Neurosci. 2017;11:338.
25. Lee J, Fernandez K, Cunningham LL. Hear and Now: Ongoing Clinical Trials to Prevent Drug-Induced Hearing Loss. Annu Rev Pharmacol Toxicol. 2024;64:211-30.
26. Dash S, Zuo J, Steyger PS. Local Delivery of Therapeutics to the Cochlea Using Nanoparticles and Other Biomaterials. Pharmaceuticals (Basel). 2022;15(9).
27. Murillo-Cuesta S, Lara E, Bermúdez-Muñoz JM, Torres-Campos E, Rodríguez-de la Rosa L, López-Larrubia P, et al. Protection of lipopolysaccharide-induced otic injury by a single dose administration of a novel dexamethasone formulation. Translational Medicine Communications. 2023;8(1):23.
28. Jung SY, Kim S, Kang Z, Kwon S, Lee J, Park JW, et al. Efficiency of a dexamethasone nanosuspension as an intratympanic injection for acute hearing loss. Drug Deliv. 2022;29(1):149-60.
29. Salt AN, Plontke SK. Pharmacokinetic principles in the inner ear: Influence of drug properties on intratympanic applications. Hear Res. 2018;368:28-40.
30. Wang X, Xiong H, Zhang P, Liu Y, Gao C, Zhou Z, et al. Intratympanic microcrystals of dexamethasone and lipoic acid for the treatment of cisplatin-induced inner ear injury. Colloids and Surfaces B: Biointerfaces. 2023;223:113191.
31. Dindelegan MG, Pașcalău V, Suciu M, Neamțu B, Perde-Schrepler M, Blebea CM, et al. Biopolymer Lipid Hybrid Microcarrier for Transmembrane Inner Ear Delivery of Dexamethasone. Gels. 2022;8(8).
32. Mooranian A, Negrulj R, Arfuso F, Al-Salami H. Multicompartmental, multilayered probucol microcapsules for diabetes mellitus: Formulation characterization and effects on production of insulin and inflammation in a pancreatic β-cell line. Artif Cells Nanomed Biotechnol. 2016;44(7):1642-53.
33. Mooranian A, Negrulj R, Takechi R, Mamo J, Al-Sallami H, Al-Salami H. The biological effects of the hypolipidaemic drug probucol microcapsules fed daily for

4 weeks, to an insulin-resistant mouse model: potential hypoglycaemic and anti-inflammatory effects. Drug Deliv Transl Res. 2018;8(3):543-51.

34. Dawson PA, Lan T, Rao A. Bile acid transporters. J Lipid Res. 2009;50(12):2340-57.

35. Ferrell JM, Chiang JYL. Bile acid receptors and signaling crosstalk in the liver, gut and brain. Liver Research. 2021;5(3):105-18.

36. DailyMed. CHENODAL- chenodiol tablet, film coated 2023 [updated 12 July 2023; cited 2024 04 March]. Available from: https://dailymed.nlm.nih.gov/dailymed/lookup.cfm?setid=769e0a3b-826d-4faf-9129-5eeb7ebe0b67.

37. DailyMed. CHOLBAM- cholic acid capsule 2023 [updated 13 March 2023; cited 2024 04 March]. Available from: https://dailymed.nlm.nih.gov/dailymed/drugInfo.cfm?setid=e5b67402-8550-4604-97a0-c7b149fbf753.

38. DailyMed. URSODIOL capsule 2023 [updated 24 July 2023; cited 2024 04 March]. Available from: https://dailymed.nlm.nih.gov/dailymed/drugInfo.cfm?setid=a061bb07-a85d-4b08-877f-ce02156f0de7.

39. Hanafi NI, Mohamed AS, Sheikh Abdul Kadir SH, Othman MHD. Overview of Bile Acids Signaling and Perspective on the Signal of Ursodeoxycholic Acid, the Most Hydrophilic Bile Acid, in the Heart. Biomolecules. 2018;8(4).

40. Arafat M, Kirchhoefer C, Mikov M, Sarfraz M, Löbenberg R. Nanosized Liposomes Containing Bile Salt: A Vesicular Nanocarrier for Enhancing Oral Bioavailability of BCS Class III Drug. J Pharm Pharm Sci. 2017;20(0):305-18.

41. Talele P, Sahu S, Mishra AK. Physicochemical characterization of solid lipid nanoparticles comprised of glycerol monostearate and bile salts. Colloids Surf B Biointerfaces. 2018;172:517-25.

42. Gagliardi A, Paolino D, Iannone M, Palma E, Fresta M, Cosco D. Sodium deoxycholate-decorated zein nanoparticles for a stable colloidal drug delivery system. Int J Nanomedicine. 2018;13:601-14.

43. Leo E, Contado C, Bortolotti F, Pavan B, Scatturin A, Tosi G, et al. Nanoparticle formulation may affect the stabilization of an antiischemic prodrug. International Journal of Pharmaceutics. 2006;307(1):103-13.

44. Kumar A, Chhatra RK, Pandey PS. Synthesis of Click Bile Acid Polymers and Their Application in Stabilization of Silver Nanoparticles Showing Iodide Sensing Property. Organic Letters. 2010;12(1):24-7.
45. Kwak K, Yu B, Mouli SK, Larson AC, Kim DH. Sodium Cholate Bile Acid-Stabilized Ferumoxytol-Doxorubicin-Lipiodol Emulsion for Transcatheter Arterial Chemoembolization of Hepatocellular Carcinoma. J Vasc Interv Radiol. 2020;31(10):1697-705.e3.
46. Faustino C, Serafim C, Rijo P, Reis CP. Bile acids and bile acid derivatives: use in drug delivery systems and as therapeutic agents. Expert Opinion on Drug Delivery. 2016;13(8):1133-48.
47. Owen H, Graham S, Werling JO, Carter PW. Anion effects on electrostatic charging of sterically stabilized, water insoluble drug particles. International Journal of Pharmaceutics. 2009;368(1):154-9.
48. Meaney CM, O'Driscoll CM. A comparison of the permeation enhancement potential of simple bile salt and mixed bile salt:fatty acid micellar systems using the CaCo-2 cell culture model. Int J Pharm. 2000;207(1-2):21-30.
49. Lajczak-McGinley NK, Porru E, Fallon CM, Smyth J, Curley C, McCarron PA, et al. The secondary bile acids, ursodeoxycholic acid and lithocholic acid, protect against intestinal inflammation by inhibition of epithelial apoptosis. Physiol Rep. 2020;8(12):e14456.
50. Ouyang H, Mei X, Zhang T, Lu B, Ji L. Ursodeoxycholic acid ameliorates diabetic retinopathy via reducing retinal inflammation and reversing the breakdown of blood-retinal barrier. Eur J Pharmacol. 2018;840:20-7.
51. Spigelman MK, Zappulla RA, Malis LI, Holland JF, Goldsmith SJ, Goldberg JD. Intracarotid Dehydrocholate Infusion: A New Method for Prolonged Reversible Blood-Brain Barrier Disruption. Neurosurgery. 1983;12(6).
52. Fiaschini N, Mancuso M, Tanori M, Colantoni E, Vitali R, Diretto G, et al. Liver Steatosis and Steatohepatitis Alter Bile Acid Receptors in Brain and Induce Neuroinflammation: A Contribution of Circulating Bile Acids and Blood-Brain Barrier. Int J Mol Sci. 2022;23(22).
53. Gookin JL, Galanko JA, Blikslager AT, Argenzio RA. PG-mediated closure of paracellular pathway and not restitution is the primary determinant of barrier recovery in acutely injured porcine ileum. Am J Physiol Gastrointest Liver Physiol. 2003;285(5):G967-79.

54. Raimondi F, Santoro P, Barone MV, Pappacoda S, Barretta ML, Nanayakkara M, et al. Bile acids modulate tight junction structure and barrier function of Caco-2 monolayers via EGFR activation. Am J Physiol Gastrointest Liver Physiol. 2008;294(4):G906-13.
55. Quinn M, McMillin M, Galindo C, Frampton G, Pae HY, DeMorrow S. Bile acids permeabilize the blood brain barrier after bile duct ligation in rats via Rac1-dependent mechanisms. Dig Liver Dis. 2014;46(6):527-34.
56. Tsutsumi K, Li SK, Hymas RV, Teng CL, Tillman LG, Hardee GE, et al. Systematic studies on the paracellular permeation of model permeants and oligonucleotides in the rat small intestine with chenodeoxycholate as enhancer. J Pharm Sci. 2008;97(1):350-67.
57. Tropitzsch A, Arnold H, Bassiouni M, Müller A, Eckhard A, Müller M, et al. Assessing cisplatin-induced ototoxicity and otoprotection in whole organ culture of the mouse inner ear in simulated microgravity. Toxicol Lett. 2014;227(3):203-12.
58. Moatti A, Silkstone D, Martin T, Abbey K, Hutson KA, Fitzpatrick DC, et al. Assessment of drug permeability through an ex vivo porcine round window membrane model. iScience. 2023;26(6):106789.
59. Kalinec G, Thein P, Park C, Kalinec F. HEI-OC1 cells as a model for investigating drug cytotoxicity. Hear Res. 2016;335:105-17.
60. Lee Ji Hyun MKP. Effects of Dimethyl Sulfoxide (DMSO) on inner ear cells. International Journal of Current Research. 2016;8(08):37166-7.
61. Qi W, Ding D, Salvi RJ. Cytotoxic effects of dimethyl sulphoxide (DMSO) on cochlear organotypic cultures. Hear Res. 2008;236(1-2):52-60.
62. Inamura N, Salt AN. Permeability changes of the blood-labyrinth barrier measured in vivo during experimental treatments. Hearing Research. 1992;61(1):12-8.
63. Sekulic M, Puche R, Bodmer D, Petkovic V. Human blood-labyrinth barrier model to study the effects of cytokines and inflammation. Front Mol Neurosci. 2023;16:1243370.
64. Le TN, Blakley BW. Mannitol and the blood-labyrinth barrier. Journal of Otolaryngology - Head & Neck Surgery. 2017;46(1):66.
65. Wang X, Gu J, Xu K, Xu B, Yu D, Wu H. Sound conditioning strategy promoting paracellular permeability of the blood-labyrinth-barrier benefits inner ear drug delivery. Bioengineering & Translational Medicine. 2024;9(1):e10596.

66. Ke Y, Ma X, Jing Y, Diao T, Yu L. The Breakdown of Blood-Labyrinth Barrier Makes it Easier for Drugs to Enter the Inner Ear. The Laryngoscope.n/a(n/a).
67. Ding D, Liu H, Qi W, Jiang H, Li Y, Wu X, et al. Ototoxic effects and mechanisms of loop diuretics. J Otol. 2016;11(4):145-56.
68. Parnes LS, Sun AH, Freeman DJ. Corticosteroid pharmacokinetics in the inner ear fluids: an animal study followed by clinical application. Laryngoscope. 1999;109(7 Pt 2):1-17.
69. Jackson LE, Silverstein H. Chemical perfusion of the inner ear. Otolaryngol Clin North Am. 2002;35(3):639-53.
70. Singh R, Birru B, Veit JGS, Arrigali EM, Serban MA. Development and Characterization of an In Vitro Round Window Membrane Model for Drug Permeability Evaluations. Pharmaceuticals (Basel). 2022;15(9).
71. Duan M-l, Zhi-qiang C. Permeability of round window membrane and its role for drug delivery: our own findings and literature review. Journal of Otology. 2009;4(1):34-43.
72. Patel J, Szczupak M, Rajguru S, Balaban C, Hoffer ME. Inner Ear Therapeutics: An Overview of Middle Ear Delivery. Front Cell Neurosci. 2019;13:261.
73. Zhang Z, Li X, Zhang W, Kohane DS. Drug Delivery across Barriers to the Middle and Inner Ear. Adv Funct Mater. 2021;31(44).
74. Li L, Chao T, Brant J, O'Malley B, Jr., Tsourkas A, Li D. Advances in nano-based inner ear delivery systems for the treatment of sensorineural hearing loss. Adv Drug Deliv Rev. 2017;108:2-12.
75. Wang X, Dellamary L, Fernandez R, Ye Q, LeBel C, Piu F. Principles of inner ear sustained release following intratympanic administration. The Laryngoscope. 2011;121(2):385-91.
76. Jeong SH, Kim Y, Lyu AR, Shin SA, Kim TH, Huh YH, et al. Junctional Modulation of Round Window Membrane Enhances Dexamethasone Uptake into the Inner Ear and Recovery after NIHL. Int J Mol Sci. 2021;22(18).
77. Vllasaliu D, Exposito-Harris R, Heras A, Casettari L, Garnett M, Illum L, et al. Tight junction modulation by chitosan nanoparticles: comparison with chitosan solution. Int J Pharm. 2010;400(1-2):183-93.
78. Lin Y-C, Chen H-C, Chen H-K, Lin Y-Y, Kuo C-Y, Wang H, et al. Ultrastructural Changes Associated With the Enhanced Permeability of the Round

Window Membrane Mediated by Ultrasound Microbubbles. Frontiers in Pharmacology. 2020;10.

79. Shih C-P, Chen H-C, Lin Y-C, Chen H-K, Wang H, Kuo C-Y, et al. Middle-ear dexamethasone delivery via ultrasound microbubbles attenuates noise-induced hearing loss. The Laryngoscope. 2019;129(8):1907-14.

80. Tavazzani E, Spaiardi P, Contini D, Sancini G, Russo G, Masetto S. Precision medicine: a new era for inner ear diseases. Front Pharmacol. 2024;15:1328460.

81. Leong S, Feng SJ, Aksit A, Olson ES, Kysar JW, Lalwani AK. Microneedles Facilitate Small-Volume Intracochlear Delivery Without Physiologic Injury in Guinea Pigs. Otol Neurotol. 2023;44(5):513-9.

82. Yang KJ, Son J, Jung SY, Yi G, Yoo J, Kim DK, et al. Optimized phospholipid-based nanoparticles for inner ear drug delivery and therapy. Biomaterials. 2018;171:133-43.

83. Zhang L, Xu Y, Cao W, Xie S, Wen L, Chen G. Understanding the translocation mechanism of PLGA nanoparticles across round window membrane into the inner ear: a guideline for inner ear drug delivery based on nanomedicine. Int J Nanomedicine. 2018;13:479-92.

84. Ge X, Jackson RL, Liu J, Harper EA, Hoffer ME, Wassel RA, et al. Distribution of PLGA nanoparticles in chinchilla cochleae. Otolaryngol Head Neck Surg. 2007;137(4):619-23.

85. Sawant PD, Luu D, Ye R, Buchta R. Drug release from hydroethanolic gels. Effect of drug's lipophilicity (logP), polymer–drug interactions and solvent lipophilicity. International Journal of Pharmaceutics. 2010;396(1):45-52.

86. Joiner JB, Prasher A, Young IC, Kim J, Shrivastava R, Maturavongsadit P, et al. Effects of Drug Physicochemical Properties on In-Situ Forming Implant Polymer Degradation and Drug Release Kinetics. Pharmaceutics. 2022;14(6).

87. Vraka C, Nics L, Wagner K-H, Hacker M, Wadsak W, Mitterhauser M. LogP, a yesterday's value? Nuclear Medicine and Biology. 2017;50:1-10.

88. Tsantili-Kakoulidou A, Demopoulos VJ. Drug-like Properties and Fraction Lipophilicity Index as a combined metric. Admet dmpk. 2021;9(3):177-90.

89. Palm K, Stenberg P, Luthman K, Artursson P. Polar Molecular Surface Properties Predict the Intestinal Absorption of Drugs in Humans. Pharmaceutical Research. 1997;14(5):568-71.

90. Schaftenaar G, de Vlieg J. Quantum mechanical polar surface area. J Comput Aided Mol Des. 2012;26(3):311-8.

91. Kelder J, Grootenhuis PD, Bayada DM, Delbressine LP, Ploemen JP. Polar molecular surface as a dominating determinant for oral absorption and brain penetration of drugs. Pharm Res. 1999;16(10):1514-9.

92. Petereit AC, Swinney K, Mensch J, Mackie C, Stokbroekx S, Brewster M, et al. Prediction of blood–brain barrier penetration of poorly soluble drug candidates using surface activity profiling. European Journal of Pharmaceutics and Biopharmaceutics. 2010;75(3):405-10.

93. PubMed. tauroursodeoxycholic acid hearing 2024 [Available from: https://pubmed.ncbi.nlm.nih.gov/?term=tauroursodeoxycholic+acid+hearing.

94. Lee CH, Park SS, Lee DH, Lee SM, Kim MY, Choi BY, et al. Tauroursodeoxycholic acid attenuates cisplatin-induced hearing loss in rats. Neurosci Lett. 2020;722:134838.

95. Zong S, Liu T, Wan F, Chen P, Luo P, Xiao H. Endoplasmic Reticulum Stress Is Involved in Cochlear Cell Apoptosis in a Cisplatin-Induced Ototoxicity Rat Model. Audiol Neurootol. 2017;22(3):160-8.

96. Klokkenburg JJ, Hoeve HL, Francke J, Wieringa MH, Borgstein J, Feenstra L. Bile acids identified in middle ear effusions of children with otitis media with effusion. Laryngoscope. 2009;119(2):396-400.

97. Develoglu ON, Yalcin E, Bulut E, Celebi S, Sahan E, Ustundag N, et al. Histopathologic changes in the middle ear mucosa after exposure to pepsin and unconjugated bile acid. J Craniofac Surg. 2014;25(6):e536-40.

98. Moreira S, Fonseca I, Nunes MJ, Rosa A, Lemos L, Rodrigues E, et al. Nrf2 activation by tauroursodeoxycholic acid in experimental models of Parkinson's disease. Exp Neurol. 2017;295:77-87.

99. Bian KY, Jin HF, Sun W, Sun YJ. DCA can improve the ACI-induced neurological impairment through negative regulation of Nrf2 signaling pathway. Eur Rev Med Pharmacol Sci. 2019;23(1):343-51.

100. Han GH, Kim SJ, Ko WK, Lee D, Lee JS, Nah H, et al. Injectable Hydrogel Containing Tauroursodeoxycholic Acid for Anti-neuroinflammatory Therapy After Spinal Cord Injury in Rats. Mol Neurobiol. 2020;57(10):4007-17.

101. Hu J, Xu M, Yuan J, Li B, Entenman S, Yu H, et al. Tauroursodeoxycholic acid prevents hearing loss and hair cell death in Cdh23(erl/erl) mice. Neuroscience. 2016;316:311-20.
102. Oishi N, Duscha S, Boukari H, Meyer M, Xie J, Wei G, et al. XBP1 mitigates aminoglycoside-induced endoplasmic reticulum stress and neuronal cell death. Cell Death Dis. 2015;6(5):e1763.
103. Jia Z, He Q, Shan C, Li F. Tauroursodeoxycholic acid attenuates gentamicin-induced cochlear hair cell death in vitro. Toxicol Lett. 2018;294:20-6.
104. Oliver D, Taberner AM, Thurm H, Sausbier M, Arntz C, Ruth P, et al. The role of BKCa channels in electrical signal encoding in the mammalian auditory periphery. J Neurosci. 2006;26(23):6181-9.
105. Bukiya AN, Vaithianathan T, Toro L, Dopico AM. The second transmembrane domain of the large conductance, voltage- and calcium-gated potassium channel beta(1) subunit is a lithocholate sensor. FEBS Lett. 2008;582(5):673-8.
106. Khurana S, Raina H, Pappas V, Raufman JP, Pallone TL. Effects of deoxycholylglycine, a conjugated secondary bile acid, on myogenic tone and agonist-induced contraction in rat resistance arteries. PLoS One. 2012;7(2):e32006.
107. Pan C, Chu H, Lai Y, Liu Y, Sun Y, Du Z, et al. Down-regulation of the large conductance Ca(2+)-activated K(+) channel expression in C57BL/6J cochlea. Acta Otolaryngol. 2016;136(9):875-8.
108. Rüttiger L, Sausbier M, Zimmermann U, Winter H, Braig C, Engel J, et al. Deletion of the Ca2+-activated potassium (BK) alpha-subunit but not the BKbeta1-subunit leads to progressive hearing loss. Proc Natl Acad Sci U S A. 2004;101(35):12922-7.
109. Xu SR, Xia ML, Deng S, Li XR, Si JQ, Li L. [The effect of large-conductance calcium-activated potassium channels on the migration of pericytes in the mice of senile cochlear stria vascularis]. Zhonghua Er Bi Yan Hou Tou Jing Wai Ke Za Zhi. 2021;56(12):1319-27.
110. Brecht EJ, Scott LL, Ding B, Zhu X, Walton JP. A BK channel-targeted peptide induces age-dependent improvement in behavioral and neural sound representation. Neurobiol Aging. 2022;110:61-72.
111. Sokolowski B, Duncan RK, Chen S, Karolat J, Kathiresan T, Harvey M. The large-conductance Ca(2+)-activated K(+) channel interacts with the apolipoprotein ApoA1. Biochem Biophys Res Commun. 2009;387(4):671-5.

112. Liang F, Schulte BA, Qu C, Hu W, Shen Z. Inhibition of the calcium- and voltage-dependent big conductance potassium channel ameliorates cisplatin-induced apoptosis in spiral ligament fibrocytes of the cochlea. Neuroscience. 2005;135(1):263-71.

113. Purcell EK, Liu L, Thomas PV, Duncan RK. Cholesterol influences voltage-gated calcium channels and BK-type potassium channels in auditory hair cells. PLoS One. 2011;6(10):e26289.

114. Dopico AM, Walsh JV, Jr., Singer JJ. Natural bile acids and synthetic analogues modulate large conductance Ca2+-activated K+ (BKCa) channel activity in smooth muscle cells. J Gen Physiol. 2002;119(3):251-73.

115. Büki B, Jünger H, Zhang Y, Lundberg YW. The Price of Immune Responses and the Role of Vitamin D in the Inner Ear. Otol Neurotol. 2019;40(6):701-9.

116. Sacks D, Baxter B, Campbell BCV, Carpenter JS, Cognard C, Dippel D, et al. Multisociety Consensus Quality Improvement Revised Consensus Statement for Endovascular Therapy of Acute Ischemic Stroke. Int J Stroke. 2018;13(6):612-32.

117. Ishizawa M, Akagi D, Makishima M. Lithocholic Acid Is a Vitamin D Receptor Ligand That Acts Preferentially in the Ileum. Int J Mol Sci. 2018;19(7).

118. Nowaczewska M, Osiński S, Marzec M, Wiciński M, Bilicka K, Kaźmierczak W. The role of vitamin D in subjective tinnitus-A case-control study. PLoS One. 2021;16(8):e0255482.

119. Bigman G. Deficiency in vitamin D is associated with bilateral hearing impairment and bilateral sensorineural hearing loss in older adults. Nutr Res. 2022;105:1-10.

120. Carpinelli MR, Wise AK, Burt RA. Vitamin D-deficient diet rescues hearing loss in Klotho mice. Hear Res. 2011;275(1-2):105-9.

121. Zou J, Minasyan A, Keisala T, Zhang Y, Wang JH, Lou YR, et al. Progressive hearing loss in mice with a mutated vitamin D receptor gene. Audiol Neurootol. 2008;13(4):219-30.

122. Sueta T, Paki B, Everett AW, Robertson D. Purinergic receptors in auditory neurotransmission. Hear Res. 2003;183(1-2):97-108.

123. Zhu Y, Zhao HB. ATP-mediated potassium recycling in the cochlear supporting cells. Purinergic Signal. 2010;6(2):221-9.

124. Loesch A. On P2X receptors in the brain: microvessels. Dedicated to the memory of the late Professor Geoffrey Burnstock (1929-2020). Cell Tissue Res. 2021;384(3):577-88.
125. Berekméri E, Szepesy J, Köles L, Zelles T. Purinergic signaling in the organ of Corti: Potential therapeutic targets of sensorineural hearing losses. Brain Res Bull. 2019;151:109-18.
126. Loesch A, Burnstock G. Ultrastructural localisation of ATP-gated P2X2 receptor immunoreactivity in vascular endothelial cells in rat brain. Endothelium. 2000;7(2):93-8.
127. Wu T, Dai M, Shi XR, Jiang ZG, Nuttall AL. Functional expression of P2X4 receptor in capillary endothelial cells of the cochlear spiral ligament and its role in regulating the capillary diameter. Am J Physiol Heart Circ Physiol. 2011;301(1):H69-78.
128. Yan D, Zhu Y, Walsh T, Xie D, Yuan H, Sirmaci A, et al. Mutation of the ATP-gated P2X(2) receptor leads to progressive hearing loss and increased susceptibility to noise. Proc Natl Acad Sci U S A. 2013;110(6):2228-33.
129. Sivcev S, Slavikova B, Ivetic M, Knezu M, Kudova E, Zemkova H. Lithocholic acid inhibits P2X2 and potentiates P2X4 receptor channel gating. J Steroid Biochem Mol Biol. 2020;202:105725.
130. Köles L, Szepesy J, Berekméri E, Zelles T. Purinergic Signaling and Cochlear Injury-Targeting the Immune System? Int J Mol Sci. 2019;20(12).
131. Nikolic P, Housley GD, Thorne PR. Expression of the P2X7 receptor subunit of the adenosine 5'-triphosphate-gated ion channel in the developing and adult rat cochlea. Audiol Neurootol. 2003;8(1):28-37.
132. Schmidt A, Joussen S, Hausmann R, Gründer S, Wiemuth D. Bile acids are potent inhibitors of rat P2X2 receptors. Purinergic Signal. 2019;15(2):213-21.
133. Wen Y, Zong S, Liu T, Du P, Li H, Xiao H. Tauroursodeoxycholic acid attenuates cisplatin-induced ototoxicity by inhibiting the accumulation and aggregation of unfolded or misfolded proteins in the endoplasmic reticulum. Toxicology. 2021;453:152736.
134. Xie Q, Khaoustov VI, Chung CC, Sohn J, Krishnan B, Lewis DE, et al. Effect of tauroursodeoxycholic acid on endoplasmic reticulum stress-induced caspase-12 activation. Hepatology. 2002;36(3):592-601.

135. Lu J, Wang W, Liu H, Liu H, Wu H. Cisplatin induces calcium ion accumulation and hearing loss by causing functional alterations in calcium channels and exocytosis. Am J Transl Res. 2019;11(11):6877-89.
136. Chien JM, Chou CT, Liang WZ, Cheng JS, Chang HT, Tseng HW, et al. Effect of deoxycholic acid on Ca2+ movement, cell viability and apoptosis in human gastric cancer cells. Toxicol Mech Methods. 2015;25(2):113-9.
137. Nakajima T, Okuda Y, Chisaki K, Shin WS, Iwasawa K, Morita T, et al. Bile acids increase intracellular Ca(2+) concentration and nitric oxide production in vascular endothelial cells. Br J Pharmacol. 2000;130(7):1457-67.
138. Devor DC, Sekar MC, Frizzell RA, Duffey ME. Taurodeoxycholate activates potassium and chloride conductances via an IP3-mediated release of calcium from intracellular stores in a colonic cell line (T84). J Clin Invest. 1993;92(5):2173-81.
139. Sharma R, Quilty F, Gilmer JF, Long A, Byrne AM. Unconjugated secondary bile acids activate the unfolded protein response and induce golgi fragmentation via a src-kinase-dependant mechanism. Oncotarget. 2017;8(1):967-78.
140. Maison SF, Liu XP, Vetter DE, Eatock RA, Nathanson NM, Wess J, et al. Muscarinic signaling in the cochlea: presynaptic and postsynaptic effects on efferent feedback and afferent excitability. J Neurosci. 2010;30(19):6751-62.
141. Stefanescu RA, Shore SE. Muscarinic acetylcholine receptors control baseline activity and Hebbian stimulus timing-dependent plasticity in fusiform cells of the dorsal cochlear nucleus. J Neurophysiol. 2017;117(3):1229-38.
142. Cheng K, Khurana S, Chen Y, Kennedy RH, Zimniak P, Raufman JP. Lithocholylcholine, a bile acid/acetylcholine hybrid, is a muscarinic receptor antagonist. J Pharmacol Exp Ther. 2002;303(1):29-35.
143. Raufman J-P, Chen Y, Cheng K, Compadre C, Compadre L, Zimniak P. Selective interaction of bile acids with muscarinic receptors: a case of molecular mimicry. European Journal of Pharmacology. 2002;457(2):77-84.
144. Raufman JP, Chen Y, Zimniak P, Cheng K. Deoxycholic acid conjugates are muscarinic cholinergic receptor antagonists. Pharmacology. 2002;65(4):215-21.
145. Wang L, Gong Z, Zhang X, Zhu F, Liu Y, Jin C, et al. Gut microbial bile acid metabolite skews macrophage polarization and contributes to high-fat diet-induced colonic inflammation. Gut Microbes. 2020;12(1):1-20.
146. Frye MD, Ryan AF, Kurabi A. Inflammation associated with noise-induced hearing loss. J Acoust Soc Am. 2019;146(5):4020.

147. Benkafadar N, François F, Affortit C, Casas F, Ceccato JC, Menardo J, et al. ROS-Induced Activation of DNA Damage Responses Drives Senescence-Like State in Postmitotic Cochlear Cells: Implication for Hearing Preservation. Mol Neurobiol. 2019;56(8):5950-69.
148. Li H, Lu M, Zhang H, Wang S, Wang F, Ma X, et al. Downregulation of REST in the cochlea contributes to age-related hearing loss via the p53 apoptosis pathway. Cell Death Dis. 2022;13(4):343.
149. Im E, Martinez JD. Ursodeoxycholic acid (UDCA) can inhibit deoxycholic acid (DCA)-induced apoptosis via modulation of EGFR/Raf-1/ERK signaling in human colon cancer cells. J Nutr. 2004;134(2):483-6.
150. Lee J, Hong EM, Kim JH, Kim JH, Jung JH, Park SW, et al. Ursodeoxycholic acid shows antineoplastic effects in bile duct cancer cells via apoptosis induction; p53 activation; and EGFR-ERK, COX-2, and PI3K-AKT pathway inhibition. Mol Biol Rep. 2021;48(9):6231-40.
151. Qiao D, Gaitonde SV, Qi W, Martinez JD. Deoxycholic acid suppresses p53 by stimulating proteasome-mediated p53 protein degradation. Carcinogenesis. 2001;22(6):957-64.
152. Ferreira DM, Afonso MB, Rodrigues PM, Simão AL, Pereira DM, Borralho PM, et al. c-Jun N-terminal kinase 1/c-Jun activation of the p53/microRNA 34a/sirtuin 1 pathway contributes to apoptosis induced by deoxycholic acid in rat liver. Mol Cell Biol. 2014;34(6):1100-20.
153. Benkafadar N, Menardo J, Bourien J, Nouvian R, François F, Decaudin D, et al. Reversible p53 inhibition prevents cisplatin ototoxicity without blocking chemotherapeutic efficacy. EMBO Mol Med. 2017;9(1):7-26.
154. Reed SM, Quelle DE. p53 Acetylation: Regulation and Consequences. Cancers (Basel). 2014;7(1):30-69.
155. Xiong H, Pang J, Yang H, Dai M, Liu Y, Ou Y, et al. Activation of miR-34a/SIRT1/p53 signaling contributes to cochlear hair cell apoptosis: implications for age-related hearing loss. Neurobiol Aging. 2015;36(4):1692-701.
156. Studer E, Zhou X, Zhao R, Wang Y, Takabe K, Nagahashi M, et al. Conjugated bile acids activate the sphingosine-1-phosphate receptor 2 in primary rodent hepatocytes. Hepatology. 2012;55(1):267-76.

157. Santos-Cortez RL, Faridi R, Rehman AU, Lee K, Ansar M, Wang X, et al. Autosomal-Recessive Hearing Impairment Due to Rare Missense Variants within S1PR2. Am J Hum Genet. 2016;98(2):331-8.
158. Ingham NJ, Carlisle F, Pearson S, Lewis MA, Buniello A, Chen J, et al. S1PR2 variants associated with auditory function in humans and endocochlear potential decline in mouse. Sci Rep. 2016;6:28964.
159. Nakayama M, Tabuchi K, Hoshino T, Nakamagoe M, Nishimura B, Hara A. The influence of sphingosine-1-phosphate receptor antagonists on gentamicin-induced hair cell loss of the rat cochlea. Neurosci Lett. 2014;561:91-5.
160. Herr DR, Reolo MJ, Peh YX, Wang W, Lee CW, Rivera R, et al. Sphingosine 1-phosphate receptor 2 (S1P2) attenuates reactive oxygen species formation and inhibits cell death: implications for otoprotective therapy. Sci Rep. 2016;6:24541.
161. Cao C, Dai L, Mu J, Wang X, Hong Y, Zhu C, et al. S1PR2 antagonist alleviates oxidative stress-enhanced brain endothelial permeability by attenuating p38 and Erk1/2-dependent cPLA(2) phosphorylation. Cell Signal. 2019;53:151-61.
162. Lee CH, Jeon J, Lee SM, Kim SY. Differential Expression of miRNAs and Their Predicted Target Pathways in Cochlear Nucleus Following Chronic Noise Exposure in Rats. Cells. 2022;11(15).
163. Dai BH, Geng L, Wang Y, Sui CJ, Xie F, Shen RX, et al. microRNA-199a-5p protects hepatocytes from bile acid-induced sustained endoplasmic reticulum stress. Cell Death Dis. 2013;4(4):e604.
164. Doukas SG, Vageli DP, Sasaki CT. NF-κB inhibition reverses acidic bile-induced miR-21, miR-155, miR-192, miR-34a, miR-375 and miR-451a deregulations in human hypopharyngeal cells. J Cell Mol Med. 2018;22(5):2922-34.
165. Sasaki CT, Vageli DP. miR-21, miR-155, miR-192, and miR-375 Deregulations Related to NF-kappaB Activation in Gastroduodenal Fluid-Induced Early Preneoplastic Lesions of Laryngeal Mucosa In Vivo. Neoplasia. 2016;18(6):329-38.
166. Rudnicki A, Shivatzki S, Beyer LA, Takada Y, Raphael Y, Avraham KB. microRNA-224 regulates Pentraxin 3, a component of the humoral arm of innate immunity, in inner ear inflammation. Hum Mol Genet. 2014;23(12):3138-46.
167. Adamowicz M, Kempinska-Podhorodecka A, Abramczyk J, Banales JM, Milkiewicz P, Milkiewicz M. Suppression of Hepatic PPARα in Primary Biliary Cholangitis Is Modulated by miR-155. Cells. 2022;11(18).

168. Pang J, Xiong H, Lin P, Lai L, Yang H, Liu Y, et al. Activation of miR-34a impairs autophagic flux and promotes cochlear cell death via repressing ATG9A: implications for age-related hearing loss. Cell Death Dis. 2017;8(10):e3079.
169. Lin Y, Shen J, Li D, Ming J, Liu X, Zhang N, et al. MiR-34a contributes to diabetes-related cochlear hair cell apoptosis via SIRT1/HIF-1α signaling. Gen Comp Endocrinol. 2017;246:63-70.
170. Castro RE, Ferreira DM, Afonso MB, Borralho PM, Machado MV, Cortez-Pinto H, et al. miR-34a/SIRT1/p53 is suppressed by ursodeoxycholic acid in the rat liver and activated by disease severity in human non-alcoholic fatty liver disease. J Hepatol. 2013;58(1):119-25.
171. Krattinger R, Boström A, Lee SML, Thasler WE, Schiöth HB, Kullak-Ublick GA, et al. Chenodeoxycholic acid significantly impacts the expression of miRNAs and genes involved in lipid, bile acid and drug metabolism in human hepatocytes. Life Sci. 2016;156:47-56.
172. Kulkarni SR, Soroka CJ, Hagey LR, Boyer JL. Sirtuin 1 activation alleviates cholestatic liver injury in a cholic acid-fed mouse model of cholestasis. Hepatology. 2016;64(6):2151-64.
173. Huang Q, Ou Y, Xiong H, Yang H, Zhang Z, Chen S, et al. The miR-34a/Bcl-2 Pathway Contributes to Auditory Cortex Neuron Apoptosis in Age-Related Hearing Loss. Audiol Neurootol. 2017;22(2):96-103.
174. Pang J, Xiong H, Yang H, Ou Y, Xu Y, Huang Q, et al. Circulating miR-34a levels correlate with age-related hearing loss in mice and humans. Exp Gerontol. 2016;76:58-67.
175. Akiyama N, Yamamoto-Fukuda T, Kojima H. miR-34a predicts the prognosis of advanced-stage external auditory canal squamous cell carcinoma. Acta Otolaryngol. 2022;142(6):537-41.
176. Wang D, Xiao Y, Li W, Feng X, Yi G, Chen Z, et al. Association of noise exposure, plasma microRNAs with arterial stiffness among Chinese workers. Environ Pollut. 2022;311:120002.
177. Cioffi JA, Yue WY, Mendolia-Loffredo S, Hansen KR, Wackym PA, Hansen MR. MicroRNA-21 overexpression contributes to vestibular schwannoma cell proliferation and survival. Otol Neurotol. 2010;31(9):1455-62.
178. Yan H, Huang W, Rao J, Yuan J. miR-21 regulates ischemic neuronal injury via the p53/Bcl-2/Bax signaling pathway. Aging (Albany NY). 2021;13(18):22242-55.

179. Ge XT, Lei P, Wang HC, Zhang AL, Han ZL, Chen X, et al. miR-21 improves the neurological outcome after traumatic brain injury in rats. Sci Rep. 2014;4:6718.
180. Hao F, Shan C, Zhang Y, Zhang Y, Jia Z. Exosomes Derived from microRNA-21 Overexpressing Neural Progenitor Cells Prevent Hearing Loss from Ischemia-Reperfusion Injury in Mice via Inhibiting the Inflammatory Process in the Cochlea. ACS Chem Neurosci. 2022;13(16):2464-72.
181. Yang T, Cai C, Peng A, Liu J, Wang Q. Exosomes derived from cochlear spiral ganglion progenitor cells prevent cochlea damage from ischemia-reperfusion injury via inhibiting the inflammatory process. Cell Tissue Res. 2021;386(2):239-47.
182. Nguyen TT, Ung TT, Li S, Sah DK, Park SY, Lian S, et al. Lithocholic Acid Induces miR21, Promoting PTEN Inhibition via STAT3 and ERK-1/2 Signaling in Colorectal Cancer Cells. Int J Mol Sci. 2021;22(19).
183. Yuan T, Ni Z, Han C, Min Y, Sun N, Liu C, et al. SOX2 interferes with the function of CDX2 in bile acid-induced gastric intestinal metaplasia. Cancer Cell Int. 2019;19:24.
184. Rodrigues PM, Afonso MB, Simão AL, Borralho PM, Rodrigues CMP, Castro RE. Inhibition of NF-κB by deoxycholic acid induces miR-21/PDCD4-dependent hepatocellular apoptosis. Sci Rep. 2015;5:17528.
185. Chen D, Jia G, Zhang Y, Mao H, Zhao L, Li W, et al. Sox2 overexpression alleviates noise-induced hearing loss by inhibiting inflammation-related hair cell apoptosis. J Neuroinflammation. 2022;19(1):59.
186. Castro RE, Ferreira DM, Zhang X, Borralho PM, Sarver AL, Zeng Y, et al. Identification of microRNAs during rat liver regeneration after partial hepatectomy and modulation by ursodeoxycholic acid. Am J Physiol Gastrointest Liver Physiol. 2010;299(4):G887-97.
187. Huang R, Huang Y, Zeng G, Li M, Jin Y. Ursodeoxycholic acid inhibits intimal hyperplasia, vascular smooth muscle cell excessive proliferation, migration via blocking miR-21/PTEN/AKT/mTOR signaling pathway. Cell Cycle. 2020;19(8):918-32.
188. Sisto R, Moleti A, Capone P, Sanjust F, Cerini L, Tranfo G, et al. MicroRNA expression is associated with auditory dysfunction in workers exposed to ototoxic solvents and noise. Front Public Health. 2022;10:958181.

189. Wang Z, Liu Y, Han N, Chen X, Yu W, Zhang W, et al. Profiles of oxidative stress-related microRNA and mRNA expression in auditory cells. Brain Res. 2010;1346:14-25.
190. Chen J, Qin J, Liu J. Elucidation of the mechanism of miR-122-5p in mediating FOXO3 injury and apoptosis of mouse cochlear hair cells induced by hydrogen peroxide. Exp Ther Med. 2022;23(6):435.
191. Yoon S, Lee H, Ji SC, Yoon SH, Cho JY, Chung JY. Pharmacokinetics and Pharmacodynamics of Ursodeoxycholic Acid in an Overweight Population With Abnormal Liver Function. Clin Pharmacol Drug Dev. 2021;10(1):68-77.
192. Lin R, Zhan M, Yang L, Wang H, Shen H, Huang S, et al. Deoxycholic acid modulates the progression of gallbladder cancer through N(6)-methyladenosine-dependent microRNA maturation. Oncogene. 2020;39(26):4983-5000.
193. Ding L, Liu J, Shen HX, Pan LP, Liu QD, Zhang HD, et al. Analysis of plasma microRNA expression profiles in male textile workers with noise-induced hearing loss. Hear Res. 2016;333:275-82.
194. Xiao T, Meng W, Jin Z, Wang J, Deng J, Wen J, et al. miR-182-5p promotes hepatocyte-stellate cell crosstalk to facilitate liver regeneration. Commun Biol. 2022;5(1):771.
195. Geng R, Furness DN, Muraleedharan CK, Zhang J, Dabdoub A, Lin V, et al. The microRNA-183/96/182 Cluster is Essential for Stereociliary Bundle Formation and Function of Cochlear Sensory Hair Cells. Sci Rep. 2018;8(1):18022.
196. Li Y, Li A, Wu J, He Y, Yu H, Chai R, et al. MiR-182-5p protects inner ear hair cells from cisplatin-induced apoptosis by inhibiting FOXO3a. Cell Death Dis. 2016;7(9):e2362.
197. Kim CW, Han JH, Wu L, Choi JY. microRNA-183 is Essential for Hair Cell Regeneration after Neomycin Injury in Zebrafish. Yonsei Med J. 2018;59(1):141-7.
198. Sedgeman LR, Beysen C, Allen RM, Ramirez Solano MA, Turner SM, Vickers KC. Intestinal bile acid sequestration improves glucose control by stimulating hepatic miR-182-5p in type 2 diabetes. Am J Physiol Gastrointest Liver Physiol. 2018;315(5):G810-g23.
199. Negrulj R, Mooranian A, Al-Salami H. Potentials and Limitations of Bile Acids in Type 2 Diabetes Mellitus: Applications of Microencapsulation as a Novel Oral Delivery System. Journal of Endocrinology and Diabetes Mellitus. 2013;1:49-59.

200. Miyazaki T, Sasaki SI, Toyoda A, Shirai M, Ikegami T, Matsuzaki Y, et al. Influences of Taurine Deficiency on Bile Acids of the Bile in the Cat Model. Adv Exp Med Biol. 2019;1155:35-44.
201. Hofmann AF. Bile Acids: The Good, the Bad, and the Ugly. News Physiol Sci. 1999;14:24-9.
202. Bellettato CM, Scarpa M. Possible strategies to cross the blood-brain barrier. Ital J Pediatr. 2018;44(Suppl 2):131.
203. Hirose K, Hartsock JJ, Johnson S, Santi P, Salt AN. Systemic lipopolysaccharide compromises the blood-labyrinth barrier and increases entry of serum fluorescein into the perilymph. J Assoc Res Otolaryngol. 2014;15(5):707-19.
204. Henriksen NL, Hansen SH, Lycas MD, Pan X, Eriksen T, Johansen LS, et al. Cholestasis alters brain lipid and bile acid composition and compromises motor function in neonatal piglets. Physiol Rep. 2022;10(13):e15368.
205. Maj MA, Gehani TR, Immoos C, Medrano MS, Fanter RK, Strand CR, et al. Olive- and Coconut-Oil-Enriched Diets Decreased Secondary Bile Acids and Regulated Metabolic and Transcriptomic Markers of Brain Injury in the Frontal Cortexes of NAFLD Pigs. Brain Sci. 2022;12(9).
206. DeMorrow S. Bile Acids in Hepatic Encephalopathy. J Clin Exp Hepatol. 2019;9(1):117-24.
207. Berendse K, Klouwer FC, Koot BG, Kemper EM, Ferdinandusse S, Koelfat KV, et al. Cholic acid therapy in Zellweger spectrum disorders. J Inherit Metab Dis. 2016;39(6):859-68.
208. Claeys W, Van Hoecke L, Geerts A, Van Vlierberghe H, Lefere S, Van Imschoot G, et al. A mouse model of hepatic encephalopathy: bile duct ligation induces brain ammonia overload, glial cell activation and neuroinflammation. Sci Rep. 2022;12(1):17558.
209. Kwan SY, Jiao J, Qi J, Wang Y, Wei P, McCormick JB, et al. Bile Acid Changes Associated With Liver Fibrosis and Steatosis in the Mexican-American Population of South Texas. Hepatol Commun. 2020;4(4):555-68.
210. Makino I, Nakagawa S, Mashimo K. Conjugated and unconjugated serum bile acid levels n patients with hepatobiliary diseases. Gastroenterology. 1969;56(6):1033-9.
211. Wang X, Chen L, Wang H, Cai W, Xie Q. Modulation of bile acid profile by gut microbiota in chronic hepatitis B. J Cell Mol Med. 2020;24(4):2573-81.

212. Kamath BM, Stein P, Houwen RHJ, Verkade HJ. Potential of ileal bile acid transporter inhibition as a therapeutic target in Alagille syndrome and progressive familial intrahepatic cholestasis. Liver Int. 2020;40(8):1812-22.
213. Paulusma CC, Elferink RP, Jansen PL. Progressive familial intrahepatic cholestasis type 1. Semin Liver Dis. 2010;30(2):117-24.
214. Li C, Guo H, Dai F, Huo X, Li Z, Zhang S, et al. SREBP-2 expression pattern contributes to susceptibility of Mongolian gerbils to hypercholesterolemia. Mol Med Rep. 2018;17(2):3288-96.
215. Doosti A, Lotfi Y, Bakhshi E. Effects of Hyperlipidemia on Noise Induced Hearing Loss (NIHL). Indian J Otolaryngol Head Neck Surg. 2016;68(2):211-3.
216. Paulusma CC, de Waart DR, Kunne C, Mok KS, Elferink RP. Activity of the bile salt export pump (ABCB11) is critically dependent on canalicular membrane cholesterol content. J Biol Chem. 2009;284(15):9947-54.
217. Lee J, Yergeau C, Kawai K, Braverman N, Géléoc GSG. A Retrospective Study of Hearing Loss in Patients Diagnosed with Peroxisome Biogenesis Disorders in the Zellweger Spectrum. Ear Hear. 2022;43(2):582-91.
218. Gholami Parizad E, Gerami Matin H, Gholami Parizad E, Khosravi A. The Prevalence of Hearing Loss in Patients with Hepatitis B Infection Compared with Healthy Volunteers. Iran J Otorhinolaryngol. 2017;29(92):127-32.
219. Sarig O, Goldsher D, Nousbeck J, Fuchs-Telem D, Cohen-Katsenelson K, Iancu TC, et al. Infantile mitochondrial hepatopathy is a cardinal feature of MEGDEL syndrome (3-methylglutaconic aciduria type IV with sensorineural deafness, encephalopathy and Leigh-like syndrome) caused by novel mutations in SERAC1. Am J Med Genet A. 2013;161a(9):2204-15.
220. Tatoli R, Tirelli S, Lampignano L, Castellana F, Bortone I, Zupo R, et al. Liver Fibrosis and Hearing Loss in an Older Mediterranean Population: Results from the Salus in Apulia Study. J Clin Med. 2022;11(23).
221. Stapelbroek JM, Peters TA, van Beurden DH, Curfs JH, Joosten A, Beynon AJ, et al. ATP8B1 is essential for maintaining normal hearing. Proc Natl Acad Sci U S A. 2009;106(24):9709-14.
222. Le Caignec C, Lefevre M, Schott JJ, Chaventre A, Gayet M, Calais C, et al. Familial deafness, congenital heart defects, and posterior embryotoxon caused by cysteine substitution in the first epidermal-growth-factor-like domain of jagged 1. Am J Hum Genet. 2002;71(1):180-6.

223. Wang H, Lin C, Yao J, Shi H, Zhang C, Wei Q, et al. Deletion of OSBPL2 in auditory cells increases cholesterol biosynthesis and drives reactive oxygen species production by inhibiting AMPK activity. Cell Death Dis. 2019;10(9):627.
224. Mohammed AA. Lipid Profile among Patients with Sudden Sensorineural Hearing Loss. Indian J Otolaryngol Head Neck Surg. 2014;66(4):425-8.
225. Chang IJ, Kang CJ, Yueh CY, Fang KH, Yeh RM, Tsai YT. The relationship between serum lipids and sudden sensorineural hearing loss: a systematic review and meta-analysis. PLoS One. 2015;10(4):e0121025.
226. Chen C, Wang M, Wang H, Xiong W, Dai Q, Wang B, et al. Impact of hyperlipidemia as a coexisting factor on the prognosis of idiopathic sudden sensorineural hearing loss: A propensity score matching analysis. Clin Otolaryngol. 2020;45(1):2-11.
227. Malgrange B, Varela-Nieto I, de Medina P, Paillasse MR. Targeting cholesterol homeostasis to fight hearing loss: a new perspective. Front Aging Neurosci. 2015;7:3.
228. Oshima T, Ikeda K, Takasaka T. Sensorineural hearing loss associated with Byler disease. Tohoku J Exp Med. 1999;187(1):83-8.
229. Li X, Chen B, Zhou X, Ye F, Wang Y, Hu W. Identification of dyslipidemia as a risk factor for sudden sensorineural hearing loss: A multicenter case-control study. J Clin Lab Anal. 2021;35(12):e24067.
230. Shi X. Physiopathology of the cochlear microcirculation. Hear Res. 2011;282(1-2):10-24.
231. Neng L, Zhang F, Kachelmeier A, Shi X. Endothelial cell, pericyte, and perivascular resident macrophage-type melanocyte interactions regulate cochlear intrastrial fluid-blood barrier permeability. J Assoc Res Otolaryngol. 2013;14(2):175-85.
232. Wu YX, Zhu GX, Liu XQ, Sun F, Zhou K, Wang S, et al. Noise alters guinea pig's blood-labyrinth barrier ultrastructure and permeability along with a decrease of cochlear Claudin-5 and Occludin. BMC Neurosci. 2014;15:136.
233. Gu J, Tong L, Lin X, Chen Y, Wu H, Wang X, et al. The disruption and hyperpermeability of blood-labyrinth barrier mediates cisplatin-induced ototoxicity. Toxicol Lett. 2022;354:56-64.
234. Pakdaman MN, Ishiyama G, Ishiyama A, Peng KA, Kim HJ, Pope WB, et al. Blood-Labyrinth Barrier Permeability in Menière Disease and Idiopathic Sudden

Sensorineural Hearing Loss: Findings on Delayed Postcontrast 3D-FLAIR MRI. AJNR Am J Neuroradiol. 2016;37(10):1903-8.

235. Shi X, Wang Z, Ren W, Chen L, Xu C, Li M, et al. LDL receptor-related protein 1 (LRP1), a novel target for opening the blood-labyrinth barrier (BLB). Signal Transduct Target Ther. 2022;7(1):175.

236. Zhang J, Chen S, Hou Z, Cai J, Dong M, Shi X. Lipopolysaccharide-induced middle ear inflammation disrupts the cochlear intra-strial fluid-blood barrier through down-regulation of tight junction proteins. PLoS One. 2015;10(3):e0122572.

237. Huang L, Chen Y, Liu R, Li B, Fei X, Li X, et al. P-Glycoprotein Aggravates Blood Brain Barrier Dysfunction in Experimental Ischemic Stroke by Inhibiting Endothelial Autophagy. Aging Dis. 2022;13(5):1546-61.

238. Saito T, Zhang ZJ, Tsuzuki H, Ohtsubo T, Yamada T, Yamamoto T, et al. Expression of P-glycoprotein in inner ear capillary endothelial cells of the guinea pig with special reference to blood-inner ear barrier. Brain Res. 1997;767(2):388-92.

239. Saito T, Zhang ZJ, Tokuriki M, Ohtsubo T, Noda I, Shibamori Y, et al. Expression of p-glycoprotein is associated with that of multidrug resistance protein 1 (MRP1) in the vestibular labyrinth and endolymphatic sac of the guinea pig. Neurosci Lett. 2001;303(3):189-92.

240. Zhang ZJ, Saito T, Kimura Y, Sugimoto C, Ohtsubo T, Saito H. Disruption of mdr1a p-glycoprotein gene results in dysfunction of blood-inner ear barrier in mice. Brain Res. 2000;852(1):116-26.

241. Elamiri A, Perwaiz S, Tuchweber B, Yousef IM. Effect of mdr2 mutation with combined tandem disruption of canalicular glycoprotein transporters by cyclosporine A on bile formation in mice. Pharmacol Res. 2003;48(5):467-72.

242. Komori Y, Arisawa S, Takai M, Yokoyama K, Honda M, Hayashi K, et al. Ursodeoxycholic acid inhibits overexpression of P-glycoprotein induced by doxorubicin in HepG2 cells. Eur J Pharmacol. 2014;724:161-7.

243. Greenwood J, Adu J, Davey AJ, Abbott NJ, Bradbury MW. The effect of bile salts on the permeability and ultrastructure of the perfused, energy-depleted, rat blood-brain barrier. J Cereb Blood Flow Metab. 1991;11(4):644-54.

244. Donovan JM, Benedek GB, Carey MC. Self-association of human apolipoproteins A-I and A-II and interactions of apolipoprotein A-I with bile salts: quasi-elastic light scattering studies. Biochemistry. 1987;26(25):8116-25.

245. Shiraya T, Araki F, Ueta T, Fukunaga H, Totsuka K, Arai T, et al. Ursodeoxycholic Acid Attenuates the Retinal Vascular Abnormalities in Anti-PDGFR-β Antibody-Induced Pericyte Depletion Mouse Models. Sci Rep. 2020;10(1):977.
246. Chung YR, Choi JA, Koh JY, Yoon YH. Ursodeoxycholic Acid Attenuates Endoplasmic Reticulum Stress-Related Retinal Pericyte Loss in Streptozotocin-Induced Diabetic Mice. J Diabetes Res. 2017;2017:1763292.
247. Palmela I, Correia L, Silva RF, Sasaki H, Kim KS, Brites D, et al. Hydrophilic bile acids protect human blood-brain barrier endothelial cells from disruption by unconjugated bilirubin: an in vitro study. Front Neurosci. 2015;9:80.
248. Fickert P, Zollner G, Fuchsbichler A, Stumptner C, Pojer C, Zenz R, et al. Effects of ursodeoxycholic and cholic acid feeding on hepatocellular transporter expression in mouse liver. Gastroenterology. 2001;121(1):170-83.
249. Brzica H, Abdullahi W, Reilly BG, Ronaldson PT. Sex-specific differences in organic anion transporting polypeptide 1a4 (Oatp1a4) functional expression at the blood-brain barrier in Sprague-Dawley rats. Fluids Barriers CNS. 2018;15(1):25.
250. Zhang Y, Csanaky IL, Selwyn FP, Lehman-McKeeman LD, Klaassen CD. Organic anion-transporting polypeptide 1a4 (Oatp1a4) is important for secondary bile acid metabolism. Biochem Pharmacol. 2013;86(3):437-45.
251. Makishima M, Okamoto AY, Repa JJ, Tu H, Learned RM, Luk A, et al. Identification of a nuclear receptor for bile acids. Science. 1999;284(5418):1362-5.
252. Huang C, Wang J, Hu W, Wang C, Lu X, Tong L, et al. Identification of functional farnesoid X receptors in brain neurons. FEBS Lett. 2016;590(18):3233-42.
253. Chen Q, Ma H, Guo X, Liu J, Gui T, Gai Z. Farnesoid X Receptor (FXR) Aggravates Amyloid-β-Triggered Apoptosis by Modulating the cAMP-Response Element-Binding Protein (CREB)/Brain-Derived Neurotrophic Factor (BDNF) Pathway In Vitro. Med Sci Monit. 2019;25:9335-45.
254. Duboc H, Taché Y, Hofmann AF. The bile acid TGR5 membrane receptor: from basic research to clinical application. Dig Liver Dis. 2014;46(4):302-12.
255. Liang H, Matei N, McBride DW, Xu Y, Tang J, Luo B, et al. Activation of TGR5 protects blood brain barrier via the BRCA1/Sirt1 pathway after middle cerebral artery occlusion in rats. J Biomed Sci. 2020;27(1):61.
256. McMillin M, Frampton G, Tobin R, Dusio G, Smith J, Shin H, et al. TGR5 signaling reduces neuroinflammation during hepatic encephalopathy. J Neurochem. 2015;135(3):565-76.

257. Zhu H, Bai Y, Wang G, Su Y, Tao Y, Wang L, et al. Hyodeoxycholic acid inhibits lipopolysaccharide-induced microglia inflammatory responses through regulating TGR5/AKT/NF-κB signaling pathway. J Psychopharmacol. 2022;36(7):849-59.
258. Weng ZB, Chen YR, Lv JT, Wang MX, Chen ZY, Zhou W, et al. A Review of Bile Acid Metabolism and Signaling in Cognitive Dysfunction-Related Diseases. Oxid Med Cell Longev. 2022;2022:4289383.
259. Grant SM, DeMorrow S. Bile Acid Signaling in Neurodegenerative and Neurological Disorders. Int J Mol Sci. 2020;21(17).
260. Koff RS, Oliai A, Sparks RW. Sensori-neural hearing loss in alcoholic cirrhosis. Digestion. 1973;8(3):248-53.
261. Zhang G, Chen H, Ren W, Huang J. Efficacy of bile acid profiles in diagnosing and staging of alcoholic liver disease. Scand J Clin Lab Invest. 2022:1-10.
262. MahmoudianDehkordi S, Arnold M, Nho K, Ahmad S, Jia W, Xie G, et al. Altered bile acid profile associates with cognitive impairment in Alzheimer's disease-An emerging role for gut microbiome. Alzheimers Dement. 2019;15(1):76-92.
263. Marksteiner J, Blasko I, Kemmler G, Koal T, Humpel C. Bile acid quantification of 20 plasma metabolites identifies lithocholic acid as a putative biomarker in Alzheimer's disease. Metabolomics. 2018;14(1):1.
264. Nho K, Kueider-Paisley A, MahmoudianDehkordi S, Arnold M, Risacher SL, Louie G, et al. Altered bile acid profile in mild cognitive impairment and Alzheimer's disease: Relationship to neuroimaging and CSF biomarkers. Alzheimers Dement. 2019;15(2):232-44.
265. Balasa R, Barcutean L, Mosora O, Manu D. Reviewing the Significance of Blood-Brain Barrier Disruption in Multiple Sclerosis Pathology and Treatment. Int J Mol Sci. 2021;22(16).
266. Rebeaud J, Peter B, Pot C. How Microbiota-Derived Metabolites Link the Gut to the Brain during Neuroinflammation. Int J Mol Sci. 2022;23(17).
267. Bhargava P, Smith MD, Mische L, Harrington E, Fitzgerald KC, Martin K, et al. Bile acid metabolism is altered in multiple sclerosis and supplementation ameliorates neuroinflammation. J Clin Invest. 2020;130(7):3467-82.
268. Brownell WE, Jacob S, Hakizimana P, Ulfendahl M, Fridberger A. Membrane cholesterol modulates cochlear electromechanics. Pflugers Arch. 2011;461(6):677-86.

269. Thomas PV, Cheng AL, Colby CC, Liu L, Patel CK, Josephs L, et al. Localization and proteomic characterization of cholesterol-rich membrane microdomains in the inner ear. J Proteomics. 2014;103:178-93.
270. Canis M, Schmid J, Olzowy B, Jahn K, Strupp M, Berghaus A, et al. The influence of cholesterol on the motility of cochlear outer hair cells and the motor protein prestin. Acta Otolaryngol. 2009;129(9):929-34.
271. Takahashi S, Homma K, Zhou Y, Nishimura S, Duan C, Chen J, et al. Susceptibility of outer hair cells to cholesterol chelator 2-hydroxypropyl-β-cyclodextrine is prestin-dependent. Sci Rep. 2016;6:21973.
272. Attili AF, Angelico M, Cantafora A, Alvaro D, Capocaccia L. Bile acid-induced liver toxicity: relation to the hydrophobic-hydrophilic balance of bile acids. Med Hypotheses. 1986;19(1):57-69.
273. Zhou Y, Maxwell KN, Sezgin E, Lu M, Liang H, Hancock JF, et al. Bile acids modulate signaling by functional perturbation of plasma membrane domains. J Biol Chem. 2013;288(50):35660-70.
274. Wang Z, Lv Q, Liu H, Wu Y, Bai Y, Cheng Y, et al. Caveolae Depletion Contributes to Vasorelaxant Effects of Chenodeoxycholic Acid. Cell Physiol Biochem. 2017;42(3):1013-24.
275. Frijters CM, Tuijn CJ, Ottenhoff R, Zegers BN, Groen AK, Elferink RP. The role of different P-glycoproteins in hepatobiliary secretion of fluorescently labeled short-chain phospholipids. J Lipid Res. 1999;40(11):1950-8.
276. Naik J, de Waart DR, Utsunomiya K, Duijst S, Mok KH, Oude Elferink RP, et al. ATP8B1 and ATP11C: Two Lipid Flippases Important for Hepatocyte Function. Dig Dis. 2015;33(3):314-8.
277. van der Mark VA, de Waart DR, Ho-Mok KS, Tabbers MM, Voogt HW, Oude Elferink RP, et al. The lipid flippase heterodimer ATP8B1-CDC50A is essential for surface expression of the apical sodium-dependent bile acid transporter (SLC10A2/ASBT) in intestinal Caco-2 cells. Biochim Biophys Acta. 2014;1842(12 Pt A):2378-86.
278. Vitale G, Gitto S, Raimondi F, Mattiaccio A, Mantovani V, Vukotic R, et al. Cryptogenic cholestasis in young and adults: ATP8B1, ABCB11, ABCB4, and TJP2 gene variants analysis by high-throughput sequencing. J Gastroenterol. 2018;53(8):945-58.

279. Rawson RB. Control of lipid metabolism by regulated intramembrane proteolysis of sterol regulatory element binding proteins (SREBPs). Biochem Soc Symp. 2003(70):221-31.
280. Zhang C, Zhang H, Zhang M, Lin C, Wang H, Yao J, et al. OSBPL2 deficiency upregulate SQLE expression increasing intracellular cholesterol and cholesteryl ester by AMPK/SP1 and SREBF2 signalling pathway. Exp Cell Res. 2019;383(2):111512.
281. Jeon TI, Esquejo RM, Roqueta-Rivera M, Phelan PE, Moon YA, Govindarajan SS, et al. An SREBP-responsive microRNA operon contributes to a regulatory loop for intracellular lipid homeostasis. Cell Metab. 2013;18(1):51-61.
282. Li T, Francl JM, Boehme S, Chiang JY. Regulation of cholesterol and bile acid homeostasis by the cholesterol 7α-hydroxylase/steroid response element-binding protein 2/microRNA-33a axis in mice. Hepatology. 2013;58(3):1111-21.
283. Shi H, Wang H, Zhang C, Lu Y, Yao J, Chen Z, et al. Mutations in OSBPL2 cause hearing loss associated with primary cilia defects via sonic hedgehog signaling. JCI Insight. 2022;7(4).
284. Xing G, Yao J, Wu B, Liu T, Wei Q, Liu C, et al. Identification of OSBPL2 as a novel candidate gene for progressive nonsyndromic hearing loss by whole-exome sequencing. Genet Med. 2015;17(3):210-8.
285. Chang SL, Hsieh CC, Tseng KS, Weng SF, Lin YS. Hypercholesterolemia is correlated with an increased risk of idiopathic sudden sensorineural hearing loss: a historical prospective cohort study. Ear Hear. 2014;35(2):256-61.
286. Sanchez VA, Dinh PC, Jr., Rooker J, Monahan PO, Althouse SK, Fung C, et al. Prevalence and risk factors for ototoxicity after cisplatin-based chemotherapy. J Cancer Surviv. 2023.
287. Carulli N, Bertolotti M, Carubbi F, Concari M, Martella P, Carulli L, et al. Review article: effect of bile salt pool composition on hepatic and biliary functions. Aliment Pharmacol Ther. 2000;14 Suppl 2:14-8.
288. Li T, Matozel M, Boehme S, Kong B, Nilsson LM, Guo G, et al. Overexpression of cholesterol 7α-hydroxylase promotes hepatic bile acid synthesis and secretion and maintains cholesterol homeostasis. Hepatology. 2011;53(3):996-1006.
289. Wang Y, Jones PJ, Woollett LA, Buckley DD, Yao L, Granholm NA, et al. Effects of chenodeoxycholic acid and deoxycholic acid on cholesterol absorption and metabolism in humans. Transl Res. 2006;148(1):37-45.

290. Uchida K, Nomura Y, Takase H, Makino S, Koga M, Takeuchi N, et al. Age-related changes in cholesterol and bile-acid metabolism in spontaneously hypertensive rats. Arch Gerontol Geriatr. 1982;1(2):171-91.
291. Gälman C, Angelin B, Rudling M. Pronounced variation in bile acid synthesis in humans is related to gender, hypertriglyceridaemia and circulating levels of fibroblast growth factor 19. J Intern Med. 2011;270(6):580-8.
292. Kim SY, Lee CH, Min C, Yoo DM, Choi HG. Association between statin medication and hearing impairment in a national health screening cohort. Sci Rep. 2021;11(1):14388.
293. Prayuenyong P, Kasbekar AV, Baguley DM. The efficacy of statins as otoprotective agents: A systematic review. Clin Otolaryngol. 2020;45(1):21-31.
294. Kurniawan C, Westendorp RG, de Craen AJ, Gussekloo J, de Laat J, van Exel E. Gene dose of apolipoprotein E and age-related hearing loss. Neurobiol Aging. 2012;33(9):2230.e7-.e12.
295. Yang A, Liu S, Yang X, Guo Z, Li J, Li X, et al. Uncovering Novel Prognostic Factors of Sudden Sensorineural Hearing Loss by Whole-Genome Sequencing of Cell-Free DNA. J Int Adv Otol. 2022;18(6):459-64.
296. Han SH, Kim JS, Lee Y, Choi H, Kim JW, Na DL, et al. Both targeted mass spectrometry and flow sorting analysis methods detected the decreased serum apolipoprotein E level in Alzheimer's disease patients. Mol Cell Proteomics. 2014;13(2):407-19.
297. Marinelli JP, Lohse CM, Fussell WL, Petersen RC, Reed NS, Machulda MM, et al. Association between hearing loss and development of dementia using formal behavioural audiometric testing within the Mayo Clinic Study of Aging (MCSA): a prospective population-based study. Lancet Healthy Longev. 2022;3(12):e817-e24.
298. Loughrey DG. Is age-related hearing loss a potentially modifiable risk factor for dementia? Lancet Healthy Longev. 2022;3(12):e805-e6.
299. Vassilaki M, Aakre JA, Knopman DS, Kremers WK, Mielke MM, Geda YE, et al. Informant-based hearing difficulties and the risk for mild cognitive impairment and dementia. Age Ageing. 2019;48(6):888-94.
300. Lin FR, Yaffe K, Xia J, Xue QL, Harris TB, Purchase-Helzner E, et al. Hearing loss and cognitive decline in older adults. JAMA Intern Med. 2013;173(4):293-9.

301. Sarant JZ, Bowe SJ, McEvoy M, Attia J. The Apolipoprotein Allele and Sensorineural Hearing Loss in Older Community-Dwelling Adults in Australia. Ear Hear. 2020;41(3):622-9.
302. Varma VR, Wang Y, An Y, Varma S, Bilgel M, Doshi J, et al. Bile acid synthesis, modulation, and dementia: A metabolomic, transcriptomic, and pharmacoepidemiologic study. PLoS Med. 2021;18(5):e1003615.
303. Cai Q, Du X, Zhou B, Cai C, Kermany MH, Zhang C, et al. Effects of simvastatin on plasma lipoproteins and hearing loss in apolipoprotein E gene-deficient mice. ORL J Otorhinolaryngol Relat Spec. 2009;71(5):244-50.
304. Kim YY, Chao JR, Kim C, Kim B, Thi-Thanh Nguyen P, Jung H, et al. Hearing loss through apoptosis of the spiral ganglion neurons in apolipoprotein E knockout mice fed with a western diet. Biochem Biophys Res Commun. 2020;523(3):692-8.
305. Guo Y, Zhang C, Du X, Nair U, Yoo TJ. Morphological and functional alterations of the cochlea in apolipoprotein E gene deficient mice. Hear Res. 2005;208(1-2):54-67.
306. Zhu S, Du X, Cai Q, Guo Y, Liu L, Cheng W, et al. Impaired stria vascularis in the inner ear of apolipoprotein E gene knockout mice. ORL J Otorhinolaryngol Relat Spec. 2008;70(6):373-80.
307. Håkansson P, Andersson I, Nyström S, Löfgren L, Amrot LF, Li H. Ontogenetic development and spatial distribution of the ileal apical sodium-dependent bile acid transporter and the ileal lipid-binding protein in apoE knockout and C57BL/6 mice. Scand J Gastroenterol. 2002;37(9):1089-96.
308. Sai N, Shi X, Zhang Y, Jiang QQ, Ji F, Yuan SL, et al. Involvement of Cholesterol Metabolic Pathways in Recovery from Noise-Induced Hearing Loss. Neural Plast. 2020;2020:6235948.
309. Srivastava RA, Srivastava N, Averna M. Dietary cholic acid lowers plasma levels of mouse and human apolipoprotein A-I primarily via a transcriptional mechanism. Eur J Biochem. 2000;267(13):4272-80.
310. Srivastava RA, Averna M, Srivastava N, Pape ME. Dietary cholate increases plasma levels of apolipoprotein B in mice by posttranscriptional mechanisms. Int J Biochem Cell Biol. 2001;33(12):1215-26.
311. Claudel T, Sturm E, Duez H, Torra IP, Sirvent A, Kosykh V, et al. Bile acid-activated nuclear receptor FXR suppresses apolipoprotein A-I transcription via a negative FXR response element. J Clin Invest. 2002;109(7):961-71.

312. Gardès C, Blum D, Bleicher K, Chaput E, Ebeling M, Hartman P, et al. Studies in mice, hamsters, and rats demonstrate that repression of hepatic apoA-I expression by taurocholic acid in mice is not mediated by the farnesoid-X-receptor. J Lipid Res. 2011;52(6):1188-99.
313. Bard JM, Dallongeville J, Hagen E, Pfister P, Ose L, Fruchart JC, et al. Comparison of the effect of fluvastatin, an hydroxymethyl glutaryl coenzyme A reductase inhibitor, and cholestyramine, a bile acid sequestrant, on lipoprotein particles defined by apolipoprotein composition. Metabolism. 1995;44(11):1447-54.
314. Leuven JA, Havekes L, Kempen HJ. Effect of deoxycholic acid on lipoprotein and apolipoprotein levels in patients with familial hypercholesterolemia. Atherosclerosis. 1986;62(1):21-5.
315. Ozel Coskun BD, Yucesoy M, Gursoy S, Baskol M, Yurci A, Yagbasan A, et al. Effects of ursodeoxycholic acid therapy on carotid intima media thickness, apolipoprotein A1, apolipoprotein B, and apolipoprotein B/A1 ratio in nonalcoholic steatohepatitis. Eur J Gastroenterol Hepatol. 2015;27(2):142-9.
316. Shah V, Mittal R, Shahal D, Sinha P, Bulut E, Mittal J, et al. Evaluating the Efficacy of Taurodeoxycholic Acid in Providing Otoprotection Using an in vitro Model of Electrode Insertion Trauma. Front Mol Neurosci. 2020;13:113.
317. Yao B, He J, Yin X, Shi Y, Wan J, Tian Z. The protective effect of lithocholic acid on the intestinal epithelial barrier is mediated by the vitamin D receptor via a SIRT1/Nrf2 and NF-κB dependent mechanism in Caco-2 cells. Toxicol Lett. 2019;316:109-18.
318. Bukiya AN, Liu J, Toro L, Dopico AM. Beta1 (KCNMB1) subunits mediate lithocholate activation of large-conductance Ca2+-activated K+ channels and dilation in small, resistance-size arteries. Mol Pharmacol. 2007;72(2):359-69.
319. McMillin M, Frampton G, Quinn M, Ashfaq S, de los Santos M, 3rd, Grant S, et al. Bile Acid Signaling Is Involved in the Neurological Decline in a Murine Model of Acute Liver Failure. Am J Pathol. 2016;186(2):312-23.
320. Dasari S, Tchounwou PB. Cisplatin in cancer therapy: molecular mechanisms of action. Eur J Pharmacol. 2014;740:364-78.
321. Schoeberl A, Gutmann M, Theiner S, Corte-Rodríguez M, Braun G, Vician P, et al. The copper transporter CTR1 and cisplatin accumulation at the single-cell level by LA-ICP-TOFMS. Frontiers in Molecular Biosciences. 2022;9.

322. Kros CJ, Steyger PS. Aminoglycoside- and Cisplatin-Induced Ototoxicity: Mechanisms and Otoprotective Strategies. Cold Spring Harb Perspect Med. 2019;9(11).
323. Hellberg V, Wallin I, Eriksson S, Hernlund E, Jerremalm E, Berndtsson M, et al. Cisplatin and Oxaliplatin Toxicity: Importance of Cochlear Kinetics as a Determinant for Ototoxicity. JNCI: Journal of the National Cancer Institute. 2009;101(1):37-47.
324. Saito T, Aran JM. Comparative ototoxicity of cisplatin during acute and chronic treatment. ORL J Otorhinolaryngol Relat Spec. 1994;56(6):315-20.
325. Brock PR, Maibach R, Childs M, Rajput K, Roebuck D, Sullivan MJ, et al. Sodium Thiosulfate for Protection from Cisplatin-Induced Hearing Loss. N Engl J Med. 2018;378(25):2376-85.
326. Yu D, Gu J, Chen Y, Kang W, Wang X, Wu H. Current Strategies to Combat Cisplatin-Induced Ototoxicity. Front Pharmacol. 2020;11:999.
327. Ramkumar V, Mukherjea D, Dhukhwa A, Rybak LP. Oxidative Stress and Inflammation Caused by Cisplatin Ototoxicity. Antioxidants (Basel). 2021;10(12).
328. Chen X, Zhang H, Wang C, Su Y, Xiong M, Feng X, et al. Curcumin-Encapsulated Chitosan-Coated Nanoformulation as an Improved Otoprotective Strategy for Ototoxic Hearing Loss. Molecular Pharmaceutics. 2022;19(7):2217-30.
329. Gu J, Wang X, Chen Y, Xu K, Yu D, Wu H. An enhanced antioxidant strategy of astaxanthin encapsulated in ROS-responsive nanoparticles for combating cisplatin-induced ototoxicity. J Nanobiotechnology. 2022;20(1):268.
330. Martín-Saldaña S, Palao-Suay R, Aguilar MR, García-Fernández L, Arévalo H, Trinidad A, et al. pH-sensitive polymeric nanoparticles with antioxidant and anti-inflammatory properties against cisplatin-induced hearing loss. Journal of Controlled Release. 2018;270:53-64.
331. Yoon JY, Yang KJ, Park SN, Kim DK, Kim JD. The effect of dexamethasone/cell-penetrating peptide nanoparticles on gene delivery for inner ear therapy. Int J Nanomedicine. 2016;11:6123-34.
332. Ding S, Xie S, Chen W, Wen L, Wang J, Yang F, et al. Is oval window transport a royal gate for nanoparticle delivery to vestibule in the inner ear? European Journal of Pharmaceutical Sciences. 2019;126:11-22.
333. Wagle SR, Ionescu CM, Kovacevic B, Jones M, Foster T, Lim P, et al. Pharmaceutical characterization of probucol bile acid-lithocholic acid nanoparticles to

prevent chronic hearing related and similar cellular oxidative stress pathologies. Nanomedicine (Lond). 2023;18(12):923-40.

334. Bochmann ES, Neumann D, Gryczke A, Wagner KG. Micro-scale solubility assessments and prediction models for active pharmaceutical ingredients in polymeric matrices. European Journal of Pharmaceutics and Biopharmaceutics. 2019;141:111-20.

335. Thybo P, Pedersen BL, Hovgaard L, Holm R, Müllertz A. Characterization and Physical Stability of Spray Dried Solid Dispersions of Probucol and PVP-K30. Pharmaceutical Development and Technology. 2008;13(5):375-86.

336. Dalsin MC, Tale S, Reineke TM. Solution-state polymer assemblies influence BCS class II drug dissolution and supersaturation maintenance. Biomacromolecules. 2014;15(2):500-11.

337. Tanida S, Yoshimoto A, Yoshida M, Uchiyama H, Kadota K, Tozuka Y. Preparation of Amorphous Composite Particles of Drugs with Ursodeoxycholic Acid as Preclinical Formulations. Chemical and Pharmaceutical Bulletin. 2019;67(9):921-8.

338. Yang S, Zhao L, Han Y, Liu Y, Chen C, Zhan M, et al. Probucol ameliorates renal injury in diabetic nephropathy by inhibiting the expression of the redox enzyme p66Shc. Redox Biol. 2017;13:482-97.

339. Colle D, Santos DB, Moreira EL, Hartwig JM, dos Santos AA, Zimmermann LT, et al. Probucol increases striatal glutathione peroxidase activity and protects against 3-nitropropionic acid-induced pro-oxidative damage in rats. PLoS One. 2013;8(6):e67658.

340. Asiri YA. Probucol attenuates cyclophosphamide-induced oxidative apoptosis, p53 and Bax signal expression in rat cardiac tissues. Oxid Med Cell Longev. 2010;3(5):308-16.

341. Colle D, Santos DB, Hartwig JM, Godoi M, Braga AL, Farina M. Succinobucol versus probucol: higher efficiency of succinobucol in mitigating 3-NP-induced brain mitochondrial dysfunction and oxidative stress in vitro. Mitochondrion. 2013;13(2):125-33.

342. Yakushiji E, Ayaori M, Nishida T, Shiotani K, Takiguchi S, Nakaya K, et al. Probucol-Oxidized Products, Spiroquinone and Diphenoquinone, Promote Reverse Cholesterol Transport in Mice. Arterioscler Thromb Vasc Biol. 2016;36(4):591-7.

343. Wolfe KL, Liu RH. Cellular antioxidant activity (CAA) assay for assessing antioxidants, foods, and dietary supplements. J Agric Food Chem. 2007;55(22):8896-907.

344. Schneider CA, Rasband WS, Eliceiri KW. NIH Image to ImageJ: 25 years of image analysis. Nat Methods. 2012;9(7):671-5.

345. Wagle SR, Kovacevic B, Walker D, Ionescu CM, Jones M, Stojanovic G, et al. Pharmacological and Advanced Cell Respiration Effects, Enhanced by Toxic Human-Bile Nano-Pharmaceuticals of Probucol Cell-Targeting Formulations. Pharmaceutics. 2020;12(8).

346. Maa Y-F, Costantino HR, Nguyen P-A, Hsu CC. The Effect of Operating and Formulation Variables on the Morphology of Spray-Dried Protein Particles. Pharmaceutical Development and Technology. 1997;2(3):213-23.

347. Porfirio T, Galindo-Rosales FJ, Campo-Deaño L, Vicente J, Semião V. Rheological characterization of polymeric solutions used in spray drying process. European Journal of Pharmaceutical Sciences. 2021;158:105650.

348. Bhattacharya A, Ray P. Studies on surface tension of poly(vinyl alcohol): Effect of concentration, temperature, and addition of chaotropic agents. Journal of Applied Polymer Science. 2004;93(1):122-30.

349. Luo J, Lin X, Li L, Tan J, Li P. β-Cyclodextrin and Oligoarginine Peptide-Based Dendrimer-Entrapped Gold Nanoparticles for Improving Drug Delivery to the Inner Ear. Front Bioeng Biotechnol. 2022;10:844177.

350. Oliva CR, Nozell SE, Diers A, McClugage SG, 3rd, Sarkaria JN, Markert JM, et al. Acquisition of temozolomide chemoresistance in gliomas leads to remodeling of mitochondrial electron transport chain. J Biol Chem. 2010;285(51):39759-67.

351. Hill BG, Benavides GA, Lancaster JR, Jr., Ballinger S, Dell'Italia L, Jianhua Z, et al. Integration of cellular bioenergetics with mitochondrial quality control and autophagy. Biol Chem. 2012;393(12):1485-512.

352. So H, Kim H, Lee JH, Park C, Kim Y, Kim E, et al. Cisplatin cytotoxicity of auditory cells requires secretions of proinflammatory cytokines via activation of ERK and NF-kappaB. J Assoc Res Otolaryngol. 2007;8(3):338-55.

353. Okada H, Kitagawa K. Risk factors associated with cisplatin-induced ototoxicity in Japanese patients with solid tumors. Cancer Med. 2023;12(7):7904-10.

354. Romano A, Rivetti S, Brigato F, Mastrangelo S, Attinà G, Maurizi P, et al. Early and Long-Term Ototoxicity Noted in Children Due to Platinum Compounds: Prevalence and Risk Factors. Biomedicines. 2023;11(2).
355. Tanaka Y, Inkyo M, Yumoto R, Nagai J, Takano M, Nagata S. Nanoparticulation of probucol, a poorly water-soluble drug, using a novel wet-milling process to improve in vitro dissolution and in vivo oral absorption. Drug Development and Industrial Pharmacy. 2012;38(8):1015-23.
356. Moribe K, Limwikrant W, Higashi K, Yamamoto K. Structural evaluation of probucol nanoparticles in water by atomic force microscopy. Int J Pharm. 2012;427(2):365-71.
357. Yoon HJ, Moon ME, Park HS, Im SY, Kim YH. Chitosan oligosaccharide (COS) inhibits LPS-induced inflammatory effects in RAW 264.7 macrophage cells. Biochemical and Biophysical Research Communications. 2007;358(3):954-9.
358. Ngo DH, Kim SK. Antioxidant effects of chitin, chitosan, and their derivatives. Adv Food Nutr Res. 2014;73:15-31.
359. Lu H, Yang G, Ran F, Gao T, Sun C, Zhao Q, et al. Polymer-functionalized mesoporous carbon nanoparticles on overcoming multiple barriers and improving oral bioavailability of Probucol. Carbohydr Polym. 2020;229:115508.
360. TM MW, Lau WM, Khutoryanskiy VV. Chitosan and Its Derivatives for Application in Mucoadhesive Drug Delivery Systems. Polymers (Basel). 2018;10(3).
361. Gulsun T, Izat N, Sahin S. Influence of permeability enhancers on the paracellular permeability of metformin hydrochloride and furosemide across Caco-2 cells. Can J Physiol Pharmacol. 2023;101(4):185-99.
362. Murillo-Cuesta S, Vallecillo N, Cediel R, Celaya AM, Lassaletta L, Varela-Nieto I, et al. A Comparative Study of Drug Delivery Methods Targeted to the Mouse Inner Ear: Bullostomy Versus Transtympanic Injection. J Vis Exp. 2017(121).
363. Cole LK, Rajala-Schultz PJ, Lorch G. Conductive hearing loss in four dogs associated with the use of ointment-based otic medications. Vet Dermatol. 2018.
364. Lin YC, Shih CP, Chen HC, Chou YL, Sytwu HK, Fang MC, et al. Ultrasound Microbubble-Facilitated Inner Ear Delivery of Gold Nanoparticles Involves Transient Disruption of the Tight Junction Barrier in the Round Window Membrane. Front Pharmacol. 2021;12:689032.
365. Saber A, Strand SP, Ulfendahl M. Use of the biodegradable polymer chitosan as a vehicle for applying drugs to the inner ear. Eur J Pharm Sci. 2010;39(1-3):110-5.

366. Nordang L, Linder B, Anniko M. Morphologic changes in round window membrane after topical hydrocortisone and dexamethasone treatment. Otol Neurotol. 2003;24(2):339-43.
367. Yu Y, Kim DH, Suh EY, Jeong SH, Kwon HC, Le TP, et al. Injectable glycol chitosan thermogel formulation for efficient inner ear drug delivery. Carbohydr Polym. 2022;278:118969.
368. Videhult Pierre P, Fransson A, Kisiel MA, Damberg P, Nikkhou Aski S, Andersson M, et al. Middle Ear Administration of a Particulate Chitosan Gel in an in vivo Model of Cisplatin Ototoxicity. Front Cell Neurosci. 2019;13:268.
369. Lajud SA, Han Z, Chi FL, Gu R, Nagda DA, Bezpalko O, et al. A regulated delivery system for inner ear drug application. J Control Release. 2013;166(3):268-76.
370. Gonçalves C, Ferreira N, Lourenço L. Production of Low Molecular Weight Chitosan and Chitooligosaccharides (COS): A Review. Polymers (Basel). 2021;13(15).
371. Kim BS, Kim CS, Lee KM. The intracellular uptake ability of chitosan-coated Poly (D,L-lactide-co-glycolide) nanoparticles. Arch Pharm Res. 2008;31(8):1050-4.
372. Chen X, Zhang H, Wang C, Su Y, Xiong M, Feng X, et al. Curcumin-Encapsulated Chitosan-Coated Nanoformulation as an Improved Otoprotective Strategy for Ototoxic Hearing Loss. Mol Pharm. 2022;19(7):2217-30.
373. Tanaka F, Whitworth CA, Rybak LP. Round window pH manipulation alters the ototoxicity of systemic cisplatin. Hear Res. 2004;187(1-2):44-50.
374. Kim K, Kwon S, Park JH, Chung H, Jeong SY, Kwon IC, et al. Physicochemical Characterizations of Self-Assembled Nanoparticles of Glycol Chitosan−Deoxycholic Acid Conjugates. Biomacromolecules. 2005;6(2):1154-8.
375. Lee KY, Jo WH, Kwon IC, Kim Y-H, Jeong SY. Structural Determination and Interior Polarity of Self-Aggregates Prepared from Deoxycholic Acid-Modified Chitosan in Water. Macromolecules. 1998;31(2):378-83.
376. Liu L, Dong W, Wang S, Zhang Y, Liu T, Xie R, et al. Deoxycholic acid disrupts the intestinal mucosal barrier and promotes intestinal tumorigenesis. Food & Function. 2018;9(11):5588-97.
377. Seicol BJ, Lin S, Xie R. Age-Related Hearing Loss Is Accompanied by Chronic Inflammation in the Cochlea and the Cochlear Nucleus. Front Aging Neurosci. 2022;14:846804.

378. Bedeir MM, Ninoyu Y, Nakamura T, Tsujikawa T, Hirano S. Multiplex immunohistochemistry reveals cochlear macrophage heterogeneity and local auditory nerve inflammation in cisplatin-induced hearing loss. Front Neurol. 2022;13:1015014.
379. Yang W, Vethanayagam RR, Dong Y, Cai Q, Hu BH. Activation of the antigen presentation function of mononuclear phagocyte populations associated with the basilar membrane of the cochlea after acoustic overstimulation. Neuroscience. 2015;303:1-15.
380. Davis S, Cirone AM, Menzie J, Russell F, Dorey CK, Shibata Y, et al. Phagocytosis-mediated M1 activation by chitin but not by chitosan. Am J Physiol Cell Physiol. 2018;315(1):C62-c72.
381. Nasrazadani S, Hassani S. Chapter 2 - Modern analytical techniques in failure analysis of aerospace, chemical, and oil and gas industries. In: Makhlouf ASH, Aliofkhazraei M, editors. Handbook of Materials Failure Analysis with Case Studies from the Oil and Gas Industry: Butterworth-Heinemann; 2016. p. 39-54.
382. Talik A, Tarnacka M, Minecka A, Hachuła B, Grelska J, Jurkiewicz K, et al. Anormal Thermal History Effect on the Structural Dynamics of Probucol Infiltrated into Porous Alumina. The Journal of Physical Chemistry C. 2021;125(7):3901-12.
383. So H, Kim H, Lee J-H, Park C, Kim Y, Kim E, et al. Cisplatin Cytotoxicity of Auditory Cells Requires Secretions of Proinflammatory Cytokines via Activation of ERK and NF-κB. Journal of the Association for Research in Otolaryngology. 2007;8(3):338-55.
384. Mondalek FG, Zhang YY, Kropp B, Kopke RD, Ge X, Jackson RL, et al. The permeability of SPION over an artificial three-layer membrane is enhanced by external magnetic field. Journal of Nanobiotechnology. 2006;4(1):4.
385. Saxena RK, Vallyathan V, Lewis DM. Evidence for lipopolysaccharide-induced differentiation of RAW264.7 murine macrophage cell line into dendritic like cells. J Biosci. 2003;28(1):129-34.
386. Holt DJ, Chamberlain LM, Grainger DW. Cell-cell signaling in co-cultures of macrophages and fibroblasts. Biomaterials. 2010;31(36):9382-94.
387. Wittaya-areekul S, Prahsarn C. Development and in vitro evaluation of chitosan–polysaccharides composite wound dressings. International Journal of Pharmaceutics. 2006;313(1):123-8.

388. Ulu A, Birhanlı E, Köytepe S, Ateş B. Chitosan/polypropylene glycol hydrogel composite film designed with TiO2 nanoparticles: A promising scaffold of biomedical applications. International Journal of Biological Macromolecules. 2020;163:529-40.
389. Kim SJ, Park C, Lee JN, Lim H, Hong GY, Moon SK, et al. Erdosteine protects HEI-OC1 auditory cells from cisplatin toxicity through suppression of inflammatory cytokines and induction of Nrf2 target proteins. Toxicol Appl Pharmacol. 2015;288(2):192-202.
390. Wang H, Lin H, Kang W, Huang L, Gong S, Zhang T, et al. miR-34a/DRP-1-mediated mitophagy participated in cisplatin-induced ototoxicity via increasing oxidative stress. BMC Pharmacol Toxicol. 2023;24(1):16.
391. Taciak B, Białasek M, Braniewska A, Sas Z, Sawicka P, Kiraga Ł, et al. Evaluation of phenotypic and functional stability of RAW 264.7 cell line through serial passages. PLoS One. 2018;13(6):e0198943.
392. Chamberlain LM, Godek ML, Gonzalez-Juarrero M, Grainger DW. Phenotypic non-equivalence of murine (monocyte-) macrophage cells in biomaterial and inflammatory models. J Biomed Mater Res A. 2009;88(4):858-71.
393. Youn CK, Park SJ, Lee MY, Cha MJ, Kim OH, You HJ, et al. Silibinin Inhibits LPS-Induced Macrophage Activation by Blocking p38 MAPK in RAW 264.7 Cells. Biomol Ther (Seoul). 2013;21(4):258-63.
394. Mai FY, He P, Ye JZ, Xu LH, Ouyang DY, Li CG, et al. Caspase-3-mediated GSDME activation contributes to cisplatin- and doxorubicin-induced secondary necrosis in mouse macrophages. Cell Prolif. 2019;52(5):e12663.
395. Zucoloto AZ, Manchope MF, Staurengo-Ferrari L, Pinho-Ribeiro FA, Zarpelon AC, Saraiva ALL, et al. Probucol attenuates lipopolysaccharide-induced leukocyte recruitment and inflammatory hyperalgesia: effect on NF-κB activation and cytokine production. Eur J Pharmacol. 2017;809:52-63.
396. Li L, Yu M, Li Y, Li Q, Yang H, Zheng M, et al. Synergistic anti-inflammatory and osteogenic n-HA/resveratrol/chitosan composite microspheres for osteoporotic bone regeneration. Bioact Mater. 2021;6(5):1255-66.
397. Zhang C, Frye MD, Sun W, Sharma A, Manohar S, Salvi R, et al. New insights on repeated acoustic injury: Augmentation of cochlear susceptibility and inflammatory reaction resultant of prior acoustic injury. Hear Res. 2020;393:107996.

398. Shin SH, Jung J, Park HR, Sim NS, Choi JY, Bae SH. The Time Course of Monocytes Infiltration After Acoustic Overstimulation. Front Cell Neurosci. 2022;16:844480.
399. Noble K, Brown L, Elvis P, Lang H. Cochlear Immune Response in Presbyacusis: a Focus on Dysregulation of Macrophage Activity. J Assoc Res Otolaryngol. 2022;23(1):1-16.
400. Sautter NB, Shick EH, Ransohoff RM, Charo IF, Hirose K. CC chemokine receptor 2 is protective against noise-induced hair cell death: studies in CX3CR1(+/GFP) mice. J Assoc Res Otolaryngol. 2006;7(4):361-72.
401. Fujioka M, Okamoto Y, Shinden S, Okano HJ, Okano H, Ogawa K, et al. Pharmacological inhibition of cochlear mitochondrial respiratory chain induces secondary inflammation in the lateral wall: a potential therapeutic target for sensorineural hearing loss. PLoS One. 2014;9(3):e90089.
402. Fujioka M, Kanzaki S, Okano HJ, Masuda M, Ogawa K, Okano H. Proinflammatory cytokines expression in noise-induced damaged cochlea. J Neurosci Res. 2006;83(4):575-83.
403. Satoh H, Firestein GS, Billings PB, Harris JP, Keithley EM. Proinflammatory cytokine expression in the endolymphatic sac during inner ear inflammation. J Assoc Res Otolaryngol. 2003;4(2):139-47.
404. Chen P, Hao JJ, Li MW, Bai J, Guo YT, Liu Z, et al. Integrative Functional Transcriptomic Analyses Implicate Shared Molecular Circuits in Sensorineural Hearing Loss. Front Cell Neurosci. 2022;16:857344.
405. Chouinard CD, Nagy G, Webb IK, Garimella SVB, Baker ES, Ibrahim YM, et al. Rapid Ion Mobility Separations of Bile Acid Isomers Using Cyclodextrin Adducts and Structures for Lossless Ion Manipulations. Anal Chem. 2018;90(18):11086-91.
406. Loftsson T, Sigurdsson HH, Jansook P. Anomalous Properties of Cyclodextrins and Their Complexes in Aqueous Solutions. Materials (Basel). 2023;16(6).
407. Holm R, Nicolajsen HV, Hartvig RA, Westh P, Ostergaard J. Complexation of tauro- and glyco-conjugated bile salts with three neutral beta-CDs studied by ACE. Electrophoresis. 2007;28(20):3745-52.
408. De Caprio J, Yun J, Javitt NB. Bile acid and sterol solubilization in 2-hydroxypropyl-beta-cyclodextrin. J Lipid Res. 1992;33(3):441-3.

409. Rinaldi L, Binello A, Stolle A, Curini M, Cravotto G. Efficient mechanochemical complexation of various steroid compounds with α-, β- and γ-cyclodextrin. Steroids. 2015;98:58-62.
410. Magnusdottir A, Másson M, Loftsson T. Self Association and Cyclodextrin Solubilization of NSAIDs. Journal of inclusion phenomena and macrocyclic chemistry. 2002;44(1):213-8.
411. Dang P, Ye R, Meng F, Han Y, Zhou Y, Gong X, et al. Microencapsulation thermodynamics of methylated β-cyclodextrins with bile salt: enthalpy, entropy, and solvent effect. Journal of Inclusion Phenomena and Macrocyclic Chemistry. 2017;88(3):181-9.
412. Paul BK, Ghosh N, Mukherjee S. Interaction of Bile Salts with β-Cyclodextrins Reveals Nonclassical Hydrophobic Effect and Enthalpy–Entropy Compensation. The Journal of Physical Chemistry B. 2016;120(16):3963-8.
413. Heřmánková E, Žák A, Poláková L, Hobzová R, Hromádka R, Širc J. Polymeric bile acid sequestrants: Review of design, in vitro binding activities, and hypocholesterolemic effects. Eur J Med Chem. 2018;144:300-17.
414. Holm R, Shi W, Hartvig RA, Askjær S, Christian Madsen J, Westh P. Thermodynamics and structure of inclusion compounds of tauro- and glyco-conjugated bile salts and β-cyclodextrin. Physical Chemistry Chemical Physics. 2009;11(25):5070-8.
415. Liu Y, Yang Y-W, Cao R, Song S-H, Zhang H-Y, Wang L-H. Thermodynamic Origin of Molecular Selective Binding of Bile Salts by Aminated β-Cyclodextrins. The Journal of Physical Chemistry B. 2003;107(50):14130-9.
416. Holm R, Schönbeck C, Askjær S, Jensen H, Westh P, Østergaard J. Complexation of tauro- and glyco-conjugated bile salts with α-cyclodextrin and hydroxypropyl-α-cyclodextrin studied by affinity capillary electrophoresis and molecular modelling. Journal of Separation Science. 2011;34(22):3221-30.
417. Zhou Z, Liu C, Chen S, Zhao H, Zhou K, Wang W, et al. Activation of the Nrf2/ARE signaling pathway by probucol contributes to inhibiting inflammation and neuronal apoptosis after spinal cord injury. Oncotarget. 2017;8(32):52078-93.
418. Dan Z, Cao H, He X, Zhang Z, Zou L, Zeng L, et al. A pH-Responsive Host-guest Nanosystem Loading Succinobucol Suppresses Lung Metastasis of Breast Cancer. Theranostics. 2016;6(3):435-45.

419. Wu N, Li M, Chen ZT, Zhang XB, Liu HZ, Li Z, et al. In vivo delivery of Atoh1 gene to rat cochlea using a dendrimer-based nanocarrier. J Biomed Nanotechnol. 2013;9(10):1736-45.
420. Jadhav D, Vavia P. Dexamethasone Sodium Phosphate Loaded Modified Cyclodextrin Based Nanoparticles: An Efficient Treatment for Rheumatoid Arthritis. J Pharm Sci. 2021;110(3):1206-18.
421. Jansook P, Pichayakorn W, Muankaew C, Loftsson T. Cyclodextrin–poloxamer aggregates as nanocarriers in eye drop formulations: dexamethasone and amphotericin B. Drug Development and Industrial Pharmacy. 2016;42(9):1446-54.
422. Loftsson T, Hreinsdóttir D, Stefánsson E. Cyclodextrin microparticles for drug delivery to the posterior segment of the eye: aqueous dexamethasone eye drops. Journal of Pharmacy and Pharmacology. 2010;59(5):629-35.
423. Sadeh P, Zeinali S, Rastegari B, Najafipour I. Size optimization of mesoporous β-Cyclodextrin Metal-Organic frameworks as Bio-MOFs. Journal of Crystal Growth. 2023;620:127348.
424. Messner M, Kurkov SV, Maraver Palazón M, Álvarez Fernández B, Brewster ME, Loftsson T. Self-assembly of cyclodextrin complexes: effect of temperature, agitation and media composition on aggregation. Int J Pharm. 2011;419(1-2):322-8.
425. Choisnard L, Gèze A, Putaux J-L, Wong Y-S, Wouessidjewe D. Nanoparticles of β-Cyclodextrin Esters Obtained by Self-Assembling of Biotransesterified β-Cyclodextrins. Biomacromolecules. 2006;7(2):515-20.
426. Messner M, Kurkov SV, Jansook P, Loftsson T. Self-assembled cyclodextrin aggregates and nanoparticles. International Journal of Pharmaceutics. 2010;387(1):199-208.
427. Zhang H-t, Fan X-d, Tian W, Suo R-t, Yang Z, Bai Y, et al. Ultrasound-Driven Secondary Self-Assembly of Amphiphilic β-Cyclodextrin Dimers. Chemistry – A European Journal. 2015;21(13):5000-8.
428. Wu A, Shen X, He Y. Micrometer-sized rodlike structure formed by the secondary assembly of cyclodextrin nanotube. J Colloid Interface Sci. 2006;302(1):87-94.
429. Yu N, Li G, Gao Y, Liu X, Ma S. Stimuli-sensitive hollow spheres from chitosan-graft-β-cyclodextrin for controlled drug release. Int J Biol Macromol. 2016;93(Pt A):971-7.

430. Mohamed MH, Wang C, Peru KM, Headley JV, Wilson LD. Characterization of the Physicochemical Properties of β-Cyclodextrin–Divinyl Sulfone Polymer Carrier–Bile Acid Systems. Molecular Pharmaceutics. 2017;14(8):2616-23.
431. Natalini B, Sardella R, Gioiello A, Ianni F, Di Michele A, Marinozzi M. Determination of bile salt critical micellization concentration on the road to drug discovery. Journal of Pharmaceutical and Biomedical Analysis. 2014;87:62-81.
432. Matsuoka K, Moroi Y. Micelle formation of sodium deoxycholate and sodium ursodeoxycholate (Part 1). Biochimica et Biophysica Acta (BBA) - Molecular and Cell Biology of Lipids. 2002;1580(2):189-99.
433. Pavlović N, Goločorbin-Kon S, Đanić M, Stanimirov B, Al-Salami H, Stankov K, et al. Bile Acids and Their Derivatives as Potential Modifiers of Drug Release and Pharmacokinetic Profiles. Frontiers in Pharmacology. 2018;9.
434. Tsuchihashi N, Hayashi K, Dan K, Goto F, Nomura Y, Fujioka M, et al. Autophagy through 4EBP1 and AMPK regulates oxidative stress-induced premature senescence in auditory cells. Oncotarget. 2015;6:3644-55.
435. Rivas-Chacón LDM, Martínez-Rodríguez S, Madrid-García R, Yanes-Díaz J, Riestra-Ayora JI, Sanz-Fernández R, et al. Role of Oxidative Stress in the Senescence Pattern of Auditory Cells in Age-Related Hearing Loss. Antioxidants (Basel). 2021;10(9).
436. Barreto J, Tita D, Orlandi M. Development of an Automated Method to Perform a Quantitative Study of Particle Size Distribution and the Effect of a Conductive Layer in Scanning Electron Microscopy. Química Nova. 2019;42.
437. Bonini M, Rossi S, Karlsson G, Almgren M, Lo Nostro P, Baglioni P. Self-Assembly of β-Cyclodextrin in Water. Part 1: Cryo-TEM and Dynamic and Static Light Scattering. Langmuir. 2006;22(4):1478-84.
438. Danaei M, Dehghankhold M, Ataei S, Hasanzadeh Davarani F, Javanmard R, Dokhani A, et al. Impact of Particle Size and Polydispersity Index on the Clinical Applications of Lipidic Nanocarrier Systems. Pharmaceutics. 2018;10(2).
439. Fissan H, Ristig S, Kaminski H, Asbach C, Epple M. Comparison of different characterization methods for nanoparticle dispersions before and after aerosolization. Analytical Methods. 2014;6(18):7324-34.
440. Yang Z, Breslow R. Very Strong Binding of Lithocholic Acid to β-Cyclodextrin. Tetrahedron Letters. 1997;38(35):6171-2.

441. Olesen NE, Westh P, Holm R. Displacement of Drugs from Cyclodextrin Complexes by Bile Salts: A Suggestion of an Intestinal Drug-Solubilizing Capacity from an In Vitro Model. Journal of Pharmaceutical Sciences. 2015;n/a(n/a).
442. Nishino K, Noguchi N, Niki E. Dynamics of action of bisphenol as radical-scavenging antioxidant against lipid peroxidation in solution and liposomal membranes. Free Radical Research. 1999;31(6):535-48.
443. Yang Z-X, Chen Y, Liu Y. Inclusion complexes of bisphenol A with cyclomaltoheptaose (β-cyclodextrin): solubilization and structure. Carbohydrate Research. 2008;343(14):2439-42.
444. Chelli S, Majdoub M, Jouini M, Aelyach S, Maurel F, Chane-Ching KI, et al. Host-guest complexes of phenol derivatives with β-cyclodextrin: An experimental and theoretical investigation. Journal of Physical Organic Chemistry. 2007;20(1):30-43.
445. Antelo A, Jover A, Galantini L, Meijide F, Alcalde MA, Pavel NV, et al. Formation of host-guest and sandwich complexes by a β-cyclodextrin derivative. Journal of Inclusion Phenomena and Macrocyclic Chemistry. 2011;69(1):245-53.
446. May BL, Gerber J, Clements P, Buntine MA, Brittain DRB, Lincoln SF, et al. Cyclodextrin and modified cyclodextrin complexes of E-4-tert-butylphenyl-4′-oxyazobenzene: UV-visible, 1H NMR and ab initio studies. Organic & Biomolecular Chemistry. 2005;3(8):1481-8.
447. Sousa T, Castro RE, Pinto SN, Coutinho A, Lucas SD, Moreira R, et al. Deoxycholic acid modulates cell death signaling through changes in mitochondrial membrane properties. J Lipid Res. 2015;56(11):2158-71.
448. Sandri G, Bonferoni MC, Rossi S, Caramella CM, Ferrari F. Effects of Particle Size, Surface Nature and Crystal Type on Dissolution Rate. In: Merkus HG, Meesters GMH, Oostra W, editors. Particles and Nanoparticles in Pharmaceutical Products: Design, Manufacturing, Behavior and Performance. Cham: Springer International Publishing; 2018. p. 303-28.
449. Csicsák D, Szolláth R, Kádár S, Ambrus R, Bartos C, Balogh E, et al. The Effect of the Particle Size Reduction on the Biorelevant Solubility and Dissolution of Poorly Soluble Drugs with Different Acid-Base Character. Pharmaceutics [Internet]. 2023; 15(1).
450. Chu KR, Lee E, Jeong SH, Park E-S. Effect of particle size on the dissolution behaviors of poorly water-soluble drugs. Archives of Pharmacal Research. 2012;35(7):1187-95.

451. Daina A, Zoete V. A BOILED-Egg To Predict Gastrointestinal Absorption and Brain Penetration of Small Molecules. ChemMedChem. 2016;11(11):1117-21.
452. Daina A, Michielin O, Zoete V. SwissADME: a free web tool to evaluate pharmacokinetics, drug-likeness and medicinal chemistry friendliness of small molecules. Scientific Reports. 2017;7(1):42717.
453. Salt A. FluidSim 5 [Available from: https://alecsalt.com/index.php/simulations/fluidsim4.
454. Salt AN, Hartsock JJ, Piu F, Hou J. Dexamethasone and Dexamethasone Phosphate Entry into Perilymph Compared for Middle Ear Applications in Guinea Pigs. Audiol Neurootol. 2018;23(4):245-57.
455. Sekulic M, Abdollahi N, Graf L, Deigendesch N, Puche R, Bodmer D, et al. Human blood-labyrinth barrier on a chip: a unique in vitro tool for investigation of BLB properties. RSC Advances. 2023;13(36):25508-17.
456. Hall MD, Telma KA, Chang KE, Lee TD, Madigan JP, Lloyd JR, et al. Say no to DMSO: dimethylsulfoxide inactivates cisplatin, carboplatin, and other platinum complexes. Cancer Res. 2014;74(14):3913-22.
457. Karbownik A, Szałek E, Urjasz H, Głęboka A, Mierzwa E, Grześkowiak E. The physical and chemical stability of cisplatin (Teva) in concentrate and diluted in sodium chloride 0.9%. Contemp Oncol (Pozn). 2012;16(5):435-9.
458. Chen X, Yao X, Wang C, Chen L, Chen X. Mesoporous silica nanoparticles capped with fluorescence-conjugated cyclodextrin for pH-activated controlled drug delivery and imaging. Microporous and Mesoporous Materials. 2015;217:46-53.
459. Pak JH, Yi J, Ryu S, Kim IK, Kim JW, Baek H, et al. Induction of Redox-Active Gene Expression by CoCl(2) Ameliorates Oxidative Stress-Mediated Injury of Murine Auditory Cells. Antioxidants (Basel). 2019;8(9).

Every reasonable effort has been made to acknowledge the owners of copyright material. I would be pleased to hear from any copyright owner who has been omitted or incorrectly acknowledged.